This is to certify that the
dissertation entitled

FAST COMPUTATIONAL TECHNIQUES FOR MULTISCALE ELECTROMAGNETIC SIMULATIONS

presented by

Vikram Melapudi

has been accepted towards fulfillment
of the requirements for the

Ph.D. degree in Electrical Engineering

Major Professor's Signature

May 14, 2009

Date

FAST COMPUTATIONAL TECHNIQUES FOR MULTISCALE ELECTROMAGNETIC SIMULATIONS

By

Vikram Melapudi

A DISSERTATION

Submitted to
Michigan State University
in partial fulfillment of the requirements
for the degree of

DOCTOR OF PHILOSOPHY

Electrical Engineering

2009

ABSTRACT

FAST COMPUTATIONAL TECHNIQUES FOR MULTISCALE ELECTROMAGNETIC SIMULATIONS

By

Vikram Melapudi

Multiscale electromagnetic simulations contain features with multiple length or frequency scales or both. Multiscale features are characteristic of realitic simulations as large degrees of freedom (N) are required to capture the minute physical details. Though integral equation (IE) approaches are well-suited for electromagnetic simulations, they require repeated evaluation of pair-wise potentials - also referred to as N-body problems. It is well known that the direct computation of these potentials scales as $\mathcal{O}(N^2)$ both in terms of computer memory and time. Even with the rapid advancements in computer technology, this places severe limitation on the size of the problem (N) that can be analyzed in a realistic time frame. Further, multiscale simulations produce badly-conditioned systems of equations that require large number of iterations when using Krylov-subspace solvers. The main goal of this thesis is to develop a suite of computational techniques that enables multiscale electromagnetic simulations in a fast, efficient and stable fashion. In this work, the accelerated Cartesian expansion (ACE) algorithm is used to overcome the quadratic cost-scaling of N-body problems. ACE was intially developed for the fast evaluation of polynomial potentials and here it is extended to the fast computation of retarded and Helmholtz potentials. These algorithms are shown to be stable and efficient for computation of electromagnetic potentials at sub-wavelength or low-frequency scales. Hybrid combination of these algorithms with existing fast methods leads to the development of multiscale electromagnetic solvers that are stable and efficient across length and frequency scales. Since the fast algorithms only reduce the time spent in each iteration, a new integral equation formulation is developed that yields better conditioned systems

of equations. This is achieved by reformulating the augmented field integral equations such that the resulting operators are bounded and compact. Further, the widespread availability of parallel distributed or cluster computers combined with the memory and speed restriction of single processor computers necessitates the development of efficient parallel implementation of the sophisticated fast algorithms. The parallel algorithms developed in this work are provably scalabale and enables simulation of problems with several millions of unknowns on large scale clusters, with hundreds of processors and beyond. In this thesis, ACE algorithm is also extended to rapid computation of time domain diffusion potentials.

ACKNOWLEDGMENT

During the past six years of my Ph.D. life at Michigan State University, I have been influenced by many people. I wish to acknowledge the select few who have left an everlasting impression on me.

I start by thanking my advisor Prof. Shanker Balasubramaniam. More than an advisor, he has been a good friend and his contagious enthusiasm and rigor in research continues to amaze me. It is difficult to encompass my gratitude and appreciation towards him in few words..

I thank my committee members Prof. Lalita Udpa, Prof. Satish Udpa and Prof. Neil Wright for all the support, advice and time they have provided me. Special regards to Prof. Lalita Udpa, my first advisor, for showing the support and confidence in me to proceed with Ph.D. The frank discussions with both Prof. Udpa(s) have helped be at home in MSU. I also thank professors E. Rothwell, A. Tamburrino and C. Y. Wang (Math Dept.) for their influential research perspectives and exciting courses.

I carry with me special memories of all the colleagues and friends in NDEL and BSer. I thank them for granting me a fun-filled research life. I am indebted to specially mention Kavitha, Naveen, Sridhar, Gokul and Yiming. I add my heart filled gratitude toward my friends Kavitha and Sanketh for their support and affection.

Finally, I would like to thank my family Mr. Karunakara Reddy (father), Mrs. Bhargavi (mother) and Mr. Vinod (brother). Their unconditional love, moral support and appreciation of my passion continues to help me lead a satisfactory life, while maintaining my unconventional perspectives.

TABLE OF CONTENTS

LIST OF TABLES

LIST OF FIGURES

Chapter 1

Introduction

This chapter provides a comprehensive introduction to the development of fast multipole methods (FMM) within the context of electromagnetics. Section 1.1 gives a brief account of the various developments in FMM that are elucidated in greater detail in rest of the chapter. Section 6.2 provides a general introduction to hierarchical algorithms, which forms the backbone of this thesis work. Section 1.3 and 1.4 details the development of various versions of FMM for Laplace and Helmholtz equation, respectively. Section 1.6 gives a preview of the developments made in this thesis work along with the outline of the thesis.

1.1 Background

The numerical solution of Maxwell's equations has typically proceeded along two different paths. The first, and perhaps the more popular, is the direct discretization of Maxwell's equations [1, 2]. Finite difference and finite element methods belong to this class of solvers. Their popularity stems from two salient features; (i) they are typically simpler to program and (ii) their memory and CPU cost scales as $\mathcal{O}(N)$, where N denotes the number of degrees of freedom. The second methodology for

solving Maxwell's equations are based on developing integral equations (IE) derived by evoking the Green's identity/equivalence theorems. While the latter was introduced in electromagnetics more than four decades ago [3], they were not a popular option for electromagnetic analysis. The bottlenecks to their adoption was due to both the memory and CPU complexity, both of which scale as $\mathcal{O}(N^2)$. This is despite some of the inherent advantages of integral equations for analyzing open region problems, viz., better condition numbers, possibility of using surface integral equations and incorporation of the radiation boundary condition in the Green's function.

The introduction of the fast multipole methods (and tree codes) significantly altered the landscape. Both these methods were developed in response to accelerating pairwise potential evaluations in N-body problems in fields ranging from biophysics to computational chemistry to astrophysics, etc. Here, it is necessary to compute long-range Coulombic potentials repeatedly between N randomly distributed particles. The tree methods [4, 5] and the fast multipole method (FMM) [6, 7, 8, 9] reduced the computational complexity of computing these pairwise potentials from $\mathcal{O}(N^2)$ to $\mathcal{O}(N)$. FMM and tree codes are based on a hierarchical decomposition of the computational domain, and using multipole/local expansions to compute the influence between sub-domains that are sufficiently separated. The FMM, as introduced in [7], exploits the representation of the potential in terms of spherical harmonics. As we shall see, this is a consequence of using addition theorems to represent the potential as a series wherein each term is a product of two functions. These functions depend either on the coordinates of the source or the observer only. The separation between source and observer is crucial to creating a fast scheme. At about the same time, an algorithm that achieves the same reduction on complexity, *albeit* using Cartesian tensors was introduced [10]. This derivation relies on using Taylor expansion of the potential function to provide the necessary addition theorems [11]. Cartesian expansions have been used extensively in tree codes. More recently, FMM codes based on

Cartesian expansions have used recurrence relations to avoid derivatives [12]. Typically, FMMs derived using the Cartesian expansion are more expensive as spherical harmonics are optimal in representing Coulombic potentials. However, it was recently shown that it is possible to develop a FMM using Maxwell-Cartesian harmonics that are *as optimal* as using spherical harmonics with one singular advantage; it avoids the need for special functions [13]. Both FMM and tree codes have revolutionized analysis in various application domains ranging from molecular dynamics [14], elastostatics [15, 16], elastic wave equations [17], flow problems [18], capacitance [19] and impedance [20] extraction in micro-electronic circuits, evaluation of splines [21] and spherical harmonics [22, 23]. The FMM framework has also been extended to the solution of potentials resulting from parabolic equations [24, 25, 26].

However, direct extension of FMM to the solution of potentials arising from hyperbolic equations is not as straightforward. The first solution to this problem was presented in two dimensions [27, 28], and soon extended to three dimensions [29, 30]. The crux to developing these algorithms was the derivation of a diagonalized form of the translation operator [30, 31, 32]. Since then, there has been a virtual explosion in research in application of these methods to various problems in electromagnetics; see [33, 34, 35] and references therein. The state of art is such that problems of the order of tens million spatial degrees of freedom have been solved [36, 37, 38, 39, 40, 41]. However, the development of FMM based method continues on many fronts [42, 43, 44, 45, 46, 47, 48, 49, 50]. This paper reviews progress in FMM technology since its inception and details current trends in FMM research.

1.2 Hierarchical Computation Scheme

The purpose of this section is to outline the structure of fast multipole methods and introduce notation that will be used in the rest of the paper.

1.2.1 Preliminaries

Consider a source distribution $q(\mathbf{r})$ such that $supp\{q(\mathbf{r})\} = \Omega \subset \mathbb{R}^3$. Likewise, it is assumed that the observers are also distributed in Ω. With no loss of generality, it is assumed that $q(\mathbf{r}) = \sum_{i=1}^{N} q_i \delta(\mathbf{r} - \mathbf{r}_i)$, where N is the number of degrees of freedom. The field due to this source constellation at any point $\mathbf{r} \in \mathbb{R}^3$ is given by

$$\phi(\mathbf{r}) = g(|\mathbf{r}|) \star q(\mathbf{r}) = \sum_{i=1}^{k} g(|\mathbf{r} - \mathbf{r}_i|) q_i \tag{1.1}$$

where $g(|\mathbf{r}|)$ is the appropriate Green's function, and $\star$ denotes a spatial convolution. It is apparent from this expression that the field evaluation scales as $\mathcal{O}(N^2)$ for N observation points. Ideas introduced by [4] to ameliorate this cost for static problems relies on exploiting the fact that the field at a point due to a cluster of sources is rank deficient, where the rank depends on the distance between the point and the center of the cluster. In other words, for a given accuracy, potential at an observation point sufficiently separated from a cluster of sources can be computed with few multipole expansions. Similarly, for given accuracy, few local expansions can be used to compute potential at a cluster of observation point due to a well-separated source. These ideas were cast in a more formal framework as tree-codes [5] and FMM [6]. At this point, we note that there is rampant confusion in terminology; both FMM and tree codes are used interchangeably. While the two methods are closely related, there are subtle but significant differences between the two [51]. Tree codes compute interactions between source pairs using one of three methods: (i) directly, (ii) evaluating fields at each observation point using multipole expansion due to a cluster of sources, or (iii) using local expansion at observation clusters to find fields. The decision on the operation used depends on which one is computationally efficient. On the other hand, the algorithmic structure of FMM enables the computation of potentials in an optimal manner [51]. Two additional operations that permit this are

aggregation and disaggregation functions. These permit the computation of information at coarser (or finer) levels using information at finer (or coarser) levels. Thus, FMM relies on a hierarchical decomposition of the computational domain. This is achieved using the following strategy [8]; the computational domain Ω is embedded in a fictitious cube that is then divided into eight sub-cubes, and so on. This process continues recursively until the desired level of refinement is reached; an N_l-level scheme implies $N_l - 1$ recursive divisions of the domain, see figure 1.1. At any level, the (sub)domain that is being partitioned is called the *parent* of all the eight *children* that it is being partitioned into. At the lowest level, all source/observers are mapped onto the smallest boxes. This hierarchical partitioning of the domain is referred to as a regular oct-tree data structure. Regular oct-tree representations are optimal only for geometries with uniform distribution [52]; non-uniform distributions can be represented using compressed oct-trees [51, 39]. In compressed oct-trees, sub-division of a domain is stopped when number of source/observer in that domain becomes less than a pre-fixed limit. While many algorithm exist for constructing a tree, the one that we have found to be efficient is the use of key data-structure to represent the nodes of a tree. In this approach the root box enclosing the entire geometry is represented with integer value 1; each of the eight (four) children of a parent is identified with a three (two) bit code which is appended to the parent box key to obtain their global unique key. Figure 1.2 shows an example compressed oct-tree where each box is represented using key-codes. This representation has several advantages: the nodes of tree at each level automatically follow Morton ordering and it plays an important role when partitioning the boxes among processors in parallel algorithm, all antecedents of a box and essential information like size of box, center position, level etc. can be readily recovered from its key-code using bit manipulations [53, 38, 54]. Mapping the computational domain onto a tree facilitates partition/classification of interactions as being either in the near or farfield. This is done using the following rule: at any

level in the tree, all boxes/sub-domains are classified as being either in the near or far field of each other using the following dictum: two sub-domains are classified as being in the farfield of each other if the distance between the centers is at least twice the side length of the domain, *and* their parents are in the near field of each other; see figure 1.3 for an illustration of these classification. Once, the interaction list have been built for all levels, the computation proceeds as follows; at the lowest level, interaction between the elements of boxes that are in the near-field of each other is computed directly, i.e., using (1.1). All other interactions are computed using a three stage algorithm: (i) compute multipoles of sources that reside in each box; (ii) convert these to local expansion at all boxes that are in its far field; (iii) from the local expansion, compute the field at each observer. This simple three stage scheme is called a one-level scheme, and necessitates the development of theorems for (i) computation of multipoles at leaf (or smallest boxes), (ii) translate multipole expansion to local expansion and (iii) finally, aggregate the local expansions in a box to compute the field at all the observers. It is apparent that one can derive a more efficient computational scheme by embedding this scheme within itself as shown in 1.4. That is, if two sets of sub-domains that interact with each other are sufficiently far away, then these clusters may be combined to form large clusters that then interact with each other at a higher level and so on; this is referred to here as a multilevel scheme. This implies that it is necessary to develop additional theorems that enable (i) shifting the origins of multipole so that effects of small clusters can be grouped together to form larger clusters and (ii) move the origin of local expansion so that expansions at the origin of the parent may be disaggregated to those of its children. In concert, these theorems enable one to traverse up and down the tree, and are presented next. This said the various steps involved in the hierarchical computing are shown in Algorithm 1.

Note that in single level algorithm the upward and downward tree traversal (steps

Algorithm 1 Hierarchical tree computation

1: Construct the tree representation for the given geometry (distribution of discrete points).
2: Build interaction list using the above definition, for all boxes in the tree and the near-field list for leafless boxes.
3: **NF**: Use direct method for computation of *nearfield* potential at observation points in each leafless box from sources contained in its near-field boxes.
4: **S2M**: compute multipole expansions for each leafless boxes from sources contained within it.
5: **M2M** (upward traversal): for all parent boxes compute the multipole expansion by combining the multipole expansions at their children boxes.
6: **M2L** (translation): for all boxes in the tree convert the multipole expansions to local expansions about centers of boxes in their interaction list.
7: **L2L** (downward traversal): *update* the local expansion information at a child box using the local expansion of their parent box.
8: **L2O**: use the local expansions about each leafless box to compute the *farfield* potential at its observation points.

5 and 7) are absent. Next, we will detail these operations for different FMMs. Starting with well known static FMM to those for Helmholtz and finally to those for wideband FMM. Details are presented for the first two despite the fact that they are well known. The rationale for doing so is two fold (i) it is important to understand when FMM for Helmholtz fails and (ii) techniques developed for static FMM and some of the new FMM approaches find their way into the development of wideband FMM.

1.3 Static fast multipole method

This section provides the appropriate theorems for fast evaluation of potential defined in terms of $g(|\mathbf{r}|) = 1/|\mathbf{r}|$. Such potentials are commonly used in study of plasma dynamics, magnetostatic problems, eddy currents etc. While on first glance, one might be inclined to exclude methods developed for rapid evaluation of the Coulomb potential but these play an important role in developing fast methods for wideband problems.

1.3.1 Single level scheme

Consider two domains $\Omega_s \in \mathbb{R}^3$ and $\Omega_o \in \mathbb{R}^3$ that comprises of randomly located source and observer points, respectively. With no loss of generality, it is assumed that the number of sources and observers are k, these domains can be embedded in spheres of radius a. The centers of Ω_s and Ω_o are denoted by $\mathbf{r}_s$ and $\mathbf{r}_o$, respectively. It is assumed that $\Omega_s \subset \bar{\Omega}_s$ and $\Omega_o \subset \bar{\Omega}_o$ and $\bar{\Omega}_s \cap \bar{\Omega}_o = \emptyset$, and the domains of Ω_s and Ω_o are sufficiently separated. In what follows, the domains $\bar{\Omega}_s$ and $\bar{\Omega}_o$ will be called parents of Ω_s and Ω_o, respectively. The parent domains can be embedded in a sphere of radius $2a$, and their center are denoted by $\mathbf{r}_s^p$ and $\mathbf{r}_o^p$, respectively. Next, we will present a single level FMM constructed using two methods; (i) spherical harmonics and (ii) Cartesian tensors.

Spherical harmonics

The theorems for a single and multilevel FMMs using spherical coordinates were introduced in a series of papers [7, 8], and have found extensive application in various disciplines; a sampling of these can be found in [6, 8, 55, 19, 20, 56, 57]. The genesis of the method is the well known generating function for Legendre polynomials [58],

$$\frac{1}{R} = \frac{1}{r\sqrt{1 - 2\frac{r'}{r}\cos\gamma + (\frac{r'}{r})^2}} = \sum_{n=0}^{\infty} \frac{r'^n}{r^{n+1}} P_n(\cos\gamma) \tag{1.2}$$

with

$$\cos\gamma = \cos\theta\cos\theta' + \sin\theta\sin\theta'\cos(\phi - \phi') \tag{1.3}$$

where $P_n(u)$ represents Legendre polynomial of degree n, $\mathbf{r}' = (r', \theta', \phi')$ and $\mathbf{r} = (r, \theta, \phi)$. Legendre polynomials in (1.2) can be represented in terms of spherical

harmonics $Y_{nm}(\theta, \phi)$ using the addition theorem [59],

$$P_n(\cos\gamma) = \sum_{m=-n}^{n} \bar{Y_n^m}(\theta, \phi) Y_n^m(\theta', \phi') \tag{1.4}$$

where the superscript $\star$ represents complex conjugate. Using (1.4) in (1.2) results in complete separation of source and observation quantities,

$$\frac{1}{R} = \sum_{n=0}^{\infty} \sum_{m=-n}^{n} r'^n \bar{Y_n^m}(\theta', \phi') \frac{Y_n^m(\theta, \phi)}{r^{n+1}} \tag{1.5}$$

These expressions enable the derivation of the following theorems necessary for steps 4, 6 and 8 in Algorithm 1.

Theorem 1.3.1 (Multipole Expansion (S2M): spherical). *Let k charges of strengths $\{q_i, i = 1, \ldots, k\}$ be located at $\mathbf{r}_i \in \Omega_s$ with $|\mathbf{r}_i - \mathbf{r}_s| < a$. Then for any $\mathbf{r} \in \Omega_o$, the potential ϕ is given by,*

$$\phi(\mathbf{r}) = \sum_{n=0}^{\infty} \sum_{m=-n}^{n} M_n^m \frac{Y_n^m(\theta, \phi)}{|\mathbf{r} - \mathbf{r}_i|^{n+1}} \tag{1.6}$$

where

$$M_n^m = \sum_{i=1}^{k} q_i |\mathbf{r}_i - \mathbf{r}_s|^n \bar{Y_n^m}(\theta_i, \phi_i) \tag{1.7}$$

where the parameters $\{\theta_i, \phi_i\}$ and $\{\theta, \phi\}$ are spherical coordinates of $\mathbf{r}_i$ and $\mathbf{r}$ w.r.t the origin at $\mathbf{r}_s$.

In Theorem 1.3.1, M_n^m is the multipole expansion at $\mathbf{r}_s$ constructed from the source quantities $q_i(\mathbf{r}_i)$. Proofs for the error bounds in the above expressions can be obtained from [8, 9]. Next, these multipoles are translated from $\mathbf{r}_s$ to $\mathbf{r}_o$.

Theorem 1.3.2 (Multipole to Local Translation operator (M2L): spherical). *Given a multipole expansion O_n^m about $\mathbf{r}_s$, it can be mapped to local expansion L_j^k at*

r_0 is

whe

p

ass

Theo

at a

ds b

cap

pos

be

ins

1.

It

en

a

e

f

$\mathbf{r}_o$ *using*

$$L_i^k = \sum_{n=0}^{\infty} \sum_{m=-n}^{n} \frac{O_n^m (-j)^{|k-m|-|m|-|k|} A_n^m A_i^k Y_{i+n}^{m-k}(\theta, \phi)}{(-1)^n A_{i+n}^{m-k} |\mathbf{r}_s - \mathbf{r}_o|^{i+n+1}} \tag{1.8}$$

where $\{\theta, \phi\}$ *are the spherical coordinates of the* $\mathbf{r}_s$ *w.r.t* $\mathbf{r}_o$*, and* $A_n^m = \frac{(-1)^n}{\sqrt{(n-m)!(n+m)!}}$.

Finally, the local expansions at any leaf node may be mapped onto the observers using the theorem presented next.

Theorem 1.3.3 (Local expansions to observer (L20): spherical). *The potential at a point* $\mathbf{r} \in \Omega_o$ *due to local expansion* L_n^m *about origin is given by,*

$$\phi(\mathbf{r}) = \sum_{n=0}^{\infty} \sum_{m=-n}^{n} L_n^m |\mathbf{r} - \mathbf{r}_o|^n Y_n^m(\theta, \phi) \tag{1.9}$$

As before, the parameters $\{\theta, \phi\}$ *are the spherical coordinates of* $\mathbf{r}$ *with respect to the origin at* $\mathbf{r}_o$.

The above theorems, in a one level setting, permit the rapid computation of potentials at all points in Ω_o due to sources in Ω_s. It is evident that this scheme can be embedded within itself to create a multilevel scheme. But prior to doing so, it is instructive to re-examine the fundamentals of FMM from a Cartesian perspective.

1.3.2 Multilevel FMM algorithm

It is apparent that the $\mathcal{O}(N^{4/3})$ cost of single level algorithm can be further reduced by embedding this scheme within itself, as is evident from figure 1.4. To implement such a scheme it is necessary to develop methods that enable one to construct multipole expansions at a parent level from those at their children. These are effected using the following theorems.

Theorem 1.3.4 (Multipole to Multipole (M2M): spherical). *A multipole ex-*

pansion O_n^m *about* $\mathbf{r}_s$ *can be mapped onto one that exists around* $\mathbf{r}_s^p$ *using*

$$M_i^k = \sum_{n=0}^{i} \sum_{m=-n}^{n} \frac{O_{i-n}^{k-m}(-j)^{|k|-|m|-|k-m|} A_n^m A_{i-n}^{k-m} \left(r_s^{cp}\right)^n \bar{Y}_n^m(\theta,\phi)}{A_i^k} \tag{1.10}$$

where $r_s^{cp} = |\mathbf{r}_s^{cp}| = \mathbf{r}_s - \mathbf{r}_s^p$, *and* $\{\theta,\phi\}$ *are the polar coordinates of* $\mathbf{r}_s$ *w.r.t.* $\mathbf{r}_s^p$.

Theorem 1.3.5 (Local to Local (L2L): spherical). *Given a local expansion* O_n^m *about* $\mathbf{r}_o^p$, *it can be mapped to one around* $\mathbf{r}_o$ *using*

$$L_i^k = \sum_{n=i}^{p} \sum_{m=-n}^{n} \frac{O_n^m(-j)^{|m|-|k|-|m-k|} A_{n-i}^{m-k} A_i^k Y_{n-i}^{m-k}(\theta,\phi) \left(r_o^{pc}\right)^{n-i}}{(-1)^{n+i} A_n^m} \tag{1.11}$$

where $\mathbf{r}_o^{pc} = |\mathbf{r}_o^{pc}| = |\mathbf{r}_o - \mathbf{r}_o^p|$, *and* $\{\theta,\phi\}$ *are the polar coordinates of* $\mathbf{r}_o$ *w.r.t.* $\mathbf{r}_o^p$.

The equivalent theorems for Cartesian expansion likewise follow.

Theorem 1.3.6 (Multipole to Multipole (M2M): Cartesian). *A traceless multipole tensor* $\mathbf{O}_t^{(m)}$ *at* $\mathbf{r}_s$ *is related to* $\mathbf{M}_t^{(m)}$ *that is centered at* $\mathbf{r}_s^p$ *via*

$$\mathbf{M}_t^{(m)} = \sum_{n=0}^{m} \frac{(-1)^n}{n!} \frac{\mathcal{D}_n \left(\mathbf{r}_s^{pc}\right)^n}{(2n-1)!!} \mathbf{O}_t^{(m-n)} \tag{1.12}$$

where $\mathbf{r}_s^{pc} = \mathbf{r}_s^p - \mathbf{r}_s$.

Theorem 1.3.7 (Local to Local (L2L): Cartesian). *Given a local expansion* $\mathbf{O}_t^{(n)}$ *that exist in the domain* $\bar{\Omega}_o$ *centered around* $\mathbf{r}_o^p$, *it can be shifted to the domain* Ω_o *centered at* $\mathbf{r}_o$ *using*

$$\mathbf{L}_t^{(m)} = \sum_{n=0}^{\infty} \begin{pmatrix} m+n \\ m \end{pmatrix} \mathbf{O}_t^{(m+n)} \cdot (m) \cdot \left(\mathbf{r}_o^{cp}\right)_t^n \tag{1.13}$$

where $\mathbf{r}_o^{cp} = \mathbf{r}_o - \mathbf{r}_c^p$

These theorems, in concert, permit traversing up and down the oct-tree, see figure 1.5. While these theorems are the bare-bones presentation of the steps required, there have been several attempts to make these more efficient [7, 8, 14, 60]. As both methods are based on Taylor expansions the upperbounds in using these approaches can be readily derived. Such a derivation is presented in [8, 13]. Alternatively, another interesting algorithm was introduced in [13] that permits *exact* evaluation of the multipole expansion at the parent given the multipole expansion at the children–this has been shown both analytically and numerically for different potential functions. However, in order to get this exact expression, one has to abandon the use of traceless tensors. It follows that the cost of using exact multipole to multipole translations is higher. But in our experience, we have found that we need a smaller number of multipoles for the same precision, and this can significantly affect the total cost, especially for large data sets [13]. Abandoning the use of traceless operators has three salient benefits; (i) the algorithms can be used for any potential function whose Taylor's series converges rapidly, (ii) it does not depend on special functions and (iii) *only* the translation operator depends on the potential function which implies that multiple potentials may be easily combined [61].

In all the above expressions, it was assumed that the number of multipoles used was infinite. The analytical estimates regarding truncation of this sum for both the spherical and Cartesian form can be found in [8, 13]. The cost analysis for multilevel approach is as follows: the total number of boxes in the tree is $\mathcal{O}(N/s)$ and the cost for S2M and L2O operations remains the same; the cost of applying M2L translation operation across levels scales as $\mathcal{O}(P^4N/s)$. In addition the cost of applying M2M and L2L operations for all boxes scales as $\mathcal{O}(N/sP^4)$. Thus, the overall computational cost associated with both schemes scales as $\mathcal{O}(P^4N)$. This cost is largely dominated by the time for multipole to local translation (M2L) and considerable research effort has been expended on reducing this cost. A closer examination of the M2L operation reveals

that (i) the number of translations per box is 189 and (ii) the cost per translation scales as $\mathcal{O}(P^4)$. The latter is due to the fact that this operation is not diagonal. Greengard *et. al.* [9] remedied this deficiency by introducing a novel algorithm that diagonalizes the translation operator. Additional modifications to the overall algorithm introduced there [42, 62] further reduces the number of translations, making the "revamped" FMM extremely efficient. Ideas behind this diagonalization can be exploited by either both varieties of FMM; spherical and Cartesian. It also plays a key role in FMMs for low-frequency, and consequently, will be presented in some detail next. An FFT based implementation of above un-diagonalized form results in a overall cost that scale as $\mathcal{O}(NP^2 \log P)$ [60], but will not be dwelt here.

1.3.3 Diagonalized translation operators

A diagonal translation operator may be derived using a spectral representation of the Green's function [9], viz.,

$$\frac{1}{R} = \frac{1}{2\pi} \int_0^\infty d\lambda e^{-\lambda z} \int_0^{2\pi} d\alpha e^{-j\lambda(x\cos(\alpha)+y\sin(\alpha)} \tag{1.14}$$

for $z > 0$. It is apparent that the inner integral is in fact a zeroth order Bessel function. The computation of potentials using the above expressions hinge on the existence of an integration rule that is efficient to a given precision and scale invariant if this formula is to be used at different levels in the FMM tree. Given the existence of such a rule [63], the potential at any point can be written as [9]

$$\phi(\mathbf{r}) = \sum_{k=1}^{s(\epsilon)} \sum_{i=1}^{M(k)} W(k,i) e^{-\lambda_k z} e^{-j\lambda_k(x\cos\alpha_i + y\sin\alpha_i)} + \mathcal{O}(\epsilon) \tag{1.15}$$

where the coefficients $W(k,i)$ are a combination of the charges q_i and integration weights w_k, $s(\epsilon)$ and $M(k)$ denotes the number of integration points for ϵ accuracy.

Evidently, in above discrete representation, the number of integration points $M(k)$ for evaluating α integral depends on k to account for the varying bandwidth, λ_k, of its integrand. The advantages of above scheme are immediately apparent in that it readily permits translation of the origin; translation of the origin is quite simply a shift in the exponentials. The similarity between (1.15) and those in Theorems (1.3.1), and (2.3.3) are readily apparent. The mapping from spherical harmonic multipole coefficients M_n^m onto exponential expansions $W(k,j)$ is given as [9],

$$W(k,i) = \frac{w_k}{M(k)} \sum_{-\infty}^{\infty} (j)^{|m|} e^{-jm\alpha_i} \sum_{n=|m|}^{\infty} \frac{M_n^m}{\sqrt{(n-m)!(n+m)!}} \lambda_k^n \tag{1.16}$$

and given $W(k,i)$ coefficients the spherical harmonic local expansion L_n^m can be computed with,

$$L_n^m = \frac{(j)^{|m|}}{\sqrt{(n-m)!(n+m)!}} \sum_{k=1}^{s(\epsilon)} (-\lambda_k)^n \sum_{i=1}^{M(k)} W(k,i) e^{-jm\alpha_i} \tag{1.17}$$

The multipole to local translation operation, with diagonalized translation forms, can be computed as a three stage process: multipole coefficients are mapped to $W(k,i)$, translate $W(k,i)$, and then map the translated coefficients back to local expansions, and then proceed as usual. It is evident that cost of all operators involving exponential expansions scale as $\mathcal{O}(P^2)$. Various symmetry considerations in implementation reduces the number of total translation count from 189 to 40. Additionally, one can exploit symmetry in the expressions involved to further reduce the overall cost, if not the asymptotic complexity [56]. Thus, properly modifying and augmenting either spherical or Cartesian multipole based algorithms with plane wave translation operators can considerably ameliorate the cost. However, a couple of issues must be noted; (i) the plane wave expression is valid for $z > 0$, this implies that the interaction list must be modified [9]; (ii) additional operators must be introduced to rotate the

multipole operators along the required axis; (iii) the operator developed should be scale invariant for the scheme to be efficient. In implementation the spherical harmonic multipole coefficient is converted into six plane wave expansions corresponding to each face of the cube and the interaction list definition is changed accordingly. For example, exponential expansions corresponding to $+z$ cube face is valid only for boxes present above $X-Y$ plane, as illustrated in figure 1.6. Boxes in original interaction list are divided into six new sets termed as *up-list, down-list, north-list, south-list, east-list* and *west-list* corresponding to $+z, -z, +y, -y, +x$ and $-x$ cube faces respectively [9]. Overall, the diagonalized version of the translation operator reduces both the total number of translation operation and per translation cost leading to a much faster algorithm. This approach is very similar to spectral approaches developed for alternative derivation of Helmholtz FMM [42, 64] and is the crux of many methods developed for wideband FMM.

1.4 FMM for Helmholtz equations

Thus far, we have seen that cascaded Taylor expansions can be used to develop static FMM. While these ideas are readily extended to the solution of parabolic equations as well [24], they are not readily extendable to Helmholtz equation kernels, especially at high frequencies. Furthermore, as was evident from last section, the scheme developed should be diagonal. Consider a problem setting that is identical to what was described in Section 6.2. We shall seek development of methods to accelerate the evaluation of the potential integral in (1.1) with $g(|\mathbf{r}|) = \exp[-j\kappa|\mathbf{r}|]/|\mathbf{r}|$. One expression that readily suggests itself is the Gegenbauer addition theorem [59, 65, 31],

$$\frac{e^{-j\kappa|\mathbf{X}+\mathbf{d}|}}{|\mathbf{X}+\mathbf{d}|} = -j\kappa\sum_{l=0}^{\infty}(-1)^l(2l+1)j_l(\kappa d)h_l^{(2)}(\kappa X)P_l(\hat{\mathbf{d}}\cdot\hat{\mathbf{X}}) \qquad (1.18)$$

wh
pa
An
in

wh
pa
of a
pa
dia

wh
kn
wa

Sub
tru

where $\mathbf{X}$ and $\mathbf{d}$ are position vectors such that $\mathbf{r} = \mathbf{X}+\mathbf{d}$ and $|\mathbf{X}| > |\mathbf{d}|$, j_l and $h_l^{(2)}$ are l^{th} order spherical Bessel and Hankel function of second kind, $X = |\mathbf{X}|$ and $d = |\mathbf{d}|$. Augmenting this theorem with another addition theorem for Legendre polynomials in (1.4) completes the separation between the source and observer coordinates.

$$\frac{e^{-j\kappa|\mathbf{X}+\mathbf{d}|}}{|\mathbf{X}+\mathbf{d}|} = -j\kappa \sum_{l=0}^{L} \sum_{m=-l}^{l} (-1)^l (2l+1) j_l(\kappa d) h_l^{(2)}(\kappa X) Y_{lm}(\theta_X, \phi_X) \bar{Y_{lm}}(\theta_d, \phi_d) \tag{1.19}$$

where L is the number of terms used in the summation, $\{\theta_X, \phi_X\}$ and $\{\theta_d, \phi_d\}$ are the polar coordinates of $\hat{X}$ and $\hat{d}$ respectively. It is evident that one may use a sequence of addition theorems to create hierarchical computational methodology. However, the principal bottleneck to such a scheme is the fact that the operators involved are not diagonal. However, diagonal operators are easily developed by recognizing that

$$4\pi(-j)^l j_l(\kappa d) P_l(\hat{\mathbf{d}} \cdot \hat{\mathbf{X}}) = \int d^2\hat{\mathbf{k}} e^{-j\mathbf{k}\cdot\mathbf{d}} P_l(\hat{\mathbf{k}} \cdot \hat{\mathbf{X}}) \tag{1.20}$$

where $d^2\hat{\mathbf{k}} = \sin\theta d\theta d\phi$ and $\mathbf{k} = \kappa\hat{\mathbf{k}}$. The relation (1.20) can be derived from well known orthogonality relation among spherical harmonics and expansion for plane waves given as.

$$\int d^2\hat{\mathbf{k}} Y_n^m(\hat{\mathbf{k}}) Y_{l'm'}^*(\hat{\mathbf{k}}) = \frac{4\pi}{2l+1}\delta_{mm'}\delta_{ll'} \tag{1.21}$$

$$e^{-jz\cos\gamma} = \sum_{l=0}^{\infty} j_l(z) P_l(\cos\gamma) \tag{1.22}$$

Substituting (1.20) in (1.18), interchanging the summation and the integral, and truncating the summation over l yields the final diagonalized form,

$$\frac{e^{-j\kappa|\mathbf{X}+\mathbf{d}|}}{|\mathbf{X}+\mathbf{d}|} = \frac{-j\kappa}{4\pi} \int d^2\hat{\mathbf{k}} e^{-j\mathbf{k}\cdot\mathbf{d}} \sum_{l=0}^{L} (-1)^l (2l+1) h_l^{(2)}(\kappa X) P_l(\hat{\mathbf{k}} \cdot \hat{X}) \tag{1.23}$$

Several derivation that result in above diagonalized form exist and are based on different set of starting formulas [30, 31, 66, 67, 32]. First scheme for diagonalizing (1.18) was presented in [30] with the use of forward and inverse far field transform defined as,

$$\tilde{f}(\theta,\phi) = \sum_{l=0}^{\infty}\sum_{m=-l}^{l}(-j)^l Y_n^m(\theta,\phi) f_{lm} \tag{1.24}$$

$$f_{lm} = \int d^2\hat{\mathbf{k}}(-j)^{-l} Y_n^m(\hat{\mathbf{k}})\tilde{f}(\theta,\phi) \tag{1.25}$$

Above definition is a simple spherical harmonic transform from $\hat{\mathbf{k}}$ to $\{l,m\}$ basis with direct analogy to Fourier transform. A simpler version of derivation in [30] is presented in [67, 35]. In [31], the expansion in (1.18) is represented as matrix vector multiplication which reveals a convolution relation in indices $\{l,m\}$. Such convolutions in $\{l,m\}$ can be computed as one-to-one multiplication in $\hat{\mathbf{k}}$ domain using the far field transform [31]. A detailed discussion on deriving the above diagonalized forms from the convolution representation of original multipole expansion for both Laplace and Helmholtz equation is presented in [31]. An alternate derivation based on similarity transform and their relation to group theory is presented in [32] to yield the same expansion in (1.23).

Single Level FMM

As before, assume that Ω_s and Ω_o denote the source and observation domain, and it is necessary to find the fields $\forall \mathbf{r} \in \Omega_o$. It is further assumed that the domains are cubes, in keeping with the data structure of oct-tree and that each domain can be embedded in a sphere of radius a. Furthermore, the clusters are assumed to be well separated. The separation distance is closely related to error bounds [30, 65], and will be dealt with in later part of the paper. Given these conditions, traversal up and

down the tree is effected using the following set of theorems:

Theorem 1.4.1 (Farfield signature). *The far field signature due a set of source q_i for $i = 1, \cdots, k$ located at $\mathbf{r}_i \in \Omega_s$ is given by*

$$\begin{aligned} M(\mathbf{r}_s, \mathbf{k}) &= \sum_{i=1}^{k} \mathcal{M}\left(q_i, \mathbf{k}, \mathbf{r}_s - \mathbf{r}_i\right) \\ &= \sum_{i=1}^{k} q_i \exp\left[-j\mathbf{k} \cdot (\mathbf{r}_s - \mathbf{r}_i)\right] \end{aligned} \tag{1.26}$$

Theorem 1.4.2 (Translation operator). *If a farfield signature exists at a point $\mathbf{r}_s$ such that it is valid for all points outside the domain Ω_s, then the translation operator that maps this farfield to the local expansion that is centered around $\mathbf{r}_o$ and valid in the domain Ω_o is given by*

$$T(\mathbf{k}, \mathbf{r}_{os}) = \sum_{l=0}^{\infty} (-1)^l (2l+1) h_l^{(2)}(\kappa |\mathbf{r}_{os}|) P_l(\hat{\mathbf{k}} \cdot \hat{\mathbf{r}}_{os}) \tag{1.27}$$

where $\mathbf{r}_{os} = \mathbf{r}_o - \mathbf{r}_s$

Finally, the potential at any point $\mathbf{r} \in \Omega_o$ can be constructed using

$$\phi(\mathbf{r}) = \frac{-jk}{4\pi} \int d^2\hat{\kappa} \mathcal{M}\left(1, -\mathbf{k}, \mathbf{r}_o - \mathbf{r}\right) T(\mathbf{k}, \mathbf{r}_{os}) M(\mathbf{r}_s, \mathbf{k}) \tag{1.28}$$

While these equations are readily derived from (1.23). More insight into the derivation of these equations can be obtained by realizing that the farfield (and local expansions) can be represented in terms of spherical harmonics. In turn, this interpretation leads to expressions that reveal convergence rates of these and error bounds as a function radius a and the separation distance. More importantly, this insight leads to the type of quadrature rules that must be used to implement these schemes numerically. In

other words, the continuous integral is evaluated using

$$\phi(\mathbf{r}) = \frac{-j\kappa}{4\pi} \sum_{p=1}^{L} \sum_{q=-p}^{p} w_{pq} \mathcal{M}\left(1, -\mathbf{k}_{pq}, \mathbf{r}_o - \mathbf{r}\right) T(\mathbf{k}_{pq}, \mathbf{r}_{os}) M(\mathbf{r}_s, \mathbf{k}_{pq}) \tag{1.29}$$

where L is the order of the Gauss Legendre rule, w_{pq} are the integration weights, p and q are the integration points in θ and ϕ axis,

$$\begin{aligned} \phi_q &= \frac{2\pi q}{2L+1} \\ \theta_p &\text{ is the } (p+1)^{th} \text{ zero of } P_{L+1}\left(\cos\theta\right) \\ w_{pq} &= \frac{4\pi\left(1-\cos^2\theta_p\right)}{(2L+1)\left[(L+1)P_L(\cos\theta_p)\right]^2} \\ \widehat{\mathbf{k}}_{pq} &= \hat{x}\sin\theta_p\cos\phi_q + \hat{y}\sin\theta_p\sin\phi_q + \hat{z}\cos\theta_p \end{aligned} \tag{1.30}$$

As is apparent form the above equations, uniform sampling is used to evaluate the integral along ϕ. Other applicable rules may be found in [68]. We have yet to elaborate the underlying factors that decide the order of Gauss-Legendre rule that is used along θ. A number of formulae exist for choosing the number of Gauss-Legendre quadrature point [30, 65, 69]. However, examination of (1.23) yields interesting insight. If only the exponential terms are considered in this integral, it is apparent that these expressions can be represented using $L = \mathcal{O}(\kappa d) = \mathcal{O}(2\kappa a)$ harmonics. This, in turn, implies that the summation is also truncated using L terms. Though the reasoning here is based on economical means to discretize the integral a deeper reason, arriving at same conclusion, exists for choice of L based on original multipole expansion [65]. Choice of L should be large enough for the series (1.19) to converge, but not too large to cause numerical instability due to the asymptotic behavior of spherical Bessel and Hankel functions. Given that only a finite number of terms are being used, one can explicitly derive error bounds that, in turn, depend on the translation distance also [30]. Deriving rigorous error bounds has been a focus of considerable work

[43, 69, 70, 71, 72], and the behavior of error is well understood [73, 74] as are the means to overcome these. A simple choice for truncation limit L applicable to most practical problems is,

$$L = \kappa d + Clog(\kappa d + \pi) \tag{1.31}$$

where C is a number that depends on the desired accuracy ϵ; typically the choice of C is {3,5,10} for an accuracy $\epsilon = \{10^{-3}, 10^{-6}, 10^{-14}\}$, respectively [65, 75]. This estimate is semi-empirical and assumes that the two boxes are well separated if they are one box apart. Other estimates [76, 73, 69] based on approximation of Bessel and Hankel function exists both in two- and three-dimensions and can account for multiple box separation between interacting boxes [72, 74]. Cost of this scheme can be computed in the same manner as in the static with $P = L$ and the diagonalized form of translation operator implies $\mathcal{O}(P^2)$ cost per operation. However choice of L depends on size of box kd, which in turn dictates the number of unknowns per box s (assuming uniform discretization). It can be show that the optimal cost of the above scheme scales as $\mathcal{O}(N^{3/2})$ for surface problems.

Multilevel FMM

While the above exposition details the necessary mathematics for implementing a single level scheme, nesting these in a hierarchical setting is the next logical extention. The first robust attempts to do so are [77, 78, 79]. Extension to multilevel is different from that encountered for the Laplace FMM; there, the number of multipoles at all level of the tree was constant. But as is evident from (1.31) and (1.29) as the size of the source/receiver boxes increases, the bandwidth increase increases by a factor of two, which implies that the number of directions increase by a factor of four. This then creates a need for developing robust methods for going up and down the tree for the stages of aggregation and disaggregation. These operators can be thought of

as filters. But before we proceed into intricate details of the methods to implement these, the theorems that help achieve these are as follows:

Theorem 1.4.3 (Translation of farfield signatures). *If the farfield signature* $M(\mathbf{r}_s, \mathbf{k})$ *around the point* $\mathbf{r}_s \in \Omega_s$ *is known, then the farfield signature* $M(\mathbf{r}_s^p, \mathbf{k})$ *around the point* $\mathbf{r}_s^p \in \Omega_s^p$ *is given by*

$$M(\mathbf{r}_s^p, \mathbf{k}) = M(\mathbf{r}_s, \mathbf{k}) e^{-j\mathbf{k}\cdot\left(\mathbf{r}_s^p - \mathbf{r}_s\right)} \tag{1.32}$$

An identical theorem for can be derived for translating local expansion at the parent level to that of its child. Numerical implementation of these theorems is not as simple as it seems. To maintain uniform accuracy across levels, employing (1.31), the L for parent is approximately twice that of its child. This implies that the number of direction for parent box is approximately four times that of its child; thus the multipole expansions for the child and parent box are defined on different grids. This process of computing a higher bandwidth representation from lower bandwidth farfield signature is referred to as interpolation and *anterpolation* is its inverse analogue applied during downward tree traversal. Implementing the above theorems calls for efficient methods to interpolate (or anterpolate). Several methods that exist have been elaborated upon in [33] and summarized as well in [69]. An efficient and exact algorithm can be devised using the forward and inverse farfield transform for both interpolation and anterpolation [79, 23, 80, 35]. This algorithm relies on the fact that at any level the farfield signature can be represented in terms of spherical harmonics., viz.,

$$M(\cdot, \mathbf{k}) = \sum_{n=0}^{\infty} \sum_{m=-n}^{n} a_{nm} Y_{nm}(\theta, \phi) \tag{1.33}$$

As is well known, the farfield signature of a source constellation is bandlimited to $\mathcal{O}(\kappa a)$ harmonics. This implies that the above expression can be truncated. Further-

more, since an Lth order rule is chosen to evaluate the spectral integral in (1.23), it follows that the upper limit in the summation over n can be chosen to be L. This said, direct computation of a_{nm} is expensive. Alternate methods both exact and approximate have been discussed in [23, 81]. Consider the computation of a_{nm} from child farfield signature $M(\mathbf{r}_s, \mathbf{k}_{kp})$ represented using $(2L^2+1)$ coefficients, i.e. $p = 1, \cdots, L$ and $q = 1, \cdots, (2L+1)$,

$$\begin{aligned} a_{nm} &= \int d^2\hat{\kappa} M(\mathbf{r}_s, \mathbf{k}) Y^*_{nm}(\theta, \phi) \\ &= \sum_{p=1}^{L} w_p P_{nm}(\cos\theta_p) \left(\sum_{q=1}^{(2L+1)} M(\mathbf{r}_s, \mathbf{k}_{pq}) e^{jn\phi_q} \right) \\ &= \sum_{p=1}^{L} w_p P_{nm}(\cos\theta_p) \alpha_m(\theta_p) \end{aligned} \tag{1.34}$$

where w_p are numerical quadrature weights. Since, the integration along ϕ is performed using uniform sampling, fast Fourier transform (FFT) can be used for summation inside the brackets. These coefficients are then used to compute samples along new polar coordinates $\left(\tilde{\theta}_p, \tilde{\phi}_q\right)$ with $p = 1, \cdots, \tilde{L}$ and $q = 1, \cdots, (2\tilde{L}+1)$ as,

$$M(\mathbf{r}_s, \tilde{\mathbf{k}}_{pq}) = \sum_{m=-\tilde{L}}^{\tilde{L}} e^{-jm\tilde{\phi}_q} \sum_{n=1}^{\tilde{L}} a_{nm} P_{nm}(\cos\tilde{\theta}_p) \tag{1.35}$$

Again, FFT can be used to evaluate the outer summation. In interpolation, $\tilde{L} > L$ to accommodate for the increase in bandwidth and $\tilde{\mathbf{k}}_{pq}$ represents the discrete directions of the farfield signature corresponding to the parent. The required multipole coefficients about parent origin $\mathbf{r}_s^p$ can be obtained using a simple shifting operation,

$$M(\mathbf{r}_s^p, \tilde{\mathbf{k}}_{pq}) = M(\mathbf{r}_s, \tilde{\mathbf{k}}_{pq}) e^{-j\tilde{\mathbf{k}}_{pq} \cdot (\mathbf{r}_s^p - \mathbf{r}_s)} \tag{1.36}$$

An inverse procedure is performed when translating local expansions from parent to

child where *anterpolation* is used in place of interpolation. First, the parent local expansion about $\mathbf{r}_o^p$ is shifted about child origin $\mathbf{r}_o$; then in *anterpolation*, the forward and inverse farfield transform are performed to reduce the bandwidth in an exact manner as described above but with $\tilde{L} < L$, where L represents the number of harmonics in parent domain. Above procedure for interpolation/anterpolation can be further accelerated with the use of fast Legendre transform [23] where the coefficients a_{nm} are not computed explicitly. Though this approach scales favorably the break-even point is large and not suitable for most practical applications [35]. This can be overcome to some extent using the 1D FMM for fast Legendre transforms [81]. Cost of Interpolation/anterpolation using this approach scales as $\mathcal{O}(Q \log Q)$, where Q denotes the number of directions in farfield signature. This said it can be shown that overall cost of the multilevel algorithm scales as $\mathcal{O}(N \log^2 N)$ [35]. Other methods used for interpolation and anterpolation have been presented in detail in [78, 33, 69]. These include the use of polynomials and approximate prolate spheroidal wave functions. The singular advantage of these methods is their cost scales linearly with the number of samples, thus the overall cost scales as $\mathcal{O}(N \log N)$. However, while interpolation is sufficiently accurate, one has to be more careful when anterpolating functions as it is necessary to remove higher order harmonics. While we have not digressed into implementation of these schemes for vector electromagnetic problems, we must caution that it is not a trivial extension. It is important to realize that the farfield component represented in terms of polar components in not bandlimited [82], whereas they are bandlimited when represented in terms of Cartesian components. This means that one either uses a fast scheme based on vector spherical harmonics [82] or converts these to Cartesian before interpolation/anterpolation. Another intriguing method for interpolation and anterpolation was introduced by Sarvas [48], wherein he introduced modifications that enabled the use of FFTs. In other words, bandlimited

farfield signatures can be represented in terms of Fourier basis as

$$M(\mathbf{k}) \approx \sum_{p=-P}^{P} \sum_{q=-Q}^{Q-1} a(p,q) e^{i(p\theta+q\phi)} \tag{1.37}$$

where,

$$\begin{aligned} a(p,q) &= DFT\{M(\mathbf{k})\} = \sum_{m=-P}^{P} \sum_{n=-Q}^{Q-1} e^{-j(m\theta+n\phi)} M(\mathbf{k}_{pq}) \\ \theta &= \frac{p2\pi}{2P+1} \\ \phi &= \frac{\pi q}{Q} \end{aligned} \tag{1.38}$$

where $DFT(\cdot)$ represents forward discrete Fourier transform, $2M$ and $2N$ are number of samples or basis function in θ and ϕ axis respectively. Then the integral over the surface of sphere can be written as,

$$\int_{-\pi}^{\pi} d\phi \int_{0}^{\pi} d\theta \sin\theta U(\theta,\phi) = \int_{-\pi}^{\pi} d\phi \int_{-\pi}^{\pi} d\theta |\sin\theta| U(\theta,\phi) \tag{1.39}$$

Note that the above modification changes the limit on θ integral to $[-\pi,\pi]$, thus it can also be evaluated in fast manner using FFT. In single level implementation, the integrand in (1.19) are first represented in terms of Fourier basis using (1.37) and then (1.39) is used for fast evaluation of integrals. In multilevel implementation the interpolation and anterpolation, for varying bandwidth of multipole and local expansion, can be achieved by zero padding and truncating the Fourier coefficients respectively. In anterpolation the Fourier coefficients of parent local expansions are symmetrically truncated before inverse Fourier transform, to obtain the local expansion about child domain with the desired bandwidth. Thus all operations, including the evaluation of integral, can be evaluated using FFT. Reader is referred to [48]

for related theorems, proofs and numerical results. Finally, the numerical implementation of multilevel FMM has been scrutinized in terms of different errors and to ensure stability. This includes discussion on the relation between truncation and integration error in (1.29) [71], and interpolation/anterpolation error using Lagrange interpolation [73] and spherical transform [69]. In addition, errors due to round-off and evaluation of special-function have been considered along with stability criterion [74]. Numerical experiments show that truncation error in (1.29) is lower bounded [43, 73]; thus for applications that routinely demand very high accuracies it is preferable to increase the distance between well-separated boxes. Evidently this amounts to an increase in number of boxes in near-field interaction.

1.4.1 Other FMMs

The above exposition presented FMMs that are apt for analyzing very general problems. However, for certain problems it is possible to develop FMM schemes that take advantage of topological features of scatterer to reduce the asymptotic complexity. The first of such algorithm was the fast steepest descent path algorithm [83] that exploited spectral representation of the Green's function. The next incarnation of this was the steepest descent FMM. It was developed following realization that when analyzing scattering from objects whose height is considerably lesser that its lateral dimension, it is not particularly useful to expand the fields using the complete spectrum. In other words, SDFMM can be interpreted to be a windowed FMM, and results in a method whose complexity scales as $\mathcal{O}(N)$. In SDFMM, it is achieved naturally using the Sommerfeld integral representation of the Green's function and evaluating this integral using a combination of two-dimension FMM and steepest

descent. More specifically,

$$\begin{aligned}\frac{e^{-jkR}}{R} &= \frac{-j}{2}\int_{-\infty}^{\infty} dk_z e^{-jk_z(z-z')} H^{(2)}\left(\kappa_\rho|\boldsymbol{\rho}-\boldsymbol{\rho}'|\right) \\ &= \frac{-j}{2}\sum_{n=1}^{N_{sd}} w_n \kappa_\rho^{(n)} H_0^{(2)}\left(\kappa_\rho|\boldsymbol{\rho}-\boldsymbol{\rho}'|\right) e^{-jk_z(z-z')}\end{aligned} \tag{1.40}$$

where N_{sd} is quadrature rule along the integration path, w_n is the integration weight, $\kappa_\rho^{(n)} = \kappa \sin\alpha_n$ and $k_z = \kappa\cos\alpha_n$, and α is defined along steepest descent path. It is immediately apparent that the summation over Hankel functions can be accelerated using a generalization of the two-dimensional FMM, and as before, this algorithm can be cast within a multilevel framework. Another algorithm along these lines was the fast inhomogeneous plane wave algorithm (FIPWA) [62, 47]. This algorithm follows directly from Weyl's identity

$$\frac{e^{-j\kappa R}}{R} = \frac{-j}{2}\int_0^{2\pi} d\phi \int_{SIP} d\theta \sin\theta e^{-j\mathbf{k}\cdot\mathbf{R}} \tag{1.41}$$

The path of integration yields contributions from both homogeneous and inhomogeneous plane waves. As written, the above integral is slowly converging, but the contour can be deformed along the steepest descent path. This integral is evaluated numerically. However, values of the radiation pattern for complex θ is obtained using interpolation/extrapolation. Manipulation of the requisite equations results in a diagonal translation operator. This method has been extended for analysis of scattering from objects above a layered medium [45, 47]. Additionally, they have been modified for developing stable algorithms for broadband applications [84]. However, we shall describe these algorithms and others [42] for rapidly computing potentials for wideband applications in the next section.

Finally, other variants of FMM exist that exploit the fact that between well separated boxes, one may construct windowed translation operators to lower the cost.

One such method is the ray propagation FMM (RPFMM) [85, 66]. Other windowed translation operators have been used in two-dimensions for the analysis of scattering from bianisotropic objects [86]. However, it follows from complexity analysis that these methods will be fruitful only when the objects are sufficiently far away from each other. This implies that the algorithm is most useful when used in a one-level setting and may not be effective with a multilevel implementation.

1.4.2 Wideband FMM

In above discussion, a significant highlight is the restrictive choice of L used to truncate the expansions. This choice, based on the asymptotic behavior of Bessel and Hankel function, reveals the behavior of above expansions when applied to low frequency problems where κ is very small. It is well known that Hankel function is singular at origin and as $\kappa \to 0$ the expansion in (1.23), though valid, becomes numerically unstable. This breakdown is referred to as *low-frequency breakdown* [43, 42]. Consequently for fixed κ the size of source domain, which also defines the translation distance, cannot be made arbitrarily small. This issue becomes significant when the geometry is densely discretized, much more than the conventional $\lambda/10$ criterion, mostly to represent intricate structural details.

Scaled expansions

At low frequencies the numerical instability can be averted by using a normalized form of the original expansion (1.23) [44, 46]. This approach is motivated by the asymptotic behaviour of spherical Bessel and Hankel function for small argument. Let t be a normalization constant such that $t = \mathcal{O}(kd)$ then the multipole expansions

in (1.23) can be written as,

$$th_0^{(2)}(-j\kappa|\mathbf{X}+\mathbf{d}|) = -j\kappa \sum_{l=0}^{L} \sum_{m=-l}^{l} (-1)^l (2l+1) \left[\frac{1}{t^l} j_l(\kappa d) \bar{Y_{lm}}(\theta_d, \phi_d)\right] t^{l+1} \\ h_l^{(2)}(\kappa X) Y_{lm}(\theta_X, \phi_X) \tag{1.42}$$

In above expression, terms inside the square brackets are the new normalized multipole coefficients. As $\kappa \to 0$, using small argument approximation for spherical functions and with $t = \kappa$, it is a straightforward exercise to show that the normalized expansions reduces to the expansions (1.2) used in static case. While the normalized forms ensures numerical stability, the low-frequency nature of the problem implies that one can choose the number of multipoles to be same at every level. This in turn implies that the multilevel version of this approach scales as $\mathcal{O}(N)$ [46]. A constant normalization factor is sufficient when the geometry is uniformly discretized. However to accommodate wide variation in domain sizes and maintain the stability of expansion different normalization factor should be chosen in different parts [33]. This approach has been successfully used in integral equation solution for scattering from sub-wavelength structures [46, 87].

Spectral representation based plane wave expansions

An alternate approach, inspired by the diagonalized form for static FMM, was introduced in [42] and later implemented in [84, 49, 50]. It is based on the following well-known spectral representation of solution to Helmholtz equation [88],

$$\frac{e^{-j\kappa R}}{R} = \frac{1}{2\pi} \int_0^\infty e^{-\sqrt{\lambda^2-\kappa^2}z} \int_0^{2\pi} e^{-j\lambda(x\cos\alpha + y\sin\alpha)} \frac{\lambda}{\sqrt{\lambda^2-\kappa^2}} d\alpha d\lambda \tag{1.43}$$

this relation is valid for $z > 0$. Further it is straight-forward to identify the purely propagating part of spectrum as $0 \leq \lambda \leq \kappa$ and the evanescent part as $\kappa < \lambda \leq \infty$;

with simple change of variables, above expression can be written as [42],

$$\frac{e^{-j\kappa R}}{R} = \left(\frac{e^{-j\kappa R}}{R}\right)_{evanescent} + \left(\frac{e^{-j\kappa R}}{R}\right)_{propagating} \tag{1.44}$$

where,

$$\begin{aligned}
\left(\frac{e^{-j\kappa R}}{R}\right)_{evanescent} &= \frac{1}{2\pi}\int_{\kappa}^{\infty} e^{-\sqrt{\lambda^2-\kappa^2}z}\int_0^{2\pi} e^{-j\lambda(x\cos\alpha+y\sin\alpha)} \\
&\quad \frac{\lambda}{\sqrt{\lambda^2-\kappa^2}} d\alpha d\lambda \\
&= \frac{1}{2\pi}\int_0^{\infty} e^{-\sigma z}\int_0^{2\pi} e^{-j\sqrt{\sigma^2+\kappa^2}(x\cos\alpha+y\sin\alpha)} d\alpha d\sigma \\
\left(\frac{e^{-j\kappa R}}{R}\right)_{propagating} &= \frac{1}{2\pi}\int_0^{\kappa} e^{-\sqrt{\lambda^2-\kappa^2}z)}\int_0^{2\pi} e^{-j\lambda(x\cos\alpha+y\sin\alpha)} \\
&\quad \frac{\lambda}{\sqrt{\lambda^2-\kappa^2}} d\alpha d\lambda \\
&= \frac{j\kappa}{2\pi}\int_0^{\pi/2} e^{-j\kappa\cos\theta}\int_0^{2\pi} e^{-j\kappa\sin\theta(x\cos\alpha+y\sin\alpha)} d\alpha d\theta
\end{aligned}$$

Notice that with $\kappa \longrightarrow 0$ the propagating part vanishes and the evanescent part reduces to the diagonalized form (1.14) used in static FMM. Now it remains to discretize the above integrals for numerical evaluation and generalized Gaussian quadratures can be employed for this. However, unlike in static case, the integrand cannot be rendered scale independent and this means quadrature points and weights should be pre-computed for all possible translation distances at all levels. It is worthwhile to recount that the multipole and local expansions are computed and stored as they appear in original spherical harmonics expansion (1.23); they are converted to exponential expansions back and forth during multipole to local translation only and these relations can be found in [50]. This approach avoids the floating point overflow as all the computed quantities and operations are regular and numerically stable. Other approaches based on above spectral representation have been presented

[84, 49, 89, 90] and they differ significantly in their numerical implementation and structure. In all these methods the multipole and local expansion are represented directly in terms of exponential expansion coefficients; hence they require new interpolation/anterpolation operators for multilevel implementation. In [84], an extension of FIPWA as introduced for multi-layered structures, the integrand is sampled along the steepest descent path (SDP) and extrapolation techniques to estimate the evanescent portion of the spectrum from samples of the propagating portion. However, one has to treat "shallow" evanescent waves differently from "deep" evanescent waves. In [49], the evanescent integrand is sampled along the traditional Sommerfeld integral path (SIP) and singular value decomposition (SVD) of the integrand is used to obtain expressions for multipole coefficient and multilevel translation operators. An interpolation matrix approach is presented in [90] to relate exponential expansions at different levels. Using sample points in child and parent domain an overdetermined system of equation is formed and solved for the interpolation matrix entries in a least square sense. The advantage of latter approaches is that they avoid the spherical harmonic to exponential expansion and reverse mapping operations.

1.5 Applications

This section provides an overview on application of above discussed algorithms in different contexts. As mentioned in introduction, FMM and other fast methods, e.g. FFT and tree code based, were developed primarily to accelerate the evaluation of potential or field in N body problems. Integral equation solutions, a common choice in simulation of many electromagnetic applications, sought through iterative solvers requires repeated evaluation of potential or field at source points itself. Thus fast algorithms play a significant role in solving real world problems within realistic time duration. The literature referenced here is only selective and not exhaustive as the

use of these algorithms have become more common during recent years. Also, only topics related to electromagnetics are listed here; for applications in other research field refer to introduction.

First, electromagnetic application of static or Laplace FMM was evaluation of electrostatic potential in 2D [6, 91]. The extension to 3D has seen lot of applications, particularly, in plasma dynamics [8, 92]. FMM based FastCap and FastHenry are widely popular tools for extraction of equivalent capacitance and impedance among multi-connects in micro-electronic components [19, 20]. Static FMM is also used in integral equation solution of magnetostatic problems predominantly for analysis and design of electric machines [93]. Simulations with non-linear materials have benefited much as they demand multiple solution before attaining stability [94, 95, 56]. It has also been applied to quasi-static case especially in simulation of eddy-current phenomena [96, 97] and micro-magnetics is another area of practical interest [98, 99].

The recently published book on fast methods in electromagnetics is a virtual treasure house of FMM methods and their applications to various problems in high frequency electromagnetics [33]. As is to be expected, Helmholtz FMM has been applied to accelerate iterative solution of surface and volume integral equations. The means to modify Helmholtz equation such that they are applicable to vector electromagnetics problems was first presented in [78]. More detailed description can be found [100, 75, 33]. Since their introduction, they have been applied extensively to scattering and radiation problems of different flavors; for instance, scattering from perfect electrically conducting surfaces [28, 65, 78, 100, 69, 101, 102, 103, 104, 105], scattering from dielectric/composite bodies [106, 107, 108, 109, 110, 111], volume integral equations [112, 70, 113, 114], anisotropic objects [115, 116], scattering from rough surfaces [117, 118, 119], application to microstrips [120], EMC/EMI analysis [121, 122, 123], antennas [124, 125, 126]. Efficient implementation of FMM in solvers with higher order geometry and basis function representations have led to the

development of fast and accurate solvers [107, 127, 128]. [129, 130]

Multipole accelerated algorithms have also been employed in various hybrid methods where solution is obtained with use of moment method combined with one or more of following techniques: to impose global radiation boundary conditions in finite element solvers [131, 132, 133], ray tracing and diffraction methods [134], multi-grid methods [135] and physical optics [136, 137]. These techniques are primarily used in applications with multi-scale scatterers like antenna interactions [138] and field predictions for urban mobile communications [139]. Implementation of FMM was also modified to accommodate perfectly matched layer (PML) assisted integral equation methods used in simulation of monolithic microwave integrated circuit (MMIC) and photonic crystals [140, 141, 142]. Fast inhomogeneous plane wave (FIPWA) method and other forms of FMM have been used to accelerate solution of scattering simulations involving layered media structures with applications in design of microstrip antennas [129, 130, 143, 144, 145, 146, 147, 148] and geophysical investigations for sub-surface scatterers [64, 149, 150, 151, 152, 153, 154, 155, 156, 157]. A combined FMM-FFT algorithm [158, 159] and SDFMM have been used in electromagnetic analysis of general quasi-planar structures with applications to rough surface scattering, grating structure design in quantum devices and radiation from microstrip patch antenna [118, 160, 161, 162]. The principle of FMM has also been extended to accelerate potential employed in time domain integral equations. Plane wave time domain (PWTD) is the time domain analogue of Helmholtz-FMM that has been used to accelerate time domain IE (TDIE) [163, 82, 164].

1.6 Thesis Objectives and Outline

As mentioned in the preceding exposition, the primary downside of conventional FMM is that they are specific to the form of Green's function. In other words, one is

required to develop new set of FMM formulaes for each form of the Green's function. The Helmholtz FMM, as detailed in Section 1.4.2, suffers from numerical instability for low excitation frequency. Analogously, plane wave time domain (PWTD), the time domain counterpart of Helmholtz FMM, also suffers from a similar breakdown when large number of unknowns are concentrated in small size domains. Consequently, the existing state of the art fast methods face severe limitations when applied to multiscale problems. These are realistic problems where certain regions are very densely discretized to accurately capture the physical details. The main goal of this thesis is develop mathematical techniques to overcome the limitations of the existing fast methods for electromagnetic simulation of multiscale problems. This is achieved with the aid of accelerated Cartesian expansion (ACE) algorithm. ACE is a recently developed, hierarchical tree computation algorithm in the vein of FMM. Unlike FMM, ACE algorithm relies on Cartesian harmonics and Taylor series expansion to derive FMM like algorithm for arbitrary, non-oscillatory potentials. In this thesis, different aspects of ACE algorithm are exploited to develop fast algorithms to overcome the *low-frequency* breakdown in both time and frequency domain.

Parallelization of FMM can be classified as a fairly recent work, with most of the literature concentrated in the last decade. The hierarchical framework of FMM qualifies it as one of the difficult algorithms to parallelize. Most of the existing algorithms are based on heuristics. Such algorithms, though successful, provide only modest scalability with maximum at 64 processors. This is a severe limitation of the FMM algorithm when considering the ever growing size of cluster computers. In this work, a parallel version of FMM algorithm is introduced that is scalable up to hundreds of processors and beyond. The proposed algorithm is provably scalable and hence allows for large scale parallelization. This work leads to the development of the state of art parallel multiscale electromagnetic solver for very large scale simulations.

The rest of the thesis is organized as follows:

Chapter 2, provides a detailed review of ACE algorithm. Here the definitions and theorems of ACE algorithm are presented in a kernel independent fashion for easy reference in later chapters. Also presented here is a detailed overview of the multi-level tree computation scheme along with the proposed modifications.

Chapter 3, addresses the sub-wavelength breakdown of PWTD method, the time domain counterpart of Helmholtz FMM. The smallest domain size used in PWTD is restricted for reasons of numerical stability. Thus, when large number of unknowns are concentrated within a sub-wavelength structure, the computational advantage offered by the PWTD algorithm is overshadowed by the direct computation cost. Here, the *almost* kernel independent framework of ACE algorithm is exploited to develop an algorithm that is stable and efficient for evaluation of retarded potentials within sub-wavelegnth structures.

Chapter 4, addresses the low-frequency breakdown of Helmholtz FMM. Here the FMM algorithm is presented in sufficient detail to identify the root cause of the breakdown. ACE expansions of the Helmholtz kernel is developed and the stability and convergence of these expansions at low-frequency limits is shown in a rigorous manner. This leads to the development of a wideband FMM algorithm, obtained by seamlessly combining the ACE and FMM algorithms. This hybrid algorithm, that is stable and efficient across length and frequency scales, is then augmented with an existing electromagnetic solver for simulation of multiscale geometries.

Chapter 5, take a slight detour from fast methods and explores the possibility of developing a new integral equation formulation that yields well conditioned systems of equations for multiscale simulation. Here the augmented electric field integral equations (AEFIE), an existing IE formulation, is considered for modification. Included here is a succinct review of the operator theory analysis of EM integral equations. These tools are used to establish the behaviour of the new formulation when applied to low-frequency and multiscale problems. The new formulation is first developed for

2D problems and then extended, with appropriate modifications, to 3D problems.

Chapter 6, presents the development of parallel implementation of above hierarchical tree computation algorithms on distributed computers using message passing interface (MPI). Here the emphasis is laid on developing a parallel framework that is provably scalable on large number, in orders of thousands, of processors. The novel schemes developed here results in a implicitly load balanced parallel algorithm. The resulting framework can be viewed as a seamless combination of different schemes already in existence. Detailed description on development of a parallel electromagnetics solver is also provided and its high efficiency is demonstrated on hundreds of processors and beyond.

Chapter 7, summarizes the various contributions of this thesis work in a succinct manner. Several possible future works are also mentioned here.

Appendix A details the development of a ACE based algorithm for rapid computation of time domain diffusion potentials and Appendix B provides a quick review of the comprehensive exam problem "Integral equation methods to model eddy current inspection of plates ".

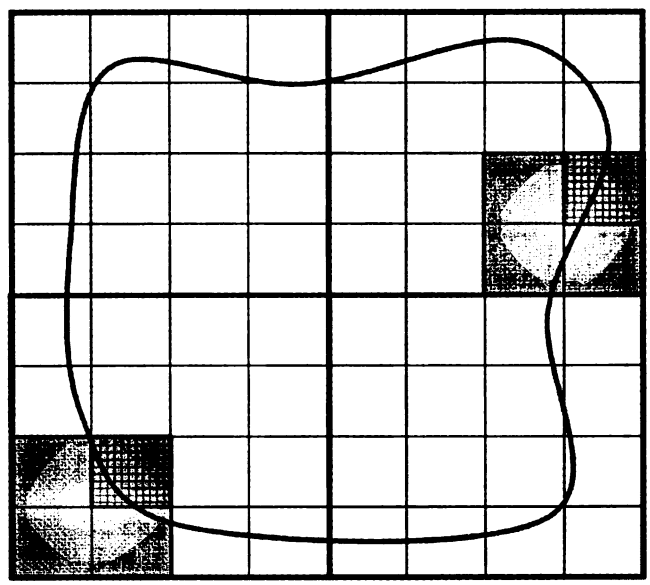

Figure 1.1: Hierarchical decomposition of a 2D computational geometry

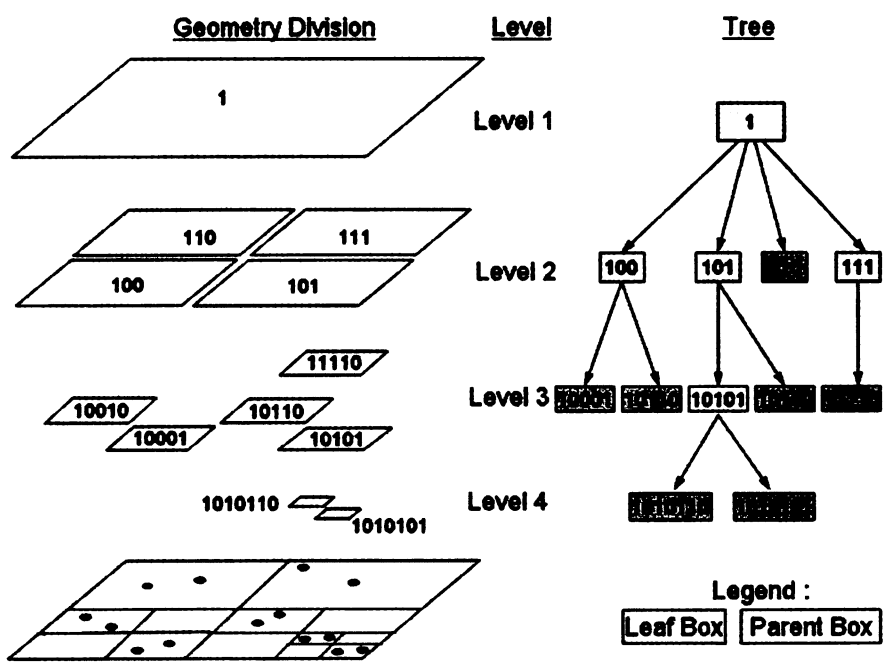

Figure 1.2: Representation of 2D computational geometry using quad-trees. Boxes at different levels and corresponding nodes in tree are represented using binary keys.

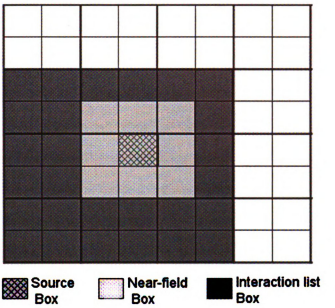

Figure 1.3: Illustration of interaction list; dark boxes are contained in the interaction list of source box.

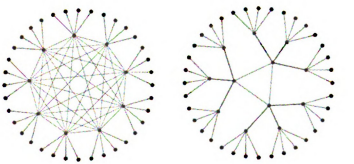

Figure 1.4: Illustration of computational load in single- and multi-level FMMs. Dark nodes correspond to actual sources while light shaded nodes represent centers of multipole and local expansions.

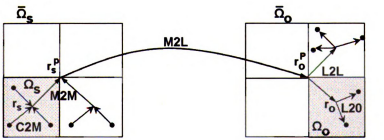

Figure 1.5: Various operators involved in a multilevel FMM

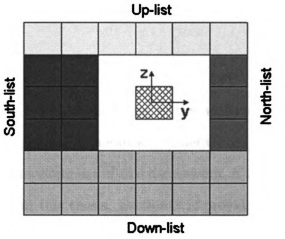

Figure 1.6: Re-grouped boxes in original interaction list, in figure 1.3, for application of diagonal translation operator (1.15)

Chapter 2

Accelerated Cartesian Expansions (ACE)

This Chapter, provides a detailed treatment of the accelerated Cartesian expansion (ACE) algorithm and a general framework for hierarchical computations. Though ACE is not the primary development of this thesis work, it is lays the foundations for the advancements made in this thesis. Section 2.1, provides a brief overview of the ACE algorithm. Section 2.2, presents the requisite introduction to definitions and notations of Cartesian tensors used in rest of this thesis. In Section 2.3, the definitions and theorems of ACE algorithm are stated. Section 2.4, provides the details of the different procedures involved in a hierarchical tree computation algorithm. Section 2.5 describes some of the algorithmic developements introduced to reduce the computational cost by half.

2.1 Introduction

Accelerated Cartesian Expansion (ACE) is a fast computational technique, in the vein of FMM, in the sense that it employs tree structure for hierarchical computation

and derives rigorous error and cost estimates. A common feature of these hierarchical computational scheme is the use of divide and conquer strategy to offer the computational advantage with a prescribed loss in accuracy. This loss of precision is justified by the fact that the numerical simulation are constrained to finite precision by other factors; and evaluation of potentials beyond this limit does not offer any advantage. Further, these schemes accelerate the computation of far-field potentials only. The dominant contribution to the total potentials arise from the near-field interactions that are evaluated *exactly* using direct computation.

ACE is the mathematical engine behind the fast method discussed in this thesis. It employs Taylor's series expansion to derive addition theorem for arbitrary, non-oscillatory functions. It is worth noting that the use of Taylor expansion for fast computation have been developed earlier also [10, 11, 12]. Typically, these FMMs derived using the Cartesian expansions were more expensive as spherical harmonics are optimal in representing Coulombic potentials. However, it was recently shown that it is possible to develop a FMM using Maxwell-Cartesian harmonics that are *as optimal* as using spherical harmonics with one singular advantage; it avoids the need for special functions [13]. Here, the entire algorithm is cast within the framework of Cartesian tensors and exploits the fact that these tensors are totally symmetric to provide an optimal representation of Cartesian harmonics. Another salient feature of ACE algorithm is that it derives exact formulaes for traversing up and down the tree, which in turn implies lesser source of error. The use of Taylor's expansion implies that the potential or its modified form be *non-oscillatory* for rapid convergence of these expansions. This technique, as presented here, was introduced for kernels of the form R^{ν}. ACE has been extended to several other forms of potentials, some of them as part of this thesis work, for e.g. Helmholtz potential [165], Yukawa (or shielded Coulomb) potentials, retarded potential, diffusion potentials, solutions to Klein-Gordon and lossy wave equations.

2.2 Cartesian Tensors

Tensor analysis is an integral tool used in development of ACE algorithm. A Cartesian tensor of rank n is denoted by $\mathbf{A}^{(n)}$ or in component notation by $A^{(n)}_{\alpha_1 \cdots \alpha_n}$, and is an array of 3^n components, for points in $\mathbb{R}^3$. A totally symmetric tensor is one that is independent of the permutation of indices $\alpha_1 \cdots \alpha_n$ and in compressed form it contains $(n+1)(n+2)/2$ independent components. Alternatively, they can be represented in compressed form as $A^{(n)}(n_1, n_2, n_3)$ where $n_1 + n_2 + n_3 = n$, and n_i is the number of times the index i is repeated. An n-fold contraction between two tensors $\mathbf{A}^{(n+m)}$ and $\mathbf{B}^{(n)}$ is represented using $\mathbf{C}^{(m)} = \mathbf{A}^{(n+m)} \,.\, n \,.\, \mathbf{B}^{(n)}$. The contraction of two totally symmetric Cartesian tensors can be written using the compressed notation as

$$C^{(m)}(m_1, m_2, m_3) = \sum_{n_1, n_2, n_3} \frac{n!}{n_1! n_2! n_3!} A^{(n+m)}(n_1 + m_1, n_2 + m_2, n_3 + m_3) \\ B^{(n)}(n_1, n_2, n_3) \tag{2.1}$$

An extensive exposition of theorems and formulae pertinent to the properties of compressed tensors, their application to the ACE algorithm, can be found in [166].

2.3 ACE: Definitions and Theorems

In this section the theorems and definitions that permit the fast evaluation of functions are outlined briefly. To this end, assume that domains Ω_s and Ω_o are sufficiently separated, and comprise of sources and observers, respectively. Also, $\Omega_s \subset \Omega_s^p$, $\Omega_o \subset \Omega_o^p$ and $\Omega_s^p \cap \Omega_o^p = \emptyset$. The centers of the domains Ω_s, Ω_o, Ω_s^p and Ω_o^p are denoted by $\mathbf{r}_s$, $\mathbf{r}_o$, $\mathbf{r}_s^p$ and $\mathbf{r}_o^p$, respectively. Further, denote the potential function that maps the effects of these sources on the observation points as $\psi(R)$, where $R = ||\mathbf{r} - \mathbf{r}'||$ and k sources exist in Ω_s. Here, the function $\psi(R)$ can stand for any interpolation function $T(t)$ convolved with the retarded potential and observed at time $t = 0$. An addition

theorem for this function may be obtained using Taylor's expansion.

Theorem 2.3.1 (Taylor Expansion). *The function* $\psi\left(\mathbf{r}-\mathbf{r}'\right)$ *can be expressed about the origin using*

$$\psi(\mathbf{r}-\mathbf{r}')=\sum_{n=0}^{\infty}\frac{(-1)^n}{n!}\mathbf{r}'^n\,.\,n\,.\,\nabla^n\psi(\mathbf{r}) \tag{2.2}$$

where $\mathbf{r}>\mathbf{r}'$

This theorem gives rise to the following corollary.

Corollary 2.3.2. *The function* $\psi(\mathbf{r}-\mathbf{r}')$ *takes the form*

$$\psi\left(\mathbf{r}-\mathbf{r}'\right)=\begin{cases}\sum_{n=0}^{\infty}\mathbf{M}^{(n)}\,.\,n\,.\,\nabla^n\psi(\mathbf{r}) & \text{for } \mathbf{r}>\mathbf{r}'\\ \sum_{n=0}^{\infty}\mathbf{r}'^n\,.\,n\,.\,\mathbf{L}^{(n)} & \text{for } \mathbf{r}'>\mathbf{r}\end{cases} \tag{2.3}$$

where $\mathbf{M}^{(n)}$ and $\mathbf{L}^{(n)}$ are the multipole and local expansions. These theorems may be used in concert to derive/prove the following five theorems that form the crux of ACE [166].

Theorem 2.3.3 (Multipole Expansion). *The total potential at any point* $\mathbf{r}\in\Omega_o$ *due to* k *sources* q_i, $i=1,\cdots,k$ *located at points* $\mathbf{r}_i\in\Omega_s$ *is given as*

$$\begin{aligned}\psi(\mathbf{r})&=\sum_{n=0}^{\infty}\mathbf{M}^{(n)}\cdot n\cdot\nabla^n\psi(\mathbf{r})\\ \mathbf{M}^{(n)}&=\sum_{i=1}^{k}(-1)^n\frac{q_i}{n!}(\mathbf{r}_i-\mathbf{r}_s)^n\end{aligned} \tag{2.4}$$

where $\mathbf{M}^{(n)}$ is the multipole tensor.

Theorem 2.3.4 (Multipole to Multipole Expansion). *Given a multipole expan-*

sion of k sources about $\mathbf{r}_s$

$$\mathbf{O}^{(n)} = \sum_{i=1}^{k} (-1)^n \frac{q_i}{n!} (\mathbf{r}_i - \mathbf{r}_s)^n \tag{2.5a}$$

then the multipole expansion about the point $\mathbf{r}_s^p$ *can be expressed in terms of (2.5a) as*

$$\mathbf{M}^{(n)} = \sum_{i=1}^{k} (-1)^n \frac{q_i}{n!} (\mathbf{r}_i - \mathbf{r}_s^p)^n = \sum_{m=0}^{n} \sum_{P(m,n)} \frac{m!}{n!} \left(\mathbf{r}_s^p - \mathbf{r}_s\right)^{n-m} \mathbf{O}^{(m)} \tag{2.5b}$$

It is evident that one can repeatedly use this theorem to translate the multipole expansion from $\mathbf{r_s}$ to $\mathbf{r_s^p}$. This expression is exact [166].

Theorem 2.3.5 (Multipole to Local Translation). *Assume that the domains* Ω_s^p *and* Ω_o^p *are sufficiently separated, and the distance between their centers* $r_{os}^p = |\mathbf{r}_{os}^p| = |\mathbf{r}_o^p - \mathbf{r}_s^p|$ *is greater that diam* $\{\Omega_s^p\}$ *and diam* $\{\Omega_o^p\}$*. If a multipole expansion* $\mathbf{M}^{(n)}$ *is located at* $\mathbf{r}_s^p$*, then another expansion* $\mathbf{L}^{(n)}$ *that produces the same field* $\forall \mathbf{r} \in \Omega_o^p$ *is given by*

$$\begin{aligned} \psi(\mathbf{r}) &= \sum_{n=0}^{\infty} \boldsymbol{\rho}^n \cdot n \cdot \mathbf{L}^{(n)} \\ \mathbf{L}^{(n)} &= \sum_{m=n}^{\infty} \frac{1}{n!} \mathbf{M}^{(m-n)} \cdot (m-n) \cdot \widetilde{\nabla}^m \psi(r_{os}^p) \end{aligned} \tag{2.6}$$

where $\boldsymbol{\rho} = \mathbf{r} - \mathbf{r}_o^p$ *and* $\widetilde{\nabla}$ *is the derivative with respect to* $\mathbf{r}_s^p$*.*

Theorem 2.3.6 (Local to Local Expansion). *A local expansion* $\mathbf{O}^{(n)}$ *that exists in the domain* Ω_o^p *centered around* $\mathbf{r}_o^p$ *can be shifted to the domain* Ω_o *centered at* $\mathbf{r}_o$ *using*

$$\mathbf{L}^{(n)} = \sum_{m=n}^{\infty} \begin{pmatrix} m \\ m-n \end{pmatrix} \mathbf{O}^{(m)} \cdot (m-n) \cdot \left(\mathbf{r}_o^{cp}\right)^{m-n} \tag{2.7}$$

It can be shown that this expression is exact as well. Finally, the fields at a set of

observation points can be computed using the following theorem.

$$\psi(\mathbf{r}) = \sum_{n=0}^{\infty} \mathbf{L}^{(n)} \cdot n \cdot (\boldsymbol{\rho}_{oi})^n \tag{2.8}$$

Proofs for these theorems for $\psi(R) = R^{\nu}$ can be found in [166] and may be trivially extended to functions of the form $\psi(R) = span\{R^{-\nu}\}$ for $\nu = -1, 0, 1, \cdots, K$, or any other non-oscillatory function. Note, that when $\psi(R) = R^{-\nu}$, evaluating the multipole to local expansion using Theorem 2.3.5 implies the computation of $\nabla^n R^{-\nu}$ which can be efficiently effected through

$$\begin{aligned} \partial_i^{n_1}\partial_j^{n_2}\partial_k^{n_3}\left(\frac{1}{R^{\nu}}\right) = (-1)^n R^{-2n-\nu} \sum_{m_1=0}^{\lfloor \frac{n_1}{2} \rfloor} \sum_{m_2=0}^{\lfloor \frac{n_2}{2} \rfloor} \sum_{m_3=0}^{\lfloor \frac{n_3}{2} \rfloor} (-1)^m \begin{bmatrix} n_1 \\ m_1 \end{bmatrix} \begin{bmatrix} n_2 \\ m_2 \end{bmatrix} \\ \begin{bmatrix} n_3 \\ m_3 \end{bmatrix} \times R^{2m} f(\nu, n-m-1)\, x^{n_1-2m_1} y^{n_2-2m_2} z^{n_3-2m_3} \end{aligned} \tag{2.9}$$

where $R^2 = x^2 + y^2 + z^2$. As was pointed out in [166], a computation scheme based on these theorems have the following characteristics:

1. The multipoles are independent of the function being translated. Only the translation operator depends on ν. This fact will be of use in developing fast methods for evaluating the retarded potential.

2. The multipole to multipole expansion (or the local to local expansion) is exact. This implies that the errors obtained do not depend on the height of the tree.

3. The formulation in terms of totally symmetric tensors permits the realization of CPU cost savings of a factor of 1/720 over a simplistic implementation.

4. Finally, since only the translation function depends on the potential function being used, it follows that the proposed methodology can be readily altered,

with very little change in the overall algorithm, for other potential functions.

2.4 Multi-level Tree Computational Framework

These theorems permit rapid evaluation of potential using either a standard or compressed oct-tree decomposition of the domain. A standard oct-tree is constructed by first embedding the entire domain in a fictitious cube that is then divided into eight sub-cubes, and so on. This process continues recursively until the desired level of refinement is reached; an N_l-level scheme implies $N_l - 1$ recursive divisions of the domain. At any level, the domain that is being partitioned is called the *parent* of all the eight *children* that it is being partitioned into. At the lowest level, all source/observers are mapped onto the smallest boxes, *leaf boxes*. This hierarchical partitioning of the domain is referred to as a regular oct-tree data structure. At any level in the tree, all boxes/domains are classified as being either in the near or far field of each other using the following dictum: two subdomains are classified as being in the far field of each other if the distance between the centers is at least twice the sidelength of the domain, *and* their parents are in the near field of each other. This definition will be used *unless* it is specially stated that an alternate definition is necessary.

The interactions between all source and observation points are now computed using traversal up and down the tree structure in the following manner. First the multipole expansions are computed at the lowest level for leaf boxes. Parent box multipoles, at all levels, are computed from its children multipoles using multipole-to-multipole translation operator, theorem 2.3.4. This process is called upward tree traversal. Second, local expansions are computed at every box from multipole expansion of the boxes in its far-field using multipole-to-local translation operator, theorem 2.3.6. Next, the local expansions of all child boxes are *updated* with the local expansion of its parent using local-to-local translation operator, theorem 2.3.6. This

procedure is referred to as downward tree traversal. Finally the potential at observer points are computed from the local expansion of leaf boxes using theorem 2.8. This the far-field potentials that accounts for contribution from all sources except from the sources in near-field region of the corresponding leaf box. The total or complete potentials is obtained by accounting for contributions from near-field sources for leaf boxes only through direct evaluation.

Cost of this scheme can be computed in the following manner. The cost associated with each operation will be denoted by C_{op} where $op \in \{NF, C2M, M2M, M2L, L2L\}$ that stand for (i) near field (ii) charge to multipole (iii) multipole to multipole (iv) multipole to local (v) local to local and (vi) local to observer. In the following analysis the total number of interaction pairs is denoted by N, number of harmonics by P, total number of levels in the tree by N_l. Let $N_{b,l}$ denote the number of boxes at each level and assume that the number of unknowns in each leaf boxes, on average, is s. It follows that $N_{b,1} = N/s$, $N_{b,l-1} = 8N_{b,l}$ and $\sum_{i=1}^{N_l} N_{b,i} \propto N/s$. With these preliminaries the cost of each operation can be computed in the following manner.

1. Near field evaluation, C_{NF}: This computation is carried out only at the lowest level $l = 1$, at leaf boxes. The cost of direct evaluation between two leaf boxes scales as s^2 and for each leaf boxes can atmost have 27 boxes in its near-field. The total cost of this operation can be written as

$$\begin{aligned} C_{NF} &\propto N/s \times 27s^2 \\ &\propto 27Ns \end{aligned} \tag{2.10}$$

2. Multipole expansion, C_{C2M}: In this operation multipoles expansion in form of totally symmetric Cartesian tensors are computed from s charges per leaf box. The distinct elements in a totally symmetric Cartesian tensor of rank p is

$(p+1)(p+2)/2$. The cost of evaluating multipole tensors up to P^{th} rank is,

$$C_{C2M} = \frac{N}{s} \times s \times \sum_{p=0}^{P} (p+1)(p+2)/2 = \frac{NP^3}{6} \tag{2.11}$$

3. Multipole to multipole expansion translation, C_{M2M}: The multipoles of parent boxes, at any level, is computed from its eight children multipoles. The number of operations to translate all $P+1$ multipole from a child to its parent is $\prod_{i=1}^{6} (P+i)/i$. Since the total number of boxes in the tree scales as N/s the cost for this operation can be expressed as

$$C_{M2M} = \frac{N}{s} \times \prod_{i=1}^{6} \frac{(P+i)}{i} \tag{2.12}$$

4. Multipole to local translation, C_{M2L}: This operation is performed on all boxes of the tree. For any box the maximum number of far-field boxes is 189. The cost of translation between two tensors is same as in previous case.

$$C_{M2L} = 189 \frac{N}{s} \prod_{i=1}^{6} \frac{(P+i)}{i} \tag{2.13}$$

5. Local to local expansion translation, C_{L2L}: As mentioned before this operation is exactly the same as multipole-to-multipole translation operation i.e. $C_{L2L} = C_{M2M}$.

6. Local to observer, C_{L2O}: cost of this operation is exactly the same as that for mapping charges to multipole expansion i.e. $C_{L2O} = C_{C2M}$.

The total cost of the scheme is the sum of all individual cost,

$$\begin{aligned} C_{total} &= C_{NF} + C_{C2M} + C_{M2M} + C_{M2L} + C_{L2L} + C_{L2O} \\ &= 27Ns + 191\frac{N}{s}\frac{P^6}{720} + \frac{NP^3}{3} \end{aligned} \tag{2.14}$$

It is readily apparent that optimal number of unknowns per box is $s \propto P^3/10$.

2.5 Algorithmic Improvements

The above discussion pertains to the classical multi-level computational framework introduced in [167]. Since its introduction several modifications and additions have been suggested to reduce the computational time and extend its applicability to general geometric distributions. Following are some of the developed in this research work for optimal implementation of ACE algorithm.

2.5.1 Reduced Interaction List

From the cost estimate of ACE algorithm it is evident that C_{M2L}, cost of multipole-to-local translation operation, is the dominant part. Both the per-translation evaluation cost and number of interaction pairs (typically 189) are very high. This observation is common to all FMM like methods [168, 169]. In FMM based on expansions in terms of spherical harmonics both the factors can be reduced with the use of plane wave basis representation and exploiting the resulting symmetry. Alternatively, in this work a new definition is introduced to classify far-field pairs: *if box a (at level $l+1$) interacts with all the children of box b (at level l) and box a, box b are in far-field of each other then box a interacts with box b.* Interaction between boxes at two consecutive levels is easily effected using Cartesian tensors. In fully populated oct-tree this results in a reduction in the number of translation operations by half with minimal increase in

error. Numerical results that support this claim is presented in chapter 3.

2.5.2 Compressed Oct-tree

Classical multi-level FMM loses its $\mathcal{O}(N_s)$ scaling when applied to geometries with non-uniformly distributed sources/observers. The root cause of this breakdown is the use of uniform or regular oct-trees where all branches of tree is grown till the lowest level. This implies that the number of source/observer per leaf box varies drastically between regions of low and high source/observer concentrations. For leaf boxes with very low number of unknowns, evaluation of potential at its far-field boxes through $\{C2M, M2L, L2O\}$ operaion can be costlier than direct evaluation. To overcome this shortcoming an adaptive version of the multi-level computational scheme was presented in [169] with compressed oct-tree representation for non-uniform geometries. In compressed oct-tree representation only boxes, at any level, with source/observer pairs greater than a pre-determined number is sub-divided into child boxes. Further, in adaptive version always the optimal form of FMM is used based on the number of points in a leaf box. The implementation of ACE algorithm closely follows the work in [169], the main deviation is that the smallest box is used to enclose some pre-fixed number of points per box, s. While this approach is not significantly different in terms of cost when compared with [169], it does provide the possibility of improving error with certain geometries as the error in multipole evaluation is reduced. On downside this method may produce large number of single child parent which in turn increases the number of tree traversal operations, however this can be remedied by eliminating these redundant parent boxes. With the elimination of single child parent nodes, the resulting oct-tree would have the same structure as in [169] except the leaf box size would be smaller here as shown in Figure 2.1.

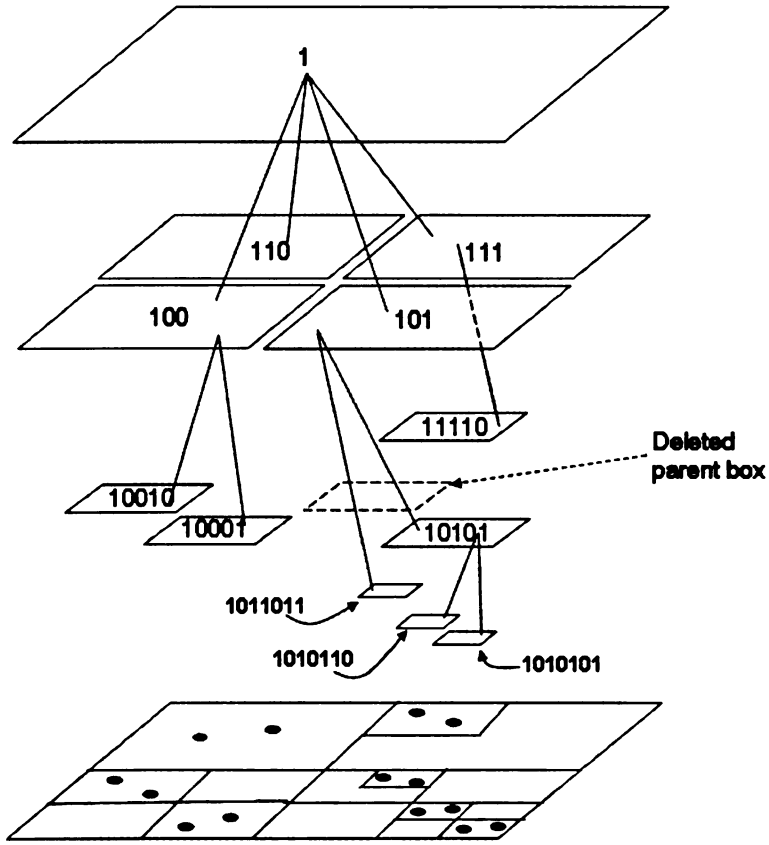

Figure 2.1: An example of compressed-quadtree with binary key representation used to label the tree nodes.

Chapter 3

Fast Evaluation of Time Domain Retarded Potential in Sub-Wavelength Structures

In this chapter, a computational scheme is presented for fast evaluation of time domain retarded potentials in sub-wavelength structure, whose principle dimension is less than or only a few orders of the maximum wavelength. Section 3.1 provides a brief review of the existing fast algorithms for evaluation of retarded potentials and their limiations when applied to sub-wavelength structures. Section 3.2 describes the problem of computing retarded potentials. Here these computation are reduced to evaluation of polynomial potentials of different orders. Section 3.3 details a fast algorithm when principal dimension of the domain is less than the maximum wavelength and Section 3.4 generalizes this to arbitrary size domains. Section 3.5 presents results and discussion of the proposed method when applied to arbitrary uniform and non-uniform geometry distributions.

3.1 Introduction

Time domain solutions to scattering problems is preferred over frequency domain methods when the analysis spans a wide range of frequencies. Examples of such analysis include characterization of wideband antennas and analysis radar signatures. Integral equation based methods for scattering from electrically large objects in time domain has been made possible via the development of acceleration techniques like plane wave time domain (PWTD) and time domain adaptive integral method (TDAIM). These methods ameliorate the computational cost when the size of overall object is several wavelengths long and the smallest feature scale is a fraction of the wavelength. However, analysis of structures that contain a mix of feature scales, poses problems for acceleration techniques in both frequency and time domain. Here, it is the geometric constraint that dictate the computational complexity. For instance, to model fine features, it is necessary to discretize that domain at a considerably higher rate than that is dictated by the smallest wavelength to capture the geometric details. These features occur in the analysis of practical problems in applied electromagnetics, ranging from EMI/EMC applications to antenna topologies to feed structures to signal integrity analysis in high speed interconnects, etc. The solution to this problem is typically sought by devising a methodology that works at sub-wavelength scales, and developing a transition to higher frequencies so that it can be integrated with existing acceleration methodologies.

The problem encountered herein is not very different from those addressed in the frequency domain fast multipole method (FMM). The PWTD algorithm is a time domain analogue of FMM, with one significant difference; the field due to a quasi-time limited and bandlimited source can be reconstructed to arbitrary accuracy using a discrete set of propagating plane waves provided certain separation conditions between the source and observers are met [170]. The separation criterion ensures that

time gating can be employed to yield causal results. Unlike in the frequency domain, the cause of breakdown is not the expansions used in the algorithm; all functions used in the expansion are regular at zero. The breakdown occurs because domains that interact with each other via the PWTD algorithm are determined indirectly by the time step size. As the time step depends only on the maximum frequency of excitation and *not* on the smallest discretization, it implies that PWTD breaks down as an acceleration tool because most of the interactions would fall under the "near" field classification. However, these arguments suggest an approach for overcoming this hurdle; develop an acceleration procedure using adaptive time stepping. The main advantage of this procedure is the seamless manner in which it can be integrated with the classical PWTD scheme for high frequencies, resulting in an acceleration scheme that is valid at all length scales [171, 172]. Alternatively, one can modify existing frequency domain low frequency algorithm to construct time domain information [173]. This implies that one needs to develop the mechanism to transition from frequency to time domain and vice versa such that the resulting system can still be cast within the framework that permits transient analysis within a marching on in time framework. It has been shown that the latter approach is considerably faster than the former [173].

This work presents an alternate method to arrive at the same objective and is founded on using Taylor expansions in a Cartesian framework, detailed in previous chapter. More specifically, the methodology presented herein will rely on the recently developed fast kernels for evaluating potential of the form R^ν for $\nu \in \mathbb{R}$, and is very competitive in terms of speed for a given accuracy with the other two methods that exist [171, 172, 173]. integrated with PWTD. Thus, the main contribution in this work are

- Development of an acceleration technique to compute retarded potentials in the sub-wavelength regime. The method presented relies on representing the

retarded potential as a function of potentials of the form R^{ν}, and then accelerating this function. The presented method can be extended to other functional representations as well.

- Development of the requisite algorithmic structure to seamlessly extend this (with very little cost overhead) to multiple time steps. Extension to multiple time steps is done with the sole aim of integrating with the PWTD algorithm.
- Application to sub-wave legnth problems with non-uniform geometric distributions

3.2 Problem Statement

Consider a set of N_s sources that are randomly distributed in a domain Ω. The location of these sources will be denoted using $\mathbf{r}_n$ and their time signatures by $f_n(\mathbf{r}_n, t)$ for $n = 1, \cdots, N_s$. It is assumed that these functions are bandlimited to an angular frequency ω_{max} and all sources are approximately quiescent for $t < 0$. As in all time domain solvers, the source functions $f_n(\mathbf{r}_n, t)$ are known only at evenly spaced time steps $t_k = k\Delta_t$ for $k = 1, \cdots, N_t$ where $\Delta_t = \pi/(\chi\omega_{max})$, $N_t\Delta_t$ is the total simulation time and χ is an oversampling factor. Typically, $\chi > 1$ and chosen between 5 to 20 to accurately reconstruct functions $f_n(\mathbf{r}_n, t)$ from its samples. The field at any point $\mathbf{r}$ due to these sources is given by

$$\Phi(\mathbf{r}, t) = \sum_{n=1}^{N_s} \frac{\delta(t - R_n/c)}{R_n} \star f_n(\mathbf{r}_n, t) \tag{3.1}$$

where c is the speed of light, $\star$ denotes convolution in time and $R_n = ||\mathbf{r} - \mathbf{r}_n||$. It is apparent that the cost of computing (3.1) scales as $\mathcal{O}(N_t N_s^2)$. Finally, in keeping with the definition of sub-wavelength regime, the size of domain is $diam(\Omega) = \mathcal{O}(c\Delta_t)$. Given the size of the domain, it is apparent that the PWTD scheme cannot be readily

used; it has to be substantially modified in order to evaluate these potentials efficiently [172].

In developing this scheme, it is necessary that the source signatures in (3.1) be known so as to facilitate the integration of the proposed algorithm with existing marching-on-in-time solvers for time domain integral equations. The starting point of the proposed method arises from the representation of the source signal. Assume that the source function can be represented in terms of $f_n(\mathbf{r}_n, t) = \sum_k I_{nk} T_k(t)$, where $T_k(t) = T(t - t_k)$ is a time basis function and I_k are the samples of the function at the discrete time step t_k. It follows from this representation that

$$\Phi(\mathbf{r}, t) = \sum_{n=1}^{N_s} \sum_{k=0}^{N_t} I_{n,k} \frac{T_k(t - R_n/c)}{R_n} \tag{3.2}$$

This implies that to realize a fast algorithm, one needs to rapidly compute functions of the form $T_k(t - R_n/c)$. To illustrate the development of a fast algorithm the temporal basis functions are chosen to be backward Lagrange polynomials. Note, however, that the methodology presented herein is *not* restricted to polynomials. To this end, the K^{th} order basis functions is defined as

$$T(t) = \begin{cases} h_k(t) g_{K-k}(t) & \text{for } (k-1)\Delta_t \le t \le k\Delta_t;\ k = 0, \cdots, K \\ 0 & \text{otherwise} \end{cases} \tag{3.3a}$$

where,

$$h_k(t) = \begin{cases} 1 & k = 0 \\ \prod_{i=1}^{k} \frac{t - i\Delta_t}{-i\Delta_t} & k \neq 0 \end{cases} \tag{3.3b}$$

and

$$g_{K-k}(t) = \prod_{i=1}^{K-k} \frac{t + i\Delta_t}{i\Delta_t} \tag{3.3c}$$

It follows, from the above equation that $T(t) = 0$ for $t \notin (-\Delta_t, K\Delta_t)$, $T(0) = 1$ and

$T(t) = 0$ for $t = -\Delta_t, \Delta_t, 2\Delta_t, \cdots, (K-1)\Delta_t$. Using the functions in (3.2), and point testing in time, results in the potential function that is a polynomial of R_n. It means that one can directly exploit acceleration methods developed for kernels of the form R^ν [166].

3.3 Single Time Step Geometries

The field at any observation point $\mathbf{r} \in \Omega$, at time instance $i\Delta_t$, due to sources at $\mathbf{r}_n \in \Omega$ for $n = 1, \cdots, N_s$ can be obtained from (3.1)

$$\Phi(i\Delta_t, \mathbf{r}) = \sum_{n=1}^{N_s} \int_0^{\Delta_t} \frac{\delta(\tau - R_n/c)}{R_n} f_n(\mathbf{r}_n, i\Delta_t - \tau) d\tau \tag{3.4}$$

where $R_n = ||\mathbf{r} - \mathbf{r}_n||$ and $f_n(\mathbf{r}_n, t)$ is the transient source strength at the nth spatial point. The limits $[0, \Delta_t]$, on above time integral is possible because $R_n/c \in [0, \Delta_t]$. Employing time-domain basis function from (3.2) and evaluating the time integral in (3.4) results in,

$$\Phi(i\Delta_t, \mathbf{r}) = \sum_{n=1}^{N_s} \sum_{j=i-K}^{i} I_{n,j} \frac{T((i-j)\Delta_t - R_n/c)}{R_n} \tag{3.5}$$

$$= \sum_{n=1}^{N_s} \sum_{j=0}^{K} I_{n,i-j} \frac{T(j\Delta_t - R_n/c)}{R_n} \tag{3.6}$$

where, K is the order of temporal basis function $T(t)$. Since $T(t)$ is chosen to be a backward Lagrange polynomial, (3.6) can be expressed in terms of powers of R_n/c as

$$\Phi(i\Delta_t, \mathbf{r}) = \sum_{n=1}^{N_s} \sum_{j=0}^{K} \sum_{h=0}^{K} I_{n,i-j} \alpha(h,j) R_n^{h-1} \tag{3.7}$$

In (3.7), $\alpha(h, j)$ is the coefficient corresponding to the polynomial of degree $(h - 1)$ for the basis function at $(i - j)$-th time step, they also depend on Δ_t and c. Evaluating these polynomials of form R^ν can be performed at $\mathcal{O}(N_s)$ cost using the ACE algorithm. Thus, the overall cost of this scheme scales as $\mathcal{O}(KN_s)$. Error bounds for using ACE to evaluate (3.7) can be obtained from the bounds derived in [166] and it can be proven that the upper bound of the error is determined by that for R^{-1}. Note, that the above derivation is not specific to using polynomials as temporal basis functions. Other basis functions may be dealt with in one of two ways; either by finding the appropriate translation functions, or by mapping these onto a space of polynomials. Using polynomials is fairly trivial as the framework for the R^ν kernel is readily available [166].

The $\mathcal{O}(KN_s)$ reduction in cost, specified above, is for brute force implementation of the ACE algorithm. It is important to recognize that the above formulation demands evaluation of the kernel $R^{-\nu}$ for different ν's. However, most of the steps in the proposed algorithm are kernel independent. In that, Theorems 2.3.3 and 2.3.4 (multipole expansion and multipole-to-multipole translation) do not depend on the kernel. Similar observation holds for local-to-local translation and evaluation of potential from local expansion, Theorem 2.3.6 and equation (2.8). Thus, only the multipole-to-local translation, Theorem 2.3.5, depends on the kernel and requires the evaluation of $\nabla^n R^\nu$ for different ν values. Therefore, evaluation of polynomials of form $\sum_n c_\nu R^\nu$ involves (almost) one tree traversal (up and down) irrespective of the kernel, only the multipole-to-local translations need to be done separately for each kernel or polynomials of different degrees. Thus, a careful implementation of the ACE algorithm results in an adaptable and significantly lower cost algorithm. Applying

the multipole to local translation (Theorem 2.3.5) in (3.7),

$$\begin{aligned}
\Phi(i\Delta_t, \mathbf{r}) &= \sum_{n=1}^{N_s}\sum_{j=0}^{K}\sum_{h=0}^{K} I_{n,i-j}\alpha(h,j)R_n^{h-1} \\
&= \sum_{n=1}^{N_s}\sum_{j=0}^{K}\sum_{h=0}^{K} I_{n,i-j}\alpha(h,j)\sum_{p=0}^{P}\nabla^p R_o^{(h-1)}\cdot p\cdot {R'_n}^{(p)} \\
&= \sum_{p=0}^{P}\sum_{j=0}^{K}\left(\sum_{h=0}^{K}\alpha(h,j)\nabla^p R_o^{(h-1)}\right)\cdot p\cdot\left(\sum_{n=1}^{N_s} I_{n,i-j}{R'_n}^{(p)}\right) \\
&= \sum_{j=0}^{K}\sum_{p=0}^{P}\mathcal{T}_j^{(p)}\cdot p\cdot\mathcal{M}_j^{(p)} \qquad (3.8)
\end{aligned}$$

where $R_o = ||\mathbf{r} - \mathbf{r}_o||$, $R'_n = ||\mathbf{r}_o - \mathbf{r}_n||$ and $\mathbf{r}_o$ is the center of sphere enclosing all sources. $\mathcal{T}_j^{(p)}$ and $\mathcal{M}_j^{(p)}$ are the optimal tensor representation of multipoles and translation operation of the ACE algorithm. Equation (3.8) implies that upward tree traversal, i.e., multipole-to-multipole translation and multipole-to-local translation should be performed K times. This is to preserve the transient information, $I_{n,i-j}$ associated with each basis function for every source. However, downward tree-traversal which include local-to-local translation and potential evaluation needs to be performed only once.

3.4 Multiple time step interaction

The above exposition was geared towards developing a scheme for computing interactions when $diam(\Omega) < c\Delta_t$. Next, the generic case of $diam\Omega > c\Delta_t$ is approached through modifications to above methodology. Consider two domains Ω_1 and Ω_2 such that, $\forall\ \mathbf{r}_1 \in \Omega_1$ and $\mathbf{r}_2 \in \Omega_2$ satisfies $(N-1)\Delta_t \leq ||\mathbf{r}_1 - \mathbf{r}_2||/c \leq N\Delta_t$, where N is any positive integer. Then, the field at any point $\mathbf{r}_1$ at i-th time step, $\Phi(i\Delta_t, \mathbf{r}_1)$,

due to N_{s,Ω_2} sources at $\mathbf{r}_n \in \Omega_2$ can be written as

$$\Phi(i\Delta_t, \mathbf{r}_1) = \sum_{n=1}^{N_{s,\Omega_2}} \int_{(N-1)\Delta_t}^{N\Delta_t} \frac{\delta(\tau - R_n/c)}{R_n} f_n(i\Delta_t - \tau, \mathbf{r}_n) d\mathbf{r} d\tau \tag{3.9}$$

where $R_n = ||\mathbf{r}_1 - \mathbf{r}_n||$. Repeating the derivation presented for single time step interaction,

$$\Phi(i\Delta_t, \mathbf{r}_1) = \sum_{n=1}^{N_s} \sum_{j=0}^{K} I_{n,i-j-(N-1)} \frac{T\left((j+N-1)\Delta_t - R_n/c\right)}{R_n} \tag{3.10}$$

When $N = 1$, (3.10) reduces to the case for interaction within one time step (3.6). It is important to preserve R/c argument of the basis function in (3.10), as a polynomial representation is necessary for acceleration using the ACE algorithm. Thus, the key in multiple time step interaction is to identify groups Ω_1 and Ω_2, and it can be done using the following argument;

$$\text{find } d_{min} \geq N\Delta_t \;\; and \;\; d_{max} \leq (N+1)\Delta_t \tag{3.11}$$

where, d_{max} and d_{min} are the maximum and minimum distance between any two points in Ω_1 and Ω_2, see Figure 3.2. For example, consider spherical domains of radii r_1 and r_2 whose centers are separated by R_o; then $d_{max} = R_o + r_1 + r_2$ and $d_{min} = R_o - r_1 - r_2$. From (3.10) and (3.8) it can be inferred that the number of upward tree traversals (multipole-to-multipole and multipole-to-local translations) equals $N_{max}K$, where $N_{max}c\Delta_t$ is the diameter of the sphere encompassing the entire low-frequency region Ω. These constraints mandate a new definition be used when developing the interaction list in the oct-tree as follows:

Definition *Interaction list rule:* Consider two child boxes whose parent boxes are in near-field. They are in each other's far-field if the distance between their centers is

at least twice the sidelength of the domain *and* they satisfy (3.11). Otherwise, they are in each other's near-field.

Some boxes may be well-separated in space and still not satisfy the temporal constraint in (3.11). For example, consider two spheres of radius $r_1 = r_2 = c\Delta_t/8$ whose centers are separated by $R_o = Nc\Delta_t$, now $d_{max} = c(N + 1/2)\Delta_t$ and $d_{min} = c(N - 1/4)\Delta_t$ which do not satisfy (3.11). In such cases one can choose either of the following options: **(i)** sub-divide the domains and perform interaction at next level (with smaller domain size); **(ii)** consider the domains to be in near-field of each other and use direct evaluation. Sub-dividing the domain without limit has two disadvantages. First, the number of unknowns per smallest box, with increasing levels, can fall below the limit for optimal computational cost. Second, sub-division into smaller size boxes does not *always* ensure compliance with constraint in (3.11); it can be shown that boxes who's centers are separated by multiples of $c\Delta_t$ ($Nc\Delta_t$), without regard to their size, will not follow the temporal constraint (3.11) and interaction between such boxes should be evaluated using direct methods. Further, using the second option on short trees can increase the total number of near-field interactions and dominate the overall computational cost. In this work, an optimal implementation is obtained by combining both, i.e., sub-dividing up-to a certain level and beyond this level domains violating (3.11) are placed in near-field interaction of each other. It is essential to note that the number of levels up-to which sub-division is used can be geometry dependent. In essence, this procedure overcomes the multiple time step interaction with a slight cost overhead that should be optimized. Further observations are presented in next section.

3.5 Results and Discussion

In this section results presented will substantiate the above claims and demonstrate the efficacy of the algorithm presented herein. As in all illustration of FMM methods, the goal is to demonstrate considerable speed-up with predetermined accuracy. Consequently, the results presented will demonstrate convergence as well as $\mathcal{O}(N_s)$ per time step CPU cost scaling. In all numerical experiments, the source/observer locations are randomly distributed. The corresponding standard/compressed oct-tree data structures (including interaction lists) are generated using the algorithmic procedure outlined in the Appendix. The accuracy of the proposed algorithm is validated against analytical data for all cases where the unknown count is numerically small. The relative error at n^{th} observer is evaluated as

$$Error_{far}(n) = \frac{||\Phi_{fast,far}(n,t) - \Phi_{analytical,far}(n,t)||_2}{||\Phi_{analytical,far}(n,t)||_2} \tag{3.12}$$

where, $||\cdot||_2$ represents L_2-norm, $\Phi_{fast,far}(t)$ and $\Phi_{analytical,far}(t)$ represent the time history of the fields produced by the sources evaluated using proposed algorithm and analytical procedure, respectively. The error reported in this work is the average error over all observers [172] when the number of observers $N_s < 32,000$. For larger number of unknowns, the analytical data (and hence the error) is computed for randomly distributed unknowns (approximately 150). Hence, the reported data is an estimate of the expected error. These value are denoted using a †. Finally, as is usually done for all fast algorithms, analytical data is computed *only* for the source/observation pairs that are in the far-field of each other, and is consequently representative of an upper bound or worst-case error. The CPU timings (in seconds) are those taken for evaluating the field at a single time step using a 2.3 GHz Intel Pentium processor with 2GB RAM running Linux OS. In all experiments that follow, the time signature

that is associated with the nth source is given by (A.16)

$$f_n(t, \mathbf{r}_n) = \kappa_n e^{-(t-t_p)^2/2\sigma^2} \tag{3.13}$$

where κ_n is the magnitude of the source randomly chosen between $[0, 1]$, $\sigma = 6.366 \times 10^{-8}$ s and $t_p = 6\sigma$ s. The effective highest frequency and minimum wavelength associated with these signal parameters are $f_{max} = 3/\pi\sigma = 15$MHz and $\lambda_{min} \approx 20m$, respectively. As prescribed in MOT solvers, the time step is chosen as $\Delta_t = 1/(20f_{max}) = 3.334$ ns and is independent of geometric feature size and only a function of f_{max}. The above parameters are chosen such that $c\Delta_t = 1m$, thus, all geometric features smaller than 1 m would fall in the sub-wavelength category. In rest of the section, P denotes the number of ACE harmonics used and K denotes the order of the time basis function.

The first set of numerical simulation is performed to demonstrate the validity of the improvements made in the kernel that reduce the number of translations by approximately a factor of two without significantly affecting the order of the error (see Appendix 2.5.1 for details). The numerical experiment performed is as follows; source points were randomly distributed within a cube of side-length 0.5 m, i.e., all points interact within one time step. The number of source/observation points is varied (as is the height of the tree), the number of unknowns at a leaf box is approximately 64, and error is obtained for the "Old" and "New" schemes. The results presented in Table 3.1 indicate what is expected, viz., the computational cost is reduced approximately by a factor of two while the increase in error is almost always marginal (the order of magnitude of the error is unchanged).

Next, set of results demonstrate that the multipole-to-multipole and local-to-local operations are exact. An important ramification of this is that the error is *independent* of the height of the tree. This experiment is effected as follows: consider two cubical

domains $\Omega_1 = (0, 1/4) \times (0, 1/4) \times (0, 1/4)$ m^3 and $\Omega_2 = (1/2, 3/4) \times (0, 1/4) \times (0, 1/4)$ m^3. Each domain contains 4000 randomly distributed source and observation points. In constructing interaction lists, it is ensured that *only* sources/observers in Ω_1 and Ω_2 interact, all others are ignored. Thus, as the number of levels in the tree are increased, the change in the error norm can be attributed solely to the multipole-to-multipole and local-to-local operations. Table A.1 shows error computed for different $\{P, K\}$ pairs and different levels in tree, where dx_0 is the size (in meters) of smallest box. It is evident from Table A.1 that, for a given $\{P, K\}$ pair, the variation in error obtained from using different levels in the tree is accurate to double precision. This is a consequence of the fact that Theorems 2.3.4 and 2.3.6 are exact, i.e., they produce the multipole (or local) expansion had the box size at that level been the leaf box. Consequently, the error bounds are much tighter. Details and proofs can be found in [166].

Next, results are presented for distribution wherein all source/observation pairs are distributed within a domain $\Omega < c\Delta_t$ and distribution sizes ranging from 8000 to 4,000,000 points. The number of unknowns per leaf box, on average, is chosen to lie between 60 and 70. From Table 3.1, it can be inferred that number of harmonics and order of time basis function are closely coupled, i.e., for a given K, arbitrarily increasing P does not improve the error and vice-versa. This is true because the two sources for error (A.17) reported here are **(a)** approximation of a time signal with polynomial basis function of order K, and **(b)** error in evaluating a polynomial through ACE (limited P) due to far-field approximation. Hence, the results for time comparison are presented only for the *optimal pairs* $\{P, K\}$. For example, $\{4, 2\}$ indicates simulation run with 4^{th} order harmonic in ACE and 2^{nd} order temporal basis functions. In general first, second and third order temporal basis function can provide up to $\mathcal{O}(10^{-4})$, $\mathcal{O}(10^{-5})$ and $\mathcal{O}(10^{-7})$ accuracies respectively, for the given source signal parameters (A.16). Table 3.3 shows the relative error for different

$\{P, K\}$ pairs and distribution sizes, N_s. It can be seen that for increasing $\{P, K\}$ combination the error decreases consistently. Table 3.4 presents the per-time-step computation time involved in both direct and proposed algorithm, the order of error corresponding to different $\{P, K\}$ pairs can be inferred from Table 3.3.

Similar results are presented for multiple time step interaction in Tables 3.5 and 3.6, where N denotes the number of distinct time step interactions and C_s denotes the sidelength of cube enclosing all sources/observers in meters. In Tables 3 to 6 empty entries, pertaining to large N_s and $\{P, K\}$ values, are due to insufficient computer memory on the chosen computer platform. Figure 3.6 shows N_s vs. T_{far} graph in log scale for data in Table 3.4. The lines plotted in the graph corresponds to a least square error linear fit for different $\{P, K\}$ pairs. Slope of these line for different $\{P, K\}$ values was approximately 1.06, thus, validating the $\mathcal{O}(N_s)$ scaling of algorithm presented here.

The evident mismatch between timings in Tables 3.6 and 3.4 is explained as follows. In the case of single-time-step interaction, the size of smallest box was chosen to accommodate 60 to 70 unknowns per box on average. However the largest box, at top of the tree (level 1), is within $c\Delta_t$ dimensions; therefore, the height of the tree increases as distribution size is increased. In case of multiple time-step interactions one can keep the leaf box size constant and increase the level-1 box size for higher distribution size, to achieve $\approx$ 64 unknowns per leaf box. However, this does not imply a direct increase in tree height because the interactions at larger boxes also need to obey (3.11). For example, for two spheres of radius r_s to interact, the limiting condition based on (3.11), is $r_s \leq c\Delta_t/4$. Boxes greater than this size interact only through their child. This is the only limitation of the algorithm presented here, however, in practice the algorithm can be strictly used to compute field interacting in few time steps *only* and PWTD will interface with this method when $\lfloor R/(c\Delta_t) \rfloor$ is beyond a certain number of time steps. Thus, an ideal algorithm should switch

between the proposed algorithm and PWTD seamlessly.

Finally, results for an adaptive version of the algorithm introduced here is shown on two types of non-uniformly distributed geometries. The first closely resembles interconnects in electronic chips as shown in Figure 3.4. The distribution of points between top and bottom planes and two interconnects were approximately the same. In applying the adaptive version, the number of unknowns per leaf node was approximately 64, was tested for source/observer distributions ranging from 8,000 to 1,000,000. Table 3.7 presents the error obtained using the proposed algorithm, and was generated for different combinations of ACE harmonics (P) and order of time basis function (K). The rate of error convergence exhibited here is fast in comparison to those in Tables 3.3 and 3.5. This outcome is primarily attributed to the consideration of smallest box enclosure and stricter enforcement of error criteria in building the interaction list; see previous chapter. The timing result for this geometry configuration is presented in Table 3.8. As explained above in uniform distribution, the timing results are presented only for certain combinations of $\{P, K\}$, each pair corresponding to different orders of accuracy given in Table 3.7. Figure 3.7 shows N_s vs. T_{far} graph in log scale. The slope of the linear fit was approximately 1.06 for different pairs of $\{P, K\}$, exhibiting the $\mathcal{O}(N_s)$ scaling produced by the adaptive version of the algorithm. The second geometry configuration considered is made of three circles with points non-uniformly distributed in each of them as shown in Figure 3.5. Each circle is 0.15 m in radius and the points were distributed so that density of points is inversely proportional to the radius. The adaptive version is applied on five different distribution sizes varying from 9,600 to 1,000,000 and the results are shown in Table 3.9. As before, it can be verified that the time scaling is $\mathcal{O}(N_s)$.

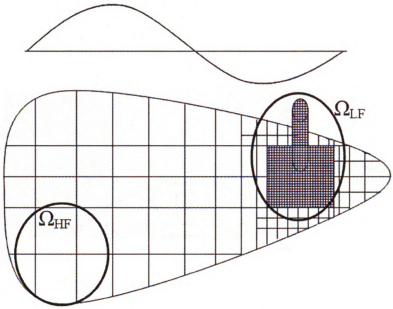

Figure 3.1: Example of antenna feed geometry with low- and high-frequency regimes denoted by Ω_{LF} and Ω_{HF} respectively. Smallest wavelength of incident pulse is also shown for reference.

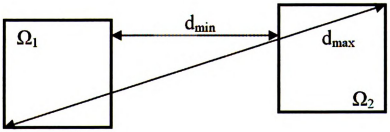

Figure 3.2: Definition for domains interacting over multiple time steps

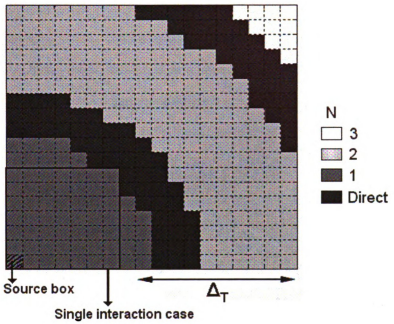

Figure 3.3: Map of N in equation 3.11 for an example single level interaction.

Table 3.1: Comparison between Old and New (reduced) scheme for interaction list for different distribution sizes (N_s) and $\{P, K\}$ pairs.

N_s	$\{P,K\}$	Old_{error}	New_{error}	Old_{time}	New_{time}	Old_{time}/New_{time}
12000	{3,1}	3.40E-4	5.96E-4	0.21	0.11	1.96
"	{4,2}	6.94E-5	1.43E-4	0.54	0.23	2.4
"	{5,2}	2.73E-5	4.87E-5	1.00	0.42	2.37
"	{9,3}	2.37E-6	4.52E-6	9.49	3.6	2.63
"	{13,3}	8.00E-7	1.62E-6	53.47	18.5	2.89
32000	{3,1}	2.36E-4	3.55E-4	0.67	0.38	1.75
"	{4,2}	3.61E-5	6.54E-5	1.97	0.91	2.16
"	{5,2}	1.70E-5	2.59E-5	3.65	1.68	2.17
"	{9,3}	1.38E-6	2.31E-6	28.54	14.42	1.98
64000	{3,1}	2.86E-4	6.38E-4	1.56	0.79	1.98
"	{4,2}	6.42E-5	1.74E-4	3.94	1.9	2.07
"	{5,2}	1.82E-5	4.01E-5	7.17	3.18	2.26
"	{9,3}	4.02E-6	8.00E-6	66.02	27.95	2.36

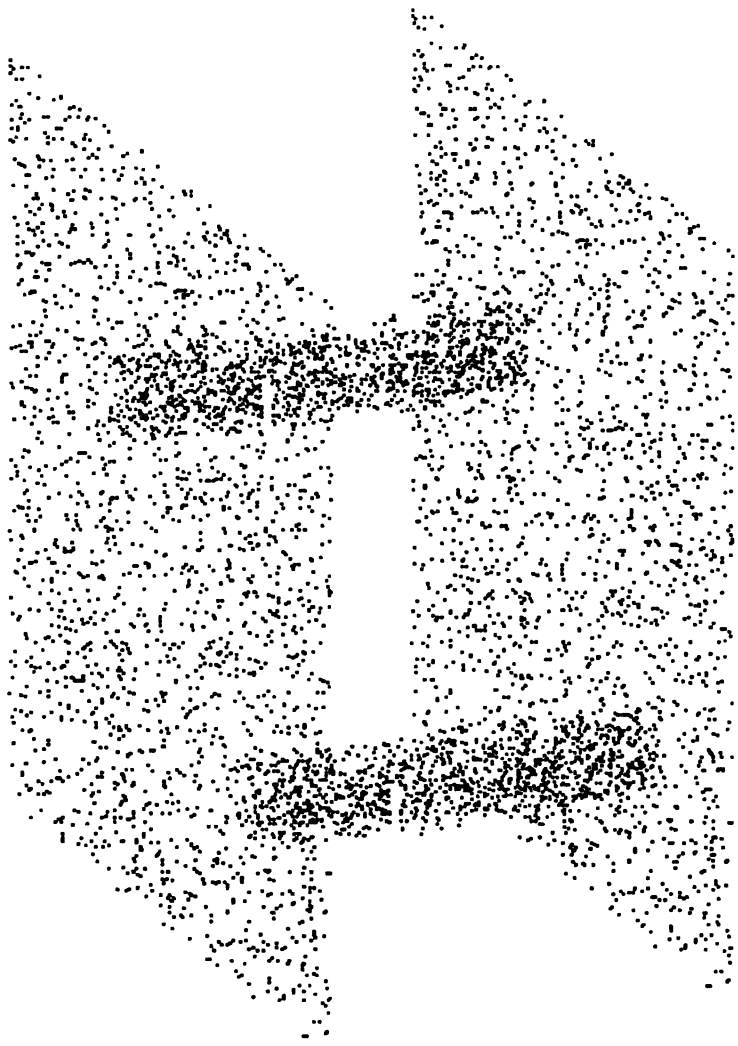

Figure 3.4: Non-uniform geometry configuration 1, resembling interconnect in electronic chips (N_s=12000).

Table 3.2: Exact multipole to multipole and local to local operators of ACE

dx_0		$\{P, K\}$	
A=0.0625	Levels	{1,1}	{4,2}
A	4	1.8800972191556 69E-2	7.03463843261 4828E-4
A/2	5	1.8800972191556 66E-2	7.03463843261 3739E-4
A/8	7	1.8800972191556 70E-2	7.03463843261 3831E-4
A/32	9	1.8800972191556 70E-2	7.03463843261 3819E-4

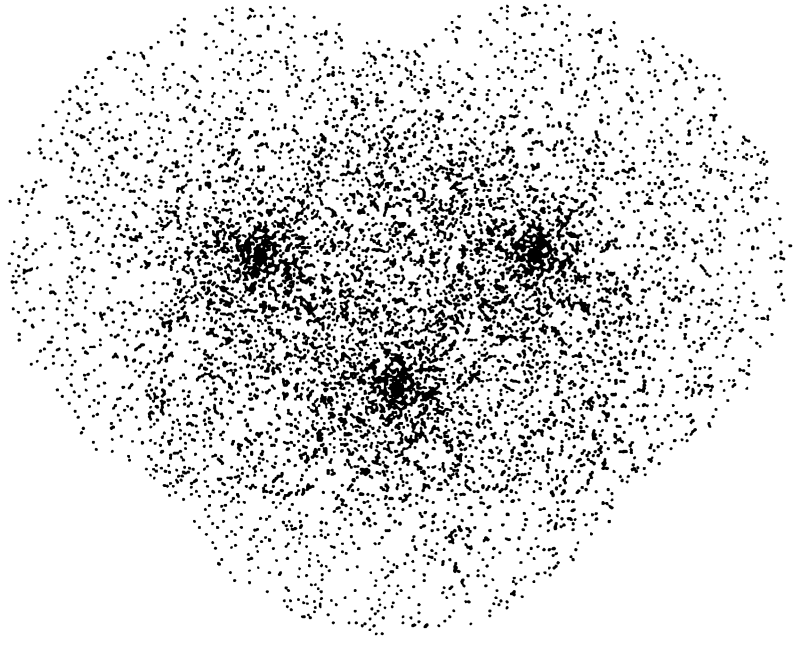

Figure 3.5: Non-uniform geometry configuration 2 (N_s=9600).

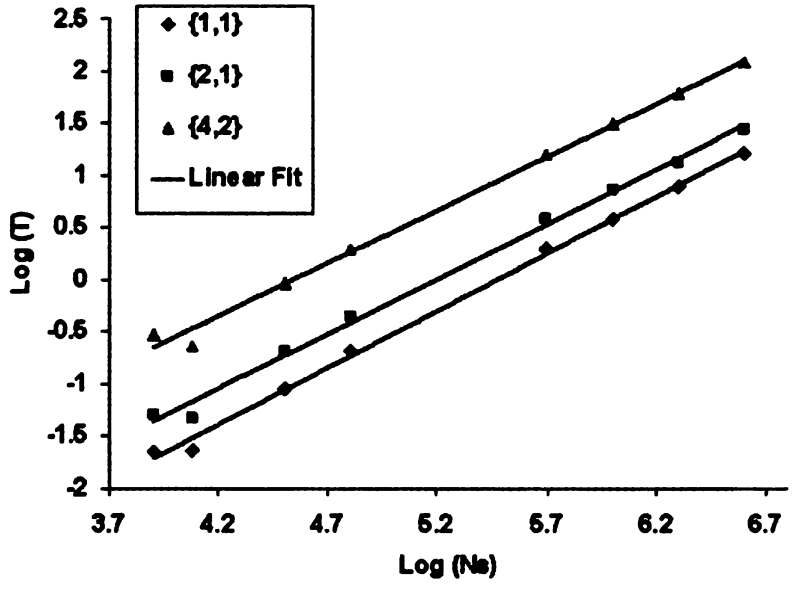

Figure 3.6: $log(N_s)$ vs. $log(T_{far})$ for single interaction case and uniform geometry

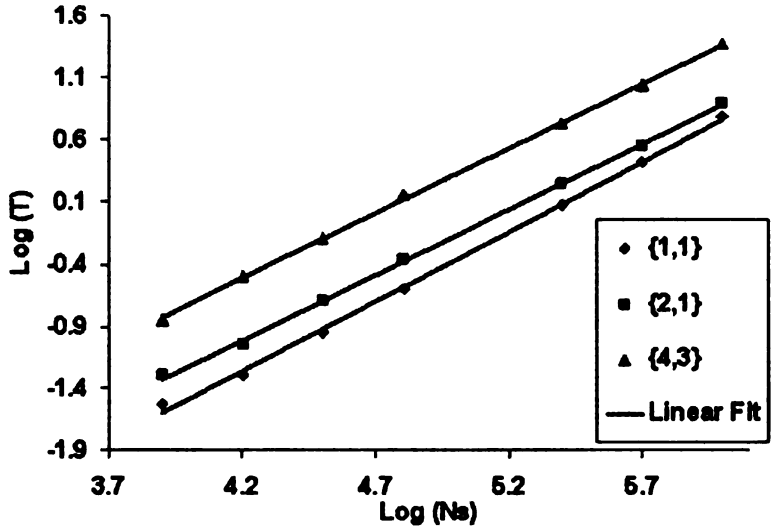

Figure 3.7: $log(N_s)$ vs. $log(T_{far})$ for single interaction case and non-uniform geometry

Table 3.3: $Error_{far}$ in single time step interaction case ($C_s = 0.5$), for various N_s and $\{P, K\}$ pairs.

N_s	8000	12000	32000	64000†	500000†
levels	4	4	4	5	6
{P,K}	$Error_{far}$				
{1,1}	0.00581	0.00995	0.00474	0.00808	0.0015
{2,1}	0.000938	0.00155	0.000637	0.000944	0.00176
{3,1}	0.000341	0.000596	0.000355	0.000638	0.00118
{4,2}	7.87E-05	0.000143	6.54E-05	0.000174	0.000406
{5,2}	2.09E-05	4.87E-05	2.59E-05	4.01E-05	2.48E-05
{9,3}	4.97E-06	4.52E-06	2.31E-06	8E-06	8.34E-06
{13,3}	8.85E-07	1.62E-06	1.03E-06	2.43E-06	-

Table 3.4: Comparison of run-time in single time step interaction case ($C_s = 0.5$).

		$T_{fast}, \{P, K\}$				
N_s	T_{Direct}	{1,1}	{2,1}	{4,2}	{9,3}	{13,3}
8000	4.47	1.40E-2	3.18E-2	0.14	2.17	10.96
12000	11.02	2.27E-2	4.61E-2	0.23	3.60	18.50
32000	97.59	8.87E-2	0.18	0.91	14.42	85.2
64000	-	0.20	0.44	1.90	27.95	173.38
500000	-	1.94	3.82	15.67	245.37	-
1000000	-	3.78	7.19	30.98	498.03	-
2000000	-	7.71	13.33	60.18	742.21	-
4000000	-	16.06	27.46	121.72	1940.15	-

Table 3.5: $Error_{far}$ in multiple time step interaction case, for various combination of N_s, N and $\{P, K\}$ pairs. N is the number of distinct time steps involved.

N_s	8000	12000	32000	32000	128000†
Levels	4	4	4	5	6
C_s	1	1	1	2	2
N	2	2	2	3	3
{P,K}	$Error_{far}$				
{1,1}	2.92E-03	2.97E-03	3.50E-03	2.11E-03	3.80E-03
{2,1}	5.79E-04	5.42E-04	7.06E-04	4.07E-04	3.33E-04
{3,1}	3.15E-04	3.07E-04	4.53E-04	3.22E-04	3.30E-04
{4,2}	6.27E-05	5.67E-05	8.14E-05	5.03E-05	7.19E-05
{5,2}	2.67E-05	2.45E-05	2.99E-05	1.54E-05	1.62E-05
{9,3}	1.97E-06	1.90E-06	3.32E-06	9.15E-07	-

Table 3.6: Comparison of run-time in multiple time step interaction case

				T_{Fast}, $\{P, K\}$			
N_s	C_s	N	T_{Direct}	{1,1}	{2,1}	{4,2}	{9,3}
8000	1.0	2	2.02	0.03	0.06	0.31	4.85
12000	1.0	2	4.69	0.04	0.10	0.49	7.68
32000	1.0	2	61.93	0.19	0.44	2.52	43.97
32000	2.0	3	34.31	0.17	0.32	1.67	28.49
64000	2.0	3	-	0.67	1.52	8.76	165.45
500000	2.0	4	-	27.89	55.47	294.06	-
1000000	1.0	2	-	45.52	83.37	433.34	-

Table 3.7: $Error_{far}$ for non-uniform geometry configuration 1.

N_s	8000	12000	32000
levels	4	5	6
$\{P, K\}$	$Error_{far}$		
{1,1}	3.81E-3	3.58E-3	3.23E-3
{2,1}	9.46E-4	8.62E-3	6.75E-4
{3,2}	1.83E-4	1.64E-4	1.14E-4
{4,2}	3.78E-5	3.43E-5	2.69E-5
{5,2}	1.62E-5	1.51E-5	1.32E-5
{6,3}	3.06E-6	2.59E-6	2.02E-6
{8,3}	1.18E-6	1.10E-7	9.46E-7
{9,3}	7.52E-7	7.27E-7	6.93E-7

Table 3.8: Comparison of run-time for non-uniform geometry configuration 1.

	T_{Fast}, $\{P, K\}$			
N_s	{1,1}	{2,1}	{4,2}	{6,3}
8000	0.03	0.05	0.14	0.49
16000	0.05	0.09	0.32	1.03
32000	0.11	0.20	0.63	2.28
64000	0.25	0.43	1.42	4.8
250000	1.19	1.75	5.33	18.86
500000	2.61	3.58	10.86	40.08
1000000	6.11	7.8	23.25	79.63

Table 3.9: Comparison of run-time for non-uniform geometry configuration 2.

	T_{Fast}, $\{P, K\}$			
N_s	{1,1}	{2,1}	{4,2}	{6,3}
9600	0.03	0.05	0.19	0.51
38400	0.13	0.23	0.79	2.88
105000	0.4	0.72	2.35	8.42
450000	2.16	3.18	10.52	37.34
1000000	5.17	7.07	24.33	82.46

Chapter 4

Wideband FMM and Multiscale Electromagnetic Solver in Frequency Domain

This chapter addresses the development of a fast algorithm for electromagnetic simulation of multiscale structures in frequency domain. Section 4.1 provides a brief review of the multiscale problem in electromagnetics and the limitation of the existing fast algorithms. Section 4.2 presents a general problem setting followed by a brief exposition on the sub-wavelength breakdown of FMM algorithm. In Section 4.3, ACE algorithm is employed for fast evaluation of Helmholtz potential in sub-wavelength scenarios; rigorous proofs are provided to establish the stability of these expansions. Section 4.4 describes the details of the hybrid algorithm, combining ACE and FMM, that is applicable to multiscale problems. Section 4.5 presents results on error and timing of the proposed schemes to demonstrate their numerical stability and efficiency. The hybrid algorithm was also integrated with an EM solver to analyze scattering from electrically large structures.

4.1 Introduction

Integral equation based methods are used extensively in scattering analysis. However, it is well known that they produce dense matrices that increase the cost and limit the size of the problem that can be solved. In past two decades, significant research effort has been dedicated to the development of efficient and accurate techniques to amortize this cost. These advances have had a widespread impact in variety of applications ranging from scattering and radiation analysis to micro-electronic packaging; an incomplete compendium of applications is presented in [88, 174]. The increased power and availability of computational resources and acceleration schemes have enabled solution of problems with very large number of unknowns, varying from few thousands to few millions [37, 40]. Another class of problems arise when analyzing structures which require a high local density of unknowns to capture geometric features. This class of problems, hereafter, referred to as multiscale problems exhibit multiple scales in frequency or length or both. For example, small length scale discretizations are required to capture sharp geometric features that are embedded within large and smooth geometries discretized at a coarser length scale. Similarly, multiple frequency scales is vital to analysis and design of ultra wideband (UWB) antennas embedded in structures [175]. In general the characteristics of a multiscale problem is the concentration of large number of unknowns in electrically small domains. Akin to the breakdown of time domain fast mathods for wave equation, existing techniques for Helmholtz equations also face limitations when applied to multiscale problems as their cost scaling is poor [46, 42] and mixed discretization also lead to badly-conditioned matrix systems [176, 177, 178, 179, 175]. The development of a fast algorithm that is stable and efficient for multiscale structures is addressed in this chapter. The latter problem of badly-conditioned system is remedied with the use of an alternate integral equation formulation, whose development is detailed in Appendix A.

As mentioned in Chapter 1, FMM has become an indispensable for large scale electromagnetic analysis [174, 34]. However, FMM becomes numerically unstable and inefficient when applied to multiscale problems [42]. This is a consequence of the fact that Helmholtz FMM does not smoothly transition to Laplace FMM as frequency tends to zero. This was first remedied by introducing a suitable scaling factor [46] that ensures the computed quantities are stable and the transition is smooth. However this approach is not suitable for problems with multiple length scales. An alternative approach based on spectral representation of free space Green's function in terms of propagating and evanescent plane waves was proposed in [42] . This approach seamlessly transitions from high to low frequency kernel for both spatial and frequency scaling [50], but it requires the evaluation of an infinite integral in $k-$space; generalized Gaussian quadratures [50] and other approaches based on contour integration in complex plane [84, 49, 180] have been explored for this purpose.

The main contributions of this chapter are,

- development of a low frequency fast method based on Accelerated Cartesian Expansion (ACE) algorithm

- development of a hybrid scheme by combining ACE with FMM for multiscale problems

- derivation of convergence proofs and bounds

- integrating the hybrid scheme with integral equation solvers and demonstrate its application to practical problems.

Though the overall structure of the hybrid algorithm developed here bears some similarity with [50], it should be emphasized that they are two different algorithms.

4.2

Let S
surfa
λ. T
curre
insid
tota
(CF

wh
be
th

4.2 Integral Equation and FMM for Helmholtz Equations

Let S denote the surface of a closed PEC object that resides in free-space. This surface is excited by a plane wave characterized by $\{\mathbf{E}^i(\mathbf{r}), \mathbf{H}^i(\mathbf{r})\}$ with wavelength λ. The scattered fields are denoted by $\{\mathbf{E}^s(\mathbf{r}), \mathbf{H}^s(\mathbf{r})\}$ and are radiated by equivalent currents $\mathbf{J}(\mathbf{r})$ on the surface S. Let S^- denote a surface that is conformal and just inside S and let $\mathbf{E}^t(\mathbf{r}) = \mathbf{E}^s(\mathbf{r}) + \mathbf{E}^i(\mathbf{r})$ and $\mathbf{H}^t(\mathbf{r}) = \mathbf{H}^s(\mathbf{r}) + \mathbf{H}^i(\mathbf{r})$ denote the total electric and magnetic fields, respectively. The combined field integral equation (CFIE) formulation for solution of $\mathbf{J}(\mathbf{r})$ is,

$$\alpha \hat{\mathbf{n}} \times \hat{\mathbf{n}} \times \mathbf{E}^t(\mathbf{r}) + (1-\alpha)\hat{\mathbf{n}} \times \mathbf{H}^t(\mathbf{r}) = 0 \; \forall \mathbf{r} \in S^- \tag{4.1}$$

where $\hat{\mathbf{n}}$ is the outward pointing normal and α is an arbitrary scalar constant chosen between 0 and 1. The scattered electric and magnetic fields are related to $\mathbf{J}(\mathbf{r})$ through the dyadic Green's function,

$$\begin{aligned}
\hat{\mathbf{n}} \times \hat{\mathbf{n}} \times \mathbf{E}^s(\mathbf{r}) &= \mathcal{L}_e\{\mathbf{J}(\mathbf{r})\} && (4.2)\\
&= \hat{\mathbf{n}} \times \hat{\mathbf{n}} \times \int_S ds \overline{\overline{G}}_\kappa(\mathbf{r}, \mathbf{r}') \cdot \mathbf{J}(\mathbf{r}') \\
\hat{\mathbf{n}} \times \mathbf{H}^s(\mathbf{r}) &= \mathcal{K}_m\{\mathbf{J}(\mathbf{r})\} && (4.3)\\
&= \hat{\mathbf{n}} \times \frac{1}{j\kappa\eta} \int_S ds \nabla \times \left[\overline{\overline{G}}_\kappa(\mathbf{r}, \mathbf{r}') \cdot \mathbf{J}(\mathbf{r}')\right] \\
\overline{\overline{G}}_\kappa(\mathbf{r}, \mathbf{r}') &= -j\kappa\eta \left(\overline{\overline{I}} + \frac{\nabla\nabla}{\kappa^2}\right) g(\mathbf{r}, \mathbf{r}') && (4.4)\\
g(\mathbf{r}, \mathbf{r}') &= \frac{e^{-j\kappa|\mathbf{r}-\mathbf{r}'|}}{4\pi|\mathbf{r}-\mathbf{r}'|} && (4.5)
\end{aligned}$$

In above relations κ is the wavenumber, η is the characteristic impedance of free space and $\overline{\overline{I}}$ is the identity dyad. The CFIE formulation is chosen to eliminate spurious

solutions

current J

Using Ga

where,

As is

terms

be re

wh

tha

dir

rec

th

fo

to

th

solutions corresponding to interior resonance problem. As is normally done, the current $\mathbf{J}(\mathbf{r})$ is represented using a space of local vector basis functions $\mathbf{f}_m(\mathbf{r})$ [181]. Using Galerkin testing results in a system of equations that may be expressed as

$$\mathcal{Z}\mathcal{I} = \mathcal{V} \tag{4.6}$$

where,

$$\begin{aligned}
\mathcal{Z}_{nm} &= \langle \mathbf{f}_n(\mathbf{r}), -\alpha\mathcal{L}_e\{\mathbf{f}_m(\mathbf{r})\} + (1-\alpha)\mathcal{K}_m\{\mathbf{f}_m(\mathbf{r})\}\rangle & (4.7)\\
\langle \mathbf{f}_n(\mathbf{r}), \mathcal{L}_e\{\mathbf{f}_m(\mathbf{r})\}\rangle &= -j\kappa\eta\langle \mathbf{f}_n(\mathbf{r}), g\mathbf{f}_m(\mathbf{r})\rangle + \frac{j\eta}{\kappa}\langle \nabla\cdot\mathbf{f}_m(\mathbf{r}), g\nabla\cdot\mathbf{f}_n(\mathbf{r})\rangle & (4.8)\\
\langle \mathbf{f}_n(\mathbf{r}), \mathcal{K}_m\{\mathbf{f}_m(\mathbf{r})\}\rangle &= \langle \mathbf{f}_n(\mathbf{r})\times\hat{\mathbf{n}}, \nabla g\times\mathbf{f}_m(\mathbf{r})\rangle & (4.9)\\
\mathcal{V}_n &= \langle \mathbf{f}_n(\mathbf{r}), \alpha\hat{\mathbf{n}}\times\hat{\mathbf{n}}\times\mathbf{E}^i(\mathbf{r}) + (1-\alpha)\hat{\mathbf{n}}\times\mathbf{H}^i(\mathbf{r})\rangle & (4.10)
\end{aligned}$$

As is evident from these equations, the evaluation of each element may be recast in terms of evaluation of scalar potentials. Thus, to better analyze the problem, it can be reposed as follows. Find the potential $\psi(\mathbf{r})$ due to a set of N sources

$$\psi(\mathbf{r}) = \sum_{i=1}^{N} \frac{e^{-j\kappa|\mathbf{r}-\mathbf{r}_i|}}{|\mathbf{r}-\mathbf{r}_i|} w_n w_i \tag{4.11}$$

where w_n and w_i represent the appropriate testing and source strengths, respectively, that include numerical quadrature weights and other constants. It is evident that a direct evaluation of potential at N observation points yields an $\mathcal{O}(N^2)$ method. FMM reduces this cost to $\mathcal{O}(N\log N)$ by utilizing spherical harmonic expansion [30, 65] of the scalar Green's function. Very briefly, the classical FMM algorithm proceeds as follows: the computational domain is embedded in a fictitious cube that is then used to construct an oct-tree. At the lowest level, interaction between the elements of boxes that are in the nearfield of each other is computed directly. All other interactions

are compu

that resid

operator

the field

a single-

While m

best und

that are

wher

expa

denc

resp

4.2

In F

the

sing

argu

are computed using a three stage algorithm: (i) compute multipoles $\mathcal{M}$ from sources that reside in each box; (ii) convert these to local expansion $\mathcal{L}$, using the translation operator $\mathcal{T}$, at all boxes that are in its far field; (iii) from the local expansions compute the field at observer points within the box. This simple three stage scheme is called a single-level algorithm and suffices to discuss the limitation of these expansions. While multilevel variants of this scheme exist [35, 69], the limitations of FMM are best understood by examining (6.8). Consider K closely spaced sources located at $\mathbf{r}_i$ that are well-separated from the testing point $\mathbf{r}$,

$$\psi(\mathbf{r}) = \frac{-j\kappa}{4\pi}\int d^2\hat{\kappa}\mathcal{M}(\mathbf{r}_s,\mathbf{k})\mathcal{T}(\mathbf{r}_o-\mathbf{r}_s,\mathbf{k})w_n e^{-j\mathbf{k}\cdot(\mathbf{r}_o-\mathbf{r})} \tag{4.12a}$$

$$= \frac{-j\kappa}{4\pi}\int d^2\hat{\mathbf{k}}w_n e^{-j\mathbf{k}\cdot(\mathbf{r}_o-\mathbf{r})}\mathcal{L}(\mathbf{r}_o,\mathbf{k}) \tag{4.12b}$$

$$\mathcal{M}(\mathbf{r}_s,\mathbf{k}) = \sum_{i=1}^{K} w_i e^{-j\mathbf{k}\cdot(\mathbf{r}_s-\mathbf{r}_i)} \tag{4.12c}$$

$$\mathcal{T}(\mathbf{r},\mathbf{k}) = \sum_{l=0}^{\infty}(-1)^l(2l+1)h_l^{(2)}(\kappa|\mathbf{r}|)P_l(\hat{\mathbf{k}}\cdot\hat{\mathbf{r}}) \tag{4.12d}$$

$$\mathcal{L}(\mathbf{r}_o,\mathbf{k}) = \mathcal{M}(\mathbf{r}_s,\mathbf{k})\mathcal{T}(\mathbf{r}_o-\mathbf{r}_s,\mathbf{k}) \tag{4.12e}$$

where $|\mathbf{r}_o-\mathbf{r}_s|>2d$, $|\mathbf{r}-\mathbf{r}_o|<d$, $\mathbf{k}=\kappa\hat{\mathbf{k}}$, $\mathbf{r}_s$ ($\mathbf{r}_o$) is the center of multipole (local) expansion for source (observation) cluster, $\mathcal{T}$ is the translation operator, $h_l^{(2)}$ and P_l denotes an order l spherical Hankel function of second kind and Legendre polynomial, respectively.

4.2.1 Sub-wavelength breakdown of Helmholtz FMM

In FMM the interaction between source and observation clusters is evaluated using the translation operator $\mathcal{T}$ in (6.8d) that contains a spherical Hankel function. The singular behaviour of spherical Hankel function implies restrictions on the size of its argument $\kappa|\mathbf{r}|$. For numerical stability, neither the translation distance $|\mathbf{r}|$ nor the

wavenumber κ can be arbitrarily small [73, 76]. Limitations on these parameters has been reported in detail in [74]. As a result, FMM is inefficient when applied to sub-wavelength problems where the principal dimension of the domain is less than or order of a wavelength only. In such problems, some of the leaf boxes have a very high density of unknowns and the overall computational complexity is dominated by the nearfield cost. Thus FMM algorithm is inefficient when applied to multiscale problems where the discretization rate is either non-uniform or uniformly dense.

4.3 ACE translation operator for Helmholtz potential

In ACE, the translation operator is the only kernel dependent quantity. The analytical form of the translation function in case of Helmholtz potential can be written as,

$$\begin{aligned}\nabla^n \frac{e^{-j\kappa R}}{R}(n_1,n_2,n_3) = \sum_{m_1=0}^{\lfloor \frac{n_1}{2} \rfloor} \sum_{m_2=0}^{\lfloor \frac{n_2}{2} \rfloor} \sum_{m_3=0}^{\lfloor \frac{n_3}{2} \rfloor} (-1)^{n+m} R^{2m-2n-1} \\ \times \begin{bmatrix} n_1 \\ m_1 \end{bmatrix} \begin{bmatrix} n_2 \\ m_2 \end{bmatrix} \begin{bmatrix} n_3 \\ m_3 \end{bmatrix} \\ x^{n_1-2m_1} y^{n_2-2m_2} z^{n_3-2m_3} \mathcal{G}(n-m, \kappa R)\end{aligned} \tag{4.13}$$

where

$$\mathcal{G}(n,\kappa R) = \sqrt{2/\pi}(j\kappa R)^{(n+0.5)} K_{n+0.5}(j\kappa R)$$

$$\begin{bmatrix} n \\ m \end{bmatrix} = \frac{n!}{2^m m!(n-2m)!}$$

In above expressions, $n = n_1 + n_2 + n_3$, $m = m_1 + m_2 + m_3$, $K_n(\cdot)$ represents the modified Hankel function of order n, $R = |\mathbf{r}|$ and $\lfloor \cdot \rfloor$ is the *floor* operation. It is well

known that above Taylor's series expansion is convergent when either the domain size or frequency is small. Consider the limiting case of low frequencies or small translation distance i.e. $\kappa R \rightarrow 0$. Using the small argument asymptotic expansion for modified Hankel function [59] and comparing with the translation operator for $1/R$ potential given in [13], (6.14) can be written as,

$$\begin{aligned} \mathcal{G}(n, \kappa R) &\approx \sqrt{2/\pi}(j\kappa R)^{(n+0.5)} \frac{\Gamma(n+0.5)}{2} \left(\frac{2}{j\kappa R}\right)^{n+0.5} \\ &\qquad \text{for} \quad 0 < x < 2n+1 \\ &\approx (2n+1)!! \end{aligned} \tag{4.14}$$

$$\lim_{\kappa R \rightarrow 0} \nabla^n \frac{e^{-j\kappa R}}{R} = \nabla^n \frac{1}{R} \tag{4.15}$$

where $(n)!!$ denotes a double factorial. Above relation shows that at low frequencies ACE translation operator for Helmholtz kernel tends to that of Laplace kernel [13]. Next, the relation between spherical and Cartesian expansions for low-frequency Helmholtz kernel is derived. Consider the spherical expansion of Helmholtz potential [65]

$$\frac{e^{j\kappa|\mathbf{X}+\mathbf{d}|}}{|\mathbf{X}+\mathbf{d}|} = -j\kappa \sum_{l=0}^{\infty} (-1)^l (2l+1) j_l(\kappa d) h_l^{(2)}(\kappa X) P_l(\hat{\mathbf{d}} \cdot \widehat{\mathbf{X}}) \tag{4.16}$$

where $\mathbf{d}$ and $\mathbf{X}$ are the location of source and observation points respectively, $d = |\mathbf{d}|$, $X = |\mathbf{X}|$ and $d << X$. The following relation between Legendre polynomial and Cartesian tensors is well known [182, 13]

$$P_n(\widehat{\mathbf{X}} \cdot \hat{\mathbf{d}}) = \frac{1}{n!} \hat{\mathbf{d}}^{(n)} \,.\, n \,.\, \mathcal{D}_n \widehat{\mathbf{X}} \tag{4.17}$$

where $\mathcal{D}_l$ is the detracer operator, using this (4.16) can be written as,

$$\frac{e^{-j\kappa|\mathbf{X}+\mathbf{d}|}}{|\mathbf{X}+\mathbf{d}|} = -j\kappa \sum_{l=0}^{\infty} \frac{(-1)^l}{l!} (2l+1) j_l(\kappa d) h_l^{(2)}(\kappa X) \left(\hat{\mathbf{d}}^{(l)} \,.\, l \,.\, \mathcal{D}_l \widehat{\mathbf{X}}\right) \tag{4.18}$$

Replacin

above re

e

Above re

ately sc

and low

4.4

Thou

sions

span

effic

com

(low

and

tisc

nei

to e

rea

Replacing spherical Bessel function j_l with its small argument approximation reduces above relation to a form similar to that prescribed in ACE (6.14) ,

$$j_l(x) \approx \frac{x^l}{(2l+1)!!} \quad \text{for small } x \tag{4.19}$$

$$\mathcal{D}_l\widehat{\mathbf{X}} = (-1)^l X^{l+1}\nabla^l \mathbf{X}^{-1} \tag{4.20}$$

$$\frac{e^{-j\kappa|\mathbf{X}+\mathbf{d}|}}{|\mathbf{X}+\mathbf{d}|} \approx \sum_{l=0}^{\infty}\left(\frac{-1^l}{l!}\mathbf{d}^{(l)}\right).l.\left(\frac{-1^{l+1}j}{(2l-1)!!}h_l^{(2)}(\kappa X)(\kappa X)^{l+1}\nabla^l\mathbf{X}^{-1}\right) \tag{4.21}$$

Above relation shows that the translation operator of ACE algorithm is an appropriately scaled version of FMM's such that it is stable for small translation distances and low frequencies.

4.4 Hybrid algorithm for multiscale problems

Though ACE algorithm is efficient for sub-wavelength problems, Cartesian expansions in (6.14) breakdown when applied to problems with high-frequency or domains spanning multiple wavelengths. Numerically it was observed that ACE algorithm is efficient when domain size is confined to 2λ. Thus, the features of ACE algorithm are complementary to that of FMM, i.e. , ACE algorithm is stable for sub-wavelength (low-frequency) problems where FMM breakdown, whereas FMM algorithm is stable and efficient for large-wavelength problems where ACE algorithm breakdown. In multiscale problems both sub- and large-wavelength problems exists simultaneously and neither of the algorithms will be efficient *individually.* Consequently, it follows that to efficiently analyze these structures, it is necessary to hybridize both algorithms to reap their respective advantages while not inheriting their disadvantages.

4.4.1 Combining ACE and FMM

The transition from ACE to FMM is readily realized by using the Taylor series expansion of the FMM multipoles. Examination of (6.8a) leads to

$$\begin{aligned} \mathcal{M}(\mathbf{r}_s, \mathbf{k}) &= \sum_{i=1}^{N} w_i \sum_{p=0}^{\infty} (\mathbf{r}_A - \mathbf{r}_i)^{(p)} \cdot p \cdot \nabla^p e^{-j\mathbf{k}\cdot(\mathbf{r}_s - \mathbf{r}_A)} \\ &= \sum_{p=0}^{\infty} \mathbf{M}^{(p)}(\mathbf{r}_A) \cdot p \cdot T_{map}^{(p)}(\mathbf{k}, \mathbf{r}_s - \mathbf{r}_A) \end{aligned} \tag{4.22}$$

where $\mathbf{r}_A$ denotes the center of ACE multipole expansion $\mathbf{M}^{(p)}$ and the mapping operator T_{map} is given as,

$$\begin{aligned} T_{map}^{(n)}(\mathbf{k}, \mathbf{r})(n_1, n_2, n_3) &= \partial_x^{n_1} \partial_y^{n_2} \partial_z^{n_3} e^{-j\mathbf{k}.\mathbf{r}} \\ &= (-j)^n \kappa_x^{n_1} \kappa_y^{n_2} \kappa_z^{n_3} e^{-j\mathbf{k}\cdot\mathbf{r}} \end{aligned} \tag{4.23}$$

In above expressions $n = n_1 + n_2 + n_3$ and $\mathbf{k} = \kappa_x \hat{x} + \kappa_y \hat{y} + \kappa_z \hat{z}$. A similar derivation follows for computation of ACE local expansion from FMM's. Consider the evaluation of potential using FMM local expansion (6.8b),

$$\psi(\mathbf{r}) = \sum_{p=0}^{\infty} w_n (\mathbf{r}_A - \mathbf{r})^{(p)} \cdot p \cdot \mathbf{L}^{(p)}(\mathbf{r}_A) \tag{4.24}$$

where

$$\mathbf{L}^{(p)}(\mathbf{r}_A) = \frac{-j\kappa}{4\pi} \int d^2\hat{\mathbf{k}} T_{map}^{(p)}(\mathbf{k}, \mathbf{r}_o - \mathbf{r}_A) \mathcal{L}(\mathbf{k}, \mathbf{r}_o) \tag{4.25}$$

Notice that the same mapping operator T_{map} is used for ACE-to-FMM multipole and FMM-to-ACE local expansion translations. In addition the translation of local expansions requires the evaluation of spectral integral.

Truncation of Taylor series expansion in (6.15) and (6.16) to P terms introduces *mapping* error. Let $Re\{y\}$ denote the real part of y, the error in *real* part of FMM

multipoles computed from Pth order ACE harmonics can be written as,

$$\begin{aligned}
\varepsilon_{map}^{R} &= \left| Re\{\mathcal{M}\} - Re\left\{ \sum_{p=0}^{P} \frac{1}{p!} (\mathbf{r}_A - \mathbf{r})^{(p)} \cdot p \cdot \nabla^p e^{-j\mathbf{k}\cdot(\mathbf{r}_s - \mathbf{r}_A)} \right\} \right| \qquad (4.26) \\
&= \left| \sum_{p=P+1}^{\infty} \frac{1}{p!} (\mathbf{r}_A - \mathbf{r})^{(p)} \cdot p \cdot \nabla^p \cos(-\mathbf{k} \cdot (\mathbf{r}_s - \mathbf{r}_A)) \right| \\
&\leq \sum_{p=P+1}^{\infty} \frac{1}{p!} \left| (\mathbf{r}_A - \mathbf{r})^{(p)} \cdot p \cdot \nabla^p \cos(-\mathbf{k} \cdot (\mathbf{r}_s - \mathbf{r}_A)) \right| \\
&\leq \sum_{p=P+1}^{\infty} \frac{3^p}{p!} (a\kappa)^p
\end{aligned}$$

where $a = max(|\mathbf{r}_A - \mathbf{r}|)$. For $P \geq 2$ above error can be written as

$$\varepsilon_{map}^{R} \leq \sum_{p=P+1}^{\infty} \frac{9}{2} \frac{3^{p-2}}{3 \cdot 4 \cdot 5 \ldots p} (a\kappa)^p \qquad (4.27)$$

$$\leq \sum_{p=P+1}^{\infty} \frac{32}{3} \left(\frac{3}{4}\right)^p (a\kappa)^p \qquad (4.28)$$

Above geometric series converges when $3a\kappa/4 < 1$ and the mapping error can be written as,

$$\varepsilon_{map}^{R} \leq \left(\frac{3a\kappa}{4}\right)^{P+1} \frac{11}{1 - 3a\kappa/4} \qquad (4.29)$$

Above bound shows that the mapping error ε_{map}^{R} decreases with increasing number of ACE harmonics P or with decreasing size of ACE domain d. Now consider the error in imaginary part of FMM multipoles computed from Pth order ACE harmonics,

$$\begin{aligned}
\varepsilon_{map}^{I} &= \left| Im\{\mathcal{M}\} - Im\left\{ \sum_{p=0}^{P} \frac{1}{p!} (\mathbf{r}_A - \mathbf{r})^{(p)} \cdot p \cdot \nabla^p e^{-j\mathbf{k}\cdot(\mathbf{r}_s - \mathbf{r}_A)} \right\} \right| \qquad (4.30) \\
&\leq \sum_{p=P+1}^{\infty} \frac{1}{p!} \left| (\mathbf{r}_A - \mathbf{r})^{(p)} \cdot p \cdot \nabla^p \sin(-\mathbf{k} \cdot (\mathbf{r}_s - \mathbf{r}_A)) \right| \\
&= \varepsilon_{map}^{R}
\end{aligned}$$

Since both real and imaginary parts satisfy same error bound, the T_{map} operator preserves both the amplitude and phase of FMM multipoles to desired precision. The error bound for FMM-to-ACE local expansion translation operation is identical to ACE-to-FMM multipole translation as they use the same mapping operator T_{map}. Furthermore, let d be the side length of the cube where ACE harmonics are defined. Then in (4.29), $a = \sqrt{3}d$ and for convergent error $d \leq \lambda/2.65$. This limit is within the range $[0.2, 2.0]\lambda$ where both ACE and FMM expansions are stable, hence the error in transition from ACE to FMM and vice versa can be controlled to arbitrary accuracy.

4.4.2 Implementation details

As shown in figure 4.1 the multiscale geometry is mapped onto a *non-uniform* oct-tree. This ensures that the number of unknowns per leaf-level box is approximately same [50, 61]. In figure 4.1(b), the dark and light nodes indicate ACE and FMM computational domains respectively. This classification of tree-nodes is based on the size of the domain they represent and introduces a *transition level* such that nodes at and above this level are of FMM type and nodes below this level are of ACE type. The hierarchical tree code computation starts with the evaluation of appropriate multipole expansion at leaf boxes. During upward tree traversal the parent multipoles are computed from their children multipoles using the multipole-to-multipole translation operator. At transition level alone the parent box FMM multipoles are computed from their children ACE multipoles using the mapping operator in (4.23). Next the appropriate multipole-to-local expansion translation operation is performed. Then the children local expansions are updated with their parent local expansion using the local-to-local expansion translation operator. Again at the transition level, the child box ACE expansion is updated with its parent box FMM local expansion using the mapping operation in (6.16). Finally the local expansion coefficients at leaf-level boxes are used to compute the farfield potential at their respective observation

points. As in all tree algorithms the complete potential is obtained after the near-field contributions are accounted through direct evaluation.

4.5 Results

This section presents plethora of results that exhibit the accuracy and efficiency of the hybrid scheme when applied to multiscale problems. First few set of results pertain to evaluation of Helmholtz potential given a set of random points. Later the hybrid scheme is integrated with an existing solver and it effectiveness, over FMM-only algorithm, is shown for several problems.

4.5.1 Helmholtz potential evaluation

First, the accuracy and stability of of ACE-only algorithm when applied to sub-wavelength problems is demonstrated. Consider the evaluation of Helmholtz potential at N source/observation pairs that are randomly distributed within a domain of size $\lambda/2$. The error incurred in computing *only* the far-field potentials using ACE are listed in Table 4.1. As is evident, the error decreases uniformly with increase in the number of harmonics. Note, that the error presented here does **not** include nearfield contributions; in general the total error including the nearfield contribution, that are computed exactly, is less by two orders of magnitude.

Next, the convergence of the mapping operators ACE to FMM (FMM to ACE is reciprocal) prescribed in (4.23) is demonstrated. Given some arbitrary number of points confined within a domain of size λ, the FMM multipoles for a given box size are computed both directly and from their children's ACE harmonics using the mapping operator T_{map}. Let $2d$ be the side-length of the FMM box, Table 4.2 shows the relative error in computation of FMM multipoles for various values of d and number of Cartesian harmonics P used in mapping. As expected the mapping error uniformly

decrease

To de

bining A

random

8,000,00

2λ to 12

structed

of doma

points is

configur

the cen

average

ACE ar

This wa

domly

of far-fi

Pentiu

L_{FMM}

distribu

Figure

distribu

uniform

scheme

tention

distribu

the hyb

to how

decreases to double precision as P increases or as d decreases.

To demonstrate the efficiency of the proposed algorithm, the hybrid scheme combining ACE and FMM is applied to both uniformly and non-uniformly distributed random points. In both cases the number of unknowns N is varied from 64,000 to 8,000,000. In case of uniform distributions the size of the domain is increased from 2λ to 12λ as the number of unknowns is increased. The non-uniform geometry is constructed of three overlapping thin disks, as shown in figure 4.1(a), and the overall size of domain was fixed at 12λ. In each disk the points were distributed so that density of points is inversely proportional to radius and linear in z-axis. Note that this geometry configuration closely resembles a multiscale scenario as the discretization rate, near the centers of disk, can be as high as $\lambda/1000$. In all cases it was ensured that the average number of points per leaf-level box is approximately 64 and the number of ACE and FMM harmonics were chosen so as to maintain an accuracy of $\mathcal{O}(10^{-4})$. This was verified by performing direct computation on few, typically 50 to 100, randomly selected points. Table 4.3 shows the time taken, in seconds, for computation of far-field potential using the hybrid algorithm on a desktop computer with 2.3 GHz Pentium IV processor 4GB RAM running Linux. In uniform distribution L_{ACE} and L_{FMM} denotes the number of ACE and FMM levels respectively. In non-uniform distribution L_{ACE} and L_{FMM} were constant at 5 and 3 respectively for all cases. Figure 4.2 shows the Log-Log plot of time vs. N for **both** uniform and non-uniform distributions. The linear line fit with slope one, indicated inside the figure, for both uniform and non-uniform case shows that the cost scaling of the proposed hybrid scheme is irrespective of how the points are distributed. It is important to draw attention to the overlapping linear line fits corresponding to uniform and non-uniform distribution of points. This, in particular, highlights the fact that the time taken by the hybrid algorithm depends purely on the number of unknowns N without regard to how the points are distributed.

4.5.2 Multiscale scattering problems

Next, the performance of integral equation solver augmented with ACE+FMM with that augmented with only FMM. The solvers employs RWG basis functions for surface currents $\mathbf{J}(\mathbf{r})$. GMRES iterative solver with a restart value of 30 was used with tolerance and maximum number of iteration fixed at 1E-3 and 1000, respectively.

In these numerical experiments geometries with different overall size and number of discretizations were considered along with different excitation frequencies. In rest of the results FMM harmonics were used when the box size is greater than or equal to $\lambda/4$ and ACE harmonics for rest of the domains. For each configuration, of chosen geometry and frequency, the CFIE solver was executed in two modes (i) *FMM-only*: where the leaf-level box size is fixed at $\lambda/4$ to ensure that only FMM harmonics are utilized (ii) *ACE+FMM*: the non-uniform tree is constructed such that the average number of unknowns per leaf-level box was approximately 10 to 20. Note that in *ACE+FMM* runs the smallest domain size can be as small as $\lambda/40$. In all cases FMM harmonics were used when box size was equal to or greater than $\lambda/4$ and ACE harmonics for rest of the domains - this defines the transition level in the hybrid algorithm. The ACE and FMM harmonics were chosen such that they yield an accuracy of $\mathcal{O}(1E-3)$. The maximum run time for each simulation was limited to 6 days and any unfinished data is denoted by $\star$. The following values are reported in table for each simulation: *near-time* and *solve-time* are the time, in seconds, for computation of sparse near-field matrix and iterative solution respectively, *speed-up* is the ratio of total time spent by the solver using *FMM-only* and *ACE+FMM* algorithms, *Avg/box* and *Max* denotes the average and maximum number of source/observer pairs per leaf-level box respectively. The ratio of maximum to minimum edge length serves as good measure of the multiscale nature of the problem as it is close to one for uniformly discretized geometries and high for discretization with multiple length scales.

First multiscale problem considered here is the cone-sphere geometry. Here the cone's tip is densely discretized in comparison to the smooth sphere part of the structure. Table 4.4 shows the results of solver using *FMM-only* and *ACE+FMM* algorithm when applied to three different cases. The geometry fits within a cuboid with aspect ratio 1 : 1 : 5 and the maximum dimension for each case is given in terms of the incident wavelength in table 4.4. Let $\hat{z}$ be the axis of rotation of cone-sphere. The propagation direction of incident plane wave $\mathbf{E}^i = \hat{x}e^{-j\kappa\hat{\mathbf{k}}.\mathbf{r}}$ was $\hat{\mathbf{k}} = \hat{y}$ for first two runs and $\hat{\mathbf{k}} = \hat{z}$ for *Run 3*, as shown in figures 4.4 and 4.3. As is evident the solver with hybrid scheme offers speed-up as high as 7 times over that using *FMM-only* algorithm. Essentially this speed-up is achieved by reducing the number of near-field interactions as indicated by the *near-time* in table. This is due to the fact that *ACE+FMM* algorithm allows domain size to be as small as $\lambda/40$ which in turn reduces the average number of unknowns per box considerably in comparision to *FMM-only* case. As expected, the speed-up offered by *ACE+FMM* algorithm reduces as the problem size increases as most interactions fall under FMM; only few number of interactions exist in sub-wavelength domains and ACE algorithm does not offer much advantage over their direct computation. Figure 4.3 and 4.4 shows the bi-static RCS corresponding to *Run 3* and *Run 2* in table 4.4. The RCS computed using both solvers exhibit excellent match to given order of accuracy.

Table 4.5 shows results from second multiscale problem - NASA almond. The entire structure fits within a cuboid with aspect ratio 1 : 6 : 4 and the maximum dimension is given in terms of incident wavelength for each case in the table 4.5. In all cases the direction of incident plane polarized along $\hat{x}$ was $\hat{\mathbf{k}} = \hat{z}$ as shown in figure 4.5. Three different meshes were considered with the number of unknowns varying from 62,000 to 250,000, the increasing multiscale nature of the problem is indicated by the max/min edge length. Here again the hybrid scheme offers speed-up as high as 7 times over *FMM-only* approach. Notice that in *Run 3* the solver with *ACE+FMM*

has completed its run while the large number of near-field interactions in *FMM-only* consumes almost the entire computational time. Figure 4.5 shows the bi-static RCS computed using both the solvers for *Run 2* in table and they agree with each other.

Table 4.6 shows results from third multiscale problem which is a toy-aircraft geometry with many sharp features. The structure fits within a cuboid with aspect ratio $3 : 1.5 : 1$ and the maximum dimension in terms of incident wavelength is reported in table. In all cases the direction of incident plane wave polarized along $\hat{x}$ was $\hat{\mathbf{k}} = \hat{z}$ as shown in figure 4.6. The number of unknowns was varied from few thousands to millions as the maximum dimension was increased from 1.5 to 20 λ. The maximum to minimum edge length ratio for this geometry was approximately 20 in all cases, indicative of a uniformly dense discretization. The solver with *ACE+FMM* exhibits speed-up as high as 14 times over the solver with *FMM-only* algorithm. Notice that in *Run 3* with 1.7 million unknowns, the large number of unknowns per box, indicated by average and maximum unknowns per box in table, in *FMM-only* case results in large number of near-field interactions which consumes the entire computational time. In comparision, with smaller domains in *ACE+FMM* algorithm the number of unknowns per box is considerably smaller and entire computation is completed within the limited time. Figure 4.6 shows the bi-static RCS corresponding to *Run 2* in table 4.6.

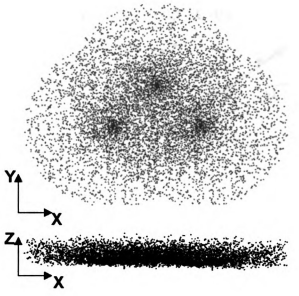

(a)

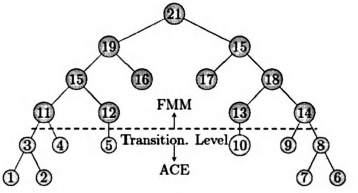

(b)

Figure 4.1: An example non-uniform (a) point distribution and (b) its tree representation.

Table 4.1: Error convergence of ACE algorithm with random points within a $\lambda/2$ size domain

P	1	3	5	7	9	12
Error	1.172E-2	4.804E-4	3.936E-5	1.236E-5	4.380E-6	7.029E-7

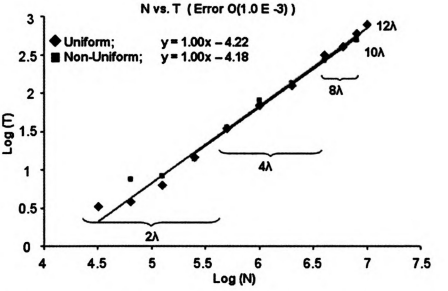

Figure 4.2: Time vs. no. of unknown in log-log plot when hybrid scheme is applied to uniform and non-uniform (fig 4.1) geometries.

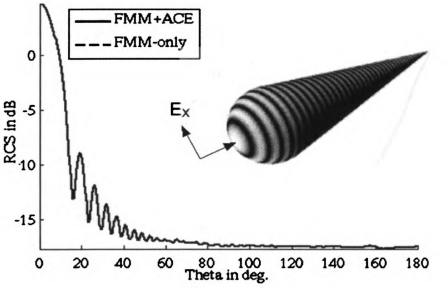

Figure 4.3: Bi-static RCS of cone-sphere geometry, corresponding to *Run 3* in table 4.4. Inset figure shows the incident excitation and magnitude of surface current.

Figure
4.4. Ins

RCS in dB

Figure
to *Ru*
surfac

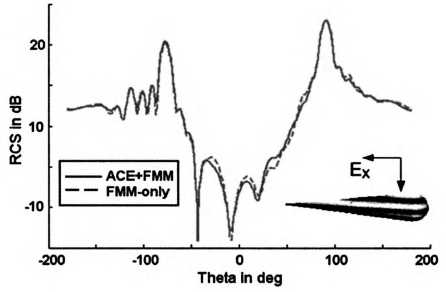

Figure 4.4: Bi-static RCS of cone-sphere geometry, corresponding to *Run 2* in table 4.4. Inset figure shows the incident excitation and magnitude of surface current.

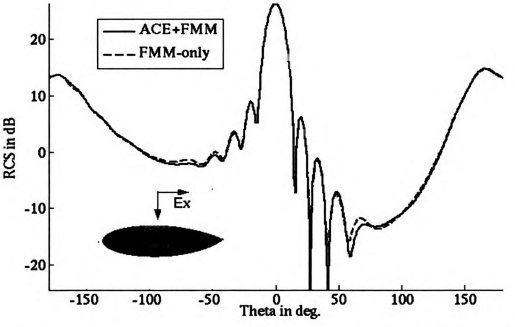

Figure 4.5: Bi-static RCS of NASA fat almond (multiscale geometry 2) corresponding to *Run 2* in table 4.5. Inset figure shows the incident excitation and magnitude of surface current

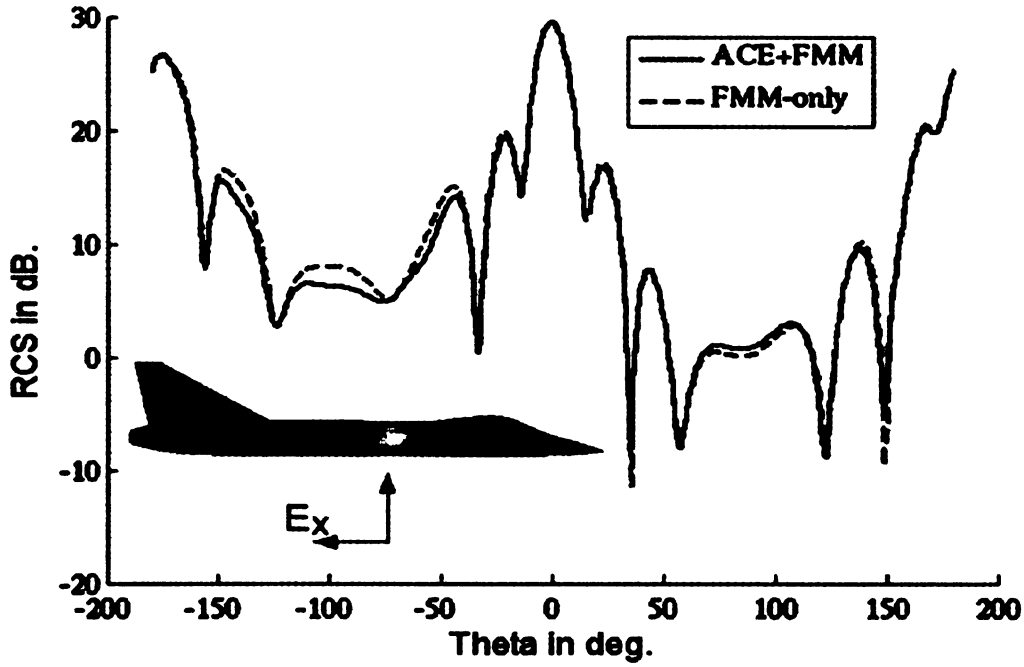

Figure 4.6: Bi-static RCS of Toy-aircraft geometry (multiscale geometry 3) corresponding to *Run 1* in table 4.6. Inset figure shows the incident excitation and magnitude of surface current

Table 4.2: Error in FMM multipoles computed from ACE multipoles using T_{map} in (4.23)

	ACE harmonics			
d	P=3	P=6	P=9	P=12
0.5	2.13	5.58E-3	9.62E-6	5.90E-09
0.25	2.58E-2	8.04E-6	1.51E-9	1.27E-13
0.125	3.49E-4	1.30E-8	1.55E-13	2.24E-15
0.0625	1.04E-5	5.34E-11	1.41E-15	1.41E-15

Table 4
tries

Table 4.3: Time for hybrid algorithm as applied to uniform and non-uniform geometries

N	Uniform				Non-uniform
	Size(λ)	Time	L_{ACE}	L_{FMM}	Time
64,000	2	3.77	3	5	7.48
125,000	2	6.29	3	5	8.13
250,000	2	14.39	3	5	13.93
500,000	4	34.57	3	6	35.71
1,000,000	4	68.7	3	6	79.53
2,000,000	4	125.26	3	6	135.43
4,000,000	**8**	310.22	3	7	263.7
8,000,000	**10**	588.94	3	7	484.02

Table 4.4: Multiscale problem 1 : Cone-sphere geometry

	Near-Time	Solve-Time	**Speed-up**	Avg/box	Max
Run 1	800 MHz, Size $\approx 2\lambda$ with 19,000 basis				
ACE+FMM	832.47	449.87	**6.21**	14	2,288
FMM	7843.59	117.87		1,329	3,424
Run 2	76 MHz, Size $\approx 7\lambda$ with 19,000 basis				
ACE+FMM	593.56	344.96	**1.39**	17	1,666
FMM	1028	277.13		100	1,926
Run 3	10 GHz, Size $\approx 21\lambda$ with 72,000 basis				
ACE+FMM	1100.28	1107.1	**0.79**	**3**	2,084
FMM	1440.7	300.28		**41**	2,224

Table 4.5: Multiscale problem 2: Almond

	Near-Time	Solve-Time	**Speed-up**	Avg/box	Max
Run 1	1 GHz, Size = 5λ with 62,550 basis				
	Max/min edge len.= 160.34				
ACE+FMM	1063.88	795.31	**7.71**	5	270
FMM-only	13532	800		242	6,118
Run 2	1.5 GHz , Size = 8λ with **107,400** basis				
	Max/min edge len.= 193.42				
ACE+FMM	1569.43	6713.38	**2.66**	4	256
FMM-only	20548.77	1475.01		175	5,464
Run 3	2 GHz , Size = 10.6λ with **269,100** basis				
	Max/min edge len.= 474.61				
ACE+FMM	22247.25	26428.42	$\star$	11	2180
FMM-only	96297.28	$\star$		265	13,110

Table 4.6: Multiscale problem 3: Toy-aircraft

	Near-Time	Solve-Time	**Speed-up**	Avg/box	Max
Run 1	76.2 MHz , Size = 1.53λ with 9,727 unknowns				
ACE+FMM	196.15	286.07	**14.29**	7	36
FMM-only	6491.35	400.66		2,784	5,178
Run 2	300 MHz, Size = 6.06λ with 26,145 unknowns				
ACE+FMM	62.54	1343.4	**6.4**	2	12
FMM-only	7800.79	1203.73		697	2,646
Run 3	1 GHz, Size = 20.27λ with **1,754,814** unknowns				
ACE+FMM	237767.37	58500.89	$\star$	98	1,174
FMM-only	$\star$	$\star$		691	4,508

Ch

A

Au

Ec

This

lead

subs

tion

dev

ters

a c

con

of

of

(A

lut

ext

Chapter 5

A Well Conditioned Formulation of Augmented Electric Field Integral Equation (AEFIE)

This chapter addresses the development of integral equation (IE) formulations that lead to well conditioned systems of equations. Typically iterative solvers, like Krylov-subspace solvers, are used for solution of large systems of equation and well conditioned systems of equation require fewer number iterations for solution. Thus the developments presented here are complementary to the discussions in previous chapters where the focus was on reducing the cost of a single iteration. Section 5.1 provides a concise account of the recent research work on the theory and development of well conditioned formulation for electromagnetic simulations. Section 5.2 introduces some of the analysis tools and the insights they provide in understanding the IE operators of EM. Section 5.3 introduces a new formulation of the augmented electric field IE (AEFIE) that leads to both better conditioned systems of equation and unique solutions at all frequencies. The new formulation is first developed for 2D and then extended to 3D case with appropriate modifications. Section 5.4 presents plethora of

results

5.1

Compu
numeri
be prir
of com
focuses
have c

Int
ulatio
electr
detail
linear
that
depe
tric fi
and
and
[184,
formu
reaso
the e
nifica
non-s
only s

results that exhibit the well-conditioned nature of the new formulation.

5.1 Introduction

Computational electromagnetic (CEM) is the field of research that concerns with numerical solution of Maxwell's equation. The rapid development in this field can be primarily attributed to the simultaneous development in power and availability of computers along with the advancements in mathematical research. This chapter focuses on the latter aspect, the mathematical developments in the past decade that have considerably altered the landscape of CEM research.

Integral equations (IE) is one of the widely adopted numerical techniques for simulation of electromagnetic problems [183]. The distinct advantage of IE approach for electromagnetic simulations over their differential equation counterparts have been detailed in the previous chapters. Typically, the IE formulations result in a set of linear system of equation, which are solved using an iterative solver. It is well known that the convergence rate of an iterative solver, the number of iterations for solution, depends directly on the condition number of the numerical system of equation. Electric field IE (EFIE) is one the most widely used formulation as it is valid for both open and closed problems. It is well known that EFIE is an integral equation of first kind and the condition number of these numerical system is not assured to be bounded [184, 185]. Further, EFIE also suffers from the low-frequency breakdown where the formulation is inherently ill-conditioned for low excitation frequencies. The physical reasons for this breakdown of EFIE at low-frequencies is well known [176]. Consider the electric field produced by an arbitrary electric current source, there exists a significant disparity in the magnitude of electric field produced by the solenoidal and non-solenoidal part of the current source. Thus, using the electric field equations, only some parts of the source can be computed in a stable and robust fashion. It

can be analytically shown that the disparity increases as the frequency tends to zero and this is known as the low-frequency breakdown of EFIE. Several computational strategies, based on quasi-Helmholtz decomposition of surface electric currents, have been proposed to overcome this limitation of EFIE. Loop-star, loop-tree and tree/co-tree are different forms of the same type of solution approach [179, 178, 87, 186]. Apart from this, recent mathematical analysis of boundary integral equations in EM have lead to the development of *analytical preconditioners* that modifies the EFIE into a well conditioned, second kind integral equations [187, 188, 189]. However, the resulting formulation suffers from the interior resonance problem and hence produce non-unique solution at resonance frequencies. Conventional techniques, like combined field IE (CFIE), also fail when applied to these new formulations. Further, the numerical implementation of these modified formulation demands careful considerations that has been the focus of several recent research works [190, 191, 192, 193].

This work explores the development of a new IE formulation for electromagnetic simulation that is both well-conditioned and resonance free. This formulation is based on the augmented field integral equations (AFIE), which were initially proposed to overcome the interior resonance problem [194]. AFIE, as originally proposed, requires the solution of an over-determined system of equations using a least-square-error approach. In this work, both the electric charges and currents are considered as unknowns and the resulting new AFIE formulation is amenable to conventional iterative solvers. However, this requires that the imposition of continuity and charge conservation conditions separately. Based on operator theory analysis, these additional constraints are imposed in a manner such that the operators in the resulting formulation are bounded and compact; leading to well-conditioned systems of equations. The validity of these formulation is shown both analytically and numerically for 2D problems. Since some of the observations in 2D case does not hold good for 3D problems, the relevant modifications are also discussed here.

5.2

Let S

surface

λ. The

current

for sol

Let S

integ

In a

elec

In

sp

5.2 Preliminaries

Let S denote the surface of a closed PEC object that resides in free-space. This surface is excited by a plane wave characterized by $\{\mathbf{E}^i(\mathbf{r}), \mathbf{H}^i(\mathbf{r})\}$ with wavelength λ. The scattered fields are denoted by $\{\mathbf{E}^s(\mathbf{r}), \mathbf{H}^s(\mathbf{r})\}$ and are radiated by equivalent currents $\mathbf{J}(\mathbf{r})$ on the surface S. The electric field integral equation (EFIE) formulation for solution of $\mathbf{J}(\mathbf{r})$ is,

$$\hat{\mathbf{n}} \times \hat{\mathbf{n}} \times \Big(\mathbf{E}^i(\mathbf{r}) + \mathbf{E}^s(\mathbf{r})\Big) = 0 \; \forall \mathbf{r} \in S \tag{5.1}$$

Let S^- denote a surface that is conformal and just inside S, then the magnetic field integral equation (MFIE) is written as

$$\hat{\mathbf{n}} \times \Big(\mathbf{H}^s(\mathbf{r}) + \mathbf{H}^i(\mathbf{r})\Big) = 0 \; \forall \mathbf{r} \in S^- \tag{5.2}$$

In above equations, $\hat{\mathbf{n}}$ is the outward pointing normal on surface S. The scattered electric and magnetic fields are related to $\mathbf{J}(\mathbf{r})$ through the dyadic Green's function,

$$\begin{aligned}
\hat{\mathbf{n}} \times \hat{\mathbf{n}} \times \mathbf{E}^s(\mathbf{r}) &= \mathcal{L}_t\{\mathbf{J}(\mathbf{r})\} && (5.3)\\
&= \hat{\mathbf{n}} \times \hat{\mathbf{n}} \times \int_S ds \overline{\overline{G}}_\kappa(\mathbf{r}, \mathbf{r}') \cdot \mathbf{J}(\mathbf{r}') && (5.4)\\
-\hat{\mathbf{n}} \times \mathbf{H}^s(\mathbf{r}) &= \mathcal{K}_t\{\mathbf{J}(\mathbf{r})\} && (5.5)\\
&= \hat{\mathbf{n}} \times \frac{1}{j\kappa\eta} \int_S ds \nabla \times \Big[\overline{\overline{G}}_\kappa(\mathbf{r}, \mathbf{r}') \cdot \mathbf{J}(\mathbf{r}')\Big] \\
\overline{\overline{G}}_\kappa(\mathbf{r}, \mathbf{r}') &= -j\kappa\eta \left(\overline{\overline{I}} + \frac{\nabla\nabla}{\kappa^2}\right) g(\mathbf{r}, \mathbf{r}') && (5.6)\\
g(\mathbf{r}, \mathbf{r}') &= \frac{e^{-j\kappa|\mathbf{r}-\mathbf{r}'|}}{4\pi|\mathbf{r}-\mathbf{r}'|} && (5.7)
\end{aligned}$$

In above relations $\kappa = \omega/c$ is the wavenumber, ω is the angular frequency, c is the speed of light in free space, η is the characteristic impedance of free space and $\overline{\overline{I}}$ is the

identity dyad. Since the above formulations are based on the boundary conditions on tangential fields, the IE operators $\mathcal{L}_t$ and $\mathcal{K}_t$ are referred to as tEFIE and tMFIE, respectively. Typically, in numerical solutions, the current $\mathbf{J}(\mathbf{r})$ is represented using a space of local vector basis functions $\mathbf{f}_m(\mathbf{r})$ [181]. Galerkin testing results in a system of equations that may be expressed as

$$\mathcal{Z}\mathcal{I} = \mathcal{V} \tag{5.8}$$

For example, in case of tEFIE, the elements of $\mathcal{Z}$ and $\mathcal{V}$ can be written as

$$\mathcal{Z}_{nm} = \langle \mathbf{f}_n(\mathbf{r}), -\mathcal{L}_t\{\mathbf{f}_m(\mathbf{r})\}\rangle \tag{5.9}$$

$$\langle \mathbf{f}_n(\mathbf{r}), \mathcal{L}_t\{\mathbf{f}_m(\mathbf{r})\}\rangle = -j\kappa\eta\langle \mathbf{f}_n(\mathbf{r}), g\mathbf{f}_m(\mathbf{r})\rangle + \frac{j\eta}{\kappa}\langle \nabla\cdot\mathbf{f}_m(\mathbf{r}), g\nabla\cdot\mathbf{f}_n(\mathbf{r})\rangle \tag{5.10}$$

$$\mathcal{V}_n = \langle \mathbf{f}_n(\mathbf{r}), \hat{\mathbf{n}}\times\hat{\mathbf{n}}\times\mathbf{E}^i(\mathbf{r})\rangle \tag{5.11}$$

5.2.1 Interior Resonance and Augmented IE

It is well known that, for closed geometries, both tEFIE and tMFIE operators have non-empty null space at excitation frequencies corresponding to interior resonance. Thus, at these frequencies the solution of the equations (5.1,5.2) is not unique [195]. Combined field IE (CFIE) is a popular alternative, where both EFIE and MFIE are solved simultaneously. Other proven approaches to overcome interior resonance problems are combined source IE (CSIE) [196] and dual surface IE [197]. All these alternatives demand additional computation in one form or the other, for e.g. CFIE requires computation of magnetic field, and CSIE doubles the number of unknowns. Augmented field integral equations (AFIE), proposed by Yaghjian [194], is an alternative approach to overcome the interior resonance problem with the computation of either electric or magnetic field only. In AFIE, a unique solution to currents $\mathbf{J}(\mathbf{r})$ is obtained by simultaneously satisfying both the tangential and normal boundary

condition of electric or magnetic field. Consider the augmented EFIE (AEFIE)

$$\mathcal{L}_t\{\mathbf{J}\} = -\hat{\mathbf{n}} \times \hat{\mathbf{n}} \times \mathbf{E}^i(\mathbf{r}) \; \forall \mathbf{r} \in S \tag{5.12}$$

$$\mathcal{L}_n\{\mathbf{J}\} = \frac{\rho_s}{\epsilon_0} - \hat{\mathbf{n}} \cdot \mathbf{E}^i(\mathbf{r}) \; \forall \mathbf{r} \in S \tag{5.13}$$

$$\mathcal{L}_n\{\mathbf{J}\} = \hat{\mathbf{n}} \cdot \int_S ds \overline{\overline{G}}_\kappa(\mathbf{r}, \mathbf{r}') \cdot \mathbf{J}(\mathbf{r}') \tag{5.14}$$

Similarly, the augmented MFIE (AMFIE) can be written as,

$$\mathcal{K}_t\{\mathbf{J}\} = \mathbf{J} - \hat{\mathbf{n}} \times \mathbf{H}^i(\mathbf{r}) \; \forall \mathbf{r} \in S \tag{5.15}$$

$$\mathcal{K}_n\{\mathbf{J}\} = -\hat{\mathbf{n}} \cdot \mathbf{H}^i(\mathbf{r}) \; \forall \mathbf{r} \in S \tag{5.16}$$

$$\mathcal{K}_n\{\mathbf{J}\} = \hat{\mathbf{n}} \cdot \frac{1}{j\kappa\eta} \int_S ds \nabla \times \left[\overline{\overline{G}}_\kappa(\mathbf{r}, \mathbf{r}') \cdot \mathbf{J}(\mathbf{r}')\right] \tag{5.17}$$

In the above equations $\mathcal{L}_n$ and $\mathcal{K}_n$ are the nEFIE and nMFIE operators that correspond to the boundary condition on electric and magnetic fields normal to the boundary surface S, respectively. It has been rigorously shown that both AEFIE and AMFIE produce unique solutions for any closed geometry except spheres. Moreover, it is evident that discretization of both the formulations lead to an overdetermined system of equations, which can be solved only in a least squares sense. Hence this approach has been relatively less popular when compared to CFIE or CSIE. A distinct feature of AFIE, also noted in the seminal work of Yaghjian [194], is that the AFIE formulation is similar to a second kind IE. However, exploiting this advantage is not trivial and forms the main focus of the work presented here.

5.2.2 Operator and Eigenvalue Analysis

In the past decade, rigorous mathematical analysis techniques have been employed to study the different boundary integral equation formulations used in computational electromagnetics. These theoretical analysis of boundary IE operators depend on the

form and size of the computational geometry and they are restricted to the study of canonical geometries such as circular cylinder and sphere in 2D and 3D, respectively. Though analytical solution exist for these geometries, the theoretical analysis have provided valuable insights that led to a better understanding of the behaviour of these IE operators. It is well known that an IE operator with finite and bounded spectrum, when discretized, yields a well-conditioned system of equations [185, 191]. In formal terms, a formulation is well-conditioned if all its operators take the form $(\mathcal{I} + \mathcal{M})$, where $\mathcal{I}$ is the identity operator and $\mathcal{M}$ is a compact operator. Intuitively, compact operators have bounded spectrum and the presence of identity operator ensures that the spectrum of overall operator is offset from origin . Hence, the spectral radius of these operators are finite and bounded, see [184, 185] for rigorous treatment on these topics. In rest of this section, for the sake of completion and clarity, these recent developments are presented in requisite detail for the 2D case. Similar observations hold for 3D case also, however with more involved derivations beyond the scope of this thesis, and these are just stated with ample references.

Consider the 2D problem of traverse electric (TEz) scattering from a PEC circular cylinder of radius a, with axis of rotation aligned along the Z-axis. The tEFIE formulation (5.1) for this problem can be written as,

$$-j\kappa\eta\hat{\mathbf{r}} \times \int_0^{2\pi} a d\phi' \left(\overline{\overline{I}} + \frac{\nabla\nabla}{\kappa^2}\right) H_0^{(2)}(\kappa R) \cdot \mathbf{J}_\phi(\phi') \;=\; -\hat{\mathbf{r}} \times \mathbf{E}^i(\phi) \qquad (5.18)$$

where $H_0^{(2)}$ is the Hankel function of second kind, $R = a||\mathbf{r}-\mathbf{r}'||$, $\mathbf{r} = a\cos\phi\hat{x}+a\sin\phi\hat{y}$ and $\mathbf{r}' = a\cos\phi'\hat{x}+a\sin\phi'\hat{y}$. For this canonical case, it is well known that $\{\hat{\phi}e^{jn\phi}, n = 0, 1, \ldots\}$ forms a complete set of eigenfunctions for the surface current $\mathbf{J}$ [183]. Then

the unknown surface current $\mathbf{J}_\phi$ can be represented as sum of these eigenfunctions,

$$\mathbf{J}_\phi = \sum_{n=0}^{\infty} I_n \hat{\phi} e^{jn\phi} \tag{5.19}$$

where I_n are the unknown coefficient to be solved for. Using the orthogonality of the eigenfunctions, the eigenvalues of operator $\mathcal{L}_t$ are given as

$$\lambda_n^{TE,tEFIE} = \frac{1}{2}(\eta\pi\kappa a) J_n'(\kappa a) H_n^{\prime(2)}(\kappa a) \tag{5.20}$$

The plot of few of these eigenvalues for different orders n and size of the object a is shown in figure 5.1. Evidently, these eigenvalues are zero whenever $J_n'(\kappa a) = 0$, indicating the non-trivial, finite dimension null space of the TE-tEFIE operator. These are also the frequencies corresponding to the interior resonance. Further, from figure 5.1, it is seen that the spread between eigenvalues is large , especially, for small values of κa. Consider the asymptotic limits when $\kappa a \to 0$,

$$\lambda_0^{TE,tEFIE} \approx j\frac{\eta\kappa a}{2} \to 0 \tag{5.21}$$

$$\lambda_n^{TE,tEFIE} \approx j\frac{\eta|n|}{2\kappa a} \to \infty \ ; n \neq 0 \tag{5.22}$$

This suggests that the tEFIE operator is unstable for electrically small scatterer. The widely spread eigenvalue spectrum also suggests that tEFIE operator is an *unbounded operator*. This is particularly a consequence of the double derivatives in (5.18) that leads to hyper-singular terms.

The same eigenvalue analysis can be extended to tMFIE operators. The tMFIE for 2D TEz scattering from a PEC cylinder of radius a can be written as,

$$\mathcal{K}_t\{\mathbf{J}_\phi(\phi)\} = \mathbf{J}_\phi + \frac{1}{4j}\hat{\mathbf{r}} \times \int_0^{2\pi} a d\phi' \hat{\phi}(\phi') \mathbf{J}_\phi(\phi') H_0^{(2)}(\kappa R) \tag{5.23}$$

As in

corre

Samp

Here.

tions

null s

nance

analys

Thus

accur

S

from

form

on su

[187]

wher

assoc

As in the case of tEFIE, $\{\hat{\phi}e^{jn\phi}\}$ form a complete set of eigenfunctions and the corresponding eigenvalues are given as,

$$\lambda_n^{TE,tMFIE} = \frac{1}{2}(j\pi\kappa a)J_n(\kappa a)H_n^{'(2)}(\kappa a) \tag{5.24}$$

Samples of these eigenvalues are plotted in figure 5.2 for different values of n and κa. Here, the eigenvalues are zero whenever $J_n(\kappa a) = 0$ and the corresponding eigenfunctions form the finite, non-trivial null space of the tMFIE operator. Notice that the null space of tEFIE and tMFIE are not the same, in other words, the interior resonance for both operators occur at different frequencies. Performing the asymptotic analysis for $\kappa a \rightarrow 0$,

$$\lambda_0^{TE,tMFIE} \approx 1 \tag{5.25}$$

$$\lambda_n^{TE,tMFIE} \approx \tfrac{1}{2} \; ; n \neq 0 \tag{5.26}$$

Thus the spectrum of tMFIE operator is bounded and for $n \rightarrow \infty$ the eigenvalues accumulate at (0.5+j0.0).

Similar analysis can be carried out in 3D for the canonical problem of scattering from a PEC sphere of radius a. Here, the vector tesseral harmonics $\mathbf{X}_{nm}$ and $\mathbf{U}_{nm}$ form the complete set of eigenfunctions for representation of the vector current fields on surface of the sphere. These are also known as the surface Helmholtz decomposition [187] on sphere and given by,

$$\mathbf{X}_{nm}(\theta,\phi) = \hat{\mathbf{r}} \times \nabla Y_n^m(\theta,\phi) \tag{5.27}$$

$$\mathbf{U}_{nm}(\theta,\phi) = \hat{\mathbf{r}} \times \mathbf{X}_{nm}(\theta,\phi) \tag{5.28}$$

where $Y_n^m(\theta,\phi) = P_n^m(\cos\theta)e^{jm\phi}$ is the spherical harmonics and P_n^m denotes the associate Legendre function of order $\{n,m\}$. The eigenvalues of tEFIE and tMFIE

operator in 3D can be derived as,

$$\mathcal{L}_t \begin{Bmatrix} \mathbf{X}_{nm} \\ \mathbf{U}_{nm} \end{Bmatrix} = \begin{Bmatrix} (\kappa a)^2 j_n(\kappa a) h_n^{(1)}(\kappa a) \mathbf{U}_{nm} \\ (\kappa a)^2 j_n'(\kappa a) h_n^{\prime(1)}(\kappa a) \mathbf{X}_{nm} \end{Bmatrix} \tag{5.29}$$

$$\mathcal{K}_t \begin{Bmatrix} \mathbf{X}_{nm} \\ \mathbf{U}_{nm} \end{Bmatrix} = \begin{Bmatrix} -j(\kappa a)^2 j_n'(\kappa a) h_n^{(1)}(\kappa a) \mathbf{U}_{nm} \\ j(\kappa a)^2 j_n(\kappa a) h_n^{\prime(1)}(\kappa a) \mathbf{X}_{nm} \end{Bmatrix} \tag{5.30}$$

Similar to 2D case, the spectrum of tEFIE operator is widespread, indicating an unbounded operator and the spectrum of tMFIE operator is bounded and accumulate about $(0.5 + j0.0)$. Here again, the interior resonance frequencies, corresponding to zero eigenvalues, are not same for tEFIE and tMFIE operators.

The above eigenvalue analysis offers more insight than just understanding the interior resonance problem and analytic nature of the IE operators. Since practical problems cannot be approximated as above canonical problems, discretized version of these IE operators are employed. In such cases, the above eigenvalue analysis can be extended as follows: assuming a uniform discretization of the geometry, increasingly fine discretization size corresponds to better representation of higher order eigenfunctions. Thus, employing a dense discretization with tEFIE operator leads to larger spread of eigenvalues and hence results in a badly-conditioned system of equations. The same geometry, when considered with tMFIE operator would lead to a well conditioned system of equation as their eigenvalues are bounded at all frequencies, except at interior resonance. These insights are used in development and investigation of the modified AEFIE formulation presented in the next section.

5.3 Well-conditioned Formulation for AEFIE

In this section, the AEFIE (5.12) is posed in a manner such that it results in a well conditioned system of equations; that is amenable for use with conventional iterative

solvers. The particular case of AEFIE was chosen so that the formulation, in future, can be extended to open geometries as well. Similar to the discussion in previous section, an eigenvalue analysis of the proposed formulation is presented in detail for the 2D problem. Extension to 3D is not trivial and requires careful consideration.

As mentioned before, if N basis function are used to represent the current, AEFIE requires the solution to satisfy $2N$ contraint equations of tEFIE and nEFIE. In this work, electric charges are also considered as unknowns so that there are $2N$ unknowns to be solved with $2N$ equations. Charge unknowns have been previously employed in MOM formulations to overcome the low-frequency breakdown of EFIE. Here we consider this choice specifically to re-formulate AEFIE as

$$\begin{bmatrix} \mathcal{A}^t_{\mathbf{J}} & \mathcal{A}^t_{\rho} \\ \mathcal{A}^n_{\mathbf{J}} & \mathcal{A}^n_{\rho} \end{bmatrix} \begin{Bmatrix} \mathbf{J} \\ \rho \end{Bmatrix} = - \begin{Bmatrix} \hat{\mathbf{n}} \times \mathbf{E}^i \\ \hat{\mathbf{n}} \cdot \mathbf{E}^i \end{Bmatrix} \tag{5.31}$$

$$\mathcal{A}^t_{\mathbf{J}} = \hat{\mathbf{n}} \times \int_S dr' g(\mathbf{r}, \mathbf{r}') \mathbf{J}(\mathbf{r}') \tag{5.32}$$

$$\mathcal{A}^n_{\mathbf{J}} = \hat{\mathbf{n}} \cdot \int_S dr' g(\mathbf{r}, \mathbf{r}') \mathbf{J}(\mathbf{r}') \tag{5.33}$$

$$\mathcal{A}^t_{\rho} = -\hat{\mathbf{n}} \times \int_S dr' \nabla g(\mathbf{r}, \mathbf{r}') \rho_s(\mathbf{r}') \tag{5.34}$$

$$\mathcal{A}^n_{\rho} = -\frac{\rho}{\epsilon_0} - \hat{\mathbf{n}} \cdot \int_S dr' \nabla g(\mathbf{r}, \mathbf{r}') \rho_s(\mathbf{r}') \tag{5.35}$$

Another motivation for employing charge unknowns is that the scalar basis function used to represent charges forms a suitable set of testing function for nEFIE. In numerical implementation, the vector basis function for currents and scalar charge basis function are used to test the tangential and normal electric field boundary conditions, respectively. However, considering both currents and charges as unknowns demands development of methodologies to impose the continuity and total-charge conservation

conditions,

$$\nabla \cdot \mathbf{J} = -j\omega\rho_s \tag{5.36}$$

$$\sum \rho_s = 0 \tag{5.37}$$

Here, the continuity condition is imposed as an external constraint using the penalty function method. In this approach, the discretized form of the differential equation is multiplied by a scalar factor α and added to the tangential field boundary condition. Here, α is a pre-determined constant chosen to be as large as possible, as per the theory of penalty functions, but within the range of available numerical precision. This causes a obvious numerical imbalance between the two equations of (5.31), hence the normal field boundary condition is also scaled by α to ameliorate this disparity. Thus, the AEFIE formulation satisfying the continuity condition is given as,

$$\begin{bmatrix} \mathcal{A}^t_{\mathbf{J}} + \alpha\nabla\cdot & \mathcal{A}^t_{\rho} + \alpha j\omega \\ \alpha\mathcal{A}^n_{\mathbf{J}} & \alpha\mathcal{A}^n_{\rho} \end{bmatrix} \begin{Bmatrix} \mathbf{J}_\phi \\ \rho_s \end{Bmatrix} = - \begin{Bmatrix} \hat{\mathbf{n}} \times \mathbf{E}^i \\ \alpha\hat{\mathbf{n}} \cdot \mathbf{E}^i \end{Bmatrix} \tag{5.38}$$

Finally, the charge conservation can be ensured either through a penalty function approach or through the deflation procedure. Since penalty function is already used to impose the continuity condition, employing it to impose charge conservation can lead to numerical overflow. Further, note that the constant current and charge vector is the only non-trivial element in the null space of the AEFIE operator in (5.31). This observation favors the use of deflation technique as it requires an approximate knowledge of the null space. Deflation is a well known procedure used in the solution of badly conditioned numerical systems. Consider an arbitrary matrix $\mathbf{M}$ with eigenvectors $\{\mathbf{e}_n\}$ and corresponding eigenvalues $\{\lambda_n\}$. $\mathbf{M}$ is a badly conditioned system of equation if one of the eigenvalues , say λ_0, is very small. However, with the knowledge of corresponding eigenvector, one can consider a modified system of

equations $\mathbf{M}'$ that is a rank one update of the original system

$$\mathbf{M}' = \mathbf{M} + (q - \lambda_0)\mathbf{e}_0\mathbf{e}_0^T \tag{5.39}$$

where q is the average eigenvalue of the original system. Notice that q becomes the new eigenvalue of eigenvector $\mathbf{e}_0$ and all other eigenvalues are unchanged.

$$\begin{aligned} \mathbf{M}'\mathbf{e}_0 &= (\mathbf{M} + (q - \lambda_0)\mathbf{e}_0\mathbf{e}_0)\mathbf{e}_0 && (5.40)\\ &= q\mathbf{e}_0 && (5.41)\\ \mathbf{M}'\mathbf{e}_n &= \mathbf{M}\mathbf{e}_n \; n \neq 0 && (5.42)\\ &= \lambda_n\mathbf{e}_n && (5.43) \end{aligned}$$

Thus the defective eigenvalue is *deflated* from the original system using the rank one update. Multiple deflations or rank one updates can be used to improve the condition number of an arbitrary system with more than one defective eigenvalues. However, the deflation procedure requires the knowledge of eigenvectors corresponding to these defective eigenvalues. Also, additional evaluations need to be performed on solution of modified system to remove the effects of deflation and obtain the correct solution. Since the null space of the AEFIE operator (5.31) is known, the deflation technique is employed to impose the charge conservation condition. At the limiting case of $\omega \rightarrow 0$, the above AEFIE equations reduces to solving the currents and charges using the normal electric field boundary condition while imposing the zero divergence constraint on currents. It is well known that nEFIE is equivalent to tMFIE and hence is well conditioned at low-frequencies also. Also, the zero divergence is the required and physically correct behaviour of currents at low-frequencies. Hence the proposed AEFIE formulation does not suffer from the low-frequency breakdown and is expected to be well conditioned across the frequency range.

5.3.1 Eigenvalue analysis in 2D

An immediate observation, looking at (5.31), is that none of the AEFIE operators contain double derivatives, which is the reason for hypersingularity that leads to unbounded operators. The following theoretical analysis is performed to investigate the analytic nature of each of the AEFIE operators. Consider the evaluation of electric field, using the above operators, produced by the current and charge sources residing on the surface of a circular cylinder of radius a. As mentioned in previous section, $\{\hat{\phi}e^{jn\phi}\}$ form a complete set of eigenfunctions for vector surface currents $\mathbf{J}_\phi$. Similarly, $\{e^{jn\phi}\}$ forms a complete set of eigenfunctions for the scalar surface charges ρ_s. Thus the mixed set $\{\hat{\phi}e^{jn\phi}, e^{jn\phi}\}$ is a complete set of basis functions for the AEFIE operator (5.31). It is a fairly straight-forward exercise to obtain the following result,

$$-\begin{Bmatrix} \hat{\mathbf{n}} \times \mathbf{E}^i \\ \alpha \hat{\mathbf{n}} \cdot \mathbf{E}^i \end{Bmatrix} = \frac{-\omega\mu\pi a}{2} \begin{bmatrix} Z_{11} & Z_{12} \\ Z_{21} & Z_{22} \end{bmatrix} \begin{Bmatrix} \hat{\phi}e^{jn\phi} \\ e^{jn\phi} \end{Bmatrix} \tag{5.44}$$

$$Z_{11} = \frac{1}{2}(J_{n+1}(\kappa a)H^{(2)}_{n+1}(\kappa a) - J_{n-1}(\kappa a)H^{(2)}_{n-1}(\kappa a)) - \alpha\frac{jn}{a} \tag{5.45}$$

$$Z_{12} = \frac{n}{\kappa a}J_n(\kappa a)H^{(2)}_n(\kappa a) - j\alpha\kappa \tag{5.46}$$

$$Z_{21} = \alpha\left(\frac{1}{2j}(J_{n+1}(\kappa a)H^{(2)}_{n+1}(\kappa a) + J_{n-1}(\kappa a)H^{(2)}_{n-1}(\kappa a))\right) \tag{5.47}$$

$$Z_{22} = \alpha\left(\frac{1}{j}J_n(\kappa a)H^{\prime(2)}_n(\kappa a) + \frac{1}{jk}\right) \tag{5.48}$$

Note that the eigenvalues of the above operator can be obtained through numerical solution only. Instead, the behaviour of the four individual operators can be studied separately. Comparing with (5.24), it can be concluded that the spectrum of the operator $\mathcal{A}^n_\phi$ is similar to that of tMFIE and hence it is bounded and compact. Figure 5.3 shows the evaluation of function $J_n(\kappa a)H_n(\kappa a)$ for different values of κa and n. It is evident that the spread of eigenvalues is bounded and accumulates at

origin for large values of n. Thus the remaining three AEFIE operators - $\mathcal{A}_{\mathbf{J}}^{t}$, $\mathcal{A}_{\mathbf{J}}^{n}$, $\mathcal{A}_{\phi}^{t}$ are also bounded. Notice that the addition of continuity condition as penalty term, to $\mathcal{A}_{\mathbf{J}}^{t}$, shifts the eigenvalues away from origin and hence acts as a *preconditioner*. Thus, this analysis shows that the operators forming the diagonal sub-matrices of the new AEFIE formulation are bounded and compact. Which in turn implies that the resulting numerical system of equations from the new AEFIE formulation is well conditioned.

5.3.2 3D Problems

The AEFIE formulation, developed above for 2D, can be extended to 3D problems also. One of the important observations in the 2D case is that the constant vector current is the only null space of the divergence $\mathcal{D}$ operator. This observation is specific for 2D closed geometries and is crucial to application of the deflation technique discussed above. In general, all solenoidal currents are elements of null space of the divergence operator $\mathcal{D}$ and there is no restriction on number of these solenoidal currents in 3D. It is well known that the surface vector field on a triangular discretization of a closed 3D surface, with N nodes and M triangles, can be represented with $3M/2$ vector basis functions. Further, these basis functions can be separated into N purely solenoidal and $3M/2 - N$ non-solenoidal vector basis functions. Hence, in the case of triangular discretizations, the dimension of the null space of the discretized operator $\mathcal{D}$ is N. This implies that one needs to perform multiple deflations, which can be costly and tedious. Instead, a domain decomposition framework is adopted in the 3D case. This approach relies on the fact that, given a set of basis function, the solenoidal and non-solenoidal contribution to the total surface current $\mathbf{J}$ can be readily identified. This decomposition of surface currents is well known in literature as loop-star, tree-co-tree, loop-tree decomposition and is not unique for a given surface triangulation. Testing functions are also decomposed in this manner. The resulting

discretized AEFIE formulation can be written as

$$\begin{bmatrix} Z^t_{LL} & A_{12} \\ A_{21} & A_{22} \end{bmatrix} \begin{Bmatrix} \mathbf{J}_L \\ \tilde{\mathbf{J}} \end{Bmatrix} = \begin{Bmatrix} \mathbf{E}^i_L \\ \tilde{\mathbf{E}^i} \end{Bmatrix} \tag{5.49}$$

$$A_{12} = \begin{bmatrix} Z^t_{LT} & Z^t_{L\rho} \end{bmatrix}^T \tag{5.50}$$

$$A_{21} = \begin{bmatrix} Z^t_{TL} & Z^n_{\rho L} \end{bmatrix}^T \tag{5.51}$$

$$A_{22} = \begin{bmatrix} Z^t_{TT} - \alpha\nabla\cdot & Z^t_{T\rho} - \alpha I \\ \alpha Z^n_{\rho T} & \alpha Z^n_{\rho\rho} \end{bmatrix} \tag{5.52}$$

$$\tilde{\mathbf{E}^i} = \begin{Bmatrix} \mathbf{E}^i_T & \alpha E^i_\rho \end{Bmatrix}^T \tag{5.53}$$

$$\tilde{\mathbf{J}} = \begin{Bmatrix} \mathbf{J}_T & \rho \end{Bmatrix}^T \tag{5.54}$$

where the subscripts $\mathbf{J}_L$ and $\mathbf{J}_T$ represent the solenoidal (loop or co-tree) and non-solenoidal (tree or star) parts of the total current $\mathbf{J}$, Z^t_{mn} and Z^n_{mn} is the respective discretized form of the tangential and normal field IE operator representing the contribution from source type $n = \{L, T, \rho\}$ and testing function of type $m = \{L, T, \rho\}$. As expected, the differential operator $\mathcal{D}$ *preconditions* the matrix elements corresponding to non-solenoidal source and testing basis functions only. Hence, in the above equation, the sub-matrix A_{22} is expected to be well conditioned with bounded spectrum and Z_{LL} is only bounded. Schur complement is a well known method to solve such decoupled system of equations. Here the Schur complement, inverse of the smaller sub-matrix, is computed and used in the iterative solution. In AEFIE, assume that the inverse of Z_{LL} is explicitly computed, then the Schur complement solution can be written as

$$\tilde{\mathbf{J}} = \left[A_{22} - A_{21} Z^{-1}_{LL} A_{12}\right]^{-1} \left(\tilde{\mathbf{E}^i} - A_{21} Z^{-1}_{LL} \mathbf{E}^i_L\right) \tag{5.55}$$

Here it cannot be guaranteed by any means that Z_{LL} will be a considerably small matrix. Since Z_{LL} is guaranteed to be well conditioned, the inverse in above equation can be replaced with an iterative solution. Thus the Schur complement solution offers a reasonable means of exploiting the well conditioned nature of the diagonal sub-matrices.

5.4 Results

In this section, results are presented to validate the well-conditioned nature of the proposed AEFIE formulation in both 2D and 3D. In both 2D and 3D, different geometrical configuration were considered and condition number was computed for a wide range of incident frequencies.

The 2D AEFIE formulation with deflation is first validated by comparing the numerical solution for surface currents on a circular cylinder with the analytical solution, as shown in figure 5.4. There is an excellent match between the two solutions and hence validates the numerical implementation of the proposed AEFIE formulation. Figure 5.5 shows the singular values of AEFIE system before and after application of deflation. As discussed in previous section, the deflation techniques successfully eliminates the defective singular values to improve the condition number of AEFIE formulation. The 2D AEFIE formulation was applied to cylindrical objects of various shapes as the frequency was varied from 3Hz to 30 GHz for each geometry. In each case, the chosen discretization rate corresponds to $\lambda/10$ at 30 GHz and the same discretization was used across the frequency range. Figure 5.6 shows the condition number of 2D AEFIE formulation and that of a conventional tEFIE approach (5.1) for circular geometry. As expected, the condition number of the tEFIE formulation monotonously increases as the frequency reduces. The condition number of AEFIE stays constant across the entire frequency range, complementing the theoretical arguments in above

section. Next, the condition number of AEFIE formulation is computed for elliptical cylinders of different aspect ratio. As expected, the condition number of AEFIE formulation remain constant across the wide range of frequencies, while that of tEFIE increases monotonously as frequency reduces. The elliptical surface were formed by nodes located $\{x_n, y_n\} = \{A\sin(n\Delta_\phi)+\cos(n\Delta_\phi), A\cos(n\Delta_\phi)+\sin(n\Delta_\phi)\}$ where Δ_ϕ controls the discretization rate and A denotes the aspect ratio. Thus the variation in discretization size is large for ellipse with larger aspect ratio. As seen from the figure 5.7, though the condition number of AEFIE increases with aspect ratio the variation is negligible and are within the same order of magnitude. With regard to tEFIE formulation, the behaviour of condition number with frequency was almost the same for different aspect ratios. Figure 5.8, presents the condition number of a singular geometry formed by an intersection of triangle and half-circle. Again, the discretization points were generated at constant angles and this geometry is representative of a multiscale structure in 2D. The condition number of AEFIE formulation remains constant and relatively low across the range of frequencies, while the condition number of tEFIE formulation increases at lower frequencies.

Next, the AEFIE formulation was applied to three different 3D geometries: sphere, NASA almond and cone-sphere geometry. Here the sphere geometry was discretized at a uniform rate. NASA almond and cone-sphere geometry are representative of multiscale structures, as they contain dense discretizations to capture sharp details. In each case, the condition number of the operators Z_{LL} and A_{22} involved in Schur complement solution (5.55) and the conventional tEFIE formulation were computed at three different frequencies - 30 Hz, 3 KHz, 3MHz. Table 5.1 shows the condition number for these numerical experiments with a simple loop-star decomposition [186] to represent the solenoidal and non-solenoidal parts of the current. As expected, the condition the number of tEFIE formulation increases as the frequency is reduced. The condition number of diagonal sub-matrices of AEFIE formulation remains constant

across the frequency range. Though the condition number behaviour is favorable with respect to frequency, these are quite high for use in practice. As an alternative, the solenoidal and non-solenoidal current decomposition were numerically orthogonalized. The resulting condition numbers of AEFIE operators Z_{LL} and A_{22} are shown in Table 5.2. For comparision, the modified tEFIE operators with the same orthogonal basis function is also included in Table 5.2. In comparision to Table 5.1, the use of orthogonal basis functions improves the condition number of AEFIE operators considerably. Further, the condition numbers of AEFIE formulation is either comparable or better than the the modified-tEFIE formulation. However, it must be noted that the construction of orthogonal basis functions is a computationally intensive process as the cost scales quadratically with the number of unknowns. Efficient means of obtaining these basis function is a current and widely investigated topic of research and is part of the future work.

Table
positi

Table 5.1: 3D AEFIE condition numbers with loop-star decomposition

Freq.	Z	A_{11}	A_{22}
	Sphere		
30 MHz	9.18E+02	2.59E+02	2.21E+03
30 Khz	9.20E+08	2.60E+02	2.03E+03
30 Hz	2.20E+15	2.60E+02	2.03E+03
	Cone-Sphere		
30 MHz	2.17E+05	2.10E+03	1.20E+06
30 Khz	2.38E+08	2.07E+03	4.48E+04
30 Hz	1.23E+18	2.00E+03	1.94E+05
	Thin-Almond		
30 MHz	3.19E+05	5.50E+05	1.80E+07
30 Khz	3.20E+11	5.50E+05	1.80E+07
30 Hz	1.38E+15	5.50E+05	4.43E+07

Table 5.2: 3D AEFIE condition numbers with orthogonal, quasi-Helmholtz decomposition

Freq.	A_{11}	A_{22}	Ortho-LS
	Sphere		
30MHz	2.80E+01	1.00E+02	359
30KHz	2.60E+01	2.46E+02	360
30 Hz	2.60E+01	2.50E+02	360
	Thin-Almond		
30MHz	8.50E+02	2.40E+05	1.20E+05
30KHz	8.50E+02	5.88E+05	5.80E+05
30 Hz	8.50E+02	2.40E+05	
	Cone-Sphere		
30MHz	1.40E+02	5.54E+02	8.08E+04
30 KHz	1.39E+02	9.79E+03	
30 Hz	1.39E+02	1.24E+03	8.08E+04

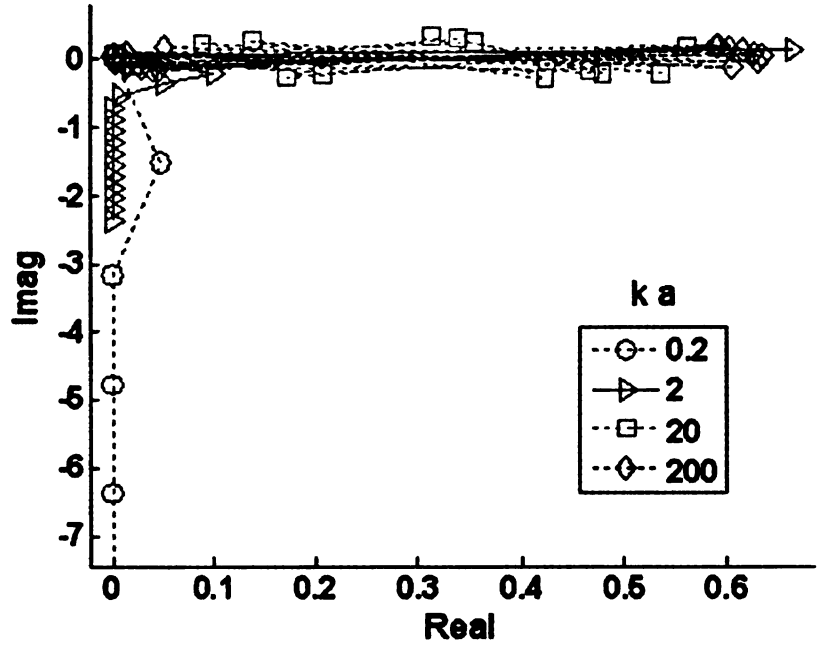

Figure 5.1: Eigenvalue spectrum of $J_n'(\kappa a)H_n^{'(2)}(\kappa a)$ corresponding to 2D-tEFIE operator (5.20).

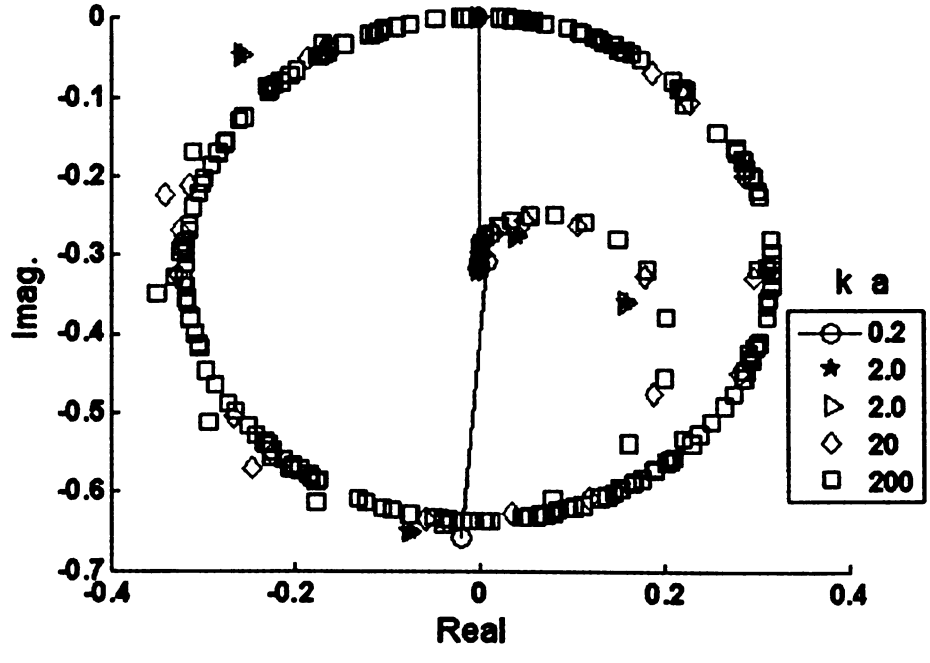

Figure 5.2: Eigenvalue spectrum of $J_n(\kappa a)H_n^{'(2)}(\kappa a)$ corresponding to 2D-tMFIE operator (5.24).

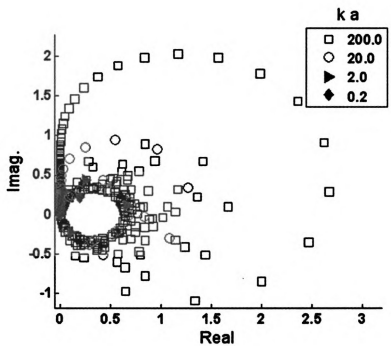

Figure 5.3: Eigenvalue spectrum of $J_n(\kappa a)H_n(\kappa a)$ corresponding to some of the AEFIE operators.

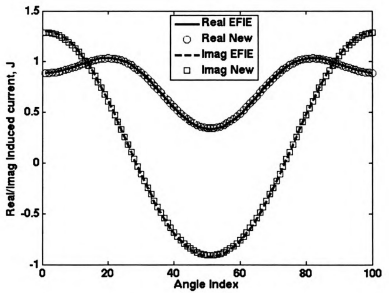

Figure 5.4: Surface current on 2D circular cylinder computed using 2D AEFIE and analytical solution.

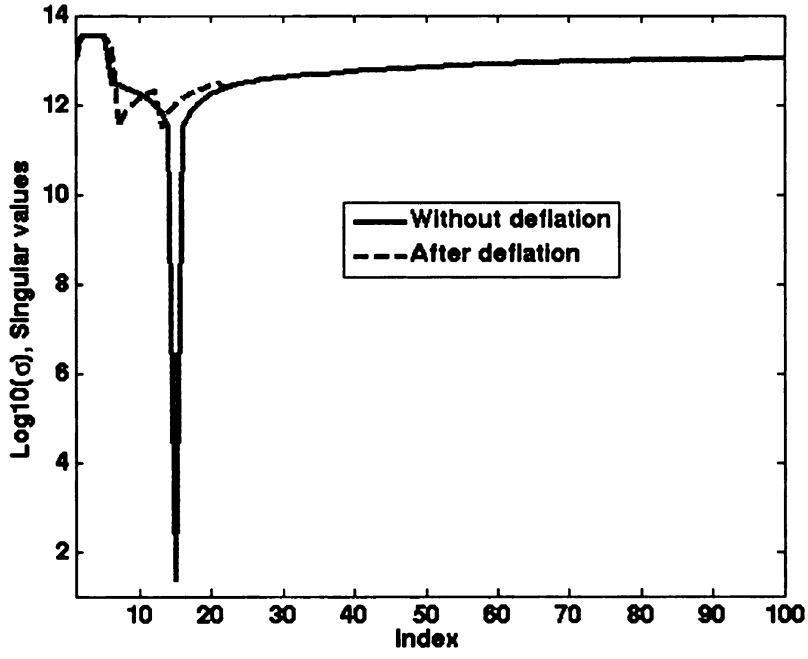

Figure 5.5: Singular values of 2D-AEFIE formulation before and after deflation.

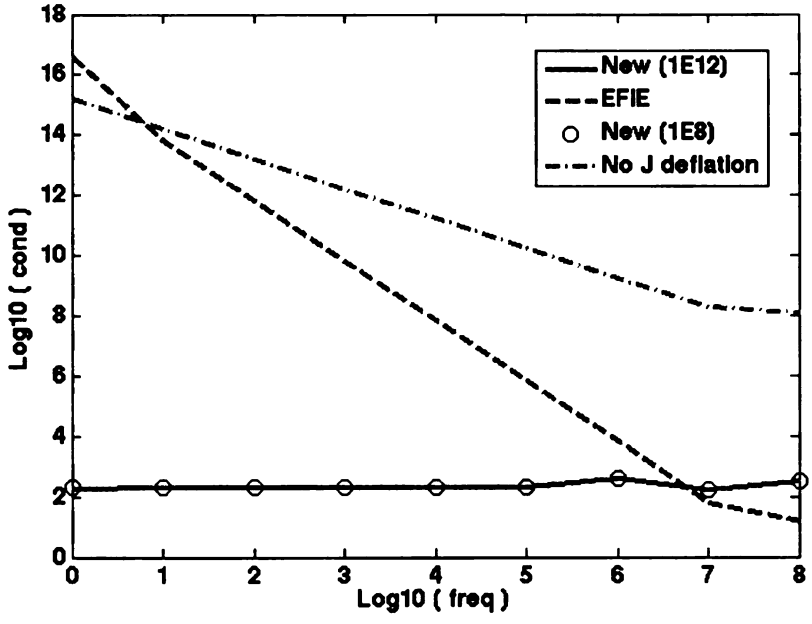

Figure 5.6: 2D AEFIE condition number vs. frequency for circular cylinder.

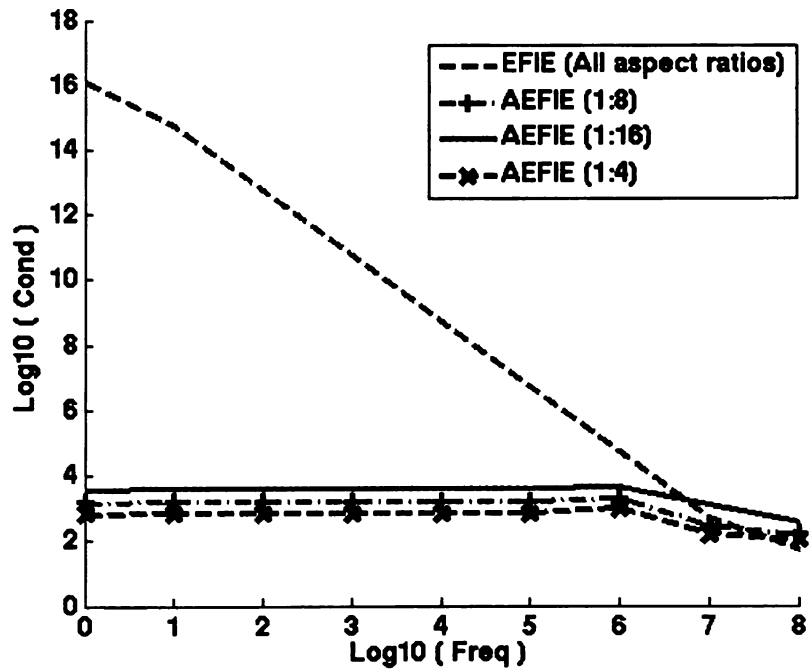

Figure 5.7: 2D AEFIE condition number vs. frequency for elliptical cylinders with different aspect ratios.

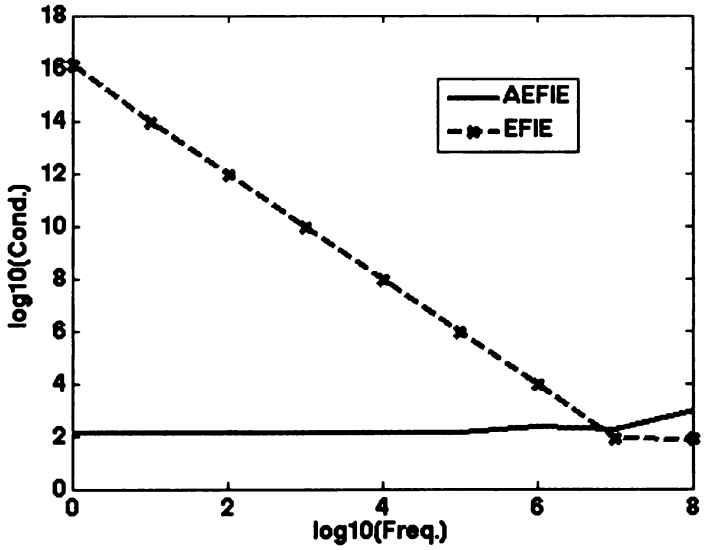

(a)

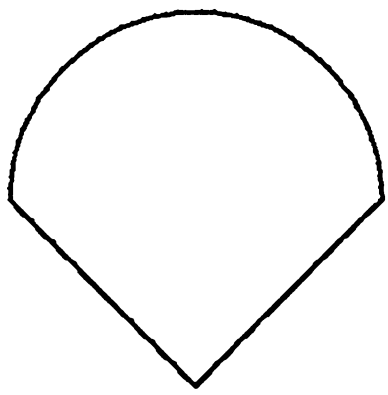

(b)

Figure 5.8: (a) Shows the 2D AEFIE condition number vs. frequency for a 3D multiscale geometry and (b) shows the geometry

Chapter 6

Algorithms for Implementation of Hierarchical Computations on Parallel, Distributed Computers

In this Chapter, parallel algorithms are developed for efficient implementation of algorithms described in previous chapters on distributed parallel or *cluster* computers. Section 6.1 provides a brief introduction to the existing approaches for parallel implementation of FMM. Section 6.2 provides a succinct summary of the integral equation solver for electromagnetic simulation (EM) and the wideband FMM, developed in the Chapter 4, for multiscale EM simulations. Section 6.3 is devoted to the details of the parallel algorithm proposed in this work. This section expounds on the parallel implementation of every step of the hierarchical tree computation. Section 6.4 presents a plethora of results that demonstrate the scalability and efficiency of the proposed algorithm.

6.1 Introduction

It is well known that integral equation (IE) methods are well-suited to model fields propagating in unbounded media as they impose exact radiation boundary condition and, in many cases, requires discretization of the boundary surfaces only [183]. The principle bottleneck to the popularity of IE based solver was its computational complexity; both memory and time scale as $\mathcal{O}(N^2)$, where N is the number of spatial degrees of freedom. In the past two decades, several fast algorithms have been developed to ameliorate the computational complexity of IE based solvers. These can be broadly classified [33] into (a) fast multipole methods (FMM), (b) fast Fourier transform (FFT) based approaches and (c) numerical compression schemes. FMM and its variants have enjoyed a widespread popularity [6, 8, 174], and the rest of the paper will focus on the further development of FMM based methods. FMM was first developed for the Laplace potential used in static problems [6, 8] and was later extended to the Helmholtz potential [30] for use in electromagnetic simulations [65]. The development of similar fast methods, combined with the explosive growth in the computing power, have enabled simulation of realistic structures with complex geometric features [198]. Many of these simulations fall under the category of multiscale problems that exhibit multiple scales in length or frequency or both. It is well known that classical FMM suffers from low frequency breakdown [42, 44], and several modifications have been proposed to overcome this limitation [46, 49, 50, 198, 180]. In this work, the wideband FMM, as described in the Chapter 4, is constructed as a hybrid combination of accelerated Cartesian expansion (ACE) and FMM is used for multiscale simulations.

The developments of fast methods has increased the size of the problems being analyzed from thousands to millions of unknowns [36, 199, 200]. As the problem size exceeds few millions of unknowns, the serial implementation of above fast algorithms

on single processor machines face severe limitations in terms of computational memory and speed. This, along with inexpensive and widespread availability of distributed or cluster computers serves as the motivation for exploring the parallel implementation of FMM [127, 37, 200, 201]. However, the algorithmic sophistication of the fast methods makes the development of efficient parallel algorithms difficult. FMM relies on (i) tree data structure to hierarchically partition the computational geometry and (ii) an alternate representation of the Greens function using multipoles. Several different approaches to partitioning the tree-data have been explored and they can be broadly classified into (a) spatial partitioning, (b) direction partitioning and (c) hierarchical partitioning. In spatial partitioning, the nodes of the tree are distributed among the P processors and harmonic expansions associated with a nodes is completely contained within the processor it resides in. This approach is effective when the number of harmonic expansions associated with a node is constant, as in the case of the Laplace FMM. While spatial partitioning has been successfully used for the computation of electrostatic interactions in molecular dynamic simulations [202, 203, 204, 205, 206, 207], it is not efficient when applied to the case of Helmholtz FMM; where the number of harmonic expansions associated with a node depend on its level in the tree. This led to the development of direction partitioning strategy [208, 209]. In this approach, spatial partitioning is used up to a particular level and beyond this level the nodes are duplicated in all processors and their harmonic expansions are partitioned among the processors [208]. The level beyond which direction partitioning is used is determined by heuristics or a one time tuning analysis. Though this approach does not ensure scalability beyond hundreds of processors, it has been well exploited to solve problems with several millions of unknowns on smaller clusters [210, 209]. Hierarchical partitioning was developed recently as a combination of spatial and direction partitioning approaches [211, 212]. Here spatial partitioning is used at the leaf level, and a systematic combination of spatial and direction partitioning is

used at all other levels. This approach shows the promise of being provably scalable albeit with a tight relation between N and P [212].

In this Chapter, a parallel implementation of the wideband FMM [198] is developed that is scalable on large number of processors. This is achieved by developing strategies that ensure self-similar distribution of tree data and lead to an algorithm that is implicitly load balanced. This work extends the recent developments in parallel algorithms for Laplace FMM [206, 213] to the Helmholtz FMM. The resulting parallel algorithm offers a seamless combination of spatial and direction partitioning strategies. It is well known, from Amdahl's law, that the maximum parallel speed-up achieved is limited by the minimum time spent on serial computations of an algorithm. Hence the parallel implementation of every step of the tree computation algorithm is presented along with their cost analysis. The main contributions of this Chapter are: we present,

1. a scalable parallel algorithm for hierarchical tree computations.

2. theoretical bounds on the parallel performance of the presented algorithm.

3. a scalable parallel EM solver for wideband-FMM.

6.2 Preliminaries

Consider the electromagnetic scattering from a closed perfect electric conductor (PEC) that is immersed in free space. Let S denote the surface of this object that is equipped with a unit outward pointing normal $\hat{\mathbf{n}}$. Electromagnetic fields denoted by $\{\mathbf{E}^i(\mathbf{r}), \mathbf{H}^i(\mathbf{r})\}$ are incident upon the object. The incident field induces an electric current $\mathbf{J}(\mathbf{r})$ that radiates scattered fields $\{\mathbf{E}^s(\mathbf{r}), \mathbf{H}^s(\mathbf{r})\}$. The unknown current $\mathbf{J}(\mathbf{r})$ can be found by solving the combined field integral equation (CFIE), that may be

written as

$$\alpha\hat{\mathbf{n}} \times \hat{\mathbf{n}} \times \mathbf{E}^t(\mathbf{r}) + (1-\alpha)\hat{\mathbf{n}} \times \mathbf{H}^t(\mathbf{r}) = 0 \quad \mathbf{r} \in S^- \tag{6.1}$$

where $\mathbf{E}^t = \mathbf{E}^i + \mathbf{E}^s$ and $\mathbf{H}^t = \mathbf{H}^i + \mathbf{H}^s$ are the total electric and magnetic fields, respectively, S^- is a surface conformal to and just inside S and $\alpha \in [0,1]$ is an arbitrary scalar constant. The scattered electromagnetic fields are related to $\mathbf{J}(\mathbf{r})$ through the dyadic Green's function,

$$\hat{\mathbf{n}} \times \hat{\mathbf{n}} \times \mathbf{E}^s(\mathbf{r}) = \mathcal{L}_e\{\mathbf{J}(\mathbf{r})\} = \hat{\mathbf{n}} \times \hat{\mathbf{n}} \times \int_S ds \overline{\overline{G}}_\kappa(\mathbf{r},\mathbf{r}') \cdot \mathbf{J}(\mathbf{r}') \tag{6.2}$$

$$-\hat{\mathbf{n}} \times \mathbf{H}^s(\mathbf{r}) = \mathcal{K}_m\{\mathbf{J}(\mathbf{r})\} = \hat{\mathbf{n}} \times \frac{1}{j\kappa\eta} \int_S ds \nabla \times \left[\overline{\overline{G}}_\kappa(\mathbf{r},\mathbf{r}') \cdot \mathbf{J}(\mathbf{r}')\right] \tag{6.3}$$

$$\overline{\overline{G}}_\kappa(\mathbf{r},\mathbf{r}') = -j\kappa\eta\left(\bar{\bar{I}} + \frac{\nabla\nabla}{\kappa^2}\right) g(\mathbf{r},\mathbf{r}') \tag{6.4}$$

$$g(\mathbf{r},\mathbf{r}') = \frac{e^{-j\kappa|\mathbf{r}-\mathbf{r}'|}}{4\pi|\mathbf{r}-\mathbf{r}'|} \tag{6.5}$$

In above relations, κ is the wavenumber, η is the characteristic impedance of free space, $\bar{\bar{I}}$ is the identity dyad and g is the scalar Green's function. Typically, the unknown currents $\mathbf{J}(\mathbf{r})$ are represented using RWG vector basis functions $\mathbf{f}_m(\mathbf{r})$ [181] and the system of matrix equations obtained by using a Galerkin testing procedure is

$$\mathcal{Z}\mathcal{I} = \mathcal{V} \tag{6.6}$$

The fast evaluation of the matrix-vector product relies on the rapid evaluation of the scalar potential. Hence, with no loss of generality, consider the evaluation of the scalar potential ψ due to N sources

$$\psi(\mathbf{r}) = \sum_{i=1}^{N} \frac{e^{-j\kappa|\mathbf{r}-\mathbf{r}_i|}}{|\mathbf{r}-\mathbf{r}_i|} w_n w_i \tag{6.7}$$

Variation to the vector case is well established [65] and will not be elucidated here.

6.2.1 The Fast Multipole Method

Consider the evaluation of the potential $\psi(\mathbf{r})$ at a point $\mathbf{r}$ that is well-separated from a cluster of sources that reside within a sphere of radius d. The FMM expansions that enables the fast evaluation of this potential is given as [65]

$$\begin{aligned}
\psi(\mathbf{r}) &= \frac{-j\kappa}{4\pi}\int d^2\hat{\kappa}\mathcal{M}(\mathbf{r}_s,\mathbf{k})\mathcal{T}(\mathbf{r}_o-\mathbf{r}_s,\mathbf{k})w_n e^{-j\mathbf{k}\cdot(\mathbf{r}-\mathbf{r}_o)} && \text{(6.8a)}\\
&= \frac{-j\kappa}{4\pi}\int d^2\hat{\mathbf{k}}w_n e^{-j\mathbf{k}\cdot(\mathbf{r}-\mathbf{r}_o)}\mathcal{L}(\mathbf{r}_o,\mathbf{k}) && \text{(6.8b)}\\
\mathcal{M}(\mathbf{r}_s,\mathbf{k}) &= \sum_{i=1}^{K} w_i e^{-j\mathbf{k}\cdot(\mathbf{r}_s-\mathbf{r}_i)} && \text{(6.8c)}\\
\mathcal{T}(\mathbf{x},\mathbf{k}) &= \sum_{l=0}^{\infty}(-j)^l(2l+1)h_l^{(2)}(\kappa|\mathbf{r}|)P_l(\hat{\mathbf{k}}\cdot\hat{\mathbf{x}}) && \text{(6.8d)}\\
\mathcal{L}(\mathbf{r}_o,\mathbf{k}) &= \mathcal{M}(\mathbf{r}_s,\mathbf{k})\mathcal{T}(\mathbf{r}_o-\mathbf{r}_s,\mathbf{k}) && \text{(6.8e)}
\end{aligned}$$

where $|\mathbf{r}_o-\mathbf{r}_s|>2d$, $|\mathbf{r}-\mathbf{r}_o|\leq d$, $|\mathbf{r}'-\mathbf{r}_s|\leq d$, $\mathbf{k}=\kappa\hat{\mathbf{k}}$, $\mathbf{r}_s$ ($\mathbf{r}_o$) is the center of multipole (local) expansion $\mathcal{M}$ ($\mathcal{L}$) for source (observation) cluster, $\mathcal{T}$ is the translation operator, $h_l^{(2)}$ and P_l denotes an order l spherical Hankel function of second kind and Legendre polynomial, respectively. The translation operator contains a spherical Hankel function which is singular at the origin. Thus, for numerical stability, neither the translation distance $|\mathbf{x}|$ nor the wavenumber κ can be arbitrarily small [73, 76]. Hence, the classical FMM is inefficient or numerically unstable when applied to sub-wavelength problems, where the domain is discretizated at a rate higher than $\lambda/10$ to capture the geometric details. These limitations have been reported in detail in [74] and several alternatives have been proposed to overcome them [46, 49, 50, 174]. In this work, the stable accelerated Cartesian expansion (ACE) [198] described in Chapters 2 and 4 is used for the sub-wavelength problems. Following section briefly presents the ACE algorithm and its integration with FMM to create a wideband FMM.

6.2.2 Accelerated Cartesian Expansion (ACE)

ACE is a hierarchical tree computation algorithm that employs the generalized Taylor's expansion to derive alternate representation of the Green's function. The construction of ACE algorithm is similar to FMM in that it uses the oct-tree for geometry processing and derives equivalent operators for tree computation. In contrast, ACE employs Cartesian harmonics as multipole and local expansions. Use of Taylor's series expansion for fast computation has been explored previously albeit with severe limitation on accuracy and performance. ACE provides a generic framework by adopting a tensorial formulation to exploit the full power of Taylor's series expansion for fast computation. In rest of the paper, $\mathbf{M}^{(n)}$ denotes a tensor of rank n, the *polyadic* associated with $\mathbf{r} = \{r_x, r_y, r_z\}$ is given by $\mathbf{r}^{(n)} = \{r_x^{n_1} r_y^{n_2} r_z^{n_3}\}$ where $n = \sum_{i=1}^{3} n_i$ and $n_i > 0$, an m fold contraction between two tensors $\mathbf{A}^{(n)}$ and $\mathbf{B}^{(m)}$ is denoted by $\mathbf{A}^{(n)} \cdot m \cdot \mathbf{B}^{(m)} = \mathbf{C}^{(n-m)}$ when $n > m$; for more details on these definitions and operations see [182, 13].

The ACE expansions for computing the potential in (6.7) can be written as

$$\psi(\mathbf{r}) = \sum_{n=0}^{\infty} w_n \mathbf{M}^{(n)}(\mathbf{r}_s) \cdot n \cdot \mathbf{T}^{(n)}(\mathbf{r}_s, \mathbf{r}) \tag{6.9}$$

$$= \sum_{n=0}^{\infty} w_n (\mathbf{r}_o - \mathbf{r})^{(n)} \cdot n \cdot \mathbf{L}^{(n)}(\mathbf{r}_o) \tag{6.10}$$

$$\mathbf{M}^{(n)}(\mathbf{r}_s) = \sum_{i=1}^{K} (-1)^n \frac{w_i}{n!} (\mathbf{r}_i - \mathbf{r}_s)^n \tag{6.11}$$

$$\mathbf{T}^{(n)}(\mathbf{r}_s, \mathbf{r}_o) = \nabla^n \frac{e^{-j\kappa|\mathbf{r}_o - \mathbf{r}_s|}}{|\mathbf{r}_o - \mathbf{r}_s|} \tag{6.12}$$

$$\mathbf{L}^{(n)}(\mathbf{r}_o) = \sum_{m=n}^{\infty} \frac{1}{n!} \mathbf{T}^{(n)}(\mathbf{r}_s, \mathbf{r}_o) \cdot (m-n) \cdot \mathbf{M}^{(m-n)} \tag{6.13}$$

where $\mathbf{M}^{(n)}$ and $\mathbf{L}^{(n)}$ denote the n-th order multipole and local expansion Cartesian harmonics and $\mathbf{T}^{(n)}$ is the ACE translation operator. ACE is an *almost kernel in-*

dependent method as (a) all quantities of the ACE algorithm, except the translation operator, are independent of the form of the kernel and (b) the ACE expansions are rapidly converging for any *non-oscillatory function* [13, 61, 174, 214]. Readers interested in the details and other salient features of the ACE algorithm are referred to [13]. In the case of the Helmholtz potential, the ACE translator operator is given as [174],

$$\begin{aligned}\mathbf{T}^{(n)}(\mathbf{r}_s,\mathbf{r}_o)=\nabla^n\frac{e^{-j\kappa R}}{R}(n_1,n_2,n_3)=&\sum_{m_1=0}^{\lfloor\frac{n_1}{2}\rfloor}\sum_{m_2=0}^{\lfloor\frac{n_2}{2}\rfloor}\sum_{m_3=0}^{\lfloor\frac{n_3}{2}\rfloor}(-1)^{n+m}R^{2m-2n-1}\\&\times\begin{bmatrix}n_1\\m_1\end{bmatrix}\begin{bmatrix}n_2\\m_2\end{bmatrix}\begin{bmatrix}n_3\\m_3\end{bmatrix}\\&x^{n_1-2m_1}y^{n_2-2m_2}z^{n_3-2m_3}\mathcal{G}(n-m,\kappa R)\end{aligned}\tag{6.14}$$

where

$$\mathcal{G}(n,\kappa R)=\sqrt{2/\pi}(j\kappa R)^{(n+0.5)}K_{n+0.5}(j\kappa R)$$

$$\begin{bmatrix}n\\m\end{bmatrix}=\frac{n!}{2^m m!(n-2m)!}$$

where, $n=n_1+n_2+n_3$, $m=m_1+m_2+m_3$, $K_n(\cdot)$ represents the modified Hankel function of order n, $R=\sqrt{x^2+y^2+z^2}$ and $\lfloor\cdot\rfloor$ is the *floor* operation. It is well known that above Taylor's series expansion is convergent when either the domain size or frequency is small or both. Further, it has been rigorously shown that as frequency tends to zero the ACE expansion seamlessly transitions to Laplace FMM [198].

6.2.3 Hybrid algorithm for multiscale problems

Multiscale problems, by definition, contains a mixture of sub-wavelength and large-wavelength problems. From above discussions it can be seen that the ACE algorithm for evaluation of Helmholtz potential is stable and efficient for sub-wavelength problems; while, FMM algorithm is efficient and optimal for large-wavelength problems. Thus, individually neither of the two algorithm is efficient for multiscale problems. A hybrid approach, where both ACE and FMM expansions are used in an optimal and seamless fashion, is required to achieve full efficiency with multiscale geometries. This implies that one needs to develop transition operators to switch from ACE to FMM and vice versa [198]. These maps are given by

$$\mathcal{M}(\mathbf{r}_s, \mathbf{k}) = \sum_{p=0}^{\infty} \mathbf{M}^{(p)}(\mathbf{r}_A) \cdot p \cdot \mathbf{T}^{(p)}_{map}(\mathbf{k}, \mathbf{r}_s - \mathbf{r}_A) \tag{6.15}$$

$$\mathbf{L}^{(p)}(\mathbf{r}_A) = \frac{-j\kappa}{4\pi} \int d^2\hat{\mathbf{k}} \mathbf{T}^{(p)}_{map}(\mathbf{k}, \mathbf{r}_o - \mathbf{r}_A) \mathcal{L}(\mathbf{k}, \mathbf{r}_o) \tag{6.16}$$

where $\mathbf{r}_A$ denotes the center of ACE multipole expansion $\mathbf{M}^{(p)}$ and the mapping operator $\mathbf{T}_{map}$. The derivation of T_{map} and the proof of convergence can be found in [198].

The overall wideband FMM algorithm proceeds as shown in Algorithm 2. The computational geometry is represented using a compressed oct-tree [51, 61]. This is constructed by first embedding a cube enclosing the computational domain and recursively sub-dividing the large *parent* cubes into eight smaller, non-overlapping *children* cubes The boxes at the lowest level of the tree, beyond which no sub-division occurs, are referred to as the leaf boxes. In rest of the paper, box and nodes are used inter-changeably. Interaction list is constructed for all nodes and nearfield list is constructed for all leaf nodes only [9, 61]. Next, the tree nodes are classified as ACE or FMM, based on the side length of the domain they represent. All nodes

representing domains less than a certain pre-determined size, typically $\lambda/4$ or $\lambda/2$, are classified as ACE nodes and rest of the nodes are labeled as FMM. The ACE to FMM multipole transition operator in (6.15) is used in step 4 and FMM to ACE local expansion transition operator in (6.16) is used in step 6 of the Algorithm 2 [198].

Algorithm 2 Wideband Multilevel Fast Multipole Algorithm

1: Construct the tree representation for the given geometry (distribution of discrete points).
2: Build interaction list for all tree nodes and the near-field list for leaf nodes only.
3: **S2M**: compute multipole expansions at each leaf node from sources contained within it.
4: **M2M** (upward traversal): compute the parent node multipole by combining the multipole expansions at their children node.
5: **M2L** (translation): for all nodes in the tree convert the multipole expansions to local expansions of the nodes in their interaction list.
6: **L2L** (downward traversal): *update* the local expansion information at a child node using the local expansion of their parent node.
7: **L2O**: use the local expansions about each leaf node to compute the *farfield* potential at its observation points.
8: **NF**: use direct method for computation of *nearfield* potential at observation points in each leaf node from sources contained in its near-field nodes.

6.3 Parallel Algorithm for FMM

This section presents the details of the parallel implementation of the ACE (PACE), FMM (PFMM) and the wideband FMM (PACEFMM) algorithm outlined in the previous section. First, a scheme for constructing and partitioning the oct-tree data structure in parallel environment is presented. This is followed by the details on parallel implementation of the individual tree computation steps in Algorithm 2. As mentioned in the introduction, the emphasis of this work is on reducing the latency among processors to ensure the scalability of the algorithm.

6.3.1 Parallel Construction of the Oct-tree

Although the construction of oct-tree is a one time effort and takes up a negligible fraction of the overall parallel run-time, it is important because (a) tree partitioning among the processors directly affects the load balancing of the rest of the algorithm and (b) creation of various interaction lists at this stage are communication-intensive. In our implementation, the tree is stored in postorder traversal order. It will be shown that the resulting ordering of nodes enables load balanced computation of various tree operations, obviating the need for explicit load balancing.

Let N denote the total number of points (sources and observers) distributed within a cubical domain of side length D and P be the number of processors. The average number of points per processor is denoted by $n = N/P$. Given the smallest side length d_0 associated with leaf boxes, the total number of levels or height of the tree is $H = \log_2(D/d_0)$. Integer coding scheme [204] is used to uniquely represent a node in the tree. This has several advantages as (a) the keys encode a wealth of information such as the center position of the box represented by the node, level of the node, its entire ancestral lineage etc., and (b) the sorted keys conform to Morton ordering [215]. Morton ordering of the sorted leaf nodes distributed across processors results in a *self-similar* structure in each processor [199, 216] as shown in figure 6.2. Self-similarity is critical to parallel processing as it ensures that each processor has an identical number of tree-operation. This leads to an implicitly load balanced scheme. The full post-order tree is constructed in a recursive fashion, in each processor, by generating the parent nodes from children nodes. Next, some comments on the distribution of tree-nodes among the processors are provided.

Each processor contains only a part of the tree with nodes at every level as shown in figure 6.3. It is evident that some nodes can occur in multiple processors. When considering the global postorder traversal tree, across processors, each such node is

associated with a processor where its occurrence is appropriate (the processor which has the rightmost leaf box in the subtree of the node). This processor is referred to as the *native* processor for that node and every tree-node has an unique *native* processor. All other occurrences of the node are termed *duplicate nodes* and the following Lemma 6.3.1 provides a bound on number of such nodes.

Lemma 6.3.1. *The number of duplicate nodes in each processor is bounded by the height of the tree, and will appear sequentially at the end of the local postorder traversal tree.*

Proof. Let H denote the height of the tree. A processor can have *at most* one duplicate nodes per level in the tree. The rationale for this statement is as follows: assume that a processor has at least two duplicate nodes at the same level in the tree. Let v_1 and v_2 be two such nodes, with v_2 occurring to the right of v_1 in the tree. A processor has a node in its local tree only if at least one of the leaf boxes in the subtree under the node falls in the same processor. Also, all the leaf boxes in a processor are consecutive in Morton ordering. Taken together, these two observations imply that the rightmost leaf box under v_1 must reside in the same processor. Thus, v_1 is native to this processor and cannot be a duplicated node. This argument demonstrates that a processor can have at most one duplicate node per level, shared with the next processor. Similarly, one can show that the number of multiply occurring nodes that are native to a processor are *limited* to one per level.

The proof that the duplicate nodes will appear sequentially at the end of local postorder traversal tree follows from the fact that the postorder sequencing always places nodes before their parents. The parent of a duplicate node is also a duplicate node in the same processor. Hence all duplicate nodes in a processor appear in sequence at the end of the local postorder traversal tree. □

Next section provides details on the parallel implementation of each step of the

tree computations shown in Algorithm 2. In rest of the Chapter, given any two nodes A and B, A is said to be *less than* B if node A appears earlier than node B in the postorder traversal sequence. This notion of comparison between tree nodes simplifies implementation of several of the processes detailed below.

6.3.2 Distribution of ACE and FMM harmonic data

The above tree partitioning scheme ensures that the nodes are uniformly partitioned among the processors. If the size of data associated with each node is same, then data is also uniformly distributed amongst the processors. This is true only for the ACE portion of the tree; in FMM, the number of expansions depends on the level of the node. Thus the total FMM expansions data contained in the *native processors* is considerably high, leading to severe load imbalance during tree computations. Though this load imbalance is bounded, due to Lemma 1, it undermines the scalability of the algorithm. A possible remedy is to re-distribute the tree nodes such that the FMM expansions data is uniformly distributed across the processors. This results in the following unfavorable scenarios. First, the optimal re-distribution of nodes may be such that some processors, especially the *native processors*, contain only higher level nodes. This induces latency during upward and downward tree traversals, steps 5 and 6 in Algorithm 2. Second the re-distributed tree is not *self-similar* across processors and affects the parallel efficiency during tree computations. As will be evident, this results in highly scalable parallel scheme.

An alternative approach developed in this is paper is the *adaptive direction partition*. To achieve uniform distribution of FMM expansion data, direction partitioning [37] is employed for duplicate nodes only. The FMM expansions data of a duplicate node is partitioned such that each copy contains an equal and distinct portion. This scheme and the self-similar distribution of the tree automatically ensures that each processor has an equal quantity of FMM harmonics data. The nodes to be parti-

tioned and the number of partitions are decided automatically, resulting in implicit load balancing. This approach bears some similarity to the recently introduced hierarchical partitioning approach, where the multipole data of all nodes except the leafs are partitioned [211, 212]. This imposes a strict relation between N and P for scalability. In contrast, the *adaptive direction partition* scheme is flexible and differs in the following manner: (a) it combines the spatial and direction partitioning in a seamless manner; (b) direction partitioning is used *only* when its optimal; and (c) it provides a means of preserving the *self similarity* of tree computations.

6.3.3 Construction of Interaction Lists

Tree computation requires the construction of interaction and nearfield lists. Interaction lists are built for all the nodes in the local tree except duplicate nodes. This operation is split into serial and parallel portions. In the serial portion, the interaction list of each node is built assuming that the *full* tree is constructed [199]. Given a node's key code, straightforward bit manipulation yields its parent node, the parent's neighbor nodes and their children. This information is used to construct the interaction list of each local node. Due to locality there is no communication cost associated with this operation. In the parallel portion, the non-existent nodes are eliminated using one time communication. At this stage, different communication *maps* are contructed for information exchange during tree traversal. The entire process is efficiently implemented with the use of a binary tree search algorithm to identify nodes in postorder traversal. A similar procedure is used to construct the nearfield list of local leaf nodes.

6.3.4 Multipole and local expansion computation

In each processor, the multipole expansions are computed at every node in the local postorder traversal tree. The postorder traversal order ensures that a parent node appears only after its children nodes (in case of *duplicate nodes*, all children that reside in the same processor). Thus, when a parent node occurs the necessary children multipoles are already computed. Multipole expansiond are computed for all the local nodes, including the *duplicate nodes*. Note that the multipole expansions at the duplicate nodes are only partially filled as they account for sources in that processor only. Thus, after the local computation, all processors with duplicate nodes send their multipole expansions to the appropriate *native processors* of the duplicate nodes they host. The *native processor* of a node simply adds the received multipole expansion data to the appropriate local node. This algorithm is a one step update process with the following bound on communication overhead.

Lemma 6.3.2. *Total number of nodes received by a processor during multipole computation is bounded by* $(P-1)H$.

Proof. This follows from the fact that the number of *duplicate nodes* in a processor is bounded by H (see Lemma 6.3.1). Since only the *duplicate nodes* are exchanged during multipole computations, the maximum number of nodes received by any processor will be no more than $(P-1)H$. □

The computation of local expansion is a reverse analogue of multipole computation. In the downward tree traversal, the child node local expansions are updated with the local expansion of their parent node. First, the processors with the duplicate nodes obtain their local expansion from its native processor. Then, the downward tree traversal is performed locally in each processor by traversing the local postorder tree from right to left.

Cost analysis: Each processor has at least one node from every level of the tree and their multipole expansions are computed in every processor by traversing the local postorder traversal tree. Thus, this part of the process is load balanced if every processor has the same number of leaf nodes. This is true even in the case of FMM where the number of multipole harmonics increases as the level increases. Since the number of duplicate nodes per processor is bounded, the communication overhead involved in exchange of their multipole information is also bounded. Hence the overall process is load balanced.

6.3.5 Translation Operation

At each node in the global postorder traversal tree, local expansions are computed using multipole expansions of the nodes in its interaction list. This process is divided into a parallel and serial portion. In the initial parallel portion, multipole information is exchanged between processors. While building the interaction lists for each node in the local postorder traversal tree, the set of processors that require their multipole expansions are identified. This list of local nodes and processors is sorted according to the processor-ID. At every processor, the requisite information is send to the appropriate processors by traversing through this list. In implementation, this data is exchanged in blocks whose size is defined by the user. This serves two purposes (a) the number of communication calls can be greatly reduced when compared to a scheme where the multipole data is exchanged one node at a time, and (b) the block size can be adjusted according to the communication architecture of the distributed environment to ensure an optimum performance. Once the required multipole expansion data is received, the actual translation operation is performed in a serial manner to compute the local expansion of nodes in the local tree. In case of FMM translations, the duplicate nodes exchange and compute only part of their FMM harmonics data in accordance with the *adaptive direction partitioning* strategy. This is possi-

ble due to the diagonal translation operation of the Helmholtz FMM algorithm. In actual implementation the serial and parallel parts are performed in an intertwined fashion such that the translation operation is performed as and when the data is received. Further, *asynchronous* communications can be used to minimize the wait time between the parallel and serial portion.

Cost analysis: The translation operation is reciprocal. Thus, if two interacting nodes are in different processors, then both processors need to exchange same amount of information. This process would be load balanced if all processors receive and process the same amount of multipole data. In case of ACE computations, where the size of harmonics data is constant for all nodes, an uniform partitioning of tree nodes automatically ensures that the data is also uniformly partitioned. The same argument is not true in the case of FMM computation where the number of harmonics is a function of the level of the node. However, the use of *adaptive direction partition* ensures that the data is distributed uniformly across the processors. Hence, this part of the algorithm is also load balanced.

6.3.6 Evaluation of Potential

The farfield potential at the observation points are evaluated from the leaf node local expansion they reside in. However, the evaluation of the potential is completed only after accounting for the nearfield interactions. These are interactions only among leaf boxes, as specified by the nearfield list. Similar to translation operation, for each leaf node a list of processors that require its information is created and then sorted by processor-ID. At every processor this list is used to communicate the leaf box information, in blocks, to appropriate processors. The nearfield potential is computed in a serial manner from the received data. This completes the evaluation of potential at every point across all processors. As in the case of translation operation, the communication and computation parts are intertwined and asynchronous communication is

used to minimize wait time.

6.3.7 Parallel Electromagnetic (EM) Solver

Next, a brief description is provided on the use of the above described parallel ACE and FMM (PACEFMM) algorithm within the framework of EM solvers. When the discretization size is in the orders of millions, the geometry processing to create basis functions, etc. becomes computationally intensive. Though this is a one time process, an efficient parallel implementation is necessary to justify the algorithmic gains obtained with the PACEFMM algorithm to reduce the overall solution time. We assume that the input to the parallel EM solver is a simple mesh file with a list of x, y, z position of each node and the element-to-node connectivity table. Each of the P processors reads an equal share of the N_n nodes and N_e elements from the input mesh file. Using the local element-to-node connectivity, a list of edges is created in each of the P processors. Each edge is represented by the two global node numbers that make the edge and this two element integer array is sorted in parallel. Thus every processor has approximately equal number of edges. The global node numbers allows one to gather the $\{x, y, z\}$ data of the nodes as they are sequentially distributed across the processors. This allows us to compute the centers of each edge which is then used to construct the oct-tree. Based on the distribution of leaf boxes the edge data are exchanged among the processors and the necessary $\{x, y, z\}$ data of related nodes are gathered from their global node number.

6.4 Results

In this Section, we present plethora of results that exhibit scalability of the parallel algorithm presented here. All the results were obtained on a IBM Blue Gene/L cluster with 1024 processors and 512 MB RAM per processor. The message passing interface

(MPI) was used for communication between the processors. In our implementation of the classical FMM, the spherical harmonic filters [23] are used for interpolation and anterpolation during upward and downward tree traversal, respectively. With 512 MB RAM per processor, pre-computation of these filter coefficients places memory constraints and restricts the maximum number of FMM levels to 10 or the overall domain size to 128 λ. First set of results correspond to evaluation of kernel only which helps to study the various aspects of the parallel algorithm. This is followed by the use of these algorithm for solving electromagnetic scattering problems. In all cases, the timings are reported in seconds and the parallel efficiency of the algorithm P_{eff} is computed using

$$P_{eff} = \frac{T_{ref} N_{ref}}{T_p N_p} \tag{6.17}$$

where T_m and N_m respectively denote the average time taken for evaluation of potential a processor and number of processors in the m-th processor set, $m \in \{32, 64, 128, 256, 512, 1024\}$ and ref is the smallest size processor set for a given N.

6.4.1 Kernel Evaluation

The PACE and PFMM algorithms were separately employed to evaluate the scalar potential (6.7) at N random, uniformly distributed source / observer pairs within a volume and surface. For volume distribution, we fill a cube of side-length a and in case of surface distribution the points were placed on a sphere of radius a.

In evaluating the PACE algorithm the overall size of the domain was fixed at λ and the leaf box size was the chosen such that the average number of sources / observers per leaf box is approximately 60. The order of ACE harmonic $p = 3$ was chosen so as to evaluate the potential to an accuracy of $\mathcal{O}(10^{-3})$ [198]. The number of points N was varied from 1 million to 80 million and in each case the number of processors was varied from 32 to 512. Table 6.1 shows, as a representative sample,

the time spent at different stages of the tree computation for the case of $N = 40$ million on different processor sets. It is evident that the time taken for parallel part of multipole-to-multipole (M2M) and local-to-local (L2L) evaluation are negligible. This is in accordance with the theoretical reasoning presented in Section 6.3.4, where Lemma 6.3.2 shows that the number of communications at this stage is bounded and small. Notice that the timing data for rest of the process is proportional to the number of processors. This is a direct consequence of the self-similar tree partition algorithm that ensures load balanced tree computation. The parallel efficiency of PACE algorithm for different cases is shown in the figure 6.4. In all cases ref was chosen to be 32 except for $N = 80$ million where ref =64 was used. The presented algorithm exhibits efficiency as high as 98% on 512 processors. Figure 6.6 shows the time spent by individual processors of a 128 processor set for N=40 million at different steps of tree computation. This exhibits the excellent load balance of the prescribed algorithm as all the processors spend almost the same amount at every step of the tree computation. Next, in figure 6.5, we plot T_m as function of N, for each processor set, to measure the cost complexity of our parallel implementation. The slope of the linear line fits are close to unity which indicates the $\mathcal{O}(N)$ scaling of our parallel implementation. Figure 6.7 plots the efficiency of our PACE algorithm for the case of spherical distribution. Here again the efficiency is as high as 96% on 512 processors. This indicates the scalability of our parallel algorithm on large number of processors.

In evaluating the PACEFMM algorithm, the side-length of the leaf box was fixed at $\lambda/4$ and overall size of the domain was chosen such that the average number of points per leaf box was approximately 60. This choice implies that the number of ACE levels is zero. Table 6.2 shows, as a representative sample, the average time taken by one processor at different stages of hierarchical tree computation for $N =$ 10 million on different processor sets. As in the case of PACE algorithm, the parallel

part of upward and downward tree traversal time are negligible and this is attributed to the bounded number of communications. Figure 6.8 shows the time taken by the individual processors in a 128 processor set during translation with and without *adaptive direction partition* strategy. Without the *adaptive direction partition*, the native processors that host the duplicate nodes spend more time in communication and computation than others. The load balance among the processors improves with *adaptive direction partition* strategy and helps to improve the scalability of the PFMM algorithm. The efficiency in case of volume distribution of points is shown in figure 6.10. The PFMM algorithm offers efficiency as high as 96% on 512 processors. Figure 6.9 shows the time taken by individual processors of a 128 processor set at different stages of tree computation. The negligible variations in time taken by different processors indicate the excellent load balance of the algorithm; which stems from the self-similar partitioning of tree nodes. In figure 6.11, the average time taken for potential evaluation T_m is plotted as a function of N for different processor sets m. The slope of the linear line fits are close to unity which indicates the linear complexity of the proposed PFMM algorithm. The efficiency of the PFMM algorithm for surface distribution of points is in shown in figure 6.12. The algorithm offers high efficiency on 512 processors even for relatively small number of points $N = 10$ million.

6.4.2 EM Simulations

The CFIE formulation is used to solve for electromagnetic scattering from closed PEC objects. The numerical system is solved by a parallel GMRES solver with diagonal preconditioner.

First, the parallel solver is validated by computing the plane wave scattering from a PEC sphere and comparing the RCS with analytical results from Mie series. Figure 6.13 shows the comparison of RCS from a PEC sphere of radius 64λ computed using the parallel solver and Mie series. As is evident there is a excellent agreement between

Table 6.1: Average time spent by an individual processor at different stages of hierarchical tree computation for N=40 million.

Proc.	Local-Multipole	Parallel-Multipole	Trans-lation	Parallel-Local-exp	Local-Local-exp	Direct
32	1.97	0.00	241.35	0.01	43.50	1307.55
64	0.99	0.00	121.31	0.00	21.75	660.91
128	0.49	0.01	60.76	0.01	10.88	332.82
256	0.25	0.01	30.72	0.01	5.43	167.19
512	0.12	0.01	15.62	0.01	2.72	83.75

the two solutions and validates our parallel implementation. Figure 6.14 shows the comparison of RCS of a PEC sphere of radius 128λ, discretized with 14 million unknowns and both the solutions exhibit excellent agreement. To compute the efficiency of the parallel solver, scattering from PEC spheres of different radius (and different number of unknowns) was considered on different processors sets. Consider spheres of radius $\{16, 32, 64\}$ with $\{500, 1500, 3240\}$ thousand unknowns. These simulations were performed on 64, 128, 256 and 512 processors. When computing the efficiency using (6.17), the time denotes the solution time averaged across the processors and 64 processor set as reference, ref =64. As shown in figure 6.15, the parallel solver exhibits efficiency as high as 90% on 512 processors with 3.24 million unknowns. The parallel solver was applied to two realistic geometries. The first geometry is a PEC toy-aircraft with fine edges that is densely discretized with 1.75 million unknowns. At 3GHz the principal dimension of the geometry was 64λ and the figure 6.16a shows the induced surface currents and the computed RCS. The total simulation time was less than 4 hours when executed on a 256 processor cluster. The second geometry is a PEC sharp arrow discretized with 3.24 million unknowns. The principal dimension was 64λ long at 3 GHz and the induced surface currents and RCS are shown in figure 6.16b. The simulation time was less than 2 hours on a 256 processor cluster.

Table 6.2: Average time spent by an individual processor at different stages of hierarchical tree computation for N=20 million points uniformly distribution within a cube of side-length 20λ.

Proc.	Local-Multipole	Parallel-Multipole	Trans-lation	Parallel-Local-exp	Local-Local-exp	Direct
32	249.98	0.04	39.01	0.02	130.99	2488.38
64	125.31	0.07	16.94	0.03	66.17	1250.01
128	62.94	0.13	9.85	0.06	33.71	626.89
256	31.77	0.28	5.09	0.11	17.52	314.1
512	16.17	0.59	3.23	0.24	9.39	157.22

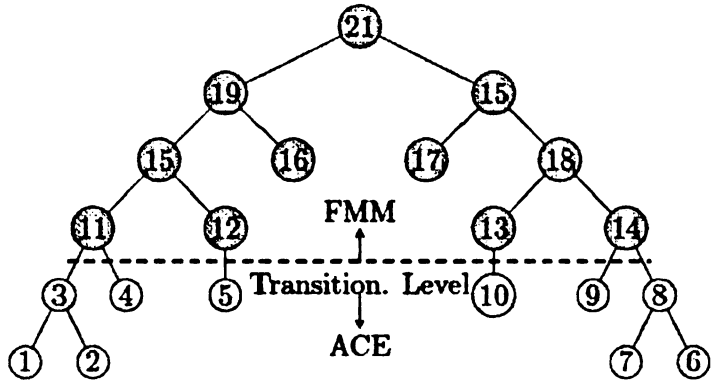

Figure 6.1: An example compressed tree used in ACE+FMM hybrid approach.

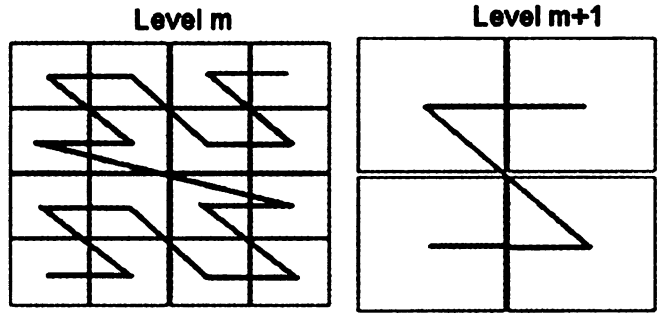

Figure 6.2: The Z-space filling curves or Morton ordering formed by the sorting the nodes of the tree at a particular level.

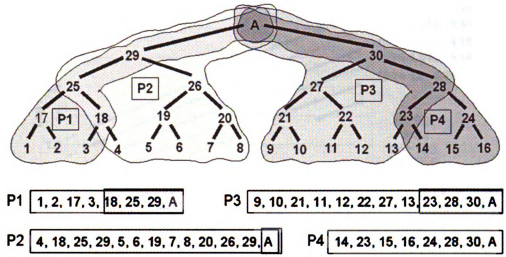

Figure 6.3: Illustration of the tree partitioning scheme proposed in this work. The subsequent distribution of nodes and duplicate nodes in each processor is also shown.

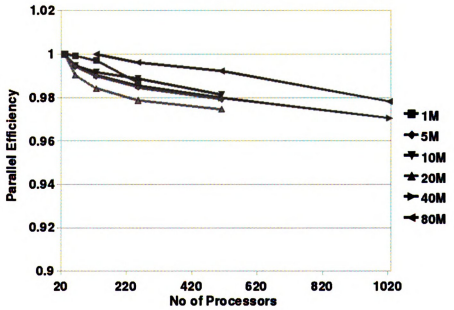

Figure 6.4: Efficiency of the parallel-ACE algorithm for computation of Helmholtz potential between N uniformly distributed random point within a cubical volume.

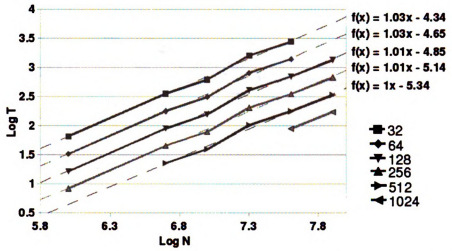

Figure 6.5: Computational complexity of the parallel-ACE algorithm for the case of uniformly distributed random points in a cubical volume. The slope of linear line fits, shown by dotted lines, are close to unity and indicates the linear complexity of parallel-ACE algorithm.

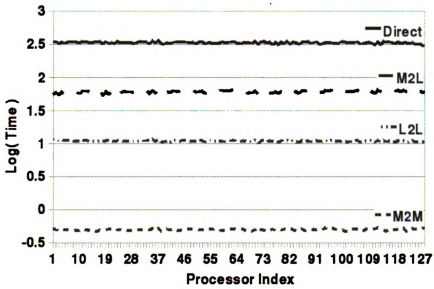

Figure 6.6: Time spent by individual processors of a 128 processor set at different steps of tree computation for N=40 million using ACE expansions.

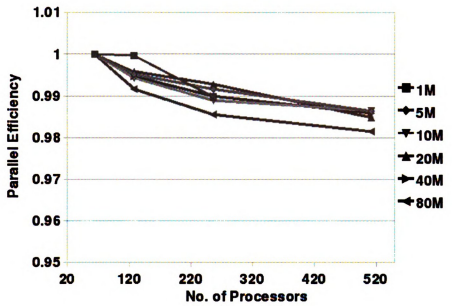

Figure 6.7: Efficiency of the parallel-ACE algorithm for computation of Helmholtz potential between N uniformly distributed random points placed on the surface of a sphere.

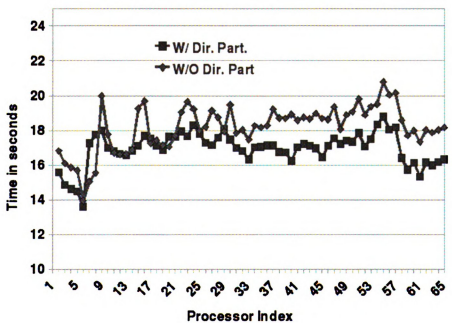

Figure 6.8: Time spent on the Helmholtz FMM translation operation by individual processors of a 128 processor set with and without *adaptive direction partition* strategy.

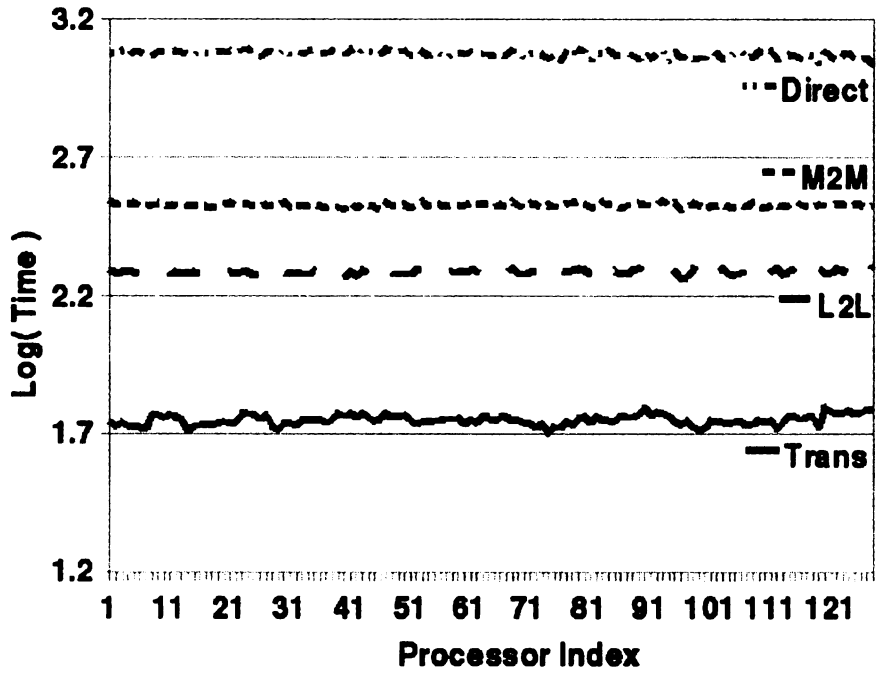

Figure 6.9: Time spent by individual processors of a 128 processor set at different steps of the tree computation for N=40 million using the Helmholtz FMM expansions.

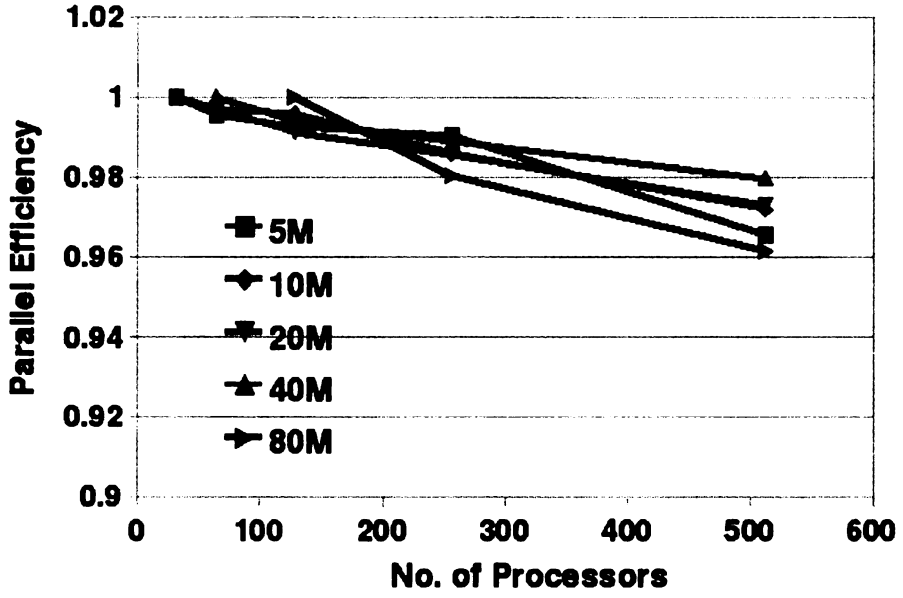

Figure 6.10: Efficiency of the parallel-FMM algorithm for evaluation of Helmholtz potential between N uniformly distributed random points within a cubical volume.

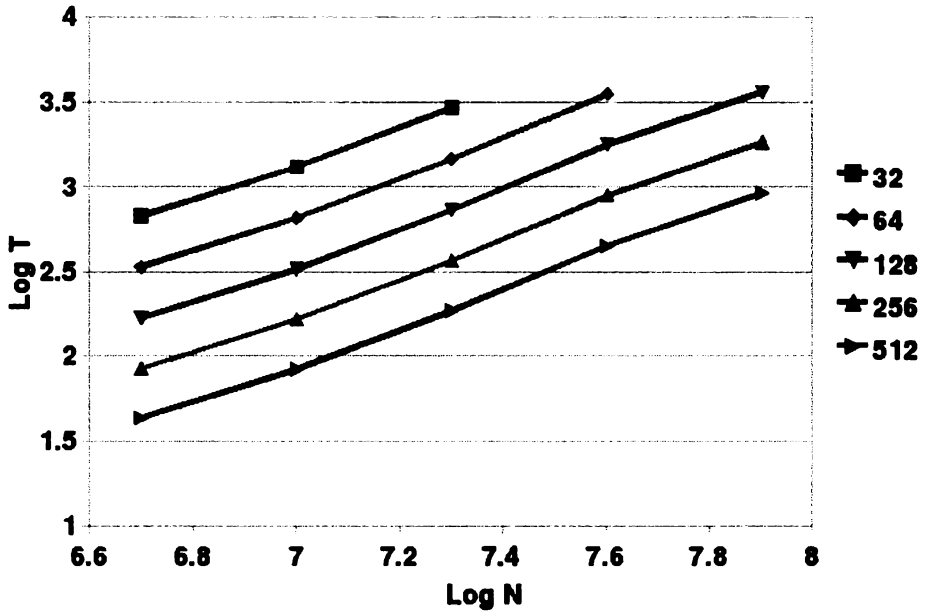

Figure 6.11: Computational complexity of parallel-FMM algorithm as a function of number of unknown N for different processor sets P. The slope of linear line fits are shown by dotted lines.

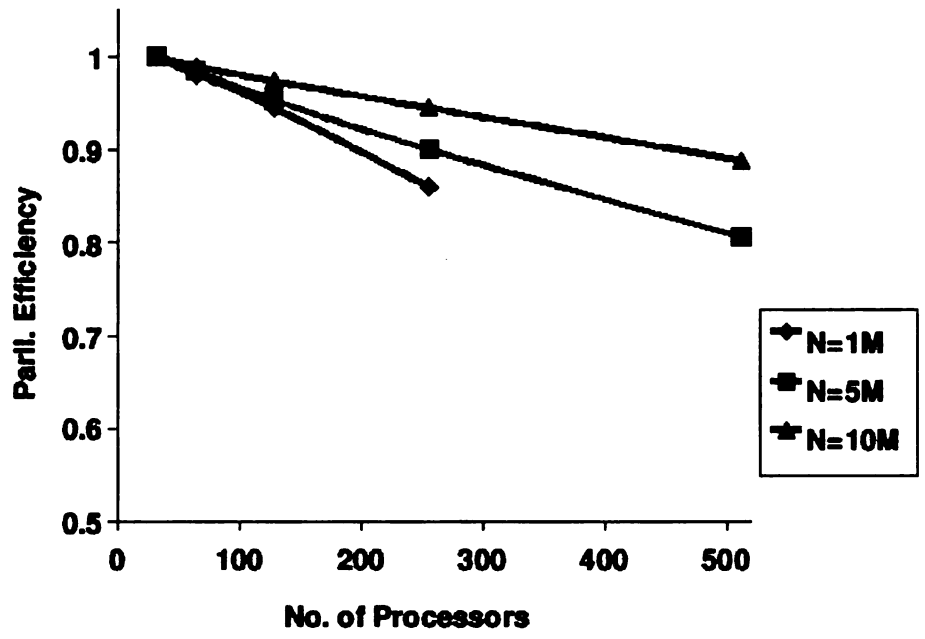

Figure 6.12: Efficiency of the parallel-FMM algorithm for evaluation of Helmholtz potential between uniformly distributed random points on the surface of a sphere.

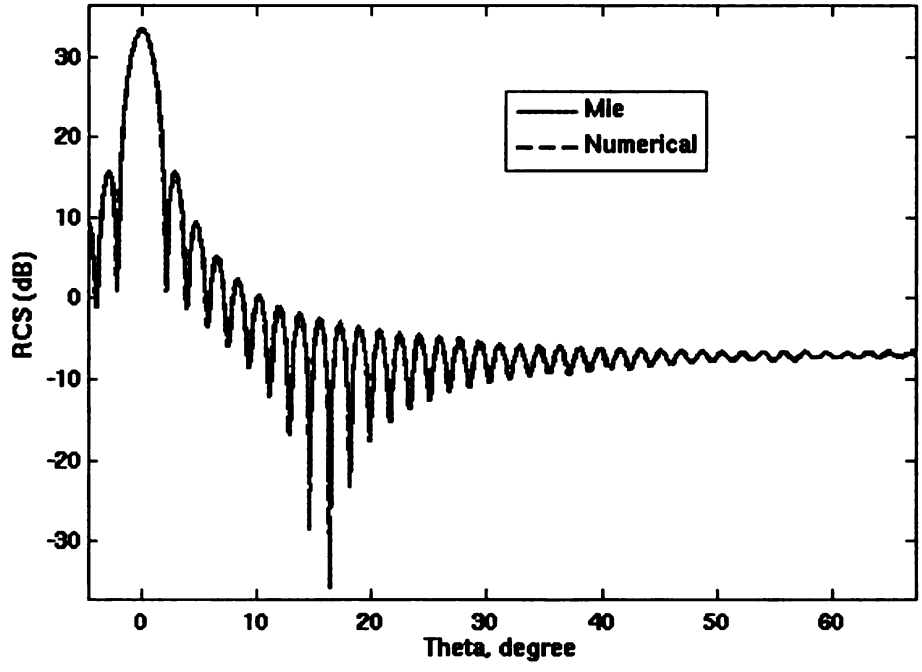

Figure 6.13: Comparison of RCS due to plane wave scattering from a 64λ PEC sphere computed using the parallel EM solver and Mie series solution. Only a portion of the RCS is shown for clarity.

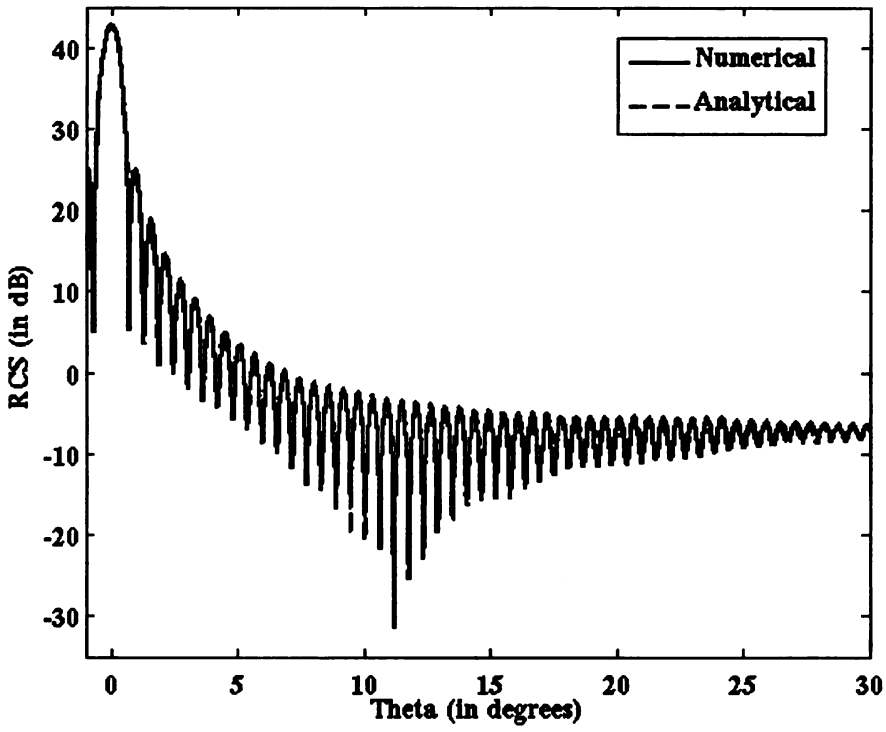

Figure 6.14: Comparison of RCS due to plane wave scattering from a 128λ PEC sphere, discretized with 14 million unknowns computed using the parallel EM solver and Mie series solution.

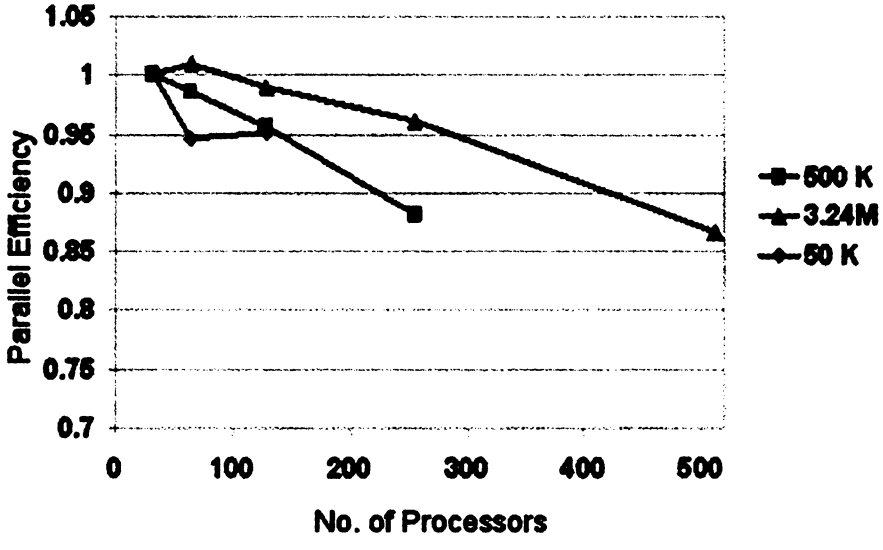

Figure 6.15: Efficiency of the parallel EM solver for the scattering from PEC sphere with different number of unknowns N and as number of processors was varied from 64 to 512.

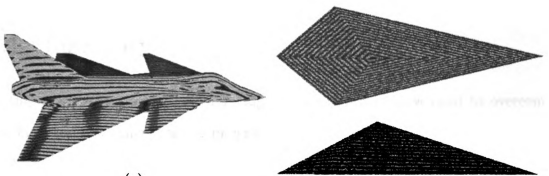

(a) (b)

Figure 6.16: Induced surface currents on multiscale geometries (a) toy-aircraft with sharp edges and (b) tetrahedron shaped arrow.

Chapter 7

Summary and Future Work

7.1 Summary

In this thesis work, several different algorithms have been developed to overcome the high computational cost of integral equation methods used in computational electromagnetics. A common feature among these proposed algorithms is the use of the recently developed accelerated Cartesian expansion (ACE) algorithm. ACE was initially introduced for fast evaluation of polynomial potentials with real exponents. This work has extended it for the fast evaluation of Helmholtz and retarded potentials that is commonly used in frequency and time domain electromagnetic simulations, respectively. It has been rigorously shown that these ACE-based algorithms are stable and efficient when applied to sub-wavelength or low-frequency problems in electromagnetics. These are the class of problems where the principal dimension of a computational domain is much smaller the dominant frequency or analogously the dominant frequency is very small.

The stability of the new algorithms at sub-wavelength regime is a features complementary to the existing acceleration schemes, like Fast multipole method (FMM) and plane wave time domain (PWTD), which have only limited success at these small

scales. Following this observation, hybrid algorithms were developed to combine positive aspects of the proposed and existing algorithms while their negative aspects mutually cancel. The hybrid algorithm in frequency domain was further integrated with an electromagnetic solver, resulting in a multiscale electromagnetic solver. This solver was used to simulate several multiscale problem with significant speed-up, as high as 14 times, over the existing solvers. The capability of the hybrid algorithm to yield arbitrary accuracy and its cost scaling were evaluated numerically. It was observed that the cost scaling of the hybrid algorithm remained purely a function of the number of unknowns, irrespective of the nature of the geometric distribution.

In the context of efficiently solving the multiscale problems, a new integral equation formulation was developed to yield well-conditioned systems of equation. Since a well-conditioned system of equation requires less number of iteration, when using iterative solver, the new formulation helps to reduce the overall solution time. This work achieves this by reformulating the existing augmented electric field integral equation (AEFIE) employed both the electric charge and current as independent unknowns. The imposition of additional constraints, like continuity and total charge conservation, have also be addressed here. The formulation was shown to be stable across frequency range for a variety of 2D and 3D problems. Though the condition numbers were in the orders of few hundreds in the 2D case, the condition number was in the order os 10^6 for 3D problems. This was reduced considerably with the use of orthogonal basis functions. However, it must be noted that the existing numerical procedure to construct orthogonal basis function are computationally intensive in terms of both memory and time.

Finally, novel strategies for parallel implementation of the hierarchical algorithms were also considered. In developing the parallel implementation of these algorithm, the emphasis was laid on improving the scalability such that they can be efficiently executed on large scale clusters with thousands of processors. A major contribution of

this work is the development of a strategy to distribute the FMM or ACE tree nodes to reflect self-similarity and the introduction of *adaptive direction partitioning.* These developments enable the derivation of theoretical bounds on communication overhead, load balanced evaluation of different steps of the tree computation and results in a parallel algorithm that is provably scalable. Plethora of results are presented to demonstrate the different aspects of the parallel algorithm; particularly the scalability of the algorithm on thousands of processors.

7.2 Future Work

The following topics are the suggested future direction of research along the lines of this thesis work:

7.2.1 Well conditioned formulation for EM solver

- As noted in the summary, the well conditioned AEFIE formulation developed here demands orthogonal basis function to obtain reasonably low condition numbers for 3D problems. Existing numerical procedures to construct orthogonal basis functions are computationally expensive. Development of methods or algorithms to efficiently construct these orthogonal basis function, either based on topology or numerical decomposition, would be of significant merit and find use in several other research areas.

- The AEFIE formulation developed in this work is specific to closed domains. In many practical applications, particularly when analyzing antennas, open structures are common. Hence, these formulations should be extended to open domain problems also.

- The AEFIE formulation is developed for PEC scattering only. Development

of similar approaches for scattering from dielectric objects would be of great benefit and extends the reach of these algorithms.

- Recent research work have successfully exploited Calderon operators to obtain well conditioned formulation for both open and closed problems. However, these analytic preconditioners have been developed for PEC scatterers only and can be extended to dielectric scattering also.

7.2.2 Fast algorithms

- The algorithms proposed in this work has extended the application of multipole methods from moderate to high frequency EM problems to very low to high frequency EM problems. This limit can be extended to include the entire frequency range, very low to very high frequency problem, by integrating FMM with ray/optics based based algorithms. This development would enable simulation of ultra wideband radiating structures in the presence of very large scatterers.

- In this work, the largest problem size solved with the parallel FMM was 128 λ. This limitation is due to the limited memory on the distributed computers. Several strategies can been developed for optimal usage of memory. Particularly, it was observed that, when considering large number of FMM levels, the memory required by interpolation and anterpolation matrix is large. Numerical compression of these matrices is a viable workaround to reduce both the memory and time spent in traversing up and down the tree structure.

- The multiscale EM solver developed in this work considers only first order basis functions to represent the unknown fields. These algorithms can be suitably modified to consider higher order geometries and basis function. This would increase the range of multiscale geometries that can be analyzed.

7.2.3 Numerical solution procedures

All the solvers used in this work utilize a simple diagonal preconditioners. More sophisticated numerical preconditioners, amenable for parallel implementation with FMM, have been developed in the past decade. Implementation and development of such preconditioners would further extend the range of the problems solved by the fast algorithms developed here.

Appendix A

A combined accelerated Cartesian expansion (ACE) and fast Fourier transform (FFT) acceleration scheme for rapid evaluation of diffusion potentials

This chapter explores the use of accelerated Cartesian expansion (ACE) algorithm for fast evaluation time domain diffusion potentials. Diffusion potentials are employed to model several physical phenomena such as heat conduction, crystal growth etc. This chapter is organized as follows: Section A.1 provides a comprehensive introduction to the use of diffusion equation to model various phyiscal system and the existing fast schemes. Section A.2 presents the formal definition the problem considered here. Section A.3 introduces in detail the temporal and spatial acceleration schemes required for rapid computation of diffusion potentials. Section A.4 presents plethora of results to demonstrate the accuracy and efficiency of the acceleration schemes presented here.

A.1 Introduction

The time domain diffusion equation is used to model a number of different physical phenomena, including eddy currents[217], heat conduction [218], crystal growth [219] and pharmacokinetics [220]. As a result, methods to efficiently solve this equation have widespread impact. Likewise, the solution to the lossy wave equation finds use in fields ranging from wave propagation physics [221] to relativistic diffusive phenomena [218]. The solution to these equations are typically obtained using either finite difference (FD) or finite element (FE) methods. The popularity of these methods may be primarily attributed to ease of implementation and, perhaps, a plethora of readily available codes. However, differential equation based methods, in general, demand the discretization of the whole domain and employ artificial or approximate boundary conditions to truncate the domain. Additionally, they are susceptible to grid dispersion. These features of FE translate to higher computational cost. Integral equation based methods offer a modality to overcome these computational bottlenecks. However, as is well known, integral equation based solvers are expensive, and their computational complexity scales quadratically with the spatial and temporal degrees of freedom,i.e., the cost scales as $\mathcal{O}(N_s^2 N_t^2)$, where N_s and N_t represent the spatial and temporal degrees of freedom, respectively.

Methods to ameliorate the cost of using integral equation based solvers have been a topic of considerable intellectual interest. These range from fast multipole like methods [222], Fourier-based methods [223], and methods that exploit spatial rank-deficiency [224]. These methods have been used extensively for solving integral equations that arise from Poisson [225], Helmholtz [27], and wave equations [170]. In what follows, we shall focus on fast methods that rely on fast multipole type methods. This class of methods was first developed to ameliorate classical N-body problems, e.g., evaluating Coulombic potentials in large systems [222] and has been widely used in a

number of different applications ranging from molecular dynamics to astrophysics to electrical engineering to fluid mechanics [34]. In this paper, the speed-up is achieved using a series of cascaded Taylor's series expansion in a hierarchical manner [166]. The methods used to develop the classical FMM can be immediately extended to computing Gauss transforms [226], that play an important role in several areas [227]. Consequently, fast Gauss transforms have seen several improvements [228]. Direct application of this method to computing diffusion potential ameliorates the quadratic spatial cost, i.e., the cost is reduced to $\mathcal{O}(N_s N_t^2)$. Acceleration in computing the temporal convolution was first addressed by considering different time scales [227], and successfully used to solve the heat equation [229]. A recent work [230] employs basis function expansions to develop a acceleration scheme whose cost scales as $\mathcal{O}(N_s N_t)$. All these methods accelerate the solution of the diffusion equation completely in real space. Alternatively the diffusion equation can be solved in Fourier space [231, 232] where the cost scales as $\mathcal{O}(N_t N_s \log N_s)$.

In this chapter, an acceleration scheme is proposed for the fast evaluation of time domain potentials that arise from the solution of diffusion equations. The proposed method scales as $\mathcal{O}(N_s N_t \log N_t)$. It is to be noted that the focus of this work is the development of acceleration kernels and not solving these equations for application to specific problems. The proposed methodology is based upon integrating the recently developed Accelerated Cartesian Expansion (ACE) [166] algorithm with either Fast Fourier Transform (FFT) schemes. The main contributions of this work can be listed as

- Developments of modified FGT based on ACE. This has exact translation operator for traversing up and down the tree
- Integration of ACE with FFT based temporal acceleration schemes. The overall cost of the scheme scales as $\mathcal{O}(N_s N_t \log N_t)$.

A.2 Mathematical Preliminaries

Consider a domain, $\Omega \subset \mathbb{R}^3 \times \mathbb{R}$, that contains a distribution of sources, $f(\mathbf{r}, t)$, that is bandlimited to f_{max} and time limited to T. The field due to this distribution of sources satisfies

$$\begin{aligned} \left(\nabla^2 - \alpha^2 \partial_t - \frac{1}{c^2}\partial_t^2\right) \Phi(\mathbf{r}, t) = f(\mathbf{r}, t) \quad \text{for} \quad \mathbf{r} \times t \in \Omega \\ \Phi(\mathbf{r}, 0) = u_0(\mathbf{r}) \quad \text{for} \quad \mathbf{r} \times 0 \in \Omega \end{aligned} \tag{A.1}$$

where $\Phi(\mathbf{r}, t)$ is the dissipative wave potential at $\mathbf{r}$ and time t, Ω is a domain of finite volume, $u_0(\mathbf{r})$ is the initial condition, α and $c \in \mathbb{R}$ are problem dependent constants, and ∂_t denotes a temporal derivative. In the limit $c \to \infty$, we recover the diffusion equation. This corresponds to the limit of an infinite velocity of propagation for solutions, i.e. changes in the spatial profile of a solution can influence the behavior of the solution at all points in space after an infinitesimal period of time.

$$\Phi(\mathbf{r}, t) = \Phi_1(\mathbf{r}, t) + \Phi_2(\mathbf{r}, t) \tag{A.2a}$$

$$\Phi_1(\mathbf{r}, t) = \int_\Omega G(\mathbf{r} - \mathbf{r}', t) u_0(\mathbf{r}') d\mathbf{r}' \tag{A.2b}$$

$$\Phi_2(\mathbf{r}, t) = \int_0^t \int_\Omega f(\mathbf{r}', t') G(\mathbf{r} - \mathbf{r}', t - t') d\mathbf{r}' dt' \tag{A.2c}$$

where $G(\mathbf{r}, t)$ is the Green's function for the diffusion equations given by,

$$G(\mathbf{r}, t) = \frac{\alpha}{(4\pi t)^{3/2}} exp\left(\frac{-\alpha^2 ||\mathbf{r}||^2}{4t}\right) \Theta(t) \tag{A.3}$$

where $\Theta(t)$ is the Heaviside distribution. The literature on the application of these Green's function to integral equation based solvers is extensive [233]. However, it is apparent that the computational cost is the principal bottleneck to the adop-

tion of these methods, despite their several advantages [230, 232]. Indeed, it can be shown from a straightforward discretization of these integrals that the cost scales as $\mathcal{O}(N_s^2 N_t + N_s^2 N_t^2)$. In what follows, we will prescribe methods to tackle the latter integral. As will be evident, evaluating the former will be a trivial use of the methods presented here.

Assume that the temporal sample size is uniform, and is denoted by Δ_t. Without loss of generality, the discrete version of (A.2c) can be written as

$$\Phi_2(\mathbf{r}, t) = \sum_{l=0}^{\lfloor t/\Delta_t \rfloor} \sum_{i=1}^{N_s} G(\mathbf{r} - \mathbf{r}_i', t - l\Delta_t) f_i(\mathbf{r}_i', l\Delta_t) \tag{A.4}$$

where $\lfloor \cdot \rfloor$ denotes the floor operation, $\mathbf{r}_i'$ and f_i are the position and strength associated with the i^{th} spatial source respectively. Testing the discretized form at N_s spatial points at time $t = t_k$ results in the following matrix equation,

$$\mathbf{P}_k = \sum_{l=0}^{k-1} \mathbf{Z}_{k-l} \mathbf{S}_l \tag{A.5}$$

where the vectors are given as

$$\begin{aligned} \mathbf{P}_k &= \left\{ \Phi_2(\mathbf{r}_1, k\Delta_t), \Phi_2(\mathbf{r}_2, k\Delta_t), \cdots, \Phi_2(\mathbf{r}_{N_s}, k\Delta_t) \right\} \\ \mathbf{S}_l &= \left\{ f(\mathbf{r}_1, l\Delta_t), f(\mathbf{r}_2, l\Delta_t), \cdots, f(\mathbf{r}_{N_s}, l\Delta_t) \right\} \end{aligned}$$

and $\mathbf{Z}_l$ is $N_s \times N_s$ matrix whose elements are $\mathbf{Z}_l(i,j) = G(\mathbf{r}_i - \mathbf{r}_j, l\Delta_t)$. In what follows, it is assumed that $\mathbf{S}_l$ is known only at $t = l\Delta_t$ and not before. Other IE formulations [230, 232, 229] can be reduced to the matrix equation of the form (B.20). As done in [234], this equation can be cast as a space time matrix equation and it is readily apparent that cost for evaluating this system scales as $\mathcal{O}(N_s^2 N_t^2)$. In the next section fast methods are developed to reduce this cost to either $\mathcal{O}(N_s N_t \log N_t)$

or $\mathcal{O}(N_s N_t)$.

A.3 Acceleration Schemes

In this section we introduce the spatial and temporal acceleration schemes that form the crux of this paper. First we employ the ACE algorithm to rapidly evaluate potentials at a particular observation time due to spatially distributed sources excited at a single time step. This corresponds to the inner summation in (A.4) and the evaluation of one matrix vector product in (B.20). Given the ACE expansions for spatial acceleration, an FFT based scheme is proposed for rapid evaluation of summation over temporal basis functions corresponding to the outer summation in (A.4). The temporal acceleration schemes presented here primarily exploit the fact that the harmonic expansion of ACE preserves the temporal convolution in (A.4). Then the Toeplitz structure among ACE expansions is identified, for which the standard FFT scheme is employed to reduce the complexity of temporal convolution from $\mathcal{O}(N_t^2)$ to $\mathcal{O}(N_t \log N_t)$. Further, the proposed schemes are cast in a block Toeplitz fashion to conform with the marching on in time (MOT) framework of existing integral equation solvers.

A.3.1 ACE for Spatial Acceleration

As mentioned in the previous section, each summation term in (B.20) corresponds to a fixed source and observation time which is denoted in the subscript. The individual matrix vector product $\mathbf{Z}_{k-l}\mathbf{S}_l$ corresponds to the evaluation of inner sum in (A.4).

This evaluation involves only spatial contributions and can be written as,

$$\mathbf{V}_{k,l} = \mathbf{Z}_{k-l}\mathbf{S}_l \tag{A.6}$$

$$\mathbf{V}^m_{k,l} = \phi_{k,l}(\mathbf{r}_m) = \sum_{n=1}^{N_s} G(\mathbf{r}_m - \mathbf{r}_n, (k-l)\Delta_t) f_n(\mathbf{r}_n, l\Delta_t) \tag{A.7}$$

where $\mathbf{V}_{k,l}$ is an intermediate vector of dimension N_s introduced for the convenience of the following discussion. It is evident that cost of computing the entire vector $\mathbf{V}_{k,l}$ scales as $\mathcal{O}(N_s^2)$. In this work, the accelerated Cartesian expansion (ACE) algorithm is adopted to accelerate computation of vector $\mathbf{V}_{k,l}$. Rapid evaluation of $\mathbf{V}_{k,j}$ through the ACE algorithm requires the definition of $\nabla^n G(\mathbf{R}, t)$ in evaluating the multipole to local expansion using Theorem 2.3.5. It is evaluated using a recursive expression as

$$\nabla^p G(\mathbf{R}, t) = \partial_x^{p_1}\partial_y^{p_2}\partial_z^{p_3} G(\mathbf{R}_x, t) G(\mathbf{R}_y, t) G(\mathbf{R}_z, t) \tag{A.8}$$

$$\partial_l^k G(\mathbf{R}_l, t) = \frac{2R_l}{4t}\partial_l^{k-1} G(\mathbf{R}_l, t) - 2(k-1)\partial_l^{k-2} G(\mathbf{R}_l, t) \quad l\epsilon\{x, y, z\}$$

where $p_i \epsilon \{0, 1, ..p\}$ and $\sum_{i=1}^{3} p_i = p$.

The ACE procedure for Gaussian kernels bears similarity to Fast Gauss Transform (FGT) [226].The use of generalized Taylor expansion and Cartesian tensors for Gaussian kernels is essentially a re-formulation of FGT, where Hermite polynomials and expansions are employed. The cost and storage savings achieved with the use of totally symmetric tensors is identical to that of the graded lexicographic order representation in improved FGT[228]. An additional advantage with ACE algorithm, as detailed in Chapter 3, is the use of *exact translation operators* for multipole-to-multipole and local-to-local expansions.

A.3.2 FFT based Temporal Acceleration

The above description details the use of ACE for the rapid evaluation of a potential at an arbitrary observation time due to spatially distributed sources all excited at a particular time instant. This corresponds to the evaluation of one of the sum terms in (B.20), hence only a part of total potential at time step ($k\Delta_t$) is computed. As mentioned in the introduction, diffusive, lossy wave and Klein-Gordon potentials exhibit an infinite temporal tail (long history) and the computation of the potential at the kth time step would involve k such partial potential evaluations. Consequently, the cost of a scheme with only spatial acceleration scales as $\mathcal{O}(N_s N_t^2)$. This complexity is undesirable when the number of time steps in the simulation is large, as would be expected for any time domain simulation of merit. A FFT based temporal acceleration scheme is deverloped here to ameliorate this cost. This scheme are formulated in a manner such that *causality* is not violated i.e. evaluation of a potential at time step ($k\Delta_t$) assumes the knowledge of sources at time steps ($m\Delta_t$), $m < k$ only. Thus the proposed acceleration schemes are in conformance with the existing solver framework and can be readily integrated.

Consider the convolution in (B.20), this can be written as one matrix vector product as illustrated in Fig. A.1, which illustrates the evaluation of the vector $\mathbf{P}_k$ at all time instants $k = 1, \ldots, N_t$. Note that each term in the figure are themselves either a matrix or vector quantity and depend on the spatial discretization. It is evident, from Fig. A.1, that the matrices $\mathbf{Z}_{i-j}$ form a Toeplitz matrix and beckons the use of fast Fourier transform to perform the matrix vector product in $\mathcal{O}(N_s^2 N_t \log N_t)$ cost. However causality allows one the knowledge of past sources only. In other words, one cannot assume the knowledge of sources $\mathbf{S}_k, \mathbf{S}_{k+1}, \ldots, \mathbf{S}_{N_t}$ when evaluating the potential at time step k. To overcome this, the matrix is divided into sub-matrices $\mathbf{T}_k$ as indicated in Fig. A.1 . The evaluation of the potential $\mathbf{P}_k$ involves different

submatrices $\mathbf{T}_l$ that are multiplied by past sources only at different time instances [234, 235]. In this scheme, computation at the k^{th} time step involves k past time source vectors $\{\mathbf{S}_{k-N}, \ldots, \mathbf{S}_{k-1}\}$ multiplied with the appropriate Toeplitz sub-matrix $\mathbf{T}_N$ to produce potential $\mathbf{P}_k$ at the k^{th} time step and partially evaluated potentials $\{\mathbf{P}_{k+1}, \ldots, \mathbf{P}_{k+N-1}\}$ at future time steps, where N depends on k. For example, evaluation of $\mathbf{P}_2$ involves the multiplication of vector $\{\mathbf{S}_0, \mathbf{S}_1\}$ with sub-matrix $\mathbf{T}_2$, however this also results in partial computation of $\mathbf{P}_3$. In the next time step, $\mathbf{P}_3$ is completely evaluated with the computation of the matrix vector product $\mathbf{T}_1\mathbf{S}_2$. Thus the sub-division scheme shown in figure A.1 also provides a means to compute potential within the MOT framework. Further each of the submatrices is Toeplitz and hence FFT can be employed to accelerate the computation. It is important to note that the this acceleration methodology does not involve any approximations and is exact. Consequently, this scheme is used to accelerate both near and far time interactions.

Next, consider the above acceleration scheme within the context of ACE algorithm introduced in previous section. The following two observations that forms the basis of integrating the Block-Toeplitz based temporal and ACE based spatial acceleration acceleration schemes,

1. Except for the multipole-to-local translation operators all other operations in ACE depend only on either the source (l) or observer (k) time.

2. The multipole-to-local translation operation in Theorem 2.3.5 preserves the convolution in time.

Consider the evaluation of potential at observation points in domain Ω_o at time $k\Delta_t$ due to sources located in domain Ω_s and excited at $l\Delta_t$. Using theorem 2.3.5 and

(2.8) of ACE algorithm in (A.4) we get

$$\Phi_2(\mathbf{r}, k\Delta_t) = \sum_{n=0}^{\infty} (\boldsymbol{\rho}_{oi})^{(n)} \cdot n \cdot \mathbf{L}_k^{(n)} \tag{A.9}$$

$$\mathbf{L}_k^{(n)} = \sum_{l=0}^{k-1} \mathbf{L}_{k,l}^{(n)} \tag{A.10}$$

$$= \sum_{m=n}^{\infty} \left(\sum_{l=0}^{k-1} \mathbf{M}_l^{(m-n)} \cdot (m-n) \cdot \frac{1}{n!} \mathbf{H}_{k-l}^{(m)} \right) \tag{A.11}$$

$$where, \quad \mathbf{H}_{k-l}^{(m)} = \nabla^m G(\mathbf{r}_{os}^p, (k-l)\Delta_t)$$

From above, we infer that the evaluation of the local expansions at the kth time step is equivalent to the evaluation of the potential at the kth time step. Considering the above equivalence we rewrite the discrete form (B.20) as

$$\mathbf{P}_k = \sum_{l=0}^{k-1} \sum_{n=0}^{\infty} (\boldsymbol{\rho}_{oi})^{(n)} \cdot n \cdot \left[\sum_{m=n}^{\infty} \left(\mathbf{M}_l^{(m-n)} \cdot (m-n) \cdot \frac{1}{n!} \mathbf{H}_{k-l}^{(m)} \right) \right] \tag{A.12}$$

$$= \sum_{n=0}^{\infty} (\boldsymbol{\rho}_{oi})^{(n)} \cdot n \cdot \sum_{m=n}^{\infty} \left[\sum_{l=0}^{k-1} \left(\mathbf{M}_l^{(m-n)} \cdot (m-n) \cdot \frac{1}{n!} \mathbf{H}_{k-l}^{(m)} \right) \right] \tag{A.13}$$

In above equation, the time dependence of translation operator and multipole expansion corresponding to a particular tensor component of ACE harmonic can be written in the block Toeplitz matrix form as illustrated in Fig A.1. This immediately suggests the evaluation of the temporal convolution in (A.13) using FFT. In addition, as described above, the block-Toeplitz structure is utilized to conform with the MOT framework of solvers. To complete the discussion we define the Fourier transform of a nth rank Cartesian tensor $\mathbf{M}^{(n)}$ as follows

$$\tilde{\mathbf{M}}^{(n)}(n_1, n_2, n_3; \omega) = \mathcal{F}\left\{ \mathbf{M}_l^{(n)}(n_1, n_2, n_3) \right\} \quad , where\ n_1 + n_2 + n_3 = n \tag{A.14}$$

where $\mathcal{F}$ denotes the forward Fourier transform operator ($t \rightarrow \omega$) and $\tilde{\mathbf{M}}^{(n)}$ denotes the n^{th} rank Cartesian tensor in Fourier space. In essence the Fourier transform of a tensor is evaluated in a term-by-term (n_1, n_2, n_3) fashion. Given this definition the local expansion at kth time step $\mathbf{L}_k$ due to all past sources is evaluated as,

$$\mathbf{L}_k^{(n)}(n_1, n_2, n_3) = \sum_{m=n}^{\infty} \frac{1}{n!} \mathcal{F}^{-1} \left\{ \sum_{\omega} \tilde{\mathbf{H}}^{(m)}(\omega) \cdot (m-n) \cdot \tilde{\mathbf{M}}^{(m-n)}(\omega) \right\} \quad \text{(A.15)}$$

where $n_1 + n_2 + n_3 = n$, $\mathcal{F}^{-1}$ is the inverse Fourier transform operator ($\omega \rightarrow t$). Since the Fourier transform is applied only in the time domain ($t \leftrightarrow \omega$) the tensor contraction definition is valid in the Fourier domain as well.

Computation of the time domain diffusion potential using the multi-level tree representation of the spatial domain requires attention to the following details. The multipole expansions for all boxes should be evaluated as we march on in time and stored at all time discretizations, this implies N_t upward tree traversals. The multipole expansions $\mathbf{M}^{(n)}$ are represented as a set of $N_t \times 1$ column vector for each tensor component as $\mathbf{M}_{\mathbf{l}}^{(\mathbf{n})}(\mathbf{n_1}, \mathbf{n_2}, \mathbf{n_3})$. In a similar fashion the translation operator for observation time $k\Delta_t$ is represented as a set of $k \times k$ matrix for each tensor component. In actual implementation only the $(2k-1)$ unique entries of this Toeplitz matrix is stored for computation with FFT. For interacting boxes, the multipole to local translation operation involves the temporal convolution (A.11) and are evaluated in a rapid manner using FFT as in (A.15). This evaluation is carried out for each of the $(n+1)(n+2)/2$ tensor components. As is evident, from figure A.1 the size of the Toeplitz system N depends on the block size which in turn depends on the observation time step k and can vary between 1 and $N_t/2$. The outcome of this process are the N local expansions from which the potentials at N future time steps are evaluated by downward tree traversal.

The cost of this scheme is computed in the following manner. The cost of one up-

ward and downward tree traversal scales as $\mathcal{O}(N_s)$. The cost of computing multipole expansions at all time instants scales as $\mathcal{O}(N_s N_t)$. The cost multipole-to-local expansion and downward tree traversal for N size Toeplitz system scales as $\mathcal{O}(N_s N \log N)$ and $\mathcal{O}(N_s N)$ respectively. In the entire scheme, Toeplitz systems of size $N_t/2$ occurs once, $N_t/4$ occurs twice and so on. Thus, the total cost of this scheme scales as

$$\mathcal{O}\left(N_s N_t + N_s\left(\frac{N_t}{2}\left(\log\frac{N_t}{2}+1\right)+2\frac{N_t}{4}\left(\log\frac{N_t}{4}+1\right)+\ldots\right)\right) \approx \mathcal{O}\left(N_s N_t \log^2 N_t\right)$$

The error in the acceleration scheme is only due to approximations in the ACE algorithm.

A.4 Results

In this section, results are presented to substantiate the above claims and demonstrate the efficacy of the algorithm presented here. The goal here is to demonstrate considerable speed-up with predetermined accuracy. Consequently, the results presented will demonstrate convergence in error as well as linear CPU cost scaling. In all numerical experiments, the source/observer locations are randomly (uniform distribution) chosen. The time signature associated with the nth source is given by (A.16)

$$f_n(t) = \kappa_n e^{-(t-t_p)^2/2\sigma^2} \tag{A.16}$$

where κ_n is the source strength, randomly chosen between $[0, 1]$, $\sigma = 6.366 \times 10^{-8}$ s and $t_p = 6\sigma$ s. In all simulations Δ_t was chosen as 1 second. These parameters were chosen arbitrarily.Error is conditioned primarily by the number of ACE harmonics used, P. While there is an error associated with the UV decomposition of the translation operator, it is conditioned to be at or below that of the error incurred in

truncating the expansion of the translation operator to P harmonics. The accuracy of the proposed algorithm is validated against direct computation for all cases where the unknown count is numerically small. The relative error at n^{th} observer is evaluated as

$$Error_{far}(n) = \frac{||\Phi_{fast,far}(n,t) - \Phi_{direct,far}(n,t)||_2}{||\Phi_{direct,far}(n,t)||_2} \tag{A.17}$$

where, $||\cdot||_2$ represents L_2-norm, $\Phi_{fast,far}(t)$ and $\Phi_{direct,far}(t)$ represent the time history of the fields produced by the sources evaluated using the proposed algorithm and a direct procedure, respectively. The final error reported throughout this work is the average error over all observers. Error is computed only with the far-field potential, i.e. direct data is computed *only* for the source/observation pairs that are in the far-field of each other, and is consequently representative of an upper bound or worst-case error. With the exception of the temporal scaling experiments, the computational time reported here is the total run-time in seconds using a 2.3 GHz Intel Pentium processor with 2GB RAM running Linux OS. High Performance Computing Center at Michigan State University was utilized to extend into very long time scales. All estimated or projected time values are marked by †.

The first set of results demonstrates the exact multipole-to-multipole and local-to-local translation operators of the ACE algorithm, in the context of evaluating Gaussian kernels. An important implication of this feature of the ACE algorithm is that the error does not increase as the height of the tree is increased. Consider two domains Ω_1 and Ω_2 of size $(0,0.5) \times (0,0.5) \times (0,0.5)m^3$ and $(1,1.5) \times (1,1.5) \times (1,1.5)m^3$ respectively. In each domain 4000 source/observer points are randomly distributed and we consider interaction between these two domains only, all other interactions are neglected. As the number of levels in tree is increased, the change in the error norm can be attributed solely to the error in multipole-to-multipole and local-to-local translations. Table A.1 shows error computed for different P and

different levels in tree. For a given accuracy (fixed P) it is evident that variation in error obtained from using different levels in the tree is accurate to double precision.

The next set of results pertain to the evaluation of the time domain diffusion potential in (A.4). Table A.2 presents errors for different ACE harmonics P, numbers of unknowns N_s, and domain sizes- represented by d - sidelength of cube enclosing all sources/observers. In all cases the number of time discretizations was maintained at a constant, $N_t = 256$ and the FFT based MOT scheme was utilized. As expected, an increase in the number of ACE harmonics, P, leads to a uniform decrease in the error for all cases. The speed-ups provided by the proposed algorithm, utilizing the FFT scheme, are exhibited in Tables A.3 and A.4. Table A.3 presents run-times for evaluating time domain diffusion potential for different size of spatial discretizations while the following parameters were kept as constants: total number of time discretization $N_t = 256$, size of domain $d = 0.5$ and number of ACE harmonics $P = 3$ corresponding to an error of $\mathcal{O}(1E-5)$. It can be seen that the proposed algorithm is 230 times faster than the direct method even for a small problem size $N_s = 4000$ and $N_t = 256$. Figure A.2 shows a log-scale graph of T_{fast} vs N_s for values in Table A.3. The line in the graph corresponds to a least-square linear fit whose slope was found to be 1.1. This validates the $\mathcal{O}(N_s)$ cost scaling of the proposed algorithm.

In Table A.4 the run-time of the proposed algorithm is shown for different numbers of time discretizations. Aside from N_t, all other parameters were kept constant at: $N_s = 8,000$, $d = 0.5$m and $P = 3$. For the FFT experiments, the expected $\mathcal{O}(N_t log N_t)$ scaling cannot be verified because of the following implementation details. In this workthe open source library FFTW3 package [236] was used which does not exhibit uniform $N_t log N_t$ scaling. This is the case with many other performance oriented FFT packages as well. Also, it was observed that it is efficient (faster) to use direct evaluation than using FFT procedure when the size of the Toeplitz system was smaller. This is important in terms of overall performance as smaller size Toeplitz

system occur more frequently ex. the Toeplitz system of size 1×1 and 2×2 occurs $N_t/2$ and $N_t/4$ times. In this work direct evaluation was used for any Toeplitz matrix of size $\leq 16 \times 16$, this may vary based on the computer platform and FFT library in use.

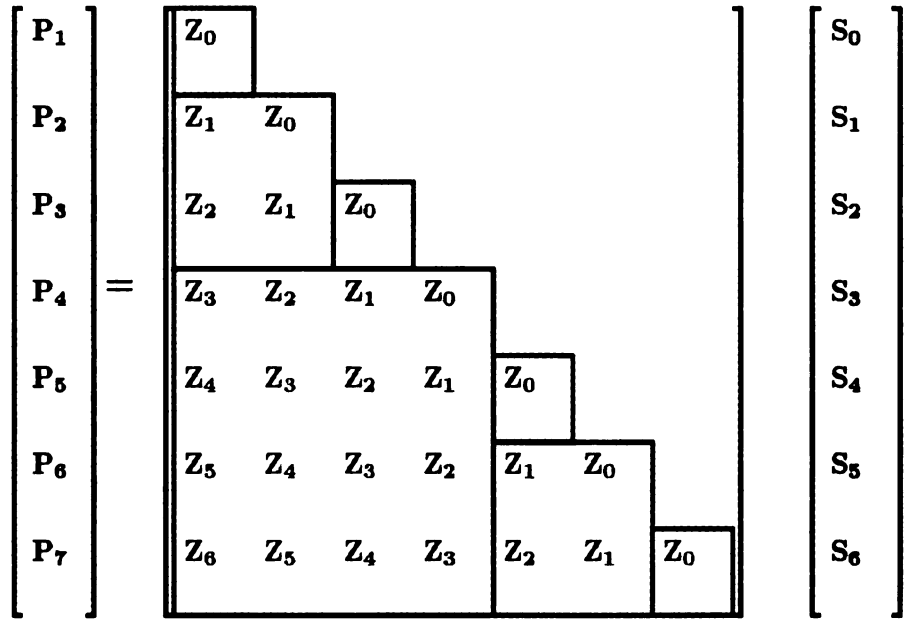

Figure A.1: Illustration of the Block-Toeplitz computational scheme

Table A.1: Exact translation operator in ACE algorithm, P denotes the number of ACE harmonics.

Levels	$P = 3$	$P = 6$
3	5.343762051614 770E-006	7.0123317207 40178E-008
4	5.343762051614 130E-006	7.0123317207 70545E-008
5	5.343762051614 279E-006	7.0123317207 63711E-008

Table A.2: Error convergence for different number of ACE harmonics (P) and different source/observer configuration (N_s, d)

	N_s, d			
P	8000, 1.0	4000, 1.0	8000, 0.5	4000, 0.5
0	4.92E-02	5.01E-02	1.39E-02	1.74E-02
1	1.12E-02	1.04E-02	3.71E-03	4.70E-03
3	9.61E-05	9.39E-05	1.22E-05	2.21E-05
5	1.20E-06	1.36E-06	3.54E-08	9.04E-08
7	1.87E-08	2.28E-08	1.20E-10	3.30E-10
9	2.77E-10	3.44E-10	6.40E-13	1.21E-12

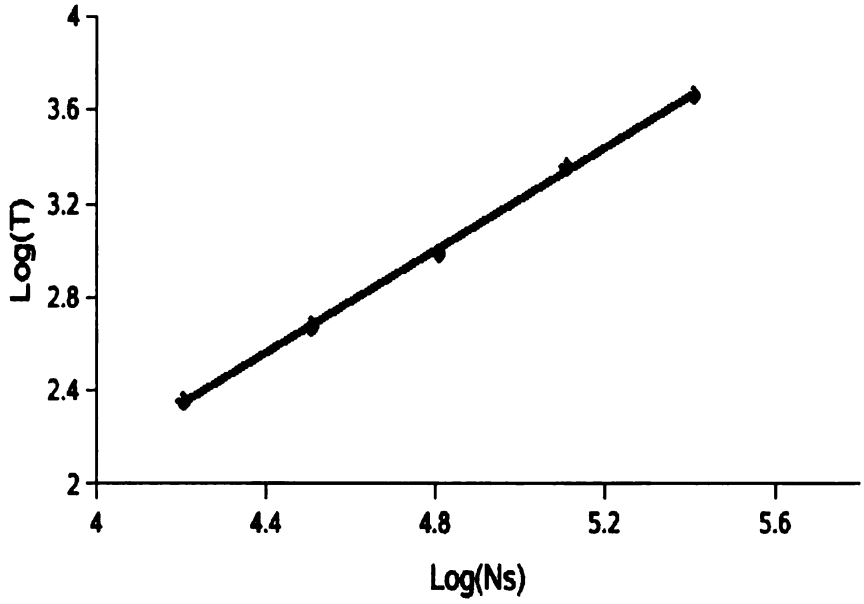

Figure A.2: *log* T_{fast} vs. *log* N_s from Table A.3, slope of linear fit = 1.1

Table A.3: Time for different problem size (N_s) within a cube of sidelength $d = 0.5$m. In all cases $N_t = 256$, $P = 3$ ($\epsilon = \mathcal{O}(1E-5)$)

N_s	T_{FFT}	T_{Direct}
4000	71.98	17195.35
8000	98.32	68781.25 †
16000	226.8	275125.60 †
32000	472.66	1100502.40 †
64000	978.07	4402009.60 †
128000	2282.01	17608038.40 †
256000	4652.78	70432153.60 †

Table A.4: T_{fast} for different N_t size. In all cases $N_s = 8,000$, $d = 0.5$, $P = 3$ ($\epsilon = \mathcal{O}(1E-5)$)

N_t	T_{FFT}	T_{Direct}
256	94.17	44169.36
512	231.95	176677.44 †
1024	554.57	706709.76 †
2048	1395.52	2826839.04 †
4096	3438.00	11307356.16 †
8192	9494.96	45229424.64 †
16384	28410.84	180917698.56 †

Appendix B

Comprehensive Exam Problem: Integral Equation Based Eddy Current Model for Defects in Layered Media

The goal of this chapter is to develop an efficient simulation scheme for eddy current testing of defects in layered media. Finite element method is the popular technique used to model eddy current testing. However, they require discretization of entire domain and is not favorable for modeling layered media. Alternatively, the less used Integral equation approach, with layered medium Green's function, demands discretization of the small defect region only. Such a formulation demands the evaluation of infinite integrals which are efficiently handled using the recently developed Discrete Complex Image Method (DCIM). A volume integral equation solver, based on tetrahedral elements, is developed here. Full details of the formulation along with results demonstrating the efficiency and accuracy of the method are presented.

B.1 Introduction

Eddy current testing (ECT) relies on the principle of magnetic induction to interrogate materials under inspection [237] at very low frequencies, of the order of kilo-Hertz (kHz). Since its inception, ECT has become an indispensable tool and covers a wide spectrum of industries from pipeline inspection to aircraft health monitoring to biomedical inspections. ECT can be used for any applications where the material to be inspected is a conducting medium. Qualitatively, the principle of operation of ECT is as follows: time varying magnetic field (produced usually by a time varying impressed currents) induces eddy currents in the conducting region, this in turn produces a measurable field outside the material region. Change in conductivity of the material affects the characteristic of the induced eddy currents–magnitude and direction of flow–causing a change in the measured field. Eddy currents are induced in regions only near the impressed currents, thus it is a local phenomena and aids in precise location of defects with appropriate signal processing.

Numerical models for ECT have played a significant role in its development and application. These models have been used to design the geometry of the excitation and measurement probes, determine optimal testing parameters and development of efficient signal processing techniques. Eddy current phenomena is governed by Maxwell's equation. Under low-frequency and high conductivity assumptions, the coupled Maxwell's equations is reduced to a single diffusion equation. Finite element methods (FEM) has been the popular choice in NDE community to model this phenomena. This is primarily due to ease of implementation and fast solution time. However, FEM requires discretization of a large domain and employs artificial boundary condition to truncate fields at boundary. Alternatively, integral equation solution have also been developed to model ECT, however these models need to be formulated appropriately to compete with the speed of FEM solutions.

In this work, an integral equation solver is developed to model ECT for analyzing defects that are embedded in a multilayered environment, e.g., cracks under rivets etc. Contrary to the existing literature in NDE [237], the low-frequency approximation is not used here. A detailed discussion of the various techniques used in this development is provided in the following sections. Section B.2 describes in detail the theory required for the development of the integral equation model. Section B.3 presents the numerical techniques used in implementation. Finally, Section B.4 provides some results to substantiate the theoretical claims.

B.2 Integral Equation Formulation

B.2.1 Formulation

Consider the homogeneous domains Ω_1 and Ω_2 in figure B.1. Assuming e^{-iwt} time convention the harmonic electromagnetic field in each region are given by Maxwell's equation,

$$\begin{aligned} \nabla \times \mathbf{E}_1 &= i\omega \mathbf{B}_1 \\ \nabla \times \mathbf{H}_1 &= -i\omega\varepsilon_1 \mathbf{E}_1 + \sigma_1 \mathbf{E}_1 + \mathbf{J}_e = -i\omega\tilde{\varepsilon_1}\mathbf{E}_1 + \mathbf{J}_e \end{aligned} \tag{B.1}$$

$$\begin{aligned} \nabla \times \mathbf{E}_2 &= i\omega \mathbf{B}_2 \\ \nabla \times \mathbf{H}_2 &= -i\omega\varepsilon_2 \mathbf{E}_2 + \sigma_2 \mathbf{E}_2 = -i\omega\tilde{\varepsilon_2}\mathbf{E}_2 \end{aligned} \tag{B.2}$$

where $\mathbf{E}_k$ and $\mathbf{H}_k$ represent the total electric and magnetic fields, respectively, in the domain Ω_k, $\mathbf{J}_e$ is the impressed or excitation source, $\{\varepsilon_k, \mu_k, \sigma_k\}$ are the electromagnetic material constants permittivity, permeability and conductivity, respectively, of the domain Ω_k, $\tilde{\varepsilon_k} = \varepsilon_k - \sigma_k/i\omega$ denotes the complex permittivity. Straight forward

manipulations reduces (B.2) to the form in (B.1)

$$\nabla \times \mathbf{H}_2 = -i\omega\tilde{\varepsilon}_1\mathbf{E}_2 + \mathbf{J}_s \tag{B.3}$$

where $\mathbf{J}_s = -i\omega(\tilde{\varepsilon}_2 - \tilde{\varepsilon}_1)\mathbf{E}_2$ is the equivalent source that depends on the field in that region. The equivalent sources introduced here allows one to treat Ω_2 same as Ω_1 but with additional sources. The total electric field, $\mathbf{E}^t$ in any region is divided into $\mathbf{E}^e$ and $\mathbf{E}^s$ corresponding to the contribution from impressed source $\mathbf{J}_e$ and equivalent source $\mathbf{J}_s$ respectively,

$$\mathbf{E}^t = \mathbf{E}^e + \mathbf{E}^s \tag{B.4}$$

The above integral equation is used to solve for the equivalent source strengths to uniquely determine the fields everywhere. Evaluation of $\mathbf{E}^s$ due to the equivalent sources $\mathbf{J}_s$ requires the prescription of the Green's function, $\overline{\overline{\mathbf{G}}}$, for a source radiating in presence of the homogeneous media Ω_1. Thus, (B.4) is written as

$$\mathbf{E} = \mathbf{E}^e + \overline{\overline{\mathbf{G}}} \star \mathbf{J}_s \tag{B.5}$$

In ECT simulations, the layered media without any defect is chosen as Ω_1 and the region corresponding to defect only is taken as Ω_2. Thus the Green's function in (B.5) corresponds to the layered media Green's function with sources outside and inside the layered media. The next section, provides a detailed treatment on the derivation of the layered media Green's function.

B.2.2 Planar Media Green's Function

In deriving the Green function, no approximation is made to reduce the governing wave equations of ECT to a diffusion equation. This is done intentionally to leverage on the existing literature in the wave propagation community and introduce the

appropriate modifications at a later stage. A vast source of literature address the derivation of Green's function in presence of layered planar media obeying the wave equation and radiation boundary condition. In the last decade, several significant developments have been made in terms of formulation and evaluation of these Green's function in a manner suitable to numerical models.

The electric and magnetic field produced by an infinitesimal electric dipole $\mathbf{d} = \delta(\mathbf{r})\hat{d}$ in homogeneous media can be written in terms of spherical waves as

$$\mathbf{E}(\mathbf{r}) = -i\omega\mu\left(\bar{\bar{\mathbf{I}}} + \frac{\nabla\nabla}{k^2}\right)\frac{e^{ikr}}{r} \star \mathbf{d} \tag{B.6}$$

$$\mathbf{H}(\mathbf{r}) = \nabla \times \frac{e^{ikr}}{r} \star \mathbf{d} \tag{B.7}$$

where $r = ||\mathbf{r}||$ and $\star$ denotes spatial convolution operation. Sommerfeld Identity [238] is used to represent spherical waves as a product of plane waves in z direction and cylindrical waves in ρ direction,

$$\frac{e^{ikr}}{r} = \frac{i}{2}\int_{SIP} dk_\rho \frac{k_\rho}{k_z} H_0^{(1)}(k_\rho\rho)e^{ik_z|z|} \tag{B.8}$$

where $k_z = \sqrt{k^2 - k_\rho^2}$, $k = w/c$, c is the speed of light in the homogeneous medium and w is the angular frequency. Now consider the effect of a layered media, stacked in z direction, whose properties vary only as a function of z. From the expansion in (B.8), it is evident that only the plane waves in z direction will get affected. In other words, the effect of introducing a layered medium in z can be accounted in terms of the reflection and transmission of the plane waves travelling in z direction. As an example, consider a vertically oriented dipole placed at origin in a homogeneous media, $\mathbf{d}_\rho = 0$. Since $\mathbf{E}_\rho = 0$, this corresponds to transverse magnetic (TM) wave excitation that is fully characterized by the $\mathbf{E}_z$ fields. Combining (B.6) and (B.8), we

get

$$\mathbf{E}_z = i\omega\mu(1+\partial_z^2/k^2)\frac{i}{2}\int_{SIP} dk_\rho \frac{k_\rho}{k_z} H_0^{(1)}(k_\rho\rho)e^{ik_z|z|} \tag{B.9}$$

When a planar layered media in z direction is introduced, its effect can be accounted for using the TM_z reflection and transmission coefficients depending on the region where field is computed. Fields on the same side of the source are called the reflected fields and is denoted by superscript R. Fields on the opposite side are called as the transmitted fields denoted by superscript T. In this case, the reflected and transmitted fields are given as,

$$\mathbf{E}_z^R = (1+\partial_z^2/k^2)\frac{-\omega\mu}{2}\int_{SIP} dk_\rho \frac{k_\rho}{k_z} H_0^{(1)}(k_\rho\rho)e^{ik_z|z|}(1+R_{TM}e^{-i2k_z|z|}) \tag{B.10}$$

$$\mathbf{E}_z^T = (1+\partial_z^2/k^2)\frac{-\omega\mu}{2}\int_{SIP} dk_\rho \frac{k_\rho}{k_z} H_0^{(1)}(k_\rho\rho)e^{ik_{2z}|z|}(1+T_{TM}) \tag{B.11}$$

where R_{TM} and T_{TM} denotes the reflection and transmission coefficient for TM_z plane waves, $k_{2z} = \sqrt{k_2^2 - k_\rho^2}$ and k_2 is the propagation constant in the layered medium. Similarly, one can perform the same derivation for TE_z fields produced by a dipole oriented in horizontal or $x-y$ plane. Since any field can be broken into TM_z and TE_z polarization, superposition of the two forms is required when considering arbitrary excitation. Depending on the intended use, several different variations of the layered media Green's function can be found in the literature. In this work, the symmetric form of the Green's function provided in [239] is used as it allows for efficient treatment of singularities in the Green's function. In addition to the source vector, this form requires a testing vector to attain symmetry. The derivation is

straight forward but laborious [239], hence only the final form is presented here

$$\hat{\alpha}.\overline{\mathbf{G}}_b^P.\hat{\alpha}' = \frac{i\omega\mu_0}{4\pi}\left(\hat{\alpha}.\hat{\alpha}' + \frac{1}{k_b^2}\hat{\alpha}.\nabla\nabla.\hat{\alpha}'\right)g^P \tag{B.12a}$$

$$\hat{\alpha}.\overline{\mathbf{G}}_b^R.\hat{\alpha}' = \frac{i\omega\mu_0}{4\pi}\left(\hat{\alpha}_s.\hat{\alpha}_s' g_{TE}^R + \hat{\alpha}_z\hat{\alpha}_z' g_{TM}^R\right) + \frac{i\omega\mu_0}{4\pi k_b^2}(\hat{\alpha}.\nabla\nabla.\hat{\alpha}'' g_{TM}^R + 2\hat{\alpha}_s.\nabla_s\nabla_s.\hat{\alpha}_s' g_{EM}^R) \tag{B.12b}$$

$$\hat{\alpha}.\overline{\mathbf{G}}_a^T.\hat{\alpha}' = \frac{i\omega\mu_0}{4\pi}\left(\hat{\alpha}_s.\hat{\alpha}_s' g_{TE}^T + \frac{1}{k_a^2}\hat{\alpha}_s.\nabla_s\nabla_s.\hat{\alpha}_s' g_{TM}^R + \frac{1}{k_b^2}\hat{\alpha}_z\hat{\alpha}_z' g_{TM_1}^T\right) \tag{B.12c}$$

where,

$$g_{TE,TM,EM}^R = \frac{i}{2}\int_{SIP} dk\rho R^{TE,TM,EM}\frac{k_\rho}{k_{bz}}H_0^{(1)}(k_\rho\rho)e^{-ik_{bz}(z+z')} \tag{B.13a}$$

$$R^{EM} = \frac{k_b^2}{2k_s^2}(R^{TE} + R^{TM})$$

$$\hat{\alpha}'' = -\hat{\alpha}_s' + \hat{\alpha}_z'$$

$$g_{TE,TM,TM1}^T = \frac{i}{2}\int_{SIP} dk_\rho T^{TE,TM,TM1}\frac{k_\rho}{k_{bz}}H_0^{(1)}(k_\rho\rho)e^{-ik_{bz}z+ik_{az}z'} \tag{B.13b}$$

$$T^{TM1} = k_\rho^2 T^{TM}$$

where $\hat{\alpha}$ is the testing vector, $\hat{\alpha}'$ is the source dipole vector, subscript t and z denotes the traverse and z components of vectors.

B.3 Numerical Implementation

This section provides details on the numerical implementation of the above theoretical formulation for ECT simulation. This includes methods to efficiently evaluate the infinite integrals of Green's function (B.12) are presented. Followed by details on the solution to the integral equation in (B.5).

B.3.1 Evaluation of Green's function

Several methods have been developed for numerical evaluation of the infinite integrals arising with the use of Sommerfeld identity in (B.8). These vary from asymptotic expansion that yield closed form, approximate solution to specialized quadrature rules. In this work, the recently developed Discrete Complex Image Method (DCIM) is used evaluate these infinite integrals in closed form. In DCIM, the integrand is approximated as a sum of exponential functions in k_z and the Sommerfeld identity is used to represent these individual infinite integrals as spherical waves.

Consider the evaluation of the following infinite integral,

$$\phi(r) = \frac{i}{2}\int_{SIP} \frac{k_\rho}{k_z} H_0^{(1)}(k_\rho \rho) e^{ik_z z} R(k_z) \tag{B.14}$$

Note that all integrals in (B.12) can be reduced to the above form with simple manipulations. Let the coefficient $R(k_z)$ in (B.14) be represented as sum of exponentials

$$R(k_z) = \sum_{n=0}^{N} A_n e^{ik_z c_n} \tag{B.15}$$

Using the Sommerfeld identity (B.8), the individual integrals in the above summation is represented as spherical waves,

$$\phi(r) = \sum_{n=0}^{N} A_n e^{ikr_n^c}/r_n^c \ , \ r_n^c = \sqrt{\rho^2 + (z+c_n)^2} \tag{B.16}$$

These spherical waves can be interpreted as emanating from image sources of strength A_n placed at complex positions r_n^c.

There exists several different approach to determine A_i and c_i, for approximating $R(k_z)$ in terms of exponential functions. Matrix Pencil Method (MPM) is a relatively new technique for representing arbitrary function in terms of exponentials. MPM is

based on singular valued decomposition (SVD) and provides a means to control the error in the resulting approximation. A major requirement of MPM is that the integrand be sampled at uniform intervals. In case of planar media Green's function, this sampling should be done respecting the Sommerfeld integral path (SIP) shown in figure B.2. In practice, this is achieved by using an intermediate parametric variable t. The integrand is sampled at uniform intervals of t and the relation between t and k_z is chosen to conform with the SIP,

$$k_z = \gamma k[it + 1] \quad 0 \leq t \leq T_0/\gamma \tag{B.17}$$

where T_0 defines the finite domain of integration and is chosen large enough until oscillations in integrand have damped sufficiently, γ controls the separation of SIP with real axis as shown in figure B.2.

The relation (B.17) prescribed in literature is suitable only for scenarios where the conductivity of the medium is zeros or negligible. When conductivity is finite and very large, as in case of ECT, k_z determined through above relation (B.17) fails to follow the SIP as shown in figure B.3. A modified relation (B.18) is introduced in this work to account for materials with high conductivity and still respect the SIP

$$k_z = \gamma Re\{k\}[it + 1] + iIm\{k\} \tag{B.18}$$

where $Re\{\cdot\}$ and $Im\{\cdot\}$ represent the real and imaginary part respectively. Note that when k is a pure real quantity, i.e. when conductivity is zero, the modified relation reduces to the original relation (B.17). Figure B.3 shows the path evaluated using the modified relation for high conductivity case. Other advantages of high conductivity are **(a)** the poles and branch cuts of the integrand are well separated from real axis and they do not affect the numerical integration; and **(b)** the integrands

are less oscillatory, which in turn implies less number of approximation terms. The maximum number of DCIM terms encountered throughtout this work did not exceed 20.

B.3.2 Solution to integral equations

For numerical solution of the integral equation in (B.5), the volume region Ω_2 is discretized into M tetrahedrons. The unknown electric field density $\mathbf{D}$ in this domain is represented in terms of divergence conforming vector basis functions defined on each face of tetrahedron [240],

$$\mathbf{D}(\mathbf{r}) = \sum_{n=1}^{M_e} \mathbf{f}_i(\mathbf{r}) D_i \tag{B.19}$$

where M_e is the total number of distinct tetrahedron faces, $\mathbf{f}_i$ is the vector basis function defined on the i^{th} face and D_i is the unknown coefficient corresponding to this basis function. Several properties of these basis function are discussed in detail in [240]. Employing this representation in (B.5) and using Galerkin testing leads to the following matrix equation,

$$\mathbf{Z}V = H \tag{B.20}$$

where V and H are vectors of size M_e and $\mathbf{Z}$ is a matrix of size $M_e \times M_e$. The elements the matrix and vectors in (B.20) are given as follows,

$$\mathbf{Z}(m,n) = \int_V d\mathbf{r} \int_V d\mathbf{r}' \mathbf{f}_m(\mathbf{r}).\overline{\overline{\mathbf{G}}}^i.\mathbf{f}_n(\mathbf{r}') \tag{B.21}$$

$$V(m) = D_m \tag{B.22}$$

$$H(m) = \int_V d\mathbf{r} E^{inc}(\mathbf{r}) \mathbf{f}_m(\mathbf{r}) \tag{B.23}$$

where V is the volume of domain Ω_2. The symmetric form of the Green's function used in this work, allows the transfer of derivatives of the Green's function onto the testing and sourcing vector basis Thus the maximum singularity encountered in this

work is of the type $1/||\mathbf{r}-\mathbf{r}'||$ which can be evaluated in closed form using the methods provided in [241].

B.4 Results and Discussion

Several results that demonstrate the efficacy of above described scheme are presented in this section. First the theoretical modifications introduced to the DCIM method for high-conductivity materials are verified. Simple semi-analytical models exists for axi-symmetric geometries. Such models exist for circular coils place over defect free layered media. The numerical implementation of DCIM and MPM procedure with the proposed modifications are compared with results these semi-analytical models for various test configuration. First, the results for evaluation of the transmitted field at various depths inside the layered medium using both the methods are shown in figure B.4. Figure B.5 shows the evaluation of transmitted fields at different frequencies using both the methods. Next, impedance of the coil evaluated using DCIM+MPM method and semi-analytical model is shown in figures B.6 and B.7 corresponding to different coil lift-off and excitation frequency, respectively. In all cases, there is an excellent match between DCIM+MPM method and semi-analytical and this implies that the proposed modifications to DCIM are valid and essential.

Next set of results corresponds to the case of a defect in the layered medium. A semi-infinite medium with finite conductivity of $\sigma = 30MS$ with a rectangular defect of size $13 \times 0.3 \times 5\ mm^3$ is considered. The frequency of excitation is 900 MHz and the solution from the integral equation solver are compared with experimental measurements. Impedance of the coil is computed at various x position, see figure B.8, with the origin at center of defect region and x position of coil is measured with respect to coil center from origin. The amplitude of coil impedance evaluated from Integral equation solution is shown in figure B.9 and the phase values of impedance is shown in

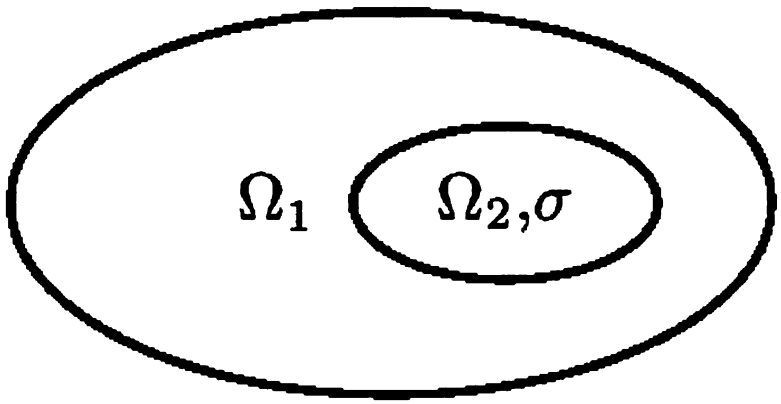

Figure B.1: Different domains in eddy current simulation

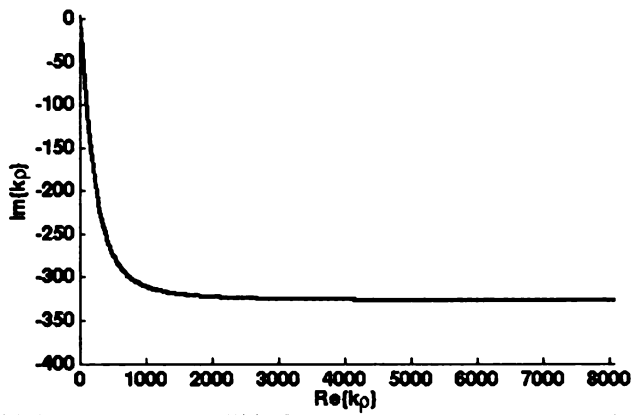

Figure B.2: DCIM path from existing literature for zero conductivity

figure B.10. Qualitatively comparing with the measurement results, provided in [242], there is a good match with results from the integral equation solver. Quantitatively, the error between the model results and measurement was evaluated to be about 10%.

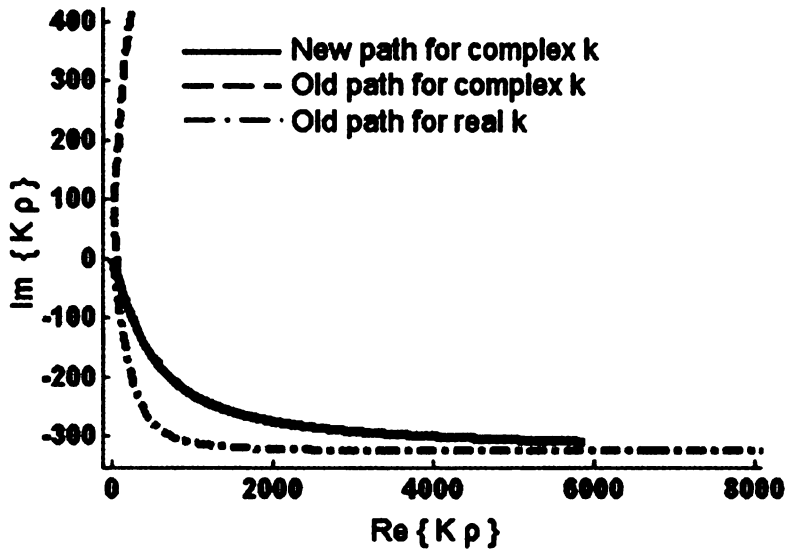

Figure B.3: Comparison between existing and Proposed DCIM path with finite conductivity.

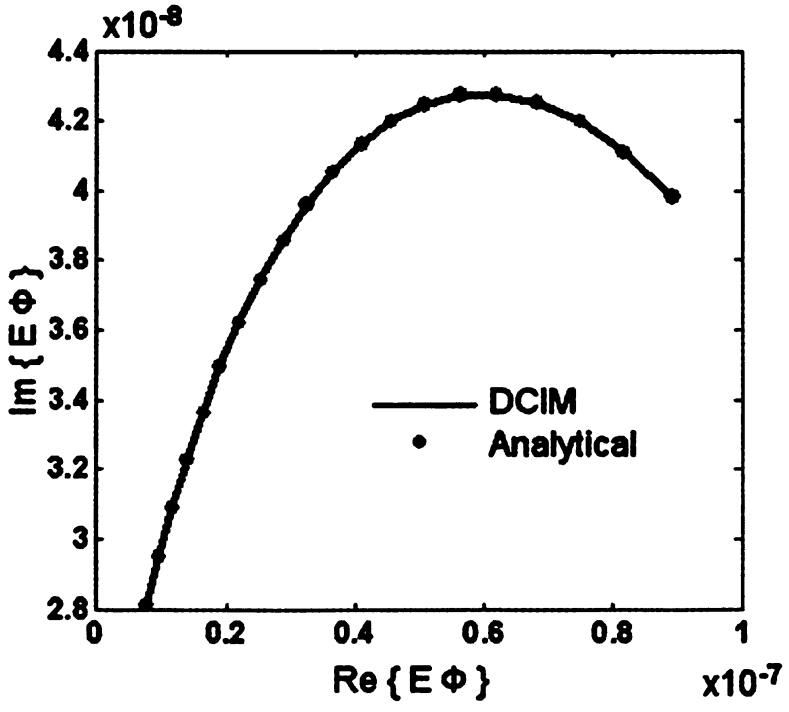

Figure B.4: Transmitted field at various depth

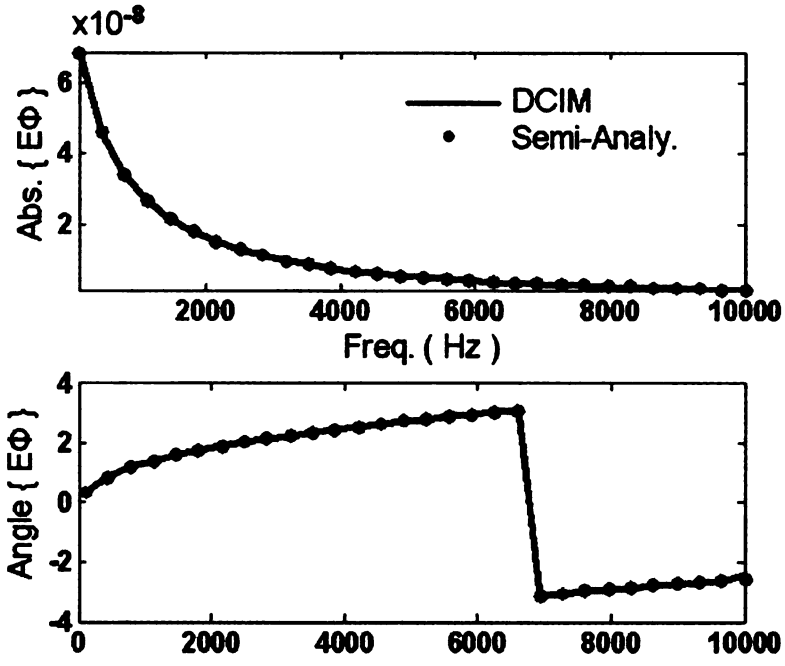

Figure B.5: Transmitted field with varying frequency

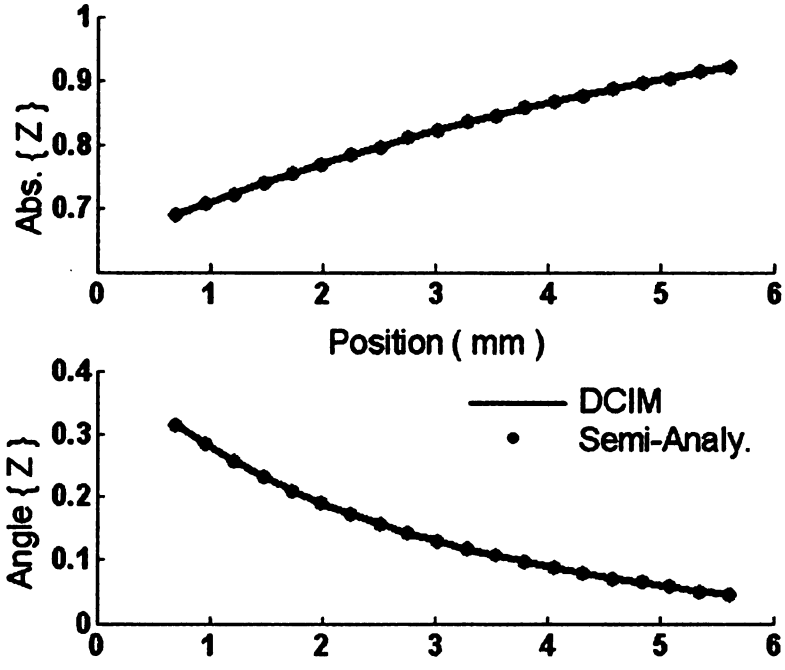

Figure B.6: Z vs. coil lift-off

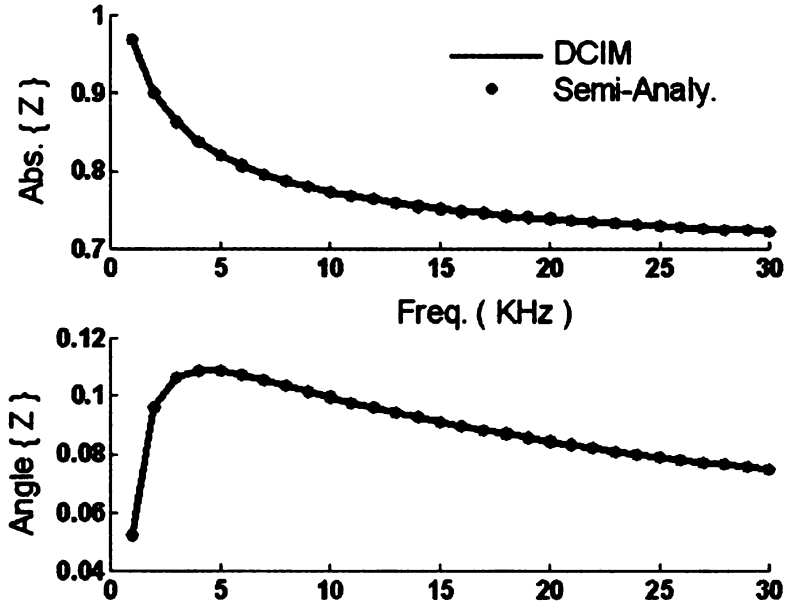

Figure B.7: Z vs. excitation frequency

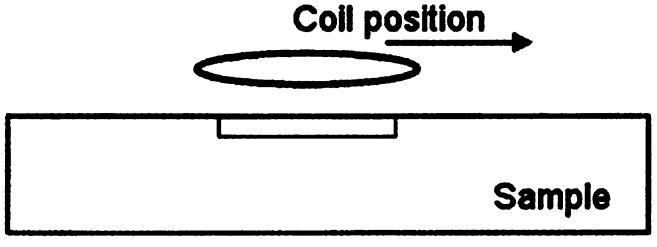

Figure B.8: Experiment to validate the integral equation model. Measurement of impedance as the coil is scanned across the defect.

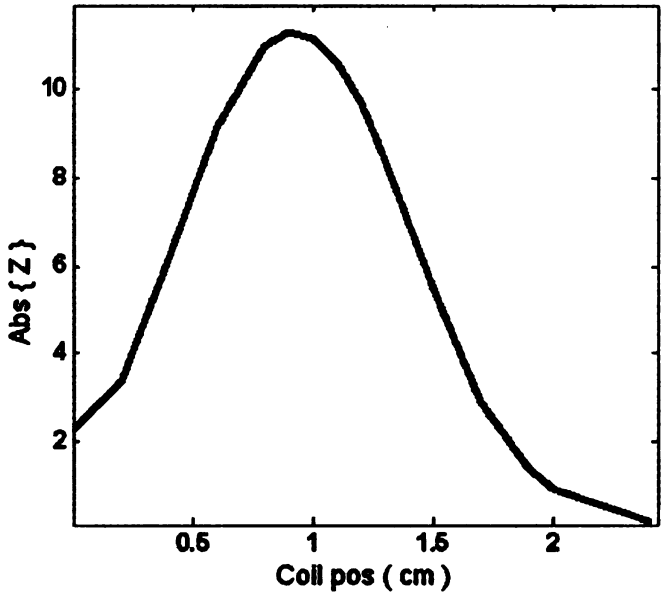

Figure B.9: Absolute value of coil impedance from the IE model.

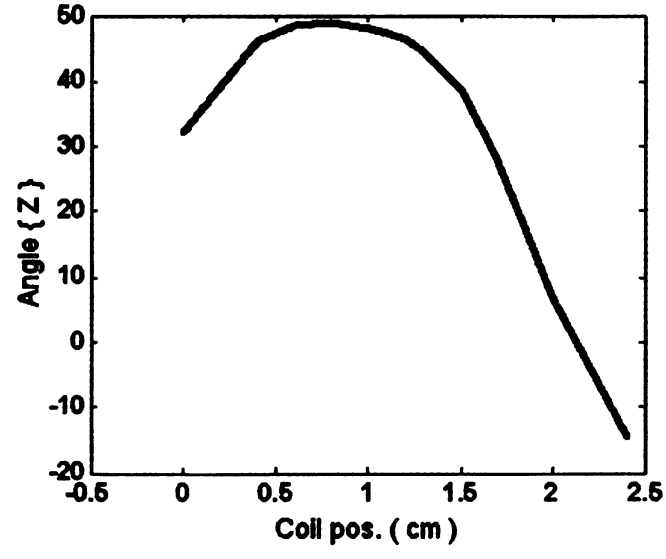

Figure B.10: Phase value of coil impedance from the IE model.

Appendix C

Curriculam Vitae

Journal Papers

1. **M Vikram**, Jun and B. Shanker, Mathematical Analysis of Single Integral Equation (SIE) for Electromagnetic Scattering from Homoegeneous Dielectric Bodies,*under preparation, to be submitted to IEEE Trans. on Antennas and Propagat.*

2. **M Vikram**, B. Shanker and S. Aluru, A Scalable Parallel Wideband FMM for Efficient Electromagnetic Simulations on Large Scale Clusters, *submitted to IEEE Trans. Antennas and Propagat*, May 2009.

3. **M Vikram**, A. Baczewski, B. Shanker and L. Kempel, "Accelerated Cartesian Expansion (ACE) unified framework for the rapid evaluation of potentials associated with the diffusion, lossy wave and Klein-Gordon equations", *under review Journal of computational physics.*

4. **M Vikram**, H. Huang, B. Shanker and V. Tri, "A Novel Wideband FMM for Electromagnetic Simulation of Multiscale Structures", *accepted for publication in IEEE Trans. Antennas and Propagat.*

5. **M. Vikram**, B. Shanker, "An incomplete review of fast multipole methods-from static to wideband-as applied to problems in computational electromagnetics", *Journal of Applied Computational Electromagnetic Society*, Accepted for publication - May 2008.

6. **M. Vikram**, B. Shanker, "Fast Evaluation of Time Domain Fields in Sub-Wavelength Source/Observer Distributions using Accelerated Cartesian Expan-

sions (ACE)", *Journal of Computational Physics*, Vol. 227, Issue 2, pp. 1007-1023, Dec. 2007.

7. K. Arunachalam, **V. R. Melapudi**, L. Udpa, and S. S. Udpa, "Microwave NDT of Cement-Based Materials Using Far Field Reflection Coefficients", NDT and E International, 39, pp. 585-593, 2006.

8. N. V. Nair, **V. R. Melapudi**, H. R. Jimenez, X. Liu, Y. Deng, Z. Zeng, L. Udpa, T. J. Moran, and S. S. Udpa, "A GMR-Based Eddy Current System for NDE of Aircraft Structures", IEEE Transactions on Magnetics, Vol. 42, Issue 10, pp. 3312-3314, Oct. 2006.

Conference Papers

1. M. Vikram, B. Shanker and S. Aluru Large Scale Parallel Electromagnetic Solver for Multiscale Simulations, Submitted to ACES International conference, to be held in March 2009.

2. N. V. Nair, M. Vikram and B. Shanker A Robust Generalized Method of Moments Scheme for Electromagnetic Analysis, Submitted to ACES International conference, to be held in March 2009.

3. M. Vikram, A. Baczewski, B. Shanker and S. Aluru Parallel Accelerated Cartesian Expansions for Particle Dynamics Simulations, Accepted in IEEE IPDPS 2009, to be held in May 2009. (**20% acceptance rate**)

4. M. Vikram, B. Shanker and T. Van Fast Solvers for Electromagnetic Simulation of Mixed-Scale Structures, Antennas Propagation Society International Symposium, San Diego, July 2008. (Received third place price in best sudent paper contest)

5. M. Vikram, B. Shanker and S. Aluru Provably Optimal Parallel Fast Solvers for Electromagnetic Simulations, Antennas Propagation Society International Symposium/URSI, San Diego, July 2008.

6. M. Vikram, B. Shanker and E. Michielssen Fast Evaluation of Transient Fields in Sub- to Long-wavelength Source/Observer Distributions, Antennas Propagation Society International Symposium/URSI, San Diego, July 2008.

7. N. V. Nair, M. Vikram and B. Shanker Mathematical Analysis of the Augmented Electric Field Integral Equation Operators, Antennas Propagation Society International Symposium/URSI, San Diego, July 2008.

8. A. Baczewski, M. Vikram and B. Shanker Fast Methods for the Evaluation of the Diffusion Kernel with Extensions to the Dissipative Kernel, Antennas Propagation Society International Symposium, San Diego, July 2008.

9. M. Vikram and B. Shanker "Fast Evaluation of Time Domain Fields in Sub-Wavelength Source/Observer Distributions using Accelerated Cartesian Expansions", URSI/UNC International conference, Ottawa, July 2007.

10. M. Vikram, H. Huang and B. Shanker "Fast Evaluation of Fields from Sub-Wavelength Structures in Frequency Domain Using Accelerated Cartesian Expansions", URSI/UNC International conference, Ottawa, July 2007.

11. M. Vikram, B. Shanker, L. Udpa and S. S. Udpa "Eddy Current Simulation of Defects in Layered Media Using Discrete Complex Image Method", URSI/UNC International conference, Ottawa, July 2007.

12. M. Vikram, Y. Jun and B. Shanker "Eigenvalue Analysis of Single Integral Equations", Electromagnetic Theory and Symposium, Ottawa, July 2007.

13. M. Vikram, H. Griffith, H. Huang and B. Shanker "Accelerated cartesian harmonics for fast computation of time and frequency domain low-frequency kernels", Antennas Propagation Society International Symposium, Hawaii, June 2007.

14. V. R. Melapudi, S. S. Udpa, L. Udpa, and W. P. Winfree "Ray Tracing Model for Terahertz Inspection of Spray On Foam Insulation (SOFI) ", 12th Biennial IEEE Conference on Electromagnetic Field Computation, 2006

15. N. V. Nair, V. R. Melapudi, L. Xin, L. Udpa, S. S. Udpa "A GMR based Eddy Current Field Sensing System for NDE of Aircraft Structures", IEEE International Magnetics Conference (INTERMAG), 2006.

16. V. R. Melapudi, S. S. Udpa, L. Udpa, and W. P. Winfree "Ray-Rracing Model for Terahertz Imaging of SOFI Inspection", Review of Quantitative Nondestructive Evaluation, D. O. Thompson and D. E. Chimenti, Eds., American Institute of Physics, 2005.

17. K. Arunachalam, R. V. Melapudi, E. J. Rothwell, L. Udpa, and S. S. Udpa, "Microwave NDE for Reinforced Concrete", Review of Quantitative Nondestructive Evaluation, D. O. Thompson and D. E. Chimenti, Eds., American Institute of Physics, 2005.

18. N. V. Nair, V. R. Melapudi, S. Ramakrishnan, L. Udpa, S. S. Udpa and W. P. Winfree, "A Wavelet Based Signal Processing Technique for Image Enhancement in Terahertz Imaging Data", Review of Quantitative Nondestructive Evaluation, D. O. Thompson and D. E. Chimenti, Eds., American Institute of Physics, 2005.

19. I. Elshafiey, V. R. Melapudi and L. Udpa " Electromagnetic?Acoustic Modeling of Fields Induced by Gradient Pulses in Diffusion Tensor Magnetic Resonance Imaging ", Review of Quantitative Nondestructive Evaluation, D. O. Thompson and D. E. Chimenti, Eds., American Institute of Physics, 2005.

20. V. R. Melapudi, S. Udpa, L. Udpa, and W. P. Winfree, "Imaging and Modeling Techniques for Terahertz Inspection of NASA-SOFI", to appear in Annual Review of Progress In Quantitative Nondestructive Evaluation 2005, Portland.

Technical Reports

1. M Vikram, H. Huang, B. Shanker and V. Tri, A Novel Wideband FMM for Electromagnetic Simulation of Multiscale Structures Michigan State University Technical Report Series, 2008.

2. M. Vikram and B. Shanker Fast Evaluation of Time Domain Fields in Sub-Wavelength Source/Observer Distributions using Accelerated Cartesian Expansions (ACE), Michigan State University Technical Report Series, 2007.

3. M. Vikram, U. Parriker and L. Udpa Automated detection and classification software for inspection of aircraft rotor structures, Technical Report submitted to FAA, 2005.

Disclosures

1. Disclosure (Spring 2007): A Free Scan GMR based Eddy Current Testing System, Inventors: M. Vikram, N. V. Nair, S. S. Udpa and L. Udpa

BIBLIOGRAPHY

[1] M. N. O. Sadiku, *Numerical techniques in electromagnetics.* CRC press, 2000.

[2] J. Jin, *The finite element method in electromagnetics.* John wiley and sons, 2002.

[3] J. H. Richmond, "Digital computer solutions of the rigorous equations for scattering problems," *Proceeding of the IEEE*, vol. 53, pp. 796–804, 1965.

[4] A. Appel, "An efficient program for many-body simulations," *SIAM J. Sci. Comput.*, vol. 6, pp. 85–103, 1985.

[5] J. Barnes and P. Hut, "A hierarchical $\mathcal{O}(n \log n)$ force calculation algorithm," *Nature*, vol. 324, pp. 446–449, 1986.

[6] V. Rokhlin, "Rapid solution of the integral equations of classical potential theory," *Journal of Computational Physics*, vol. 60, pp. 187–207, 1985.

[7] L. Greengard and V. Rokhlin, "A fast algorithm for particle simulations," *Journal of Computational Physics*, vol. 20, pp. 63–71, 1987.

[8] L. Greengard, *The rapid evaluation of potential fields in particle systems.* Cambridge, MA: MIT Press, 1988.

[9] L. Greengard and V. Rokhlin, "A new version of the fast multipole method for the Laplace equation in three dimensions," *Acta Numerica*, vol. 6, pp. 229–269, 1997.

[10] F. Zhao, "An $\mathcal{O}(n)$ algorithm for three-dimensional n-body simulation," Master's thesis, Massachusetts Institute of Technology, 1987.

[11] E. J. Weniger, "Addition theorems as three-dimensional Taylor expansions," *International Journal of Quantum Chemistry*, vol. 76, pp. 280–295, 2000.

[12] P. B. Visscher and D. M. Apalkov, "Charge based recursive fast multipole micromagnetics," *Physica B: Physics of Condensed Matter*, vol. 343, pp. 184–188, 2004.

[13] B. Shanker and H. Huang, "Accelerated Cartesian expansions - a fast method for computing of potentials of the form $R^{-\nu}$ for all real ν," *Journal of Computational Physics*, vol. 226, pp. 732–753, 2007. Technical Report; MSU-ECE-Report-2006-5.

[14] W. D. Elliott and J. A. Board, "Multipole algorithms for molecular dynamics simulation on high performance computers," Tech. Rep. TR95-003.html, Duke University, 1995.

[15] Y. Fu, K. J. Klimkowski, G. J. Rodin, E. Berger, J. C. Browne, J. K. Singer, R. A. van de Geijin, and K. S. Vemaganti, "A fast solution method for three-dimensional many-particle problems of linear elastosticity," *J. Numer. Methods Eng.*, vol. 42, pp. 1215–1229, 1998.

[16] K. Yoshida, N. Nishimura, and S. Kobayashi, "Application of fast multipole Galerkin boundary integral equationmethod to elastostatic crack problems in 3D," *Int. J. Numer. Methods Eng.*, vol. 50, pp. 525–527, 2001.

[17] Y. H. Chen, W. C. Chew, and S. Zeroug, "Fast multipole method as an efficient solver for 2D elastic wavesurface integral equations," *Computational mechanics*, vol. 20, pp. 495–506, 1997.

[18] Y. Fu and G. J. Rodin, "Fast solution method for three-dimensional Stokesian many-particle problems," *Commun. Numer. Meth. Eng.*, vol. 16, pp. 145–149, 2000.

[19] K. Nabors and J. White, "Fastcap: A multipole accelerated 2-D capacitance extraction program," *IEEE Trans. Computer Aided Design*, vol. 10, pp. 1447–1459, 1991.

[20] M. Kamon, M. J. Tsuk, and J. K. White, "FASTHENRY: A multipole accelerated 3-D inductance extraction program," *IEEE Trans. Microwave Theory Tech.*, vol. 42, pp. 1750–1758, 1994.

[21] F. Chen and D. Suter, "Using a fast multipole method to accelerate spline evaluations," *IEEE Computational Science and Engineering*, vol. 5, pp. 24–31, 1998.

[22] J. R. Driscoll and J. D. M. Healy, "Asymptotically fast algorithms for spherical and related transforms," in *30th annual symposium on foundations of computer science*, (Research Triangle Park, NC), pp. 344–349, IEEE Computer Society Press, 1989.

[23] R. J. Chien and B. K. Alpert, "A fast spherical filter with uniform resolution," *Journal of Computational Physics*, vol. 136, pp. 580–584, 1997.

[24] L. Greengard and J. Strain, "A fast algorithm for the evaluation of heat potentials," *Comm. Pure Appl. Math.*, vol. 43, pp. 949–963, 1990.

[25] J. Tausch, "A fast method for solving the heat equation by layer potentials," *Journal of Computational Physics*, vol. 224, no. 2, pp. 956–969, 2007.

[26] J.-R. Li and L. Greengard, "On the numerical solution of the heat equation I: fast solvers infree space," *Journal of Computational Physics*, vol. 226, pp. 1891–1901, 2007.

[27] V. Rokhlin, "Rapid solutions of integral equations of scattering theory in two dimensions," *Journal of Computational Physics*, vol. 86, pp. 414–439, 1990.

[28] C. C. Lu and W. C. Chew, "Fast algorithm for solving hybrid integral equations," *IEE Proceedings H: Microwaves and Antennas*, vol. 140, pp. 455–460, 1992.

[29] N. Engheta, W. D. Murphy, V. Rokhlin, and M. S. Vassiliou, "The fast multipole method (FMM) for electromagnetic scattering problems," *IEEE Trans. Antennas Propagat.*, vol. 40, pp. 634–641, 1992.

[30] V. Rokhlin, "Diagonal forms of translation operators for the Helmholtz equation in three dimensions," *Applied and Computational Harmonic Analysis*, vol. 1, pp. 82–93, 1993.

[31] M. A. Epton and B. Dembart, "Multipole translation theory for three dimensional Laplace and Helmholtz equations," *SIAM J. Sci. Compt.*, vol. 16, pp. 865–897, 1995.

[32] W. C. Chew, S. Koc, J. M. Song, C. C. Lu, and E. Michielssen, "A succint way to diagonalize the translation matrix in three dimensions," *IEEE AP-S Int. Symp.*, pp. 2072–2075, 1997.

[33] W. C. Chew, J.-M. Jin, E. Michielssen, and J. Song, eds., *Fast and Efficient Algorithms in Computational Electromagnetics.* Artech House Publishers, 2001.

[34] N. Nishimura, "Fast multipole accelerated boundary integral equation methods," *Appl Mech Rev*, vol. 55, pp. 299–324, 2002.

[35] M. F. Gyure and M. A. Stalzer, "A prescription for the multilevel Helmhotz FMM," *IEEE Computational Science and Engineering*, vol. 5, no. 3, pp. 39–47, 1998.

[36] S. Velamparambil, J. M. Song, W. C. Chew, and G. K., "ScaleME: A portable scalable multipole engine for electromagnetic and acoustic integral equation solvers," *IEEE AP-S Int. Symp.*, vol. 3, pp. 1774–1777, 1998.

[37] S. Velamparambil, W. C. Chew, and J. Song, "10 million unknowns: is it that big?," *IEEE Trans. Antennas and Propagat.*, vol. 45, pp. 43–58, 2003.

[38] B. Hariharan, S. Aluru, and B. Shanker, "A scalable parallel fast multipole method for analysis of scattering from perfect electrically conducting surfaces," in *Supercomputing, ACM/IEEE 2002 Conference*, pp. 42–42, 16-22 Nov. 2002.

[39] B. Hariharan and S. Aluru, "Efficient parallel algorithms and software for compressed octrees with applications to hierarchical methods," *Parallel Computing*, vol. 31, pp. 311–331, 2005.

[40] L. Gurel and O. Ergul, "Fast and accurate solutions of extremely large integral-equation problems discretised with tens of millions of unknowns," *Electronics Letters*, vol. 43, no. 9, pp. 499–500, April 26 2007.

[41] O. Ergul and L. Gurel, "Hierarchical parallelisation strategy for multilevel fast multipole algorithm in computational electromagnetics," *Electronics Letters*, vol. 44, no. 1, pp. 3–5, January 3 2008.

[42] L. Greengard, J. Huang, V. Rokhlin, and S. Wandzura, "Accelerating fast multipole methods for the Helmholtz equation at low frequencies," *IEEE Computational Science and Engineering*, vol. 5, pp. 32–38, 1998.

[43] B. Dembart and E. Yip, "The accuracy of fast multipole methods for Maxwell's equations," *IEEE Computational Science and Engineering*, vol. 5, pp. 48–56, 1998.

[44] J. S. Zhao and W. C. Chew, "MLFMA for solving boundary equations of 2D electromagnetic scattering from static to electrodynamic," *Microwave and Optical Technology Letters*, vol. 20, pp. 306–311, 1999.

[45] T. J. Cui and W. C. Chew, "Fast algorithm for electromagnetic scattering by buried conducting plates of large size," *IEEE Trans. Antennas and Propagat.*, vol. 47, no. 6, pp. 1116–1118, 1999.

[46] J. S. Zhao and W. C. Chew, "Three-dimensional multilevel fast multipole algorithm from static to electrodynamic," *Microwave and Optical Technology Letters*, vol. 26, pp. 43–48, 2000.

[47] B. Hu and W. C. Chew, "Fast inhomogenous plane wave algorithm for scattering from objects above the multilayered medium," *IEEE Trans. Geoscience and Remote Sensing*, vol. 39, pp. 1028–1038, 2001.

[48] J. Sarvas, "Performing interpolation and anterpolation entirely by fast Fourier transform in the 3-D multilevel fast multipole algorithm," *SIAM Journal on Numerical Analysis*, vol. 41, pp. 2180–2196, 2003.

[49] E. Darve and P. Have, "Efficient fast multipole method for low-frequency scattering," *Journal of Computational Physics*, vol. 197, pp. 341–363, January 2004.

[50] H. Cheng, W. Y. Crutchfield, Z. Gimbutas, L. F. Greengard, J. F. Ethridge, J. Huang, V. Rokhlin, and N. Y. andJ. Zhao, "A wideband fast multipole method for the Helmholtz equation in three dimensions," *Journal of Computational Physics*, vol. 216, pp. 300–325, 2006.

[51] H. Cheng, L. Greengard, and V. Rokhlin, "A fast adaptive multipole algorithm in three dimensions," *Journal of Computational Physics*, vol. 155, pp. 468–498, 1999.

[52] S. Aluru, "Greengard's N-body algorithm is not order N," *SIAM J. Sci. Comput.*, vol. 17, pp. 773–776, 1996.

[53] M. S. Warren and J. K. Salmon, "A parallel hashed oct-tree N-body algorithm," in *Supercomputing '93: Proceedings of the 1993 ACM/IEEE conference on Supercomputing*, (New York, NY, USA), pp. 12–21, ACM, 1993.

[54] F. Sevilgen, S. Aluru, and N. Futamura, "Parallel algorithms for tree accumulations," *Journal of Parallel and Distributed Computing*, vol. 65, pp. 85–93, 2005.

[55] J. T. J. White, "A multiscale method for fast capacitance extraction," in *Proceedings of the IEEE/ACM DAC*, 1998.

[56] S. Balasubramanian, L. N. Subramaniam, and B. Shanker, "Fast integral equation based analysis of magneto-static fields in bulk non-linear media," *IEEE Trans. Magnetics*, vol. 35, pp. 100–107, 2002.

[57] V. Rokhlin and S. M. Wandzura, "The fast multipole method for periodic structure," in *IEEE AP-S Int. Symp.*, pp. 424–427, 1994.

[58] J. A. Stratton, *Electromagnetic theory.* McGraw-Hill New York, 1941.

[59] M. Abramowitz and I. A. Stegun, *Handbook of Mathematical Functions with Formulas, Graphs, and Mathematical Tables.* New York, NY: Dover Publications, Inc., 1972.

[60] W. D. Elliott and J. A. Board, "Fast Fourier transform accelerated fast multipole algorithm," *SIAM J. Sci. Comput.*, vol. 17, pp. 398–415, 1996.

[61] M. Vikram and B. Shanker, "Fast evaluation of time domain fields in subwavelength source/observer distributions using accelerated Cartesian expansions (ACE)," *Journal of Computational Physics*, vol. 227, pp. 1007–1023, 2007.

[62] B. Hu, W. C. Chew, E. Michielssen, and J. Zhao, "An improved fast steepest descent algorithm for the fast analysis of two-dimensional scattering problems," *Radio Sci.*, vol. 34, pp. 759–772, 1999.

[63] N. Yarvin and V. Rokhlin, "Generalized Gaussian quadratures and singular value decompositions of integral operators," tech. rep., Department of Computer Science, Yale University, 1996.

[64] B. Hu, W. C. Chew, E. Michielssen, and J. Zhano, "Fast inhomogeneous plane wave algorithm for fast analysis of two-dimensional scattering problems," *Radio Science*, vol. 34, pp. 759–772, 1999.

[65] R. Coifman, V. Rokhlin, and S. Wandzura, "The fast multipole method for the wave equation: A pedestrian prescription," *IEEE Antennas and Propagation Magazine*, vol. 35, pp. 7–12, June 1993.

[66] V. Rokhlin, "Sparse diagonal forms for translation operators for the Helmholtz equation in two dimensions," Tech. Rep. YALEU/DCS/RR-1095, Yale University, 1995.

[67] J. Rahola, "Diagonal forms of the translation operators in the fast multipole algorithm for scattering problems," *BIT Numerical Mathematics*, vol. 36, pp. 333–358, 1996.

[68] A. D. McLaren, "Optimal numerical integration on a sphere," *Mathematics of Computation*, vol. 17, pp. 361–383, 1963.

[69] E. Darve, "The fast multipole method: Numerical implementation," *Journal of Computational Physics*, vol. 160, pp. 195–240, 2000.

[70] J. Song and W. C. Chew, "Error analysis for the truncation of multipole expansion of vector Green's functions," *IEEE Microwave and Wireless Components letters*, vol. 11, pp. 311–313, 2001.

[71] J.-Y. Li, L.-W. Li, B.-L. Ooi, P.-S. Kooi, and M.-S. Leong, "On the accuracy of the addition theorem for a scalar green's function used in the FMM," *Microwave and Optical Technology Letters*, vol. 31, pp. 439–442, 2001.

[72] M. L. Hastriter, S. Ohnuki, and W. C. Chew, "Error control of the translation operator in 3D MLFMA," *Microwave and Optical Technology Letters*, vol. 37, pp. 184–188, 2003.

[73] S. Koc, J. Song, and W. C. Chew, "Error analysis for the numerical evaluation of the diagonal forms of the scalar spherical addition theorem," *SIAM J. Numer. Anal.*, vol. 36, no. 3, pp. 906–921, 1999.

[74] M. Nilsson, "Stability of the high frequency fast multipole method for helmholtz equation in three dimensions," *BIT Numerical Mathematics*, vol. 44, pp. 773–791, 2004.

[75] J. M. Song, C. C. Lu, W. C. Chew, and S. W. Lee, "Fast illinois solver code (FISC)," *IEEE Antennas Propagat. Mag.*, vol. 40, pp. 27–34, 1998.

[76] E. Darve, "The fast multipole method I: Error analysis and asymptotic complexity," *SIAM J. Numer. Anal.*, vol. 38, pp. 98–128, 2000.

[77] C. C. Lu and W. C. Chew, "A multilevel algorithm for solving boundary integral wave scattering," *Microwave and Optical Technology Letters*, vol. 7, pp. 466–470, 1994.

[78] J. M. Song and W. C. Chew, "Multilevel fast-multipole algorithm for solving combined field integral equations of electromagnetic scattering," *Microwave and Optical Technology Letters*, vol. 10, no. 1, pp. 14–19, 1995.

[79] B. Dembart and E. Yip, "A 3D fast multipole method for electromagnetics with multiple levels," in *Proceedings of the 11th Annual Conference on Applied Computational Electromagnetics*, vol. 1, (Monterey, CA), pp. 621–628, 1995.

[80] T. Hrycak and V. Rokhlin, "An improved fast multipole algorithm for potential fields," *SIAM Journal on Scientific Computing*, vol. 19, pp. 1804–1826, 1998.

[81] N. Yarvin and V. Rokhlin, "A generalized 1D fast-multipole method, with applications to filtering of spherical harmonics," tech. rep., Yale University, 1998.

[82] B. Shanker, A. Ergin, M. Lu, and E. Michielssen, "Fast analysis of transient electromagnetic scattering phenomena using the multilevel plane wave time domain algorithm," *IEEE Trans. Antennas and Propagat.*, vol. 51, no. 3, pp. 628–641, March 2003.

[83] E. Michielssen and W. C. Chew, "Fast steepest descent path algorithm for analyzing scattering from two-dimensional objects," *Radio Sci.*, vol. 31, pp. 1215–1224, 1996.

[84] L. J. Jiang and W. C. Chew, "Low-frequency fast inhomogeneous plane-wave algorithm (LF-FIPWA)," *Microwave and Optical Technology Letters*, vol. 20, pp. 117–122, 2004.

[85] R. L. Wagner and W. C. Chew, "A ray-propagation fast multipole algorithm," *Microwave and Optical Technology Letters*, vol. 7, pp. 435–438, 1994.

[86] B. Shanker, S.-K. Han, and E. Michielssen, "A fast multipole approach to computing scattering from an inhomogeneous bianisotropic cylindrical object using Beltrami fields," *Radio Science*, vol. 33, pp. 17–31, 1998.

[87] T. J. Cui and W. C. Chew, "Accurate analysis of wire structures from very-low frequency to microwave frequency," *IEEE Trans. Antennas and Propagat.*, vol. 50, pp. 301–307, 2002.

[88] W. C. Chew, *Waves and Fields in Inhomogeneous Media.* IEEE Press New York, 1995.

[89] L. Xuan, A. Zhu, A. R. J., and S. D. Gedney, "A broadband multilevel fast multipole algorithm," *IEEE AP-S Int. Symp. and USNC/URSI National Radio Science Meeting*, vol. 2, pp. 1195–1198, 2004.

[90] H. Wallen and J. Sarvas, "Translation procedures for broadband MLFMA," *Progress in Electromagnetics Research*, vol. 55, pp. 47–78, 2005.

[91] J. Carrier, L. Greengard, and V. Rokhlin, "A fast adaptive multipole algorithm for particle simulations," *SIAM J. Sci. Stat. Comput.*, vol. 9, pp. 669–686, 1988.

[92] K. Nabors and J. White, "Multipole-accelerated capacitance extraction for 3-D structures with multilayer dielectrics," *IEEE Tran. Circ. Syst.*, vol. 39, pp. 946–954, 1992.

[93] A. Adedoyin and P. Andrei, "3-D magnetostatic using the fast multiple method," *IEEE Trans. Magnetics*, vol. 43, no. 6, pp. 2914–2916, June 2007.

[94] I. Mayergoyz, P. Andrei, and M. Dimian, "Nonlinear magnetostatic calculations based on fast multipole method," *IEEE Trans. Magnetics*, vol. 39, no. 3, pp. 1103–1106, May 2003.

[95] W. Hafla, A. Buchau, F. Groh, and W. Rucker, "Efficient integral equation method for the solution of 3-D magnetostatic problems," *IEEE Trans. Magnetics*, vol. 41, no. 5, pp. 1408–1411, May 2005.

[96] Y. Takahashi, Y. Fujishima, and S. Wakao, "Large-scale analysis of surface charge in eddy-current problems by the fast multipole method," *IEEE Trans. Magnetics*, vol. 41, no. 5, pp. 1700–1703, May 2005.

[97] G. Rubinacci, A. Tamburrino, S. Ventre, and F. Villone, "A fast 3-D multipole method for eddy-current computation," *IEEE Trans. Magnetics*, vol. 40, no. 2, pp. 1290–1293, March 2004.

[98] C. Seberino and H. Bertram, "Concise, efficient three-dimensional fast multipole method for micromagnetics," *IEEE Trans. Magnetics*, vol. 37, no. 3, pp. 1078–1086, May 2001.

[99] D. Apalkov and P. Visscher, "Fast multipole method for micromagnetic simulation of periodic systems," *IEEE Trans. Magnetics*, vol. 39, no. 6, pp. 3478–3480, Nov. 2003.

[100] J. M. Song, C. C. Lu, and W. C. Chew, "MLFMA for electromagnetic scattering by large complex objects," *IEEE Trans. Antennas and Propagat*, vol. 45, pp. 1488–1493, 1997.

[101] T. Eibert, "Some scattering results computed by surface-integral-equation and by the multilevel fast multipole method," *IEEE Antennas and Propagation Magazine*, vol. 49, no. 2, pp. 61–69, April 2007.

[102] L. Hamilton, P. Macdonald, M. Stalzer, R. Turley, J. Visher, and S. Wandzura, "3D method of moments scattering computations using the fast multipole method," *Antennas and Propagation Society International Symposium, 1994. AP-S. Digest*, vol. 1, pp. 435–438, 20-24 Jun 1994.

[103] T. J. Cui, W. C. Chew, G. Chen, and J. Song, "Efficient MLFMA, RPFMA, and FAFFA algorithms for EM scattering by very large structures," *IEEE Trans. Antennas and Propagat.*, vol. 52, no. 3, pp. 759–770, March 2004.

[104] K. Sertel and J. L. Volakis, "Effects of the fast multipole method (FMM) parameters on radar cross section computations," *IEEE AP-S Int. Symp.*, pp. 624–627, 1999.

[105] Z. Q. Zhang, Q. H. Liu, and X. M. Xu, "RCS computation of large inhomogeneous objects using fast integral equation solver," *IEEE Trans. Antennas Propagat.*, vol. 51, pp. 613–618, March 2003.

[106] J. M. Song and W. C. Chew, "Fast multipole method solution using parametric geometry," *Micro. Opt. Tech. Lett.*, vol. 7, pp. 760–795, 1994.

[107] K. Donepudi, J. M. Jin, and W. C. Chew, "A higher order multilevel fast multipole algorithm for scattering from mixed conducting/dielectric bodies," *IEEE Trans. Antennas Propag.*, vol. 51, pp. 2814–2821, 2003.

[108] K. Donepudi, J. Song, J.-M. Jin, G. Kang, and W. Chew, "A novel implementation of multilevel fast multipole algorithm for higher order Galerkin's method," *IEEE Trans. Antennas and Propagat.*, vol. 48, no. 8, pp. 1192–1197, Aug 2000.

[109] J. Liu and J.-M. Jin, "A novel hybridization of higher order finite element and boundary integral methods for electromagnetic scattering and radiation problems," *IEEE Trans. Antennas Propogat.*, vol. 49, no. 12, pp. 1794–1806, Dec 2001.

[110] H. Wallen, S. Jarvenpaa, P. Yla-Oijala, and J. Sarvas, "Broadband Muller-MLFMA for electromagnetic scattering by dielectric objects," *IEEE Trans. Antennas Propagat.*, vol. 55, no. 5, pp. 1423–1430, May 2007.

[111] V. Jandhyala, B. Shanker, E. Michielssen, and W. Chew, "Fast algorithm for the analysis of scattering by dielectric rough surfaces," *Journal of Optical Society of America*, vol. 15, pp. 1877–1885, 1998.

[112] X. Q. Sheng, J. J. M., J. M. Song, C. W. C., and C. C. Lu, "Solution of combined-field integral equation using multilevel fast multipole algorithm for scattering from homogeneous bodies," *IEEE Antennas and Propagation Magazine*, vol. 46, pp. 1718–1726, 1998.

[113] C.-C. Lu, "A fast algorithm based on volume integral equation for analysis of arbitrarily shaped dielectric radomes," *IEEE Trans. Antennas Propogat.*, vol. 51, no. 3, pp. 606–612, March 2003.

[114] J.-Y. Li and L.-W. Li, "Characterizing scattering by 3d arbitrarily shaped homogeneous dielectric objects using fast multipole method," *IEEE Antennas and Wireless Propagation Letters*, vol. 3, pp. 1–4, 2004.

[115] G. Kobidze, K. Aygun, and B. Shanker, "Efficient integral equation based analysis of scattering from PEC-anisotropic bodies," in *Antennas and Propagation Society International Symposium, 2004. IEEE*, vol. 4, pp. 3887–3890Vol.4, 20-25 June 2004.

[116] G. Kobidze and B. Shanker, "Integral equation based analysis of scattering from 3-d inhomogeneous anisotropic bodies," *Antennas and Propagation, IEEE Transactions on*, vol. 52, pp. 2650–2658, Oct. 2004.

[117] R. Wagner, J. Song, and W. Chew, "Monte carlo simulation of electromagnetic scattering from two-dimensional random rough surfaces," *Antennas and Propagation, IEEE Transactions on*, vol. 45, no. 2, pp. 235–245, 1997.

[118] M. El-Shenawee, C. Rappaport, E. Miller, and M. Silevitch, "Three-dimensional subsurface analysis of electromagnetic scattering from penetrable/PEC objects buried under rough surfaces: use of the steepest descent fast multipole method," *IEEE Trans. Geoscience and Remote Sensing*, vol. 39, no. 6, pp. 1174–1182, Jun 2001.

[119] V. Jandhyala, B. Shanker, E. Michielssen, and W. Chew, "A combined steepest descent-fast multipole algorithm for the analysis of three-dimensional scattering by rough surfaces," in *Antennas and Propagation Society International Symposium, 1997. IEEE., 1997 Digest*, vol. 4, pp. 2308–2311vol.4, 13-18 July 1997.

[120] V. Jandhyala, E. Michielssen, B. Shanker, and W. Chew, "SDFMM-based fast analysis of radiation and scattering from finite microstrip structures," in *Antennas and Propagation Society International Symposium, 1998. IEEE*, vol. 3, pp. 1530–1533vol.3, 21-26 June 1998.

[121] G. Hoyler and R. Unbehauen, "The fast multipole method for EMC problem," *Electrical Engineering*, vol. 80, pp. 403–411, 1997.

[122] H. Y. Chao, W. C. Chew, E. Michielssen, and J. M. Song, "The multilevel fast multipole algorithm for electromagnetic compatibility analysis," *IEEE-EMC Int. Symp.*, vol. 2, pp. 844–847, 1999.

[123] T. J. Cui, W. C. Chew, J.-S. Zhao, and H.-Y. Chao, "Full-wave analysis of complicated transmission-line circuits using wire models," *Antennas and Propagation, IEEE Transactions on*, vol. 50, no. 10, pp. 1350–1360, 2002.

[124] Z. Z. Oo, L. Le-Wei, J.-Y. Li, and E.-P. Li, "Analysis and design of reflector and horn antennas using multilevel fast multipole algorithms (MLFMA)," *IEEE AP-S Int. Symp.*, vol. 2, pp. 758–761, 22-27 June 2003.

[125] J. Lord, S. Benham, and R. Mittra, "Multi-level fast multipole for antenna modelling," *Antennas and Propagation, 2003. (ICAP 2003). Twelfth International Conference on (Conf. Publ. No. 491)*, vol. 1, pp. 308–311, 31 March-3 April 2003.

[126] H.-Y. Chao, J.-S. Zhao, and W. C. Chew, "Application of curvilinear basis functions and MLFMA for radiation and scattering problems involving curved PEC structures," *IEEE Trans. Antennas and Propagat.*, vol. 51, no. 2, pp. 331–336, Feb 2003.

[127] K. Donepudi, J. M. Jin, S. Velamparambil, J. M. Song, and W. C. Chew, "A higher-order parallelized fast multipole algorithm for 3D scattering," *IEEE Trans. Antennas Propagat.*, vol. 49, pp. 1069–1078, 2001.

[128] K. Donepudi, J. M. Song, J. M. Jin, G. Kang, and W. C. Chew, "Point-based MLFMA for Galerkin's method," *IEEE Trans. Antennas Propagat.*, vol. 48, pp. 1192–1197, 2000.

[129] L. Gurel and M. Aksun, "Fast multipole method in layered media: 2-D electromagnetic scattering problems," in *IEEE AP-S Int. Symp.*, pp. 1734–1737, 1996.

[130] L. Gurel and M. Aksun, "Electromagnetic scattering solution of conducting strips in layered media using the fast multipole method," *IEEE Microwave and Guided Wave Letters*, vol. 6, pp. 277–??, 1996.

[131] J. M. Jin, *The Finite Element Method in Electromagnetics.* New York: Wiley, 2002.

[132] S. Bindiganavale and J. Volakis, "A hybrid FE-FMM technique for electromagnetic scattering," *IEEE Trans. Antennas Propagat.*, vol. 45, no. 1, pp. 180–181, Jan 1997.

[133] N. Lu and J.-M. Jin, "Application of fast multipole method to finite-element boundary-integral solution of scattering problems," *IEEE Trans. Antennas Propogat.*, vol. 44, no. 6, pp. 781–786, Jun 1996.

[134] Z. Zhao, L. Li, J. Smith, and L. Carin, "Analysis of scattering from very large three-dimensional rough surfaces using MLFMM and ray-based analyses," *IEEE Antennas and Propagation Magazine*, vol. 47, no. 3, pp. 20–30, June 2005.

[135] P.-L. Rui, R.-S. Chen, D.-X. Wang, and E. Kai-Ning Yung, "A spectral multigrid method combined with MLFMM for solving electromagnetic wave scattering problems," *IEEE Trans. Antennas Propagat*, vol. 55, no. 9, pp. 2571–2577, Sept. 2007.

[136] T. Eibert, "Modeling and design of offset parabolic reflector antennas using physical optics and multilevel fast multipole method accelerated method of moments," *Multitopic Conference, 2006. INMIC '06. IEEE*, pp. 377–382, 23-24 Dec. 2006.

[137] L. Gurel, A. Manyas, and O. Ergul, "PO-MLFMA hybrid technique for the solution of electromagnetic scattering problems involving complex targets," *Antennas and Propagation, 2007. EuCAP 2007. The Second European Conference on*, pp. 1–5, 11-16 Nov. 2007.

[138] A. Tzoulis and T. Eibert, "Antenna modeling with the hybrid finite element - boundary integral - multilevel fast multipole - uniform geometrical theory of diffraction method," *Antennas, 2007. INICA '07. 2nd International ITG Conference on*, pp. 91–95, 28-30 March 2007.

[139] X. Yin, X. Zai, W. Hong, and X. Zhu, "A fast algorithm based on MEI and FMM for field prediction in urban mobile communications," *IEEE AP-S Int. Symp.*, vol. 2, pp. 1384–1387, Aug 1999.

[140] D. Pissoort, E. Michielssen, D. Ginste, and F. Olyslager, "Fast-multipole analysis of electromagnetic scattering by photonic crystal slabs," *Lightwave Technology, Journal of*, vol. 25, no. 9, pp. 2847–2863, Sept. 2007.

[141] D. Ginste, E. Michielssen, F. Olyslager, and D. De Zutter, "An efficient perfectly matched layer based multilevel fast multipole algorithm for large planar microwave structures," *IEEE Trans. Antennas Propagat.*, vol. 54, no. 5, pp. 1538–1548, May 2006.

[142] D. Pissoort, D. Ginste, and F. Olyslager, "Including PML-based absorbing boundary conditions in the MLFMA," *IEEE Antennas and Wireless Propagation Letters*, vol. 4, pp. 312–315, 2005.

[143] V. Jandhyala, E. Michielssen, and R. Mittra, "Multipole-accelerated capacitance computatiion for 3-d structures in a stratified dielectric medium using a closed form green's function," *Int. J. Microwave. Millimeter Wave Comput. Aided Eng.*, vol. 5, pp. 68–78, 1995.

[144] L. Gurel and M. I. Aksun, "Electromagnetic scttering solution of conducting strips in layered media using the fast multipole method," *IEEE Microwave Guided Wave Letters*, vol. 6, pp. 277–279, 1996.

[145] P. A. MacDonald and T. Itoh, "Fast simulation of microstrip structures using the fast multipole method," *Int. J. Numerical Modelling: Electron. Networks, Devices and Fields*, vol. 9, pp. 345–357, 1996.

[146] J. Zhao, W. C. Chew, C. C. Lu, E. Michielssen, and J. M. Song, "Thin-stratified medium fast-multipole algorithm for solving microstrip structures," *IEEE Trans. Microwave Theory Tech.*, vol. 46, pp. 395–403, 1998.

[147] V. Jandhyala, E. Michielssen, B. Shanker, and W. C. Chew, "A fast algorithm for the analysis of radiation and scattering from arrays on finite substrates," *Micro. Opt. Tech. Lett.*, vol. 23, pp. 306–310, 1999.

[148] F. Ling, J. M. Song, and J. M. Jin, "Multilevel fast multipole algorithm for analysis of large scale microstripstructures," *IEEE Microwave and Guided Wave Letts.*, vol. 9, pp. 508–510, 1999.

[149] B. Hu and W. C. Chew, "Fast inhomogeneous plane wave algorithm for electromagnetic solutions in layered medium structures-2D case," *Radio Science*, vol. 35, 2000.

[150] B. Hu and W. C. Chew, "Fast inhomogeneous plane wave algorithm for multilayered medium problems," *IEEE Trans. Geoscience. Remote Sensing*, vol. 39, pp. 1028–1038, 2001.

[151] N. Geng, A. Sullivan, and L. Carin, "Multi-level fast-multipole algorithm for scattering from conducting targets above or embedded in a lossy half space," *IEEE Trans. Geoscience Remote Sensing*, vol. 38, pp. 1567–1579, 2000.

[152] N. Geng, A. Sullivan, and L. Carin, "Fast multipole method analysis of scattering from a three-dimensional target in a half-space environment," *IEEE Trans. Antennas Propagat.*, vol. 49, pp. 740–748, 2001.

[153] Z. Liu, J. He, Y. Xie, A. Sullivan, and C. L., "Multi-level fast multipole algorithm for general targets on a half-space interface," *IEEE Trans. Antennas Propagat.*, vol. 50, pp. 1838–1849, 2002.

[154] Z. Liu, R. J. Adams, and C. L., "New MLFMA formulation for closed pec targets in the vicinity of a half space," *IEEE Trans. Antennas Propagat.*, vol. 51, pp. 2822–2829, 2003.

[155] X. Dong, Z. Liu, and L. Carin, "Volume and surface MLFMA formulations for dielectric targets in the presence of a half space," *Radio Science*, vol. 39, 2004.

[156] L. Li and L. Carin, "Multi-level fast multipole method calibration of ray models with application to wireless propagation," *IEEE Trans. Antennas Propagat.*, vol. 52, pp. 2794–2799, 2004.

[157] M. A. Seville, *Multilevel Multipole Free Fast Algorithm for Elecgromagnetic Scattering Problems in Layered Media.* PhD thesis, University of Illinois at Urbana, 2006.

[158] R. L. Wagner, *Efficient computational techniques for electromagnetic propagation and scattering.* PhD thesis, University of Illinois at Urbana-Champaign, 1996.

[159] R. L. Wagner, J. Song, and C. W. C., "Monte Carlo simulation of electromagnetic scattering from two-dimensional random rough surfaces," *IEEE Trans. Antennas Propogat.*, vol. 45, pp. 235–245, 1997.

[160] V. Jandhyala, B. Shanker, E. Michielssen, and W. C. Chew, "A combined steepest descent fast multipole algorithm for the fast analysis of three-dimensional scattering by rough surfaces," *IEEE Trans. Geoscience Remote Sensing*, vol. 36, pp. 738–748, 1998.

[161] V. Jandhyala, D. Sengupta, B. Shanker, E. Michielssen, M. Feng, and G. Stillman, "Two-dimensional rough surface couplers for broadband quantum-well infrared photodetectors," *Appl. Phys. Lett.*, vol. 73, pp. 3495–3497, 1998.

[162] V. Jandhyala, D. Sengupta, B. Shanker, E. Michielssen, M. Feng, and G. Stillman, "Efficient electromagnetic analysis of two-dimensional finite quasi-random gratings of quantum well infrared photodetectors," *J. Appl. Phys.*, vol. 83, pp. 3360–3363, 1998.

[163] A. Ergin, B. Shanker, and E. Michielssen, "The plane-wave time-domain algorithm for the fast analysis of transient wave phenomena," *Antennas and Propagation Magazine, IEEE*, vol. 41, pp. 39–52, Aug. 1999.

[164] B. Shanker, A. Ergin, K. Aygun, and E. Michielssen, "Analysis of transient electromagnetic scattering phenomena using a two-level plane wave time-domain algorithm," *Antennas and Propagation, IEEE Transactions on*, vol. 48, no. 4, pp. 510–523, 2000.

[165] M. Vikram, H. Griffith, H. Huang, and B. Shanker, "A uniform framework for time and frequency domain low-frequency problems," in *Proceedings of the 2007 IEEE Internation Symposium on Antennas and Propagation Society International*, 2007.

[166] B. Shanker and H. Huang, "Accelerated cartesian expansions–a fast method for computing of potentials of the form $r^{-\nu}$ for all real ν," *J. Comp. Phys.*, p. doi:10.1016/j.jcp.2007.04.033, 2007.

[167] L. Greengard and V. Rokhlin, "A new version of the fast multipole method for the laplace equation in three dimensions," *Acta Numerica*, vol. 6, pp. 229–269, 1997.

[168] L. Greengard and V. Rokhlin, "A fast algorithm for particle simulations," *Journal of Computational Physics*, vol. 73, pp. 325–348, Dec. 1987.

[169] H. Cheng, L. Greengard, and V. Rokhlin, "A fast adaptive multipole algorithm in three dimensions," *J. Comput. Phys.*, vol. 155, no. 2, pp. 468–498, 1999.

[170] B. Shanker, A. Ergin, M. Lu, and E. Michielssen, "Fast analysis of transient electromagnetic scattering phenomena using the multilevel plane wave time domain algorithm," *Antennas and Propagation, IEEE Transactions on*, vol. 51, pp. 628–641, March 2003.

[171] K. Aygün, *Novel fast algorithms for time domain integral equation analysis of antennas and circuits.* PhD thesis, University of Illinois at Urbana, 2002.

[172] J. Meng, M. Lu, and E. Michielssen, "Towards efficient and stable low frequency time domain integral equation solvers," in *Proceeding of the 2006 IEEE International Symposium on Antennas and Propagation*, pp. 2955–2958, 2006.

[173] J. Meng, M. Lu, and E. Michielssen, "A fast space-adaptive algorithm to evaluate transient wave fields due to low-frequency source constellations," in *Proceedings of the 2005 IEEE International Symposium on Antennas and Propagation*, vol. 3A, pp. 171–174, July 2005.

[174] M. Vikram and B. Shanker, "An incomplete review of fast multipole methods -from static to wideband -as applied to problems in computational electromagnetics," *ACES (accepted for publication)*, 2008.

[175] J.-S. Zhao and W. C. Chew, "Integral equation solution to Maxwell's equations from zero frequency to microwave frequency," *IEEE Trans. Antennas Propagat.*, vol. 48, pp. 1635–1645, 2000.

[176] J. Mautz and R. Harrington, "An E-field solution for a conducting surface small or comparable to the wavelength," *Antennas and Propagation, IEEE Transactions on*, vol. 32, pp. 330–339, Apr 1984.

[177] E. Arvas, R. Harrington, and J. Mautz, "Radiation and scattering from electrically small conducting bodies of arbitrary shape," *Antennas and Propagation, IEEE Transactions on*, vol. 34, pp. 66–77, Jan 1986.

[178] W. Wu, W. Glisson, and D. Kajfez, "A study of two numerical solution procedures for the electric field integral equation at low frequency," *Appl. Computat. Electromagn. Soc. J.*, vol. 10, pp. 69–80, 1995.

[179] M. Burton and S. Kashyap, "A study of a recent, moment-method algorithm that is accurate to very low frequencies," *Appl. Computat. Electromagn. Soc. J.*, vol. 10, pp. 69–80, 1995.

[180] I. Bogaert, J. Peeters, J. Fostier, and F. Olyslager, "NSPWMLFMA: A low frequency stable formulation of the mlfma in three dimensions," *Antennas and Propagation Society International Symposium, 2008. AP-S 2008. IEEE*, pp. 1–4, July 2008.

[181] S. Rao, D. Wilton, and A. Glisson, "Electromagnetic scattering by surfaces of arbitrary shape," *Antennas and Propagation, IEEE Transactions on*, vol. 30, pp. 409–418, May 1982.

[182] J. Applequist, "Traceless cartesian tensor forms for spherical harmonic functions: new theorems and applications to electrostatics of dielectric media," *J. Phys. A: Math. Gen.*, vol. 22, pp. 4303–4330, 1989.

[183] A. Peterson, S. Ray, and R. Mittra, *Computational Methods for Electromagnetics.* Institute of Electrical and Electronic Engineers (IEEE) Press, 1997.

[184] D. L. Colton and R. Kress, *Integral equation methods in scattering theory.* New York: Wiley, 1983.

[185] K. E. Atkinson, *The numerical solution of integral equations of the second kind.* Cambridge, U.K: Cambridge Univ. Press, 1997.

[186] G. Vecchi, "Loop-star decomposition of basis functions in the discretization of the efie," *IEEE Trans. Antennas and Propagat.*, vol. 47, pp. 339–346, 1999.

[187] G. Hsiao and R. E. Kleinman, "Mathematical foundations for error estimation in numerical solution of integral equations in electromagnetics," *IEEE Trans. Antennas and Propagat.*, vol. 45, pp. 316–328, 1997.

[188] R. J. Adams and G. S. Brown, "Stabilization procedure for electric field integral equation," *Electronic Letters*, vol. 35, pp. 2015–2016, 1999.

[189] R. J. Adams, "Physical and analytical properties of a stabilied electric field integral equation," *IEEE Trans. Antennas and Propagat.*, vol. 52, pp. 362–372, 2004.

[190] S. H. Christiansen and J.-C. Nédélec, "A preconditioner for the electric field integral equation based on calderon formulas," *SIAM J. Numer. Anal.*, vol. 40, no. 3, pp. 1100–1135, 2002.

[191] H. Contopanagos, B. Dembart, M. Epton, J. J. Ottusch, V. Rokhlin, J. Visher, and S. Wandzura, "Well-conditioned boundary integral equations for three-dimensional electromagnetic scattering," *IEEE Trans. Antennas and Propagat.*, vol. 50, pp. 1824–1830, 2002.

[192] R. J. Adams and N. J. Champagne, "A numerical implementation of the modified electric field integral equation," *IEEE Trans. Antennas and Propagat.*, vol. 52, pp. 2262–2266, 2004.

[193] F. Andriulli, K. Cools, H. Bagci, F. Olyslager, A. Buffa, S. Christiansen, and E. Michielssen, "A multiplicative calderon preconditioner for the electric field integral equation," *Antennas and Propagation, IEEE Transactions on*, vol. 56, pp. 2398–2412, Aug. 2008.

[194] A. D. Yaghjian, "Augmented electric- and magnetic-field integral equation," *Radio Science*, vol. 16, pp. 987–1001, 1981.

[195] J. R. Mautz and R. F. Harrington, "H-field, E-field and combined-field solutions for conducting bodies of revolution," *Electronics and Communications*, vol. 32, pp. 157–164, 1978.

[196] J. Mautz and R. Harrington, "A combined-source solution for radiation and scattering from a perfectly conducting body," *Antennas and Propagation, IEEE Transactions on*, vol. 27, pp. 445–454, Jul 1979.

[197] R. Shore and A. Yaghjian, "Dual-surface integral equations in electromagnetic scattering," *Antennas and Propagation, IEEE Transactions on*, vol. 53, pp. 1706–1709, May 2005.

[198] M. Vikram, H. Huang, B. Shanker, and V. Tri, "A novel wideband FMM for fast integral equation solution of multiscale problems in electromagnetics," *to appear in IEEE Trans. Antennas and Propagat.*, July 2009.

[199] B. Hariharan, S. Aluru, and B. Shanker, "A scalable parallel fast multipole method for analysis of scattering from perfect electrically conducting surfaces," in *Supercomputing '02: Proceedings of the 2002 ACM/IEEE conference on Supercomputing*, (Los Alamitos, CA, USA), pp. 1–17, IEEE Computer Society Press, 2002.

[200] L. Gurel and O. Ergul, "Fast and accurate solutions of extremely large integral-equation problems discretised with tens of millions of unknowns," *Electronics Letters*, vol. 43, pp. 499–500, April 2007.

[201] C. Waltz, K. Sertel, M. Carr, B. Usner, and J. Volakis, "Massively parallel fast multipole method solutions of large electromagnetic scattering problems," *IEEE Trans. Antennas and Propagat.*, vol. 55, no. 6, pp. 1810–1816, June 2007.

[202] P. B. Callahan and S. R. Kosaraju, "A decomposition of multidimensional point sets with applications to k-nearest neighbors and n-body potential fields," *Journal of the ACM*, vol. 42, pp. 67–90, 1995.

[203] M. S. Warren and J. K. Salmon, "Astrophysical n-body simulations using hierarchical tree data structures," *Proceedings of Supercomputing*, p. 570576, 1992.

[204] M. Warren and J. Salmon, "A parallel hashed oct-tree n-body algorithm," *Proceedings of Super-computing*, pp. 1–12, 1993.

[205] P. Liu and S. Bhatt, "Experiences with parallel n-body simulation," *IEEE Transactions on Parallel and Distributed Systems*, vol. 11, pp. 1306–1323, 2000.

[206] F. Sevilgen, S. Aluru, and N. Futamura, "A provably optimal, distribution-independent parallel fast multipole method," *Proceedings of International Parallel and Distributed Processing Symposium IEEE Computer Society Press*, pp. 77–84, 2000.

[207] S. H. Teng, "Provably good partitioning and load balancing algorithms for parallel adaptive n-body simulation," *SIAM Journal on Scientific Computing*, vol. 19, pp. 635–656, 1998.

[208] S. Velamparambil, J. E. Schutt-Aine, J. G. Nickel, J. M. Song, and W. C. Chew, "Solving large sclae electromagnetic problems using a linux cluster and parallel MLFMA," *IEEE AP-S Int. Symp.*, vol. 1, pp. 636–639, 1999.

[209] O. Ergul and L. Gurel, "Efficient parallelization of the multilevel fast multipole algorithm for the solution of large-scale scattering problems," *IEEE Trans. Antennas Propagat.*, vol. 56, pp. 2335–2345, 2008.

[210] S. Velamparambil and W. C. Chew, "Analysis and performance of a distributed memory multilevel fast multipole algorithm," *IEEE Trans. Antennas Propagat.*, vol. 8, pp. 2719–2727, 2005.

[211] O. Ergul and L. Gurel, "Hierarchical parallelisation strategy for multilevel fast multipole algorithm in computational electromagnetics," *Electronics Letters*, vol. 44, 2008.

[212] J. Fostier and F. Olyslager, "A provably scalable parallel multilevel fast multipole algorithm," *Electronics Letters*, vol. 44, pp. 1111–1113, Sept. 2008.

[213] M. Vikram, A. Baczewski, B. Shanker, and S. Aluru, "Parallel accelerated cartesian expansions for particle dynamics simulations," *to appear in Proceedings of International Parallel and Distributed Processing Symposium IEEE Computer Society Press*, 2009.

[214] M. Vikram, A. Baczewski, B. Shanker, and L. Kempel, "Accelerated cartesian expansion (ace) unified framework for the rapid evaluation of potentials associated with the diffusion, lossy wave and klein-gordon equations," *Submitted to Journal of Computational Physics*, 2008.

[215] G. M. Morton, "A computer oriented geodetic data base and a new technique in file sequencing," tech. rep., Tech. Rep. IBM.

[216] M. Griebel, S. Knapek, and G. Zumbusch, *Numerical simulation in Molecular Dynamics.* Springer-Verlag, 2007.

[217] A. Tamburrino, R. Fresa, S. Udpa, and Y. .Tian, "Three-dimensional defect localization from time-of-flight/eddy current testing data," *IEEE Transactions on Magnetics*, vol. 40(2), pp. 1148–1151, 2004.

[218] P. M. Morse and H. Feshbach, *Methods of Theoretical Physics.* McGraw-Hill Science/Engineering/Math, 1953.

[219] W. Boettinger, J. Warren, C. Beckermann, and A. Karma, "Phase-simulation of solidification," *Annual Review of Materials Research*, vol. 32, pp. 163–94, 2002.

[220] D. Arifin, L. Lee, and C. Wang, "Mathematical modeling and simulation of drug release from microspheres: Implications to drug delivery systems," *Advanced Drug Delivery Reviews*, vol. 58, pp. 1274–1325, 2006.

[221] A. E. Yilmaz, D. S. Weile, B. Shanker, J.-M. Jin, and E. Michielssen, "Fast analysis of transient scattering in lossy media," *IEEE Antennas and Wireless Propagation Letters*, vol. 1, pp. 14–17, 2002.

[222] V. Rokhlin, "Rapid solution of integral equations of classical potential theory," *J. Comput. Phy.*, vol. 60, pp. 187–207, 1985.

[223] E. Bleszynski, M. Bleszynski, and T. Jaroszewicz, "Aim: Adaptive integral method for solving large-scale electromagnetic scattering and radiation problems," *Radio Sci.*, vol. 31, no. 5, pp. 1225–1251, 1996.

[224] S. Kapur and D. E. Long, "Ies3: Efficient electrostatic and electromagnetic simulation," *IEEE Computational Science and Engineering*, vol. 5, pp. 60–67, Oct. 1998.

[225] L. Greengard and V. Rokhlin, "A new version of the fast multipole method for the laplace equation in three dimensions," *Acta Numerica*, vol. 6, pp. 229–269, 1997.

[226] L. Greengard and J. Strain, "The fast gauss transform," *SIAM J. Sci. Stat. Comput.*, vol. 12, pp. 79–94, January 1991.

[227] J. Strain, "Fast adaptive methods for the free-space heat equation," *SIAM J. Sci. Statist. Comput.*, vol. 15, pp. 186–206, 1992.

[228] C. Yang, R. Duraiswami, N. A. Gumerov, and L. Davis, "Improved fast gauss transform and efficient kernel density estimation," in *ICCV '03: Proceedings of the Ninth IEEE International Conference on Computer Vision*, (Washington, DC, USA), p. 464, IEEE Computer Society, 2003.

[229] L. Greengard and J. Strain, "A fast algorithm for the evaluation of heat potentials," *Comm. Pure Appl. Math.*, vol. 43, no. 8, pp. 949–963, 1990.

[230] J. Tausch, "A fast method for solving the heat equation by layer potentials," *Journal of Computational Physics*, vol. 224, no. 2, pp. 956–969, 2007.

[231] L. Greengard and P. Lin, "Spectral approximation of the free-space heat kernel," *Appl. Comput. Harmon. Anal.*, vol. 9, no. 1, pp. 83–97, 2000.

[232] J.-R. Li and L. Greengard, "On the numerical solution of the heat equation i: fast solvers in free space," *Journal of Computational Physics*, 2007.

[233] R. Harrington, *Field Computation by Moment Methods.* Wiley-IEEE Press, 1993.

[234] M. Lu, K. Yegin, B. Shanker, and E. Michielssen, "Fast time domain integral equation solvers for analyzing two-dimensional scattering phenomena, part i: temporal acceleration," *Electromagnetics*, vol. 24, no. 6, pp. 425–449, 2004.

[235] A. E. Yilmaz, J. M. Jin, and E. Michielssen, "Analysis of low-frequency electromagnetic transients by an extended time-domain adaptive integral metho," *IEEE Trans. on Advanced Packaging*, vol. 30, pp. 301–312, May 2007.

[236] *The Design and Implementation of FFTW3*, vol. 93, 2005.

[237] S. S. Udpa (Editor) and P. O. Moore (Editor), *Handbook of Nondestructive Evaluation: Electromagnetic Testing*, vol. 5. ASNT, 2004.

[238] W. C. Chew, *Waves and Fields in Inhomogeneous Media*. Piscataway, NJ: IEEE Press, 1995.

[239] T. J. Cui and W. C. Chew, "Fast algorithm for electromagnetic scattering by buried 3-D dielectric objects of large size," *IEEE Transactions on Geoscience and Remote Sensing*, vol. 37, pp. 2597–2608, Sept. 1999.

[240] D. H. Schaubert, D. R. Wilton, and A. W. Glisson, "A tetrahedral modeling method for electromagnetic scattering by arbitrarily shaped inhomogenous dielectric bodies," *IEEE Trans. Antennas and Propogat.*, vol. 32, pp. 77–85, Jan 1984.

[241] D. Wilton, S. Rao, A. Glisson, D. Schaubert, O. Al-Bundak, and C. Butler, "Potential integrals for uniform and linear source distributions on polygonal and polyhedral domains," *IEEE Transactions on Antennas and Propagation*, vol. 32, pp. 276–281, Mar. 1984.

[242] H. A. Sabbagh, J. R. Bowler and L. D. Sabbagh, "A Volume Integral Code for Eddy-Current Non-destructive Evaluation," *Journal of Applied Computational Electromagnetics Society*, vol. 4, pp. 3–22, 1989.